Role of Fragile X Mental Retardation Protein in lung

A THESIS TO BE SUBMITTED TO

THE UNIVERSITY OF TRANS-DISCIPLINARY HEALTH SCIENCES AND TECHNOLOGY

FOR THE AWARD OF THE DEGREEOF

DOCTOR OF PHILOSOPHY

BY

DEBLINA SAIN BASU

UNDER THE GUIDANCE OF

DR. ARJUN GUHA

JULY, 2022

THE UNIVERSITY OF TRANS-DISCIPLINARY HEALTH SCIENCES AND TECHNOLOGY

Private University Established in Karnataka by ACT 35 of 2013

BENGALURU - 560064

DECLARATION BY THE CANDIDATE

I declare that this thesis entitled "**Role of Fragile X Mental Retardation Protein in lung**" submitted for the award of Doctor of Philosophy to THE UNIVERSITY OF TRANS-DISCIPLINARY HEALTH SCIENCES AND TECHNOLOGY, Bengaluru, is my original work, conducted under the supervision of my guide **Dr. Arjun Guha**. I also wish to inform that no part of the research has been submitted for a degree or examination at any university. References, help and material obtained from other sources have been duly acknowledged. I hereby confirm the originality of the work and that there is no plagiarism in any part of the dissertation.

Place: Bengaluru **Signature of the Candidate**

Date: 21-Jul-2022

Name of candidate: Deblina Sain Basu

Reg. No.: 20318020210

THE UNIVERSITY OF TRANS-DISCIPLINARY HEALTH SCIENCES AND TECHNOLOGY

Private University Established in Karnataka by ACT 35 of 2013

BENGALURU - 560064

CERTIFICATE

This is to certify that the work incorporated in this thesis **"Role of Fragile X Mental Retardation Protein in lung"** submitted by Deblina Sain Basu was carried out under my supervision. No part of this thesis has been submitted for a degree or examination at any university. References, help and material obtained from other sources have been duly acknowledged. I hereby confirm the originality of the work and that there is no plagiarism in any part of the dissertation.

Research Supervisor

Date: 21-Jul-2022

Dr. Arjun Guha

inStem, GKVK Post, Bellary Road,

Bangalore 560065, India

Institute for Stem Cell Biology and Regenerative Medicine
Autonomous Institute of the Department of Biotechnology, Government of India

inStem

July 21, 2022

To Whom It May Concern

I am writing to forward Ms. Deblina Sain Basu's (Registration number: 20318020210) doctoral thesis for your consideration. Deblina as a graduate student in my laboratory since December 2016.

Please do not hesitate to get in touch if you have any questions or concerns.

Arjun Guha, PhD
Principal Investigator, Regulation of Cell Fate Theme, Institute for Stem Cell Biology and Regenerative Medicine.
arjung@instem.res.in Tel:
(9180) 61948110
https://www.instem.res.in/faculty/arjun

Dedication

I would like to dedicate this work to my Babaji Maharaj Dr. Swami Prajnadas Kathia. His inspirations and blessings always helped me to overcome all obstacles of the inner and outer world.

Acknowledgements

I would like to express my sincere gratitude to my advisor Dr. Arjun Guha for his guidance and support throughout my work. His valuable suggestions and insights allowed me to move in the right direction. I would like to thank my Doctoral Advisory Committee Members, Dr. Rajesh Thimmulappa, Dr. Ravi Muddashetty, Dr. Sumantra Chatterji and Dr. Aditi Bhattacharya for their valuable comments, discussions and insights. I would like to convey my thanks to Dr. Narmada Khare for her immense help in composing this thesis.

I am very thankful to my present colleagues and past members of Guha lab, whom I have worked closely to complete this thesis work: Dr. Rital Bhavsar, Aditya Deshpande, Sai Manoz L., Imtiyaz Gulami, Saraswati Chavwda, Amrutha, Piyush, Steffy, Archit and the unforgettable group of under graduate trainees; Harlin, Mamta and Megha. I hope for your success in all your future endeavors and continue friendship in the coming days. I am also thankful to Dr. Ravi Muddashetty's group and Dr. Sumantra Chatterji's group, for their extensive help during collaboration.

I convey my gratitude to the academic coordinator in Transdisciplinary University (TDU), Mr. Ravi Kumar for all his kind help regarding thesis submission and other official works at University.

I wish to thank my parents, in-law parents, brothers, sister and all the members of my extended family, especially my grandfather, Late Mr. Rabindranath Sain and my husband, Mr. Saswata Basu for their constant support and sacrifice during this journey. I would like to thank all my teachers who helped me to learn, adapt and achieve self-confidence. Though this list is long but I would like take few names: Mr. Biswadeep Mondal, Mrs. Sonali Ghosh, Dr. Dilip Guha, Dr. Prasanta Kumar Mondal, Dr. Baidyanath Chakravorty, Dr. Anindya Sinha, Mr. Ashok kr. Das. Last but not the least, I would like to thank all my friends on campus and outside campus, Rose, Roopkatha, Arka, Adwitiya, Sumit and my wonderful group of school friends. Your support has always helped me to overcome odds and to grow with new spirit.

Contribution

Thesis advises: Dr. Arjun Guha, Dr. Ravi Muddashetty, Dr. Rajesh Thimmulappa, Dr. Sumantra Chatterji and Dr. Aditi Bhattacharya
Study design: Dr. Arjun Guha, Deblina Sain Basu
Data collection and analysis: Deblina Sain Basu, Rital Bhavsar, Imtiyaz Gulami, Saraswati Chavda
Manuscript preparation: Dr. Arjun Guha, Deblina Sain Basu, Saraswati Chavda
Manuscript correction: Dr. Arjun Guha, Dr. Narmada Khare

I also thank Harlin Kaur, Binita Dam, Megha Balachanda, Mamta Yadav and Arnab Karmakar for their contribution. They worked together to validate some of the findings and hypothesis. Their data is not presented in the thesis but helped us for conceptual advancement.

List of contents

List of Symbols and Abbreviation

FMRP	Fragile X Mental Retardation Protein
ISR	Integrated Stress Response
SG	Stress granule
SIG	Stress induced granules
Fmr1	Notation for the gene of Fragile X Mental Retardation Protein in mouse
FMR1	Notation for the gene of Fragile X Mental Retardation Protein in human
WT	Wild type
KO	Knocked out
KD	Knocked down
RT-PCR	Reverse transcription Polymerase Chain Reaction
KDa	Kilodalton
SDS	Sodium dodecyle sulfate
ATF4	Activating transcription factor 4 protein; notation for the related gene in human
Atf4	Notation for the ATF4 gene in mouse
ATF3	Activating transcription factor 3
SOD1	Superoxide dismutase 1
G3BP	Ras GTPase-activating protein-binding protein
Atxn2	Ataxin 2
Tia1	T cell-restricted intracellular antigen-1
eIF2α	Notation for the protein of eukaryotic initiation factor 2α
P-eIF2α	Notation for the protein of phosphorylated form of eukaryotic initiation factor 2α
siRNA	Short interfering RNA
4HNE	4-Hydroxy-2-nonenal
γ-H2AX	Phosphorylated form of H2A histone family member X
DMSO	Dimethyl sulfoxide
DMEM	Dulbecco’s Modified Eagle Medium
FBS	Fetal bovine serum

GCN2	General control nondepressible 2
PERK	PKR-like endoplasmic reticulum kinase
PKR	Protein kinase double stranded RNA-dependent
HRI	Heme regulated inhibitor
OD	Optical density
mg	Milligram
ug	Microgram
uM	Micro molar
Nap	Naphthalene
PQ	9,10-Phenanthrenequinone
Actub	Acetylated tubulin
Scgb1a1	Secretoglobin Family 1A Member 1
um	Micro meter
uM	Micromolar
mL	Milliliter
CO_2	Carbon dioxide
Cyp2f2	Cytochrome P450 2F2
DPX	Dibutylphthalate polystyrene xylene
COPD	Chronic obstructive pulmonary disorder
ALI	Acute lung injury
DDR	DNA damage response
CYFIP1/2	Cytoplasmic FMRP interacting protein 1/2
DDX3X	DEAD-box helicase 3 X-linked
PARP1	Poly [ADP-Ribose] polymerase 1
RPS6K	Ribosomal protein S6 kinase
PP2A	Protein Phosphatase 2 Catalytic Subunit Alpha
mTOR	Mammalian target of rapamycin
ERK	Extracellular regulated kinase
PI3K	Phosphoinositide 3-kinase
AKT	Serine/Threonine-specific protein kinases
Nrf2	Nuclear factor-erythroid factor 2-related factor 2
PRMP5	Pathogen-associated molecular patterns 5
YBX1	Y-Box Binding Protein 1

APC	Adenomatous polyposis coli
TNFα	Tumour Necrosis Factor alpha
EIF4E	Eukaryotic initiation factor 4F
Tdrd3	Tudor domain containing 3
FXTAS	Fragile X-associated Tremor/ Ataxia Syndrome
FXPOI	Fragile X-associated Primary Ovarian Insufficiency

List of Tables

List of Figures

SYNOPSIS

Lung is the organ of gaseous exchange. The epithelium of lung is exposed to inhaled air containing airborne pollutants, pathogens, particulate matters during the breathing process. Some of these chemicals are directly cytotoxic and some of them produce hazardous metabolic byproducts. Altogether these chemicals cause huge amount of redox burden on respiratory system. Lung epithelial cells must have unique repertoires to balance this redox burden or xenobiotic stress. In order understand the stress regulation in lung this study was initiated.

Integrated stress response (ISR) is a major pathway for cellular stress management in lung. There are four upstream kinases, GCN2, PERK, PKR and HRI. In presence of stress stimuli like, amino acid starvation, protein misfolding, double stranded DNA break or oxidative stress these kinases become phosphorylated and activate eIF2α. Activated or phosphorylated eIF2α falls off from the translation machinery to stop global translation. The mRNAs are stored in stress granules during this process and some stress regulator genes are activated by a non-canonical translation machinery. ATF4 is such a master regulator which gets activated and activate many other downstream genes.

According to previous studies FMRP was established as a multifunctional protein that helps in regulation of oxidative and genotoxic stress in the cells from different origin. In absence of this protein more oxidative stress in murine brain, perturbed DNA damage response during replication stress and perturbed stress granule biogenesis were reported. These reports suggested that FMRP may have an important role in cellular stress response pathways.

Expression of FMRP in lung epithelium and indication of FMRP involvement in cellular stress response, led us to investigate the role of this protein in the stress response of lung and lung derived cells.

The current study entitled “Role of Fragile X Mental Retardation Protein in Lung” is divided in to five chapters.

Chapter-I is the introduction, where literature reviews on FMRP and scope of the study has been described. **Chapter –II** describes the experimental procedures. A major part of this chapter has been published in the Journal of

Cell Science. **Chapter –III** describes the study related to the protecting role of FMRP in lung and lung derived cell line. This chapter includes expression of FMRP and associated phenotype in murine lung, establishment of C22 cell line as an ex vivo model system, replicating FMRP phenotype in ex vivo model and role of FMRP in the Integrated Stress Response pathway. This chapter also talks about the role of FMRP in human lung. The dataset of this chapter has been published in the Journal of Cell Science. **Chapter-IV** deals with three alternative possibilities to explain FMRP phenotype in the lung. This chapter concludes that none of the known mechanisms like, FMRP dependent superoxide dismutase 1 translation, FMRP dependent activation of DNA damage response in replication stress or FMRP dependent stress granule biogenesis can sufficiently explain the susceptibility of FMRP deficient lung or lung derived cells to xenobiotic stress across species or stressors. The chapter also concludes that FMRP dependent actuation of ISR can fit as a plausible mechanism for the FMRP phenotype in the lung. A part of this chapter has been published in the Journal of Cell Science. **Chapter- V** is the discussion and future prospects of the study.

Chapter –III: The study was initiated to probe the role of FMRP in the regulation of stress response in the lung epithelial cells. This chapter deals with the major part of the study. The result section starts with the immunohistochemical analysis that shows expression of FMRP in murine lung epithelium, predominantly in the airway club and ciliated cells. It also shows that, in absence of FMRP there is no obvious histological difference in the lung tissue or any detectable difference in the expression of oxidative and genotoxic stress markers. Next, the animals were challenged with conventional dosage of naphthalene to create xenobiotic stress in the mouse lung. It was observed that in absence of FMRP airway epithelium had faster and greater club cell loss. Higher level of oxidative and genotoxic stress marker expression and their longer persistence were also observed in the airway club cells. In order to investigate the cell autonomous function of FMRP in the murine lung, the next study was performed on a club cell like, C22 cell line using naphthalene as a stress inducer. The cell line experiments gaveus opportunity to probe the time dependent events of cellular stress response more closely and mounting of

ISR within 3 h of acute stress stimuli could be observed. Here it was also noticed that in absence of FMRP, ISR was perturbedin the cells from very initial step of eIF2α phosphorylation. Knocking down ATF4 phenocopied FMRP, which led us to conclude that ISR is the major pathway of stress response during naphthalene induced stress and FMRP is involved in this process.

Next we went on to probe the role of FMRP in human lung. This section, describes expression of FMRP in human airway epithelium and a non-ciliated, bronchial cell line BEAS2B. The section also deals with the study of FMRP in BEAS2B cells during 9, 10-PQ injury. The study suggests that the protecting role of FMRP and its involvement in ISR is conserved in human bronchial cell line. It was that FMRP dependent activation of ISR is also applicable for the alveolar epithelial cell line A549 in response to PQ stress.

Overall the chapter concludes that FMRP is important for lung health, as it protects airway cells from xenobiotic stress by activating ISR. As we could not comment on all four upstream kinases, due to lack of reliable western blot based data, we could only say that at least for PKR mediated activation of ISR is dependent on FMRP in the lung epithelial cells. Though this study could not delineate the underlined molecular mechanism of FMRP dependent eIF2α phosphorylation in response to stress, but can propose a plausible mechanism that FMRP may physically interact with its binding partner Caprin1 and G3BP1 to facilitate phosphorylation of eIF2α.

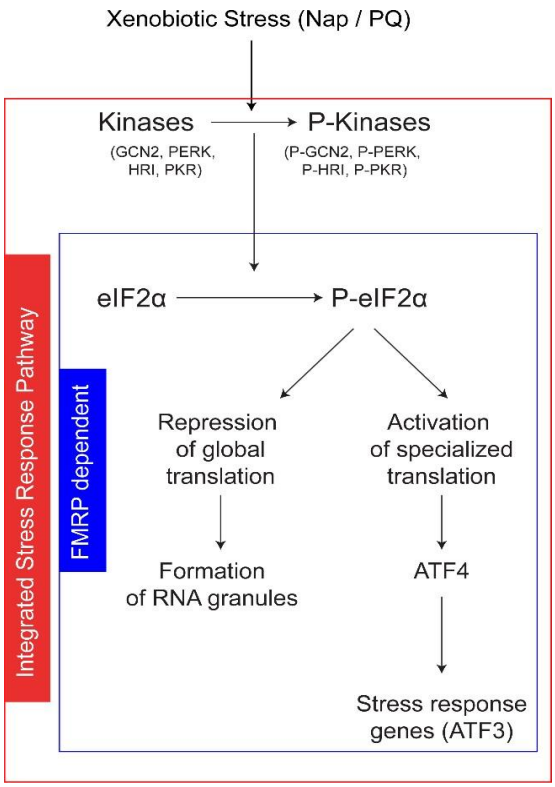

Model for the role of FMRP in the regulation of the Integrated Stress Response in the lung. Exposure to xenobiotics such as Naphthalene (Nap) and 9, 10-Phenanthrenequinone (PQ) result in the activation of at least one of four stress-responsive kinases (PKR) and to the induction of Integrated Stress Response Pathway (ISR, outlined in red). Our findings suggest that FMRP has an essential role downstream to PKR phosphorylation (outline in blue).

Chapter- IV: This chapter deals with the alternatively possible mechanisms, which may explain the FMRP phenotype in the lung. First of all, we tried to probe the FMRP and Superoxide dismutase 1 (SOD) interaction in lung in order to understand the role of FMRP dependent SOD1 translation in the susceptibility of FMRP deficient cells. SOD1 is one of the most important enzyme, which regulates the redox balance in lung. SOD1 converts free oxygen radicals in to oxygen molecule and hydrogen peroxide and further degrades hydrogen peroxide to water and hydrogen molecule. Severe lung phenotypes and pathological conditions are associated with mutation of SOD1 gene or loss of function of the protein. A study in mouse brain by Bechara et al, showed FMRP binds with SOD1 mRNA and facilitates its translation. In absence of FMRP there is decreased SOD1 expression in mouse brain.

In light of this study, we tried to probe the role of FMRP in regulating SOD1 expression in lung. Though we could recapitulate the deficiency of SOD1 in mouse brain, but could not detect any significant difference of SOD1 expression in the lung of FMRP deficient mice. This data primarily suggested that SOD1 translation is not dependent on FMRP in mouse lung. But further study during naphthalene insult revealed a possible injury dependent role of FMRP in the upregulation of SOD1 post injury. Studies in mouse cell line with naphthalene and 9, 10 PQ suggests that post injury SOD1 upregulation could be fully or partially dependent on FMRP according to the type of stressors or stress level. But, studies in BEAS2B cell line showed that post injury SOD1 upregulation is not dependent on FMRP in this human bronchial cell line. Altogether the data allow us to conclude that FMRP may regulate post injury SOD1 expression ina context specific way and may not explain the phenotype of FMRP in lung.

Next, we tried to probe the role of FMRP in stress granule biogenesis under the experimental condition. When we treated the cells with arsenite, we observed FMRP and Tia1 are forming large granular structures and mostly they are overlapping with each other. In absence of FMRP these granules were largely absent. Though when we treated the cells with Nap/PQ we did not observe such conspicuous granule formation. We found that maximum percentage of intensity is coming from the diffused staining of FMRP and Tia1 in the control cells (Sc treated) and in absence of FMRP the overall intensity of Tia1 is less compared to control. These results suggest that there may not be any stress granule formation under the experimental condition, even in the presence of FMRP. So, FMRP dependent stress granule biogenesis cannot sufficiently explain the phenotype in the lung.

Next, we logically concluded that FMRP dependent activation of DNA damage response during replication stress cannot explain the phenotype in the lung. FMRP was found to be involved in γ-H2AX mediated activation of DNA damage response during replication stress (Alpatov et al, 2014). It was also reported that in absence of FMRP γ-H2AX foci formation was reduced. Though the report also said that γ-H2AX foci formation may not depend on FMRP in case of certain stressors like γ-irradiation. Under our experimental condition it was

found that γ-H2AX foci formation was not perturbed, in fact increased in the absence of FMRP. This section also dealt with the fact that lung epithelial cells and C22 cells under experimental condition should not acquire any replication stress as they were largely non-mitotic. In case of other two cell lines (BEAS2B and A549) however this argue does not apply but increased γ-H2AX foci formation in absence of FMRP clearly tells that perturbation of DNA damage response unable to explain the susceptibility of FMRP deficient pulmonary epithelial cells to xenobiotic stress.

Taken together, in this chapter it was concluded that FMRP dependent actuation of ISR can only explain the underlined mechanism of susceptibility of FMRP deficient pulmonary epithelial cells to the xenoiotic stress across species and stressor.

LIST OF PUBLICATIONS

1. Deblina Sain Basu, Rital Bhavsar, Imtiyaz Gulami, Saraswati Chavda, SaiManoz Lingamallu, Ravi Muddashetty, Chandrakanth Veeranna, Sumantra Chattarji, Rajesh Thimmulappa, Aditi Bhattacharya, Arjun Guha. FMRP protects the lung from xenobiotic stress by facilitating the Integrated Stress Response. J Cell Sci. 2022 Mar 23; DOI: 10.1242/jcs.258652c

2. Amrutha Kizhedathu, Piyush Chhajed, Lahari Yamala, Deblina Sain Basu, Tina Mukherjee, Vinothkumar Kutti Ragunath and Arjun Guha. Duox generated reactive oxygen species activate ATR/Chk1 to induce G2 arrest in Drosophila tracheoblasts. Elife, 2021 Oct 8; 10:e68636, doi: 10.7554/eLife.68636

REFERENCES

1. **Adjibade P, Grenier St-Sauveur V, Bergeman J, Huot ME, Khandjian EW, Mazroui R**. DDX3 regulates endoplasmic reticulum stress-induced ATF4 expression. Scientific reports. **2017** Oct 23;7(1):1-2.

2. **Alpatov R, Lesch BJ, Nakamoto-Kinoshita M, Blanco A, Chen S, Stützer A, Armache KJ, Simon MD, Xu C, Ali M, Murn J.** A chromatin-dependent role of the fragile X mental retardation protein FMRP in the DNA damage response. Cell. **2014** May 8;157(4):869-81.

3. **Anderson P, Kedersha N.** Stress granules: the Tao of RNA triage. Trends in biochemical sciences. **2008** Mar 1;33(3):141-50.

4. **Anderson P. KedershaN.(2006)**. RNA Granules. J. Cell Biol.;172:803-8.

5. **Bakker CE, Verheij C, Willemsen R, van der Helm R, Oerlemans F, Vermey M, Bygrave A, Hoogeveen A, Oostra BA, Reyniers E, De Boule K.** Fmr1 knockout mice: a model to study fragile X mental retardation. Cell. **1994** Jul 15;78(1):23-33.

6. **Bardoni B, Schenck A, Mandel JL.** The Fragile X mental retardation protein. Brain research bulletin. **2001** Nov 1;56(3-4):375-82.

7. **Bechara EG, Didiot MC, Melko M, Davidovic L, Bensaid M, Martin P, Castets M, Pognonec P, Khandjian EW, Moine H, Bardoni B.** A novel function for fragile X mental retardation protein in translational activation. PLoS Biol. **2009** Jan 20;7(1):e1000016.

8. **Blackwell E, Ceman S.** A new regulatory function of the region proximal to the RGG box in the fragile X mental retardation protein. Journal of cell science. **2011** Sep 15;124(18):3060-5.

9. **Buckpitt A, Boland B, Isbell M, Morin D, Shultz M, Baldwin R, Chan K, Karlsson A, Lin C, Taff A, West J.** Naphthalene-induced respiratory tract toxicity: metabolic mechanisms of toxicity. Drug metabolism reviews. **2002** Jan 1;34(4):791-820.

10. **Casingal CR, Kikkawa T, Inada H, Sasaki Y, Osumi N.** Identification of FMRP target mRNAs in the developmental brain: FMRP might coordinate Ras/MAPK, Wnt/β-catenin, and mTOR signaling during corticogenesis. Molecular brain. **2020** Dec;13(1):1-3.

11. **Cheever A, Ceman S.** Phosphorylation of FMRP inhibits association with Dicer. Rna. **2009** Mar 1;15(3):362-6.

12. **Chen E, Joseph S.** Fragile X mental retardation protein: a paradigm for translational control by RNA-binding proteins. Biochimie. **2015** Jul 1;114:147-54.

13. **Constantino L, Gonçalves RC, Giombelli VR, Tomasi CD, Vuolo F, Kist LW, de Oliveira GM, de Bittencourt Pasquali MA, Bogo MR, Mauad T, Horn A.** Regulation of lung oxidative damage by endogenous superoxide dismutase in sepsis. Intensive care medicine experimental. **2014** Dec;2(1):1-1.

14. **Dahlhaus R.** Of men and mice: modeling the fragile X syndrome. Frontiers in Molecular Neuroscience. **2018** Mar 15;11:41.

15. **Darnell JC, Mostovetsky O, Darnell RB.** FMRP RNA targets: identification and validation. Genes, Brain and Behavior. **2005** Aug;4(6):341-9.

16. **Davis JK, Broadie K.** Multifarious functions of the fragile X mental retardation protein. Trends in Genetics. **2017** Oct 1;33(10):703-14.

17. **de Diego-Otero Y, Romero-Zerbo Y, el Bekay R, Decara J, Sanchez L, Rodriguez-de Fonseca F, del Arco-Herrera I**. α-tocopherol protects against oxidative stress in the fragile X knockout mouse: an experimental therapeutic approach for the Fmr1 deficiency. Neuropsychopharmacology. **2009** Mar;34(4):1011-26.

18. **Debrey SM, Leehey MA, Klepitskaya O, Filley CM, Shah RC, Kluger B, Berry-Kravis E, Spector E, Tassone F, Hall DA.** Clinical phenotype of adult fragile X gray zone allele carriers: a case series. The Cerebellum. **2016** Oct;15(5):623-31

19. **Demello DE, Mahmoud S, Ryerse J, Hoffmann JW.** Generation and characterization of a conditionally immortalized lung clara cell line from the H-2K b-tsA58 transgenic mouse. In Vitro Cellular & Developmental Biology-Animal. **2002** Mar 1;38(3):154-64.

20. **Deng PY, Rotman Z, Blundon JA, Cho Y, Cui J, Cavalli V, Zakharenko SS, Klyachko VA.** FMRP regulates neurotransmitter release and synaptic information transmission by modulating action potential duration via BK channels. Neuron. **2013** Feb 20;77(4):696-711.

21. **Devys D, Lutz Y, Rouyer N, Bellocq JP, Mandel JL.** The FMR–1 protein is cytoplasmic, most abundant in neurons and appears normal in carriers of a fragile X premutation. Nature genetics. **1993** Aug;4(4):335-40.

22. **Diao C, Chen Z, Qiu T, Liu H, Yang Y, Liu X, Wu J, Wang L.** Inhibition of PRMT5 attenuates oxidative stress-induced pyroptosis via activation of the Nrf2/HO-1 signal pathway in a mouse model of renal ischemia-reperfusion injury. Oxidative Medicine and Cellular Longevity. **2019** Oct;2019.

23. **Didiot MC, Subramanian M, Flatter E, Mandel JL, Moine H.** Cells lacking the fragile X mental retardation protein (FMRP) have normal RISC activity but exhibit altered stress granule assembly. Molecular biology of the cell. **2009** Jan 1;20(1):428-37.

24. **El Bekay R, Romero-Zerbo Y, Decara J, Sanchez-Salido L, Del Arco-Herrera I, Rodríguez-de Fonseca F, De Diego-Otero Y.** Enhanced markers of oxidative stress, altered antioxidants and NADPH-oxidase activation in brains from Fragile X mental retardation 1-deficient mice, a pathological model for Fragile X syndrome. European Journal of Neuroscience. **2007** Dec;26(11):3169-80.

25. **Fähling M, Mrowka R, Steege A, Kirschner KM, Benko E, Förstera B, Persson PB, Thiele BJ, Meier JC, Scholz H.** Translational regulation of the human achaete-scute homologue-1 by fragile X mental retardation protein. Journal of Biological Chemistry. **2009** Feb 13;284(7):4255-66.

26. **Feng Y, Absher D, Eberhart DE, Brown V, Malter HE, Warren ST.** FMRP associates with polyribosomes as an mRNP, and the I304N mutation of severe fragile X syndrome abolishes this association. Molecular cell. **1997** Dec 1;1(1):109-18.

27. **Fernández-Blanco Á, Dierssen M.** Rethinking intellectual disability from neuro-to astro-pathology. International Journal of Molecular Sciences. **2020** Jan;21(23):9039.

28. Fu, Y. H., Kuhl, D. P., Pizzuti, A., Pieretti, M., Sutcliffe, J. S., Richards, S., ... & Caskey, C. T. (**1991**). Variation of the CGG repeat at the fragile X site results in genetic instability: resolution of the Sherman paradox. Cell, 67(6), 1047-1058.

29. **Gilks N, Kedersha N, Ayodele M, Shen L, Stoecklin G, Dember LM, Anderson P.** Stress granule assembly is mediated by prion-like aggregation of TIA-1. Molecular biology of the cell. **2004** Dec;15(12):5383-98.

30. **Gong C, Yang H, Wang S, Liu J, Li Z, Hu Y, Chen Y, Huang Y, Luo Q, Wu Y, Liu E.** hTERT Promotes CRC Proliferation and Migration by Recruiting YBX1 to Increase NRF2 Expression. Frontiers in cell and developmental biology. **2021** May 17;9:1136.

31. **Guha A, Vasconcelos M, Cai Y, Yoneda M, Hinds A, Qian J, Li G, Dickel L, Johnson JE, Kimura S, Guo J.** Neuroepithelial body microenvironment is a niche for a distinct subset of Clara-like precursors in the developing airways. Proceedings of the National Academy of Sciences. **2012** Jul 31;109(31):12592-7.

32. **Guha A, Vasconcelos M, Zhao R, Gower AC, Rajagopal J, Cardoso WV.** Analysis of Notch signaling-dependent gene expression in developing airways reveals diversity of Clara cells. PLoS One. **2014** Feb 21;9(2):e88848.

33. **Hatch EM, Kulukian A, Holland AJ, Cleveland DW, Stearns T.** Cep152 interacts with Plk4 and is required for centriole duplication. Journal of Cell Biology. **2010** Nov 15;191(4):721-9.

34. **He CH, Gong P, Hu B, Stewart D, Choi ME, Choi AM, Alam J.** Identification of activating transcription factor 4 (ATF4) as an Nrf2-interacting protein: implication for heme oxygenase-1 gene regulation. Journal of biological chemistry. **2001** Jun 15;276(24):20858-65.

35. **Hernandez K, Lau KJ, Ba M, Singer CA.** C108 GETTING INFLAMED: MARKERS OF LUNG INJURY AND REMODELLING: Microrna-25 And-188 Target Myosin-5a To Attenuate Mucin Hypersecretion In Asthma. American Journal of Respiratory and Critical Care Medicine. **2017**;195.

36. Hu Y, Chen Z, Fu Y, He Q, Jiang L, Zheng J, Gao Y, Mei P, Chen Z, Ren X. The amino-terminal structure of human fragile X mental retardation protein obtained using precipitant-immobilized imprinted polymers. Nature communications. **2015** Mar 23;6(1):1-1.

37. **Kim M, Ceman S.** Fragile X mental retardation protein: past, present and future. Current Protein and Peptide Science. **2012** Jun 1;13(4):358-71.

38. **Koike E, Yanagisawa R, Takano H.** Toxicological effects of polycyclic aromatic hydrocarbons and their derivatives on respiratory cells. Atmospheric environment. **2014** Nov 1;97:529-36.

39. **Konsavage WM, Zhang L, Wu Y, Shenberger JS.** Hyperoxia-induced activation of the integrated stress response in the newborn rat lung. American Journal of Physiology-Lung Cellular and Molecular Physiology. **2012** Jan 1;302(1):L27-35.

40. **Krawczun MS, Jenkins EC, Brown WT.** Analysis of the fragile-X chromosome: localization and detection of the fragile site in high resolution preparations. Human genetics. **1985** Mar 1;69(3):209-11.

41. **Lavrich KS, Corteselli EM, Wages PA, Bromberg PA, Simmons SO, Gibbs-Flournoy EA, Samet JM**. Investigating mitochondrial dysfunction in human lung cells exposed to redox-active PM components. Toxicology and applied pharmacology. **2018** Mar 1;342:99-107.

42. **Lee FH, Lai TK, Su P, Liu F.** Altered cortical Cytoarchitecture in the Fmr1 knockout mouse. Molecular brain. **2019** Dec;12(1):1-2.

43. **Li G, Scull C, Ozcan L, Tabas I.** NADPH oxidase links endoplasmic reticulum stress, oxidative stress, and PKR activation to induce apoptosis. Journal of Cell Biology. **2010** Dec 13;191(6):1113-25.

44. **Li ZM, Xue CJ, Wang JH, Wang QM.** Comparative study of the characteristics of typical mineral deposits in Xinjiang, China, and its neighboring countries and regions. Geology in China. **2006**;33(1):160-8.

45. **Lima-Cabello E, Garcia-Guirado F, Calvo-Medina R, el Bekay R, Perez-Costillas L, Quintero-Navarro C, Sanchez-Salido L, de Diego-Otero Y.** An abnormal nitric oxide metabolism contributes to brain oxidative stress in the mouse model for the fragile X syndrome, a possible role in intellectual disability. Oxidative medicine and cellular longevity. **2016** Oct;2016.

46. **Linder B, Plöttner O, Kroiss M, Hartmann E, Laggerbauer B, Meister G, Keidel E, Fischer U.** Tdrd3 is a novel stress granule-associated protein interacting with the Fragile-X syndrome protein FMRP. Human molecular genetics. **2008** Oct 15;17(20):3236-46.

47. **Lozon TI, Eastman AJ, Matute-Bello G, Chen P, Hallstrand TS, Altemeier WA.** PKR-dependent CHOP induction limits hyperoxia-induced lung injury. American Journal of Physiology-Lung Cellular and Molecular Physiology. **2011** Mar 1.

48. Lubs HA. A marker X chromosome. American journal of human genetics. **1969** May;21(3):231.

49. **Luo X, Kraus WL.** On PAR with PARP: cellular stress signaling through poly (ADP-ribose) and PARP-1. Genes & development. **2012** Mar 1;26(5):417-32.

50. **Mateu-Regue A, Christiansen J, Bagger FO, Winther O, Hellriegel C, Nielsen FC**. Single mRNP analysis reveals that small cytoplasmic mRNP granules represent mRNA singletons. Cell reports. **2019** Oct 15;29(3):736-48.

51. **Matsunaga T, Arakaki M, Kamiya T, Endo S, El-Kabbani O, Hara A.** Involvement of an aldo-keto reductase (AKR1C3) in redox cycling of 9, 10-phenanthrenequinone leading to apoptosis in human endothelial cells. Chemico-biological interactions. **2009** Sep 14;181(1):52-60.

52. **Movaghar A, Page D, Brilliant M, Baker MW, Greenberg J, Hong J, DaWalt LS, Saha K, Kuusisto F, Stewart R, Berry-Kravis E.** Data-driven phenotype discovery of FMR1 premutation carriers in a population-based sample. Science advances. **2019** Aug 21;5(8):eaaw7195.

53. **Myrick LK, Hashimoto H, Cheng X, Warren ST.** Human FMRP contains an integral tandem Agenet (Tudor) and KH motif in the amino terminal domain. Human molecular genetics. **2015** Mar 15;24(6):1733-40.

54. **Nabih HK.** Crosstalk between NRF2 and Dicer through metastasis regulating MicroRNAs; mir-34a, mir-200 family and mir-103/107 family. Archives of Biochemistry and Biophysics. **2020** Jun 15;686:108326.

55. **Noguchi E, Yokouchi Y, Zhang J, Shibuya K, Shibuya A, Bannai M, Tokunaga K, Doi H, Tamari M, Shimizu M, Shirakawa T.** Positional identification of an asthma susceptibility gene on human chromosome 5q33. American journal of respiratory and critical care medicine. **2005** Jul 15;172(2):183-8.

56. **Obeidat ME, Hall IP**. Genetics of complex respiratory diseases: implications for pathophysiology and pharmacology studies. British journal of pharmacology. **2011** May;163(1):96-105.

57. **Pasciuto E, Bagni C. SnapShot:** FMRP interacting proteins. Cell. **2014** Sep 25;159(1):218-.

58. **Peng T, Frank DB, Kadzik RS, Morley MP, Rathi KS, Wang T, Zhou S, Cheng L, Lu MM, Morrisey EE**. Hedgehog actively maintains adult lung quiescence and regulates repair and regeneration. Nature. **2015** Oct;526(7574):578-82.

59. **Piazzon N, Rage F, Schlotter F, Moine H, Branlant C, Massenet S.** In vitro and in cellulo evidences for association of the survival of motor neuron complex with the fragile X mental retardation protein. Journal of Biological Chemistry. **2008** Feb 29;283(9):5598-610.

60. **Pietrzak J, Spickett CM, Płoszaj T, Virág L, Robaszkiewicz A.** PARP1 promoter links cell cycle progression with adaptation to oxidative environment. Redox biology. **2018** Sep 1;18:1-5.

61. **Prieto M, Folci A, Martin S.** Post-translational modifications of the Fragile X Mental Retardation Protein in neuronal function and dysfunction. Molecular psychiatry. **2020** Aug;25(8):1688-703.

62. **Protic D, Salcedo-Arellano MJ, Dy JB, Potter LA, Hagerman RJ.** New targeted treatments for fragile X syndrome. Current pediatric reviews. **2019** Nov 1;15(4):251-8.

63. **Protter DS, Parker R.** Principles and properties of stress granules. Trends in cell biology. **2016** Sep 1;26(9):668-79.

64. **Ramos A, Hollingworth D, Adinolfi S, Castets M, Kelly G, Frenkiel TA, Bardoni B, Pastore A.** The structure of the N-terminal domain of the fragile X mental retardation protein: a platform for protein-protein interaction. Structure. **2006** Jan 1;14(1):21-31.

65. **Reineke LC, Cheema SA, Dubrulle J, Neilson JR.** Chronic starvation induces noncanonical pro-death stress granules. Journal of cell science. **2018** Oct 1;131(19):jcs220244.

66. **Reineke LC, Kedersha N, Langereis MA, van Kuppeveld FJ, Lloyd RE.** Stress granules regulate double-stranded RNA-dependent protein kinase activation through a complex containing G3BP1 and Caprin1. MBio. **2015** Mar 17;6(2):e02486-14.

67. **Richter JD, Zhao X.** The molecular biology of FMRP: new insights into fragile X syndrome. Nature Reviews Neuroscience. **2021** Feb 19:1-4.

68. **Romero-Zerbo Y, Decara J, El Bekay R, Sanchez-Salido L, Del Arco-Herrera I, De Fonseca FR, De Diego-Otero Y.** Protective effects of melatonin against oxidative stress in Fmr1 knockout mice: a therapeutic research model for the fragile X syndrome. Journal of pineal research. **2009** Mar;46(2):224-34.

69. **Santoro MR, Bray SM, Warren ST.** Molecular mechanisms of fragile X syndrome: a twenty-year perspective. Annual Review of Pathology: Mechanisms of Disease. **2012** Feb 28;7:219-45.

70. **Sarcinelli C, Dragic H, Piecyk M, Barbet V, Duret C, Barthelaix A, Ferraro-Peyret C, Fauvre J, Renno T, Chaveroux C, Manié SN.** ATF4-Dependent NRF2 transcriptional regulation promotes antioxidant protection during endoplasmic reticulum stress. Cancers. **2020** Mar;12(3):569.

71. **Sharma A, Hoeffer CA, Takayasu Y, Miyawaki T, McBride SM, Klann E, Zukin RS.** Dysregulation of mTOR signaling in fragile X syndrome. Journal of Neuroscience. **2010** Jan 13;30(2):694-702.

72. **Sherman, S. L., Morton, N. E., Jacobs, P. A., & Turner, G. (1984).** The marker (X) syndrome: a cytogenetic and genetic analysis. Annals of human genetics, 48(1), 21-37.

73. Shih JW, Wang WT, Tsai TY, Kuo CY, Li HK, Wu Lee YH. Critical roles of RNA helicase DDX3 and its interactions with eIF4E/PABP1 in stress granule assembly and stress response. Biochemical Journal. **2012** Jan 1;441(1):119-29**.**

74. **Siedlinski M, van Diemen CC, Postma DS, Vonk JM, Boezen HM.** Superoxide dismutases, lung function and bronchial responsiveness in a general population. European Respiratory Journal. **2009** May 1;33(5):986-92.

75. **Singh A, Ling G, Suhasini AN, Zhang P, Yamamoto M, Navas-Acien A, Cosgrove G, Tuder RM, Kensler TW, Watson WH, Biswal S.** Nrf2-dependent sulfiredoxin-1 expression protects against cigarette smoke-induced oxidative stress in lungs. Free Radical Biology and Medicine. **2009** Feb 1;46(3):376-86.

76. S**olomon S, Xu Y, Wang B, David M, Schubert P, Kennedy D, Schrader JW.** Distinct structural features of Caprin-1 mediate its interaction with G3BP-1 and its induction of phosphorylation of eIF2α, entry to cytoplasmic stress granules, and selective interaction with a subset of mRNAs. Molecular and Cellular Biology. **2007** Jan 8.

77. **Song G, Napoli E, Wong S, Hagerman R, Liu S, Tassone F, Giulivi C.** Altered redox mitochondrial biology in the neurodegenerative disorder fragile X-tremor/ataxia syndrome: use of antioxidants in precision medicine. Molecular Medicine. **2016** Jan;22(1):548-59.

78. **Specchia V, Puricella A, D'Attis S, Massari S, Giangrande A, Bozzetti MP.** Drosophila melanogaster as a model to study the multiple phenotypes, related to genome stability of the fragile-X syndrome. Frontiers in genetics. **2019** Feb 13;10:10.

79. **Stoica L, Keeler AM, Xiong L, Kalfopoulos M, Desrochers K, Brown Jr RH, Sena-Esteves M, Flotte TR, ElMallah MK.** Restrictive lung disease in the Cu/Zn superoxide-dismutase 1 G93A amyotrophic lateral sclerosis mouse model. American journal of respiratory cell and molecular biology. **2017** Mar;56(3):405-8.

80. **Stripp BR, Maxson KA, Mera RA, Singh G.** Plasticity of airway cell proliferation and gene expression after acute naphthalene injury. American Journal of Physiology-Lung Cellular and Molecular Physiology. **1995** Dec 1;269(6):L791-9.

81. **Sutherland GR.** Heritable fragile sites on human chromosomes I. Factors affecting expression in lymphocyte culture. American journal of human genetics. **1979** Mar;31(2):125.

82. **Taha MS, Haghighi F, Stefanski A, Nakhaei-Rad S, Kazemein Jasemi NS, Al Kabbani MA, Görg B, Fujii M, Lang PA, Häussinger D, Piekorz RP.** Novel FMRP interaction networks linked to cellular stress. The FEBS journal. **2021** Feb;288(3):837-60.

83. **Tang S, Qin F, Wang X, Liang Z, Cai H, Mo L, Huang Y, Liang B, Wei X, Ao Q, Xu Y.** H2O2 induces PP2A demethylation to downregulate mTORC1 signaling in HEK293 cells. Cell Biology International. **2018** Sep;42(9):1182-91.

84. **Tankersley CG, Haenggeli C, Rothstein JD.** Respiratory impairment in a mouse model of amyotrophic lateral sclerosis. Journal of applied physiology. **2007** Mar;102(3):926-32.

85. **Valverde R, Edwards L, Regan L.** Structure and function of KH domains. The FEBS journal. **2008** Jun;275(11):2712-26.

86. **Valverde R, Pozdnyakova I, Kajander T, Venkatraman J, Regan L.** Fragile X mental retardation syndrome: structure of the KH1-KH2 domains of fragile X mental retardation protein. Structure. **2007** Sep 11;15(9):1090-8.

87. **Van Winkle LS. Buckpitt AR, Nishio SJ, Isaac JM, Plopper CG.** Cellular response in naphthalene-induced Clara cell injury and bronchiolar epithelial repair in mice. Am J Physiol Lung Cell Mol Physiol. **1995**;269:L800-18.

88. **van't Wout EF, Hiemstra PS, Marciniak SJ.** The integrated stress response in lung disease. American journal of respiratory cell and molecular biology. **2014** Jun;50(6):1005-9.

89. **Vasic V, Jones MS, Haslinger D, Knaus LS, Schmeisser MJ, Novarino G, Chiocchetti AG.** Translating the Role of mTOR-and RAS-Associated Signalopathies in Autism Spectrum Disorder: Models, Mechanisms and Treatment. Genes. **2021** Nov;12(11):1746.

90. **Vasilyev N, Polonskaia A, Darnell JC, Darnell RB, Patel DJ, Serganov A.** Crystal structure reveals specific recognition of a G-quadruplex RNA by a β-turn in the RGG motif of FMRP. Proceedings of the National Academy of Sciences. **2015** Sep 29;112(39):E5391-400.

91. **Verkerk AJ, Pieretti M, Sutcliffe JS, Fu YH, Kuhl DP, Pizzuti A, Reiner O, Richards S, Victoria MF, Zhang F, Eussen BE.** Identification of a gene (FMR-1) containing a CGG repeat coincident with a breakpoint cluster region exhibiting length variation in fragile X syndrome. Cell. **1991** May 31;65(5):905-14.

92. **Virág L.** Poly (ADP-ribosyl) ation in asthma and other lung diseases. Pharmacological research. **2005** Jul 1;52(1):83-92.

93. **Wallace AM, Hardigan AA, Gaffney A, Mirochnitchenko O, Thankachen J, Poon K, Arellanos L, Salim S, Thompson V, D'Armiento JM, Foronjy R.** Redox Regulation Of Protein Phosphatase 2A (PP2A) Phosphorylation Prevents Smoke-Induced Lung Injury. InD97. EMERGING OXIDATIVE STRESS-RELATED MECHANISMS IN INJURY AND REPAIR **2011** May (pp. A6142-A6142). American Thoracic Society.

94. **Wang Z, Sun W, Cao J, Cui H, Ma Z.** Repeated Aurora-A siRNA Transfection Results in Effective Apoptosis of A549 Cells Compared to Single Transfection. Clinical laboratory. **2016** Jan 1;62(4):697-703.

95. **Wheeler AC, Bailey Jr DB, Berry-Kravis E, Greenberg J, Losh M, Mailick M, Milà M, Olichney JM, Rodriguez-Revenga L, Sherman S, Smith L.** Associated features in females with an FMR1 premutation. Journal of neurodevelopmental disorders. **2014** Dec;6(1):1-4.

96. **White B, Schmidt M, Murphy C, Livingstone W, O'toole D, Lawler M, O'Neill L, Kelleher D, Schwarz HP, Smith OP.** Activated protein C inhibits

lipopolysaccharide-induced nuclear translocation of nuclear factor κB (NF-κB) and tumour necrosis factor α (TNF-α) production in the THP-1 monocytic cell line. British journal of haematology. **2000** Jul;110(1):130-4.

97. **Wong HR, Wispe JR.** The stress response and the lung. American Journal of Physiology-Lung Cellular and Molecular Physiology. **1997** Jul 1;273(1):L1-9.

98. **Wu Y, Zhu J, Huang X, Du Z.** Crystal structure of a dimerization domain of human Caprin-1: insights into the assembly of an evolutionarily conserved ribonucleoprotein complex consisting of Caprin-1, FMRP and G3BP1. Acta Crystallographica Section D: Structural Biology. **2016** Jun 1;72(6):718-27.

99. **Xu J, Ji L, Liang Y, Wan Z, Zheng W, Song X, Gorshkov K, Sun Q, Lin H, Zheng X, Chen J.** CircRNA-SORE mediates sorafenib resistance in hepatocellular carcinoma by stabilizing YBX1. Signal transduction and targeted therapy. **2020** Dec 26;5(1):1-4.

100. **Yang M, Ahmed H, Wu W, Jiang B, Jia Z.** Cytotoxicity of air pollutant 9, 10-Phenanthrenequinone: role of reactive oxygen species and redox signaling. BioMed research international. **2018** Jun 10;2018.

101. **Yao M, Wang X, Tang Y, Zhang W, Cui B, Liu Q, Xing L.** Dicer mediating the expression of miR-143 and miR-155 regulates hexokinase II associated cellular response to hypoxia. American Journal of Physiology-Lung Cellular and Molecular Physiology. **2014** Dec 1;307(11):L829-37.

102. **Younus H.** Therapeutic potentials of superoxide dismutase. International journal of health sciences. **2018** May;12(3):88.

103. **Zalfa F, Bagni C.** Molecular insights into mental retardation: multiple functions for the Fragile X mental retardation protein?. Current issues in molecular biology. **2004**;6(2):73-88.

104. **Zelko IN, Mariani TJ, Folz RJ.** Superoxide dismutase multigene family: a comparison of the CuZn-SOD (SOD1), Mn-SOD (SOD2), and EC- SOD (SOD3) gene structures, evolution, and expression. Free Radical Biology and Medicine. **2002** Aug 1;33(3):337-49.

105. **Zhang P, Abdelmohsen K, Liu Y, Tominaga-Yamanaka K, Yoon JH, Ioannis G, Martindale JL, Zhang Y, Becker KG, Yang IH, Gorospe M.** Novel RNA-and FMRP-binding protein TRF2-S regulates axonal mRNA transport and presynaptic plasticity. Nature communications. **2015** Nov 20;6(1):1-5.

106. **Zhou Z, Cao M, Guo Y, Zhao L, Wang J, Jia X, Li J, Wang C, Gabriel G, Xue Q, Yi Y.** Fragile X mental retardation protein stimulates ribonucleoprotein assembly of influenza A virus. Nature communications. **2014** Feb 10;5(1):1-2.

Chapter 1

Introduction

1.1 Lung injury repair

The Lung is an internal organ which deals with the exchange of oxygen and carbon dioxide. The epithelium of lung is mainly divided into two compartments, bronchial epithelium or the lining of airways, and the alveolar epithelium, the lining of alveolar sacs. Bronchial compartment takes a major role in transport of gases in and out of the lung, whereas alveolar epithelium is the main site forthe gaseous exchange.

Both the compartments of pulmonary epithelium are readily exposed to airborne pollutants on a daily basis during gas exchange. Some man-made pollutants or xenobiotic substances damage cell health directly and some are metabolically processed inside the epithelial cells and generate reactive oxygen species (ROS) and other toxic byproducts that, in turn, damage cell health. In both cases, the xenobiotic substances affect cell heath by generating cellular stress and activate stress response pathways, anti-oxidant expression, and inflammatory responses in the pulmonary epithelium. A defective stress response system or altered antioxidant expression can be associated with poor lung health or diseases.

A deeper understanding of the stress response pathways in the lung epithelial cells will reveal mechanisms that restore lung health post exposure to environmental toxicants. This knowledge can augment efforts to promote lung health or identify genetic susceptibilities to lung disease. More precisely a gene responsible for activation of a major stress response pathway may be found to protect the lung from xenobiotic stress. So, in order to understand the mechanism of stress response in the lung, we initiated this investigation.

1.2 Expression of Fragile X mental retardation protein in the lung

Fragile X mental retardation protein (FMRP) is an RNA binding protein having multiple roles. Till now, researchers studying the function of FMRP have primarily focused on the brain and neurons. However, studies in humans and mice have indicated that there is very little tissue specificity in FMRP expression. Along with tissues like thyroid, heart, liver, stomach, kidney and

gonadal tissues, pulmonary epithelium also expresses FMRP in humans. According to the Human Protein Atlas, there is high expression of FMRP in nasopharynx, alveolar cells and alveolar macrophages, and a medium expression in bronchial epithelium (https://www.proteinatlas.org/ENSG00000102081-FMR1/tissue). In support of this, our preliminary data in human and murine lungs also showed abundant expression of FMRP (See chapter III).

Some recent reports suggest that FMRP actively participates in different pathways to mitigate stress (Kim et al, 2006; Didiot MC et al, 2008; Linder B et al, 2008; Bechara et al, 2009; Alpatov et al, 2014). This made us curious to know the role of FMRP in stress responses in the lung.

1.3 Brief history of Fragile X mental retardation protein and the model systems used in research

1.3.1 Fragile X syndrome as a heritable form of intellectual disability

Fragile X syndrome (FXS) is a common form of inherited intellectual disability (ID) in humans. Most of the affected individuals possess one or more phenotypes like developmental delay, cognitive disorder, Autism Spectrum Disorder (ASD), speech disorder. FXS is caused due to the mutation of a gene called Fragile X Mental Retardation 1 (FMR1), located on the X chromosome. This inherited form of ID is observed in about 1 in 4000 to 5000 males and in about 1 in 8000 females (Zalfa F et al, 2004; Protic D et al, 2019). FXS follows a X-linked recessive pattern of inheritance. As a result, males having one X chromosome, have higher chances of developing FXS if they get a mutated X chromosome from their parents. Whereas a female having two X chromosomes, will remain unaffected even if one of the X chromosomes is mutated. The unaffected female can, however, transmit the mutation to the next generation.

1.3.2 Preliminary reports on heritable form of ID leading to the discovery of Fragile X mental retardation gene

In 1943, James Purdon Martin and Julia Bell first reported a form of X-linked inherited ID. Hence, this disorder is also known as Martin-Bell syndrome. In 1969, H.A. Lubs reported a peculiarity of the X- chromosome that was linked to heritable ID. According to his report on a study carried out on a family, four affected males from three consecutive generations, and two unaffected females from the second generation were found to have X-chromosomes with satellites (Lubs HA, 1969). A satellite is a feature of a chromosome, where a small portion of the chromosome is connected to the main arm by a constriction. Generally, satellites on chromosomes are visible during the metaphase, when the chromosomes are condensed. The constrictions make the chromosomes fragile, and hence are often known as “fragile sites”. Lubs’s report predicted that the cause of the mental retardation was a recessive mutation in a gene that was probably located near the site of constriction on the long arm of the X-chromosome (Fig 1.1). Later on, Sutherland found many other fragile sites on chromosomes along with the one at Xq27 or Xq28, which could be heritable (Sutherland GR, 1979). These discoveries revealed that a fragile site is located near a gene on X chromosome long arm that is linked to a form of heritable intellectual disability. In 1985, Krawczun et al. confirmed that the fragile site on the X-chromosome that was linked with the heritable ID was located at Xq27.3 (Krawczun MS et al, 1985).

1.3.3 Sherman paradox, indicating complexity in the nature of hereditary transmission of the Fragile X gene mutation

In 1983, Jacobs and Turner described the clinical features of this X-linked mental retardation. A year later, in 1984, the same group of researchers explained the complexity of its inheritance pattern. Stephanie L. Sherman observed that the frequency of this fragile X syndrome increases with each passing generation (Sherman et al, 1983). She also reported that clinically asymptomatic males could pass the disease to their daughters. To explain this phenotype, she proposed a hypothesis that the gene

responsible for the heritable ID has two steps of mutation. An intermediate asymptomatic phase or “premutation” could be carried forward with higher chances of acquiring “full mutation” or diseased condition in successive generation. This observation changed the understanding about X-linked inheritance. A X-linked recessive gene mutation cannot be transferred to the next generation by an asymptomatic male in general. But in this case, an asymptomatic father can transfer a premutation containing X-chromosometo the daughter. The X-chromosome may acquire full mutation in this generation and carried forward to the next generation, where manifestation of syndrome may occur (especially in males). This pattern of X-linked inheritance became famous as the “Sherman paradox” later on.

Finally, in 1991, Fragile X Mental Retardation 1 (FMR1) gene was cloned by Verkerk et al. It was found that FMR1 gene, located at Xq27.3 contains a CGG repeat sequence at the 5’ untranslated region (5’UTR) of the gene, just before the start codon. When the number of these repeats exceeded 200, the promoter of the gene became hyper-methylated and inactivated, causing inability to produce the protein product. This condition was found to directly correlate to FXS.

In the same year, Sherman paradox was also explained by Ying-Hui-Fu et al. They introduced a new term called “premutation” (Fu et al, 1991).The fragile X site usually contains up to 55 CGG repeats, which can increase to 200 or above. When the repeat number exceeds 200, the gene is hyper methylated and loses translational activity. As a result FXS related phenotypes can be observed. But, a premutation allele contains 55-200 CGG repeats at the FMR1 locus. Carriers of the premutation allele do not present any mental retardation symptoms, but can pass on the mutated allele to the next generation. Premutation alleles are unstable and may acquire more copy numbers during meiotic division to get a length of fully mutated condition (i.e. more than 200 repeats). This explains how a clinically asymptomatic father can pass a mutated allele to his daughter, and why the risk of disease manifestation increases with successive

generations.

1.3.4 Model systems used in FMRP studies

The protein structure of FMRP is conserved from Drosophila to humans (Specchia V et al, 2019). Because of this, many of the neurological aspects such as synaptic plasticity and learning behavior can be studied in Drosophila, mouse and rat. For the studies related to genetic pathways involving FMRP, Drosophila is used as a model system. For the studies of FMRP dependent brain function, usually mice and rats are used as model systems. But behavioral complexity of ASD patients cannot be recapitulated in a mouse model (Dahlhaus R, 2018). Apart from that, thereare a few more dissimilarities between mouse and human regarding FMR genetics. In mice, hyper-methylation does not occur up to 300 CGG repeats, whereas in humans more than 200 copy numbers cause gene inactivation. In the case of the mouse model, the Fmr1 gene is silenced by genetic engineering tools with a disrupted Fmr1 DNA sequence (by inserting a 5’ exon), hence the protein product is completely absent (Kazdoba et al, 2014). Human population has a different degree of gene silencing due to the variable number of CGG repeats on gene locus. As a result, protein can be lost, reduced and even present in a mosaic pattern, i.e expressed in a certain percentage of cells in an organ or tissue, in the human body. Genetic interrelations of FMR1 and other ID related genes are not necessarily similar between mice and higher primates (Dahlhaus R, 2018).

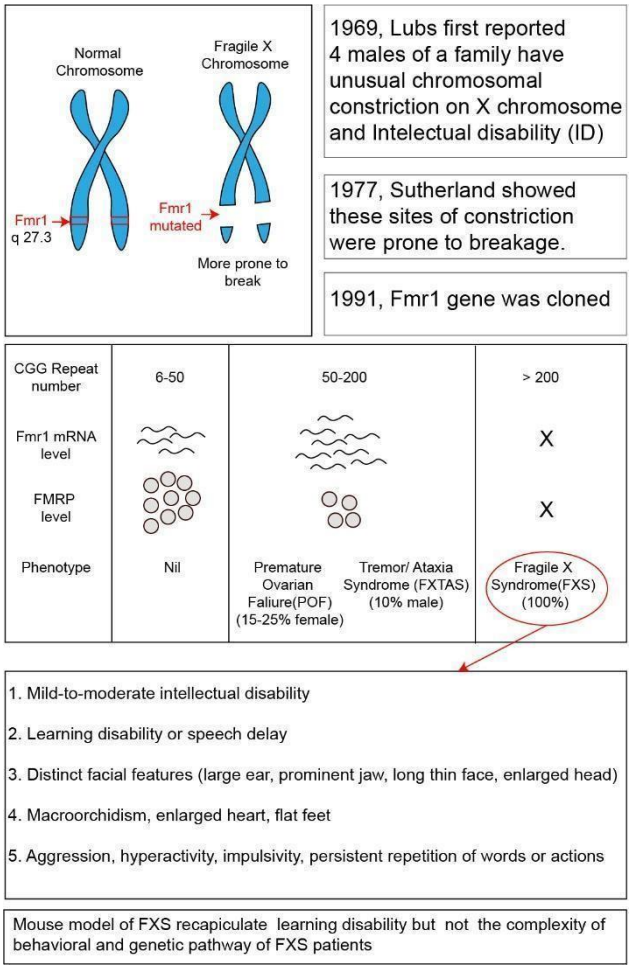

Fig 1.1: Brief history of Fmr1 gene and the role of Fmr1 mutation in Fragile X Syndrome. About twenty years of study have concluded FMR1 gene is located at Xq27.3 position and contains a CGG repeat expansion. Expansion of CGG repeat to more than 200 in numbers can cause hyper-methylation and gene inactivation, which is related to autism spectrum disorder. CGG repeat from 55 to 200 is associated with partial loss of the protein product and clinical conditions in a subset of this group.

1.4 Emerging evidence of FMRP function in cellular stress regulation

FMRP is a 71 kDa protein, which contains two agenet domains, three K-homology domains and a RGG box along with few sites for post-translational modification (PTM) like phosphorylation, methylation among others (see details in chapter 5). These RGG box, KH and agenet domains and specialized PTM sites of FMRP facilitate binding with multiple proteins, RNAs and chromatin. The large interactome of FMRP indicates its direct or indirect involvement in

cellular stress regulation (Taha et al, 2021; Didiot MC et al, 2008, Bechara et al, 2009). In the following section three such prominent studies have been discussed to elucidate the evidence of FMRP function in cellular stress regulation.

1.4.1 FMRP-SOD1 interaction in regulation of oxidative stress in brain

Along with this neuronal function of FMRP, recent studies have identified the protein to be linked with cellular stress, not only in the brain but also in the tissues and cells of other organs. Abnormal nitric oxide metabolism and high levels of ROS have been found in the brains of Fmr1 Knockout (KO) mice, causing increased oxidative stress (Bekay R et al, 2007; Cabello EL et al, 2016). This finding has been supported by Bechara *et al*, when the group reported that FMRP regulates expression of Superoxide Dismutase 1 (SOD1), a ROS quenching enzyme, in the mouse brain. According to this work, FMRP knockout mice brain tissue shows higher levels of ROS and decreased SOD1 expression compared to the wild type control (Bechara et al, 2009).

1.4.2 Association of FMRP with stress granules indicate its role in cellular stress responses in cells and tissues other than neuronal origin

Stress granules are membrane-less protein-RNA aggregates formed during cellular stress. Relations between FMRP and cellular stress became stronger with the evidence of the presence of FMRP in stress granules (Kim et al, 2006; Didiot MC et al, 2008; Linder B et al, 2008). Didiot et al showed altered stress granule assembly in the absence of FMRP or in the presence of a mutated form of FMRP (1304N mutation) in mouse fibroblast cells (MEF) and HeLa cells (Fig 1.2). According to this study, in response to oxidative stress (by arsenite treatment) or heat shock, FMRP deficient cells produce less stress granules compared to

control. They found a stronger phenotype in case of 1304N mutation, a mutation in the KH domain of FMRP.

1.4.3 Role of FMRP in actuating DNA damage response during replication stress in mouse fibroblast and spermatocyte cells

Apart from chemically induced oxidative stress, importance of FMRP has been also reported in DNA damage response during replication stress (Alpatov R et al, 2014). Alpatov et al have shown that FMRP deficient cells fail to mount γ-H2AX (phosphorylated form of histone 2A protein) mediated DNA damage response during replication stress caused by aphidicolin (APH), hydroxyurea (HU) or ultra-violate ray (UV) in a dividing cell. APH, HU or UV usually block DNA synthesis in a replicating cell and they create a single stranded DNA break. According to this report, FMRP deficient cells fail to dock γ-H2AX at the site of DNA damage, hence fail to actuate DNA damage response. They have also reported that while γ-H2AX mediated DNA damage response is affected in FMRP deficient cells in response to APH, HU or UV, it remains unaffected in response to other types of stress such as gamma irradiation (possibly a double stranded DNA break). This study has revealed a chromatin binding role of FMRP and has shown that the N-terminal agenet domain of FMRP physically interacts with chromatin and recruits γ-H2AX during meiosis in the mouse spermatocytes.

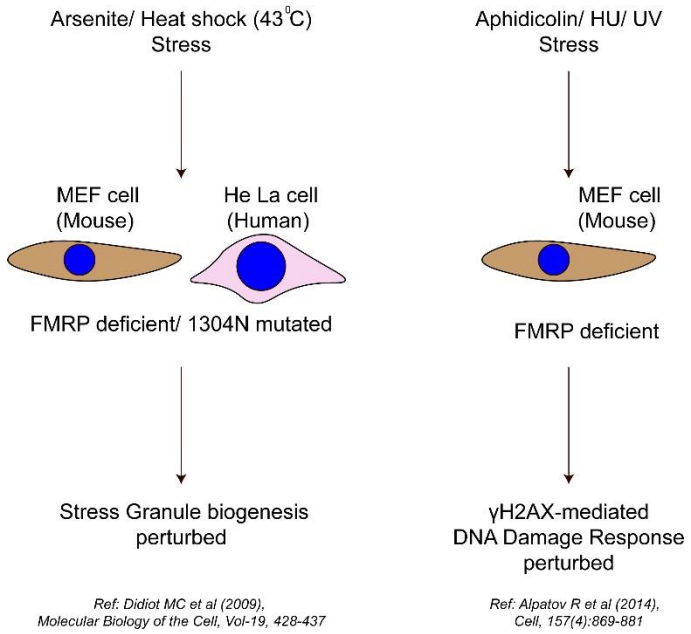

Fig 1.2: Recent studies suggest the role of FMRP in oxidative and genotoxic stresses outside the brain. Studies in mouse and human cell lines suggest FMRP could be involved in stress response pathways induced by oxidative stress, heat shock stress and replicative stress.

1.4.4 New perspective on the functionality of FMRP

These few important discoveries have opened up new opportunities and given a new perspective to look into the functionality of FMRP outside the brain. The Bechara *et al* study has shown that FMRP is not only a translational repressor, but it could be for a translational activator of the translation of some specific mRNAs. This may imply that FMRP can regulate the translation machinery in such a way that it causes repression of many genes, but allows translation of some specialized genes in the brain. The studies which have reported the association of FMRP with stress granules, and certain dependency of stress granule biogenesis on this protein, may suggest that FMRP could be linked with a general form of stress response, such as the integrated stress response or ISR. The Alpatov et al study has established the role of FMRP as a chromatin binding protein, which is required to mount a DNA damage response during replication stress. Altogether they suggest

FMRP could be involved in the cellular stress response pathways apart from its classical role in neurons.

1.5 Molecular structure of FMRP facilitates interaction with large number of nucleic acids, proteins and ribosomes

FMRP is known as an RNA binding protein, though its structural complexity provides interactions with a large number of proteins, ribosomes as well as chromatin. The N-terminal end of FMRP (1-215 amino acid residue) contains two methyl-lysine/arginine recognizing Agenet domains, Age1 stretching from amino acid 3 to amino acid 49, and Age2 stretching from amino acid 63 to amino acid 113 (Fig 1.3). A nuclear localization signal (NLS) is flanked by the amino acids of Age2 domain and a nuclear export signal (NES) is located near the C-terminal end of the protein. These two signals help FMRP shuttle between nucleus and cytoplasm.

Apart from Agenet domains, FMRP has KH domains and RGG boxes. FMRP KH domains or K-homology domain 1 and 2 contain G-X-X-G motifs between β1α1 and β2α2 protein folds (Fig 5.1). But there is one more KH domain that was recently discovered. It has an A-K-E-A motif, and is referred to as KH0 (Myrick et al, 2015). KH0 is connected to KH1 and KH2 by a nine-residue flexible loop. These KH domains generally interact with RNA or single stranded DNA (ssDNA). KH1-KH2 loop also interacts with polyribosomes (Darnell JC et al, 2005).

With the help of these specialized domains FMRP interacts with 180 proteins, hundreds of mRNAs, non-coding RNAs and some microRNAs (Taha MS et al, 2020, Fernandez E et al, 2013). 102 of these proteins interact at the C-terminal domain of FMRP, 48 interact at both ends, and 28 are found to be specific for N-terminal interaction (Taha MS et al, 2020). RNAs mostly interact through KH domains of FMRP. A point mutation of this KH2 domain, known as 1304N disrupts nucleoprotein binding and was found to facilitate ribonucleoprotein (RNP) assembly

during influenza virus infection in lung (Zhou Z et al, 2014).

FMRP contains a C-terminal arginine-glycine rich domain, called RGG box for binding G-quadruplex structures of RNAs, like SOD1 SoSLIP (Bechara et al, 2009).

In light of the discussion regarding the role of FMRP in stress response, specifically in ISR, the interactions of different proteins at different domains of FMRP become very crucial. The C-terminal domain of FMRP is known to physically interact with caprin-1 and PKR (Taha MS et al, 2020). This interaction could be very important in elucidating the role of FMRP in ISR, as caprin1 is already known to facilitate eIF2α phosphorylation along with G3BP1 (detailed discussion in section 5.2).

On the other hand, CYFIP1 interacts with FMRP at N terminal end and this interaction suggests another possibility to regulate eIF2α phosphorylation in an indirect way. CYFIP1-FMRP complex binds with eIF4E and restricts eIF4E to join the translation machinery (Clifton NE et al, 2020). That is how, CYFIP1-FMRP interaction indirectly facilitates eIF2α phosphorylation and represses translation machinery.

Taken together, the complex structure of FMRP and its various interacting partners suggest that FMRP can directly or indirectly regulate translation machinery and could be involved in other stress response pathways.

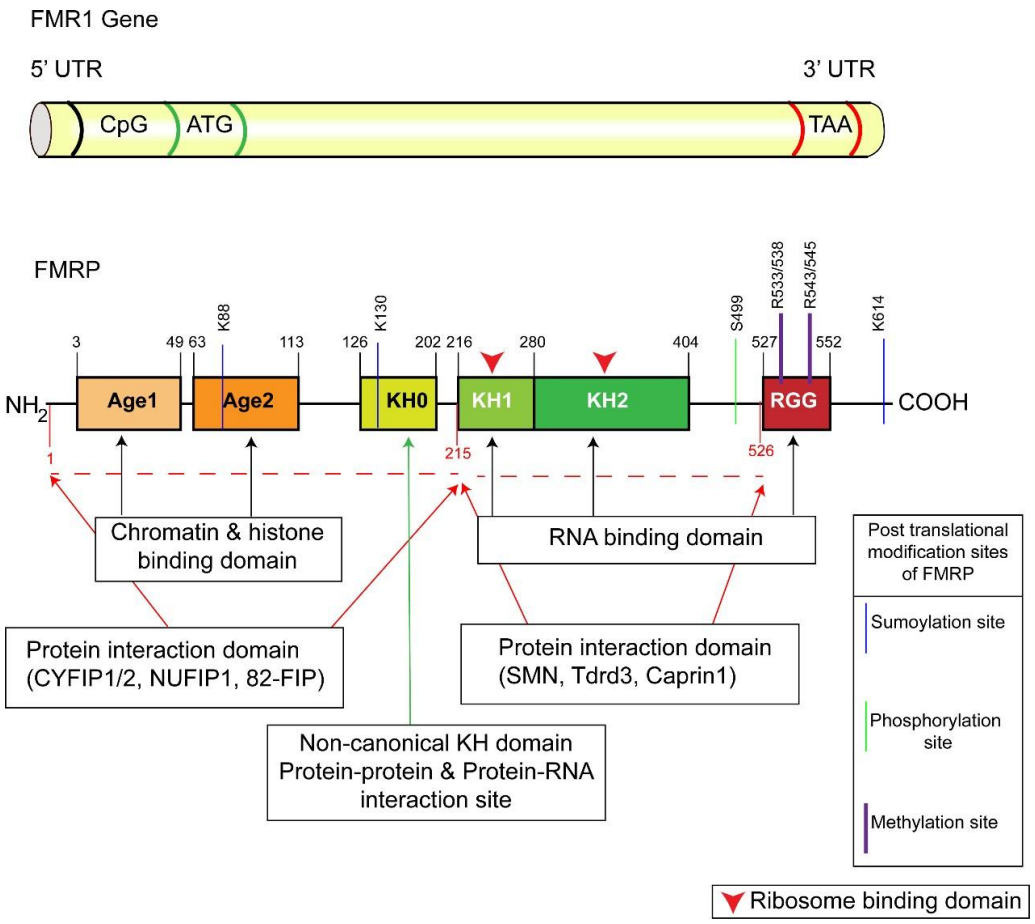

Fig 1.3: Fmr1 gene and different functional domains of Fragile X Mental Retardation Protein. Illustration of Fmr1 gene showing the position of CGG repeat (upper panel). Illustration of FMRP protein showing RNA, DNA and protein interacting domains along with the sites for post-translational modification.

1.6 Insight about FMRP function from the classically known molecular mechanism of FMRP in the neuron

1.6.1 Role of FMRP in neuron

Since it was found that the trinucleotide expansion in the promoter region of FMR1 gene is associated with a heritable ID, researchers focused primarily on brain and neurons. FMRP is abundantly expressed in the brain tissue, mainly hippocampal and cerebellar regions. Many neurons of the forebrain and the hindbrain are also FMRP-positive (Devys D et al, 1993; Yue Feng et al, 1997). This protein is mainly expressed in the cytoplasm, however it is known to shuffle between nucleus and cytoplasm.

Neuronal role of FMRP has been extensively studied in the past two decades. This includes presynaptic action potential regulation, post synaptic glutamate signaling and CYFIP1 (Cytoplasmic FMRP interacting Protein 1) dependent cytoskeletal remodeling (Fig 1.4).

1.6.2 Presynaptic role of FMRP controlling action potential and neurotransmitter release

Many studies have reported that FMRP has a prominent role in the presynaptic neuronal activity. FMRP interacts with the BK channel β4 subunit (large conductance Ca^{+} activated K^{+} channel). BK channels are voltage gated potassium channels, which can be activated by intracellular increase in Ca+ and subsequent binding of Ca+ to the high affinity binding sites. Interaction of FMRP and BKβ4 subunit modulates calcium sensitivity of BK channel, duration of action potential (AP) in the presynaptic neuron and neurotransmitter release. Fmr1 KO mice have shown excessive broadening of AP, elevated presynaptic calcium influx and increased neurotransmitter release (Deng PY et al, 2013).

1.6.3 Postsynaptic activity of FMRP to maintain synaptic plasticity via regulating translation machinery

Apart from the above discussed roles of FMRP in neuronal activity and development, FMRP has a unique role in regulating synaptic plasticity in the postsynaptic neuron. Most of the neurological problems found in FXS patients were found to be associated with metabotropic glutamate receptor (mGluR)-mediated long-term depression (LTD) pathway. Stimulation of mGluR1/5 receptor activates the phosphatidylinositol 3-kinase (PI3K)-mammalian target of rapamycin (mTOR) - extracellular signal–related kinase (ERK) pathway, which phosphorylates FMRP. On the other hand, FMRP itself negatively regulates mTOR pathway by inhibiting the catalytic subunit of PI3K and phosphatidylinositol 3-kinase enhancer (PIKE) (Sharma A et al, 2010; Santoro MR et al, 2012). FMRP plays an important role in translation of mRNAs containing 5’ methylated guanosine triphosphate (5’m7GTP) cap. For cap-dependent translation, translation initiation complex eIF4F needs to communicate with the 5'm7GTP cap of mRNA template. 4E-binding protein (4E-BP) inhibits this interaction. FMRP binding partner CYFIP1 has been found to act as 4E-BP. CYFIP1-FMRP interaction acts as translational repression signal in neurons (Fig 1.3). As a result, in absence of FMRP, levels of dendritic messenger proteins increase and dense, immature dendritic spines appear (Santoro MR et al, 2012). In the absence of FMRP, activity of mTOR kinase and cap-dependent translation has been found to be highin the mouse brain (Sharma A et al, 2010).

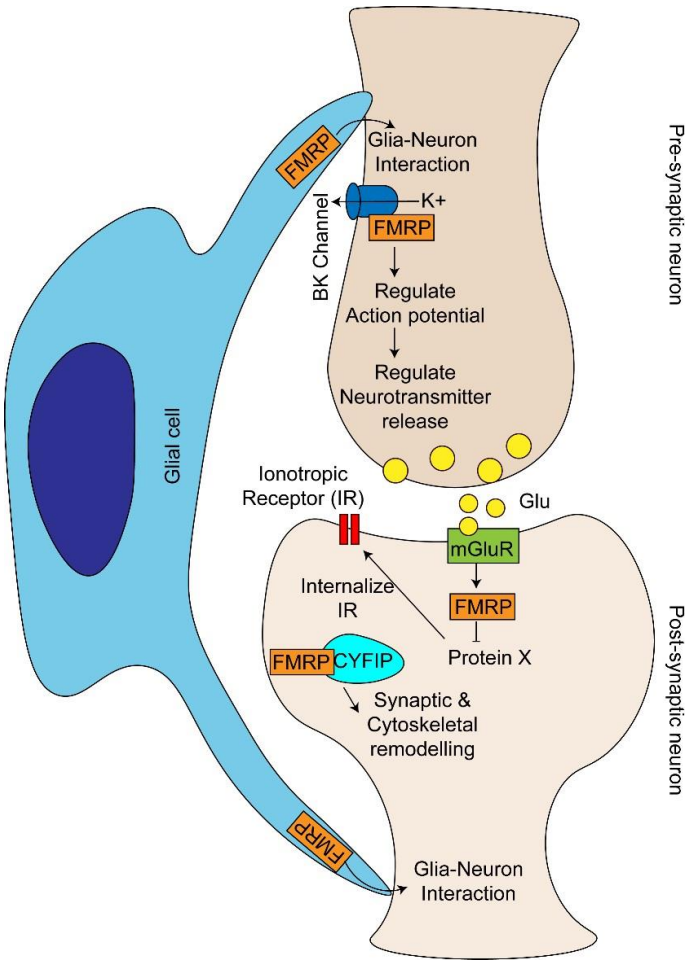

Fig 1.4: Role of FMRP in neuronal plasticity. FMRP interacts with the BK channel and regulates action potential in presynaptic neurons. FMRP is involved in the major pathways of synaptic plasticity and long term memory formation.

In a nutshell, it can be said that FMRP has major involvement in neuronal development and functional pathways. Most importantly, the post synaptic activity of FMRP indicates its involvement with the translational machinery to control the global translation in the neuron.

1.6.4 Role of FMRP in neurodevelopment

FMRP expression was detected in glial cells during early developmental stages (Fig 1.4). In the Fmr1 KO mice brain, an altered number of oligodendrocytes and increased level of glial fibrillary acidic protein (GFAP) in astrocytes were observed. These could be related to altered

myelination of neurons and synaptic transmission (Lee FH et al, 2019; Fernández-Blanco Á et al, 2020).

1.7 FXS link to lung health

Interestingly, cytoplasmic FMR interacting protein 2 (CYFIP2) is found to be significantly associated with the development of pulmonary diseases like asthma and chronic obstructive pulmonary disorder (COPD) (Noguchi E et al, 2005; Obeidat M and Hall IP, 2010). A dataset of gene expression analysis reports more than 2.8 fold decrease of FMR1 expression in case of COPD (http://www.ncbi.nlm.nih.gov/geo/query/acc.cgi?acc=GSE3320). On the other hand, an important study on the clinical profile of pre-mutation carriers of Fragile x syndrome reveals that the people who carry 55 to 200 copy numbers of CGG repeats in FMR1 gene have significantly different lung function profiles compared to the control group. Moreover, this group of people shows higher rates of respiratory diseases and pulmonary system related symptoms such as chronic sinusitis, dyspnea (P value between 0.05 and 0.01) (Movaghar A et al, 2019). These studies strongly motivate us to investigate the role of FMRP during stress response in the lung.

1.8 Scope of investigation

Considering the fact that lung epithelium is readily exposed to xenobiotic stress caused by various airborne chemicals and pathogens during the breathing process, it can be said that the burden of free radicals, ROS and other oxygen species in this tissue is higher than any other tissue. ROS has a paradoxical role in lung health. It is required to kill the pathogens and remove hazardous chemicals, but simultaneously, excessive ROS damages the epithelial cells. To maintain the balance of ROS, lung epithelial cells must have unique mechanisms. One of such mechanisms is integrated stress response (ISR) (Konsavage WM et al, 2012; Li G et al, 2010).

1.8.1 Integrated stress response

Stress response pathways generally help to metabolize or efflux the

chemicals to get rid of the stressor. Integrated stress response is a regulatory mechanism which involves the activation of stress induced genes to cope up with the stress, either by controlling the damage or by removing the damaged cell. Various stress stimuli such as oxidative stress, protein misfolding, double stranded DNA breaks, viral infection converge into phosphorylation of eIF2α at serine 51 residue. As a result the global translation is turned off and protein synthesis is reduced in great extent. Along with the translational attenuation, stress induced genes, such as activating transcription factor 4 (ATF4) and its downstream genes are activated. This process of cellular stress response is commonly known as integrated stress response (ISR) (Fig 1.5). The phosphorylation of eIF2α is carried out by a family of four kinases, general control non-depressible-2 (GCN2), protein kinase double stranded RNA-dependent (PKR), PKR-like ER kinase (PERK) and heme-regulated inhibitor (HRI). These four serine-threonine kinases are responsible for sensing different type of cellular stresses.

GCN2 is a sensor for amino acid deprivation or glucose deprivation. Although recent studies have found that viral infection and UV irradiation can also activate GCN2 (Deng J et al, 2002). The cytosolic kinase GCN2 is activated by dimerization and auto-phosphorylation followed by direct binding of uncharged tRNA or viral genomic RNA to the HisRS (histidyl-tRNA synthetase) domain of the protein (Donnelly N et al, 2013). PKR is present in cytosol and nucleus of the cell. The N-terminal part of PKR contains a double stranded DNA binding domain. Whereas, the C-terminal part of the protein contains kinase domain and dimerization interface. PKR can be activated in response to various stresses such as, oxidative stress, viral infection and ER stress (Li G et al, 2010). PERK is a trans-membrane protein located on the ER membrane. The N-terminal end of the protein faces the ER lumen and bind to immunoglobulin binding protein (BiP). The C-terminal part contains auto-phosphorylation sites and kinase domains. The misfolded proteins in the ER lumen competes with PERK for BiP binding. As a result PERK is dissociated from BiP and gets activated by dimerization and auto phosphorylation. Protein misfolding and oxidative stress can trigger PERK activation

(Donnelly N et al, 2013). The N-terminal end of HRI contains heme binding domain whereas, the protein contains two kinase domains flanking a kinase insert domain. HRI is activated by intermolecular auto-phosphorylation sensing lower heme concentration.

Activation of these four kinases leads to the phosphorylation of eIF2α at serine 51 residue. EIF2α bound to GTP and Met-tRNA scans for 43S complex, which is a rate limiting phase of translation initiation. EIF2B is responsible for the exchange of GDP-GTP on eIF2. When eIF2α is phosphorylated at serine 51 residue, eIF2B is inhibited and level of GTP bound eIF2α decreases. As a result protein synthesis dramatically decreases. During this time mRNAs are sequestered in to stress granules and some stress induced genes gets activated. One of such stress induced gene is ATF4, which is also a key regulator of this ISR pathway. ATF4 mRNA has four upstream ORFs (uORFs), among which uORF2 and 4 are inhibitory. In stressed cell when GTP bound eIF2α decreases, the scanning ribosome does not reach to the inhibitory uORFs, rather starts translating the coding region of ATF4 (Vattem KM and Wek RC, 2004). Increase in the level of ATF4 protein allows the transcription factor activity of the protein and subsequent activation of downstream genes such as ATF3. Activation of eIF2α and ATF4 could be pro-apoptotic or anti-apoptotic, depending on the duration and level of eIF2α phosphorylation and activation of different downstream activator genes.

Given the fact that FMRP and its interacting proteins are closely associated with cellular stress, it became interesting to us to probe the role of FMRP in xenobiotic stress generated in pulmonary epithelial cells and in due course in the context of the Integrated Stress Response Pathway (Fig 1.5).

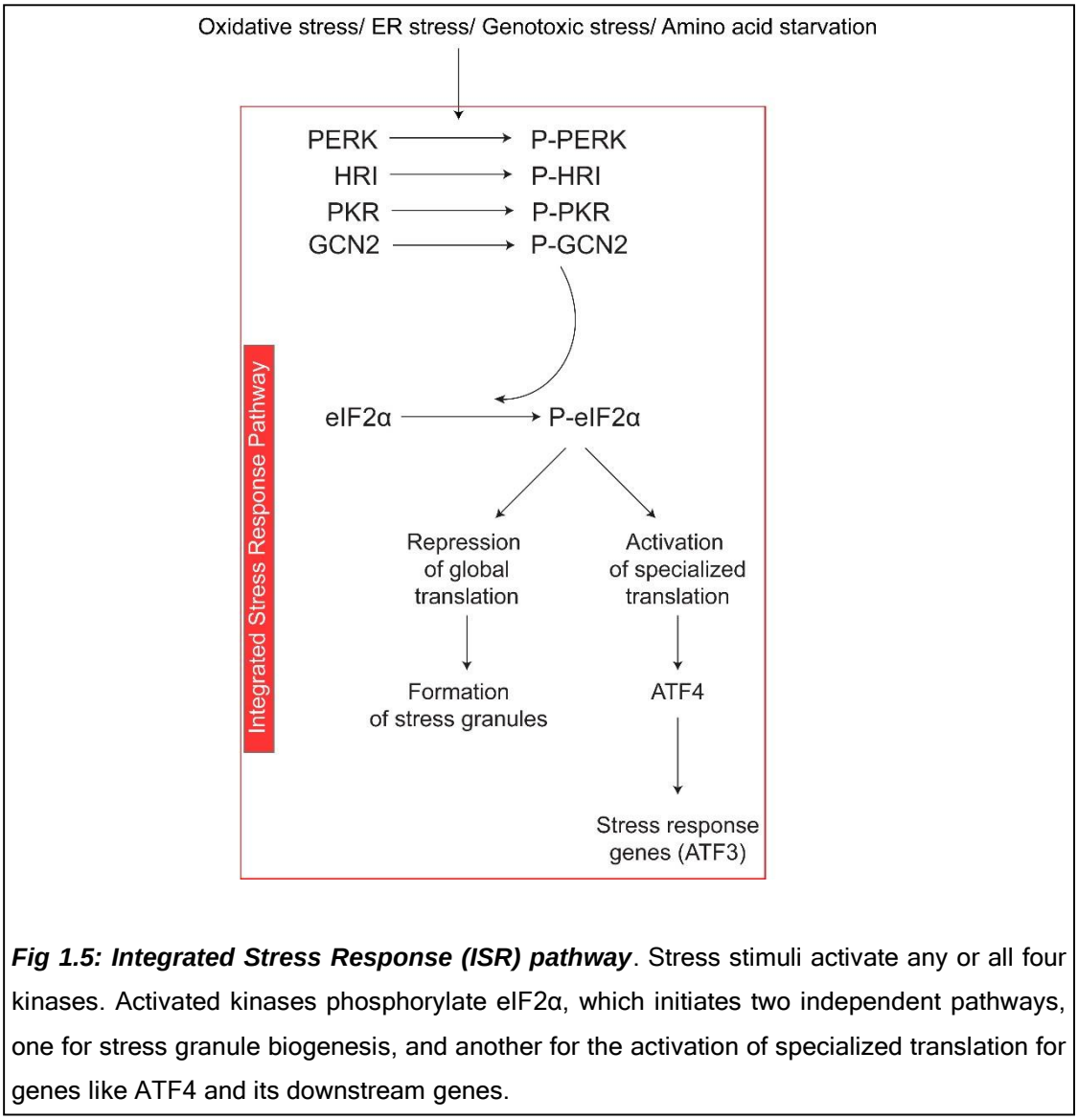

Fig 1.5: Integrated Stress Response (ISR) pathway. Stress stimuli activate any or all four kinases. Activated kinases phosphorylate eIF2α, which initiates two independent pathways, one for stress granule biogenesis, and another for the activation of specialized translation for genes like ATF4 and its downstream genes.

References

1. **Alpatov R, Lesch BJ, Nakamoto-Kinoshita M, Blanco A, Chen S, Stützer A, Armache KJ, Simon MD, Xu C, Ali M, Murn J.** A chromatin-dependent role of the fragile X mental retardation protein FMRP in the DNA damage response. Cell. **2014** May 8;157(4):869-81.

2. **Bechara EG, Didiot MC, Melko M, Davidovic L, Bensaid M, Martin P, Castets M, Pognonec P, Khandjian EW, Moine H, Bardoni B.** A novel function for fragile X mental retardation protein in translational activation. PLoS Biol. **2009** Jan 20;7(1):e1000016.

3. **Cheever A, Ceman S.** Phosphorylation of FMRP inhibits association with Dicer. Rna. **2009** Mar 1;15(3):362-6.

4. **Dahlhaus R.** Of men and mice: modeling the fragile X syndrome. Frontiers in Molecular Neuroscience. **2018** Mar 15;11:41.

5. **de Diego-Otero Y, Romero-Zerbo Y, el Bekay R, Decara J, Sanchez L, Rodriguez-de Fonseca F, del Arco-Herrera I.** α-tocopherol protects against oxidative stress in the fragile X knockout mouse: an experimental therapeutic approach for the Fmr1 deficiency. Neuropsychopharmacology. **2009** Mar;34(4):1011-26.

6. **Debrey SM, Leehey MA, Klepitskaya O, Filley CM, Shah RC, Kluger B, Berry-Kravis E, Spector E, Tassone F, Hall DA.** Clinical phenotype of adult fragile X gray zone allele carriers: a case series. The Cerebellum. **2016** Oct;15(5):623-31

7. **Deng J, Harding HP, Raught B, Gingras AC, Berlanga JJ, Scheuner D, Kaufman RJ, Ron D, Sonenberg N.** Activation of GCN2 in UV-irradiated cells inhibits translation. Current Biology. **2002** Aug 6;12(15):1279-86.

8. **Deng PY, Rotman Z, Blundon JA, Cho Y, Cui J, Cavalli V, Zakharenko SS, Klyachko VA.** FMRP regulates neurotransmitter release and synaptic information transmission by modulating action potential duration via BK channels. Neuron. **2013** Feb 20;77(4):696-711.

9. **Devys D, Lutz Y, Rouyer N, Bellocq JP, Mandel JL.** The FMR–1 protein is cytoplasmic, most abundant in neurons and appears normal in carriers of a fragile X premutation. Nature genetics. **1993** Aug;4(4):335-40.

10. **Diao C, Chen Z, Qiu T, Liu H, Yang Y, Liu X, Wu J, Wang L.** Inhibition of PRMT5 attenuates oxidative stress-induced pyroptosis via activation of the Nrf2/HO-1 signal pathway in a mouse model of renal ischemia-reperfusion injury. Oxidative Medicine and Cellular Longevity. 2019 Oct;**2019.**

11. **Didiot MC, Subramanian M, Flatter E, Mandel JL, Moine H.** Cells lacking the fragile X mental retardation protein (FMRP) have normal RISC activity but exhibit altered stress granule assembly. Molecular biology of the cell. **2009** Jan 1;20(1):428-37.

12. **Donnelly N, Gorman AM, Gupta S, Samali A.** The eIF2α kinases: their structures and functions. Cellular and molecular life sciences. **2013** Oct;70:3493-511.

13. **El Bekay R, Romero-Zerbo Y, Decara J, Sanchez-Salido L, Del Arco- Herrera I, Rodríguez-de Fonseca F, De Diego-Otero Y.** Enhanced markers of oxidative stress, altered antioxidants and NADPH-oxidase activation in brains from Fragile X mental retardation 1-deficient mice, a pathological model for Fragile X syndrome. European Journal of Neuroscience. **2007** Dec;26(11):3169-80.

14. **Fernández-Blanco Á, Dierssen M.** Rethinking intellectual disability from neuro-to astro-pathology. International Journal of Molecular Sciences. **2020** Jan;21(23):9039.

15. **Fu, Y. H., Kuhl, D. P., Pizzuti, A., Pieretti, M., Sutcliffe, J. S., Richards, S.,... & Caskey, C. T. (1991)**. Variation of the CGG repeat at the fragile X site results in genetic instability: resolution of the Sherman paradox. Cell, 67(6), 1047-1058.

16. **Gong C, Yang H, Wang S, Liu J, Li Z, Hu Y, Chen Y, Huang Y, Luo Q, Wu Y, Liu E.** hTERT Promotes CRC Proliferation and Migration by Recruiting YBX1 to Increase NRF2 Expression. Frontiers in cell and developmental biology. **2021** May 17;9:1136.

17. **Hernandez K, Lau KJ, Ba M, Singer CA.** C108 GETTING INFLAMED: MARKERS OF LUNG INJURY AND REMODELLING: Microrna-25 And-188 Target Myosin-5a To Attenuate Mucin Hypersecretion In Asthma. American Journal of Respiratory and Critical Care Medicine. **2017**;195.

18. **Kazdoba TM, Leach PT, Silverman JL, Crawley JN.** Modeling fragile X syndrome in the Fmr1 knockout mouse. Intractable & rare diseases research. **2014** Nov 30;3(4):118-33.

19. **Khayachi A, Gwizdek C, Poupon G, Alcor D, Chafai M, Cassé F, Maurin T, Prieto M, Folci A, De Graeve F, Castagnola S.** Sumoylation regulates FMRP-mediated dendritic spine elimination and maturation. Nature communications. **2018** Feb 22;9(1):1-7.

20. **Kim M, Ceman S.** Fragile X mental retardation protein: past, present and future. Current Protein and Peptide Science. **2012** Jun 1;13(4):358-71.

21. **Konsavage WM, Zhang L, Wu Y, Shenberger JS.** Hyperoxia-induced activation of the integrated stress response in the newborn rat lung. American Journal of Physiology-Lung Cellular and Molecular Physiology. **2012** Jan 1;302(1):L27-35.

22. **Krawczun MS, Jenkins EC, Brown WT.** Analysis of the fragile-X chromosome: localization and detection of the fragile site in high resolution preparations. Human genetics. **1985** Mar 1;69(3):209-11.

23. **Lee FH, Lai TK, Su P, Liu F.** Altered cortical Cytoarchitecture in the Fmr1 knockout mouse. Molecular brain. **2019** Dec;12(1):1-2.

24. **Li G, Scull C, Ozcan L, Tabas I.** NADPH oxidase links endoplasmic reticulum stress, oxidative stress, and PKR activation to induce apoptosis. Journal of Cell Biology. **2010** Dec 13;191(6):1113-25.

25. **Lima-Cabello E, Garcia-Guirado F, Calvo-Medina R, el Bekay R, Perez- Costillas L, Quintero-Navarro C, Sanchez-Salido L, de Diego-Otero Y.** An abnormal nitric oxide metabolism contributes to brain oxidative stress in the mouse model for the fragile X syndrome, a possible role in intellectual disability. Oxidative medicine and cellular longevity. **2016** Oct;2016.

26. **Linder B, Plöttner O, Kroiss M, Hartmann E, Laggerbauer B, Meister G, Keidel E, Fischer U.** Tdrd3 is a novel stress granule-associated protein interacting with the Fragile-X syndrome protein FMRP. Human molecular genetics. **2008** Oct 15;17(20):3236-46.

27. **Loesch DZ, Bui QM, Huggins RM, Mitchell RJ, Hagerman RJ, Tassone F.** Transcript levels of the intermediate size or grey zone fragile X mental retardation 1 alleles are raised, and correlate with the number of CGG repeats. Journal of medical genetics. **2007** Mar 1;44(3):200-4.

28. **Lubs HA.** A marker X chromosome. American journal of human genetics. **1969** May;21(3):231.

29. **Luo X, Kraus WL.** On PAR with PARP: cellular stress signaling through poly (ADP-ribose) and PARP-1. Genes & development. **2012** Mar 1;26(5):417-32.

30. **Mateu-Regue A, Christiansen J, Bagger FO, Winther O, Hellriegel C, Nielsen FC.** Single mRNP analysis reveals that small cytoplasmic mRNP granules represent mRNA singletons. Cell reports. **2019** Oct 15;29(3):736-48.

31. **Movaghar A, Page D, Brilliant M, Baker MW, Greenberg J, Hong J, DaWalt LS, Saha K, Kuusisto F, Stewart R, Berry-Kravis E.** Data-driven phenotype discovery of FMR1 premutation carriers in a population-based sample. Science advances. **2019** Aug 21;5(8):eaaw7195.

32. **Nabih HK.** Crosstalk between NRF2 and Dicer through metastasis regulating MicroRNAs; mir-34a, mir-200 family and mir-103/107 family. Archives of Biochemistry and Biophysics. **2020** Jun 15;686:108326.

33. **Noguchi E, Yokouchi Y, Zhang J, Shibuya K, Shibuya A, Bannai M, Tokunaga K, Doi H, Tamari M, Shimizu M, Shirakawa T.** Positional identification of an asthma susceptibility gene on human chromosome 5q33. American journal of respiratory and critical care medicine. **2005** Jul 15;172(2):183-8.

34. **Obeidat ME, Hall IP.** Genetics of complex respiratory diseases: implications for pathophysiology and pharmacology studies. British journal of pharmacology. **2011** May;163(1):96-105.

35. **Pietrzak J, Spickett CM, Płoszaj T, Virág L, Robaszkiewicz A.** PARP1 promoter links cell cycle progression with adaptation to oxidative environment. Redox biology. **2018** Sep 1;18:1-5.

36. **Prieto M, Folci A, Martin S.** Post-translational modifications of the Fragile X Mental Retardation Protein in neuronal function and dysfunction. Molecular psychiatry. **2020** Aug;25(8):1688-703.

37. **Protic D, Salcedo-Arellano MJ, Dy JB, Potter LA, Hagerman RJ.** New targeted treatments for fragile X syndrome. Current pediatric reviews. **2019** Nov 1;15(4):251-8.

38. **Reineke LC, Kedersha N, Langereis MA, van Kuppeveld FJ, Lloyd RE.** Stress granules regulate double-stranded RNA-dependent protein kinase activation through a complex containing G3BP1 and Caprin1. MBio. **2015** May 1;6(2).

39. **Santoro MR, Bray SM, Warren ST.** Molecular mechanisms of fragile X syndrome: a twenty-year perspective. Annual Review of Pathology: Mechanisms of Disease. **2012** Feb 28;7:219-45.

40. **Schneider A, Winarni TI, Cabal-Herrera AM, Bacalman S, Gane L, Hagerman P, Tassone F, Hagerman R.** Elevated FMR1-mRNA and lowered FMRP–a double-hit mechanism for psychiatric features in men with FMR1 premutations. Translational psychiatry. **2020** Jun 23;10(1):1-8.

41. **Sharma A, Hoeffer CA, Takayasu Y, Miyawaki T, McBride SM, Klann E, Zukin RS.** Dysregulation of mTOR signaling in fragile X syndrome. Journal of Neuroscience. **2010** Jan 13;30(2):694-702.

42. **Sherman, S. L., Morton, N. E., Jacobs, P. A., & Turner, G. (1984).** The marker (X) syndrome: a cytogenetic and genetic analysis. Annals of human genetics, 48(1), 21-37.

43. **Shih JW, Wang WT, Tsai TY, Kuo CY, Li HK, Wu Lee YH.** Critical roles of RNA helicase DDX3 and its interactions with eIF4E/PABP1 in stress granule assembly and stress response. Biochemical Journal. **2012** Jan 1;441(1):119-29.

44. **Specchia V, Puricella A, D'Attis S, Massari S, Giangrande A, Bozzetti MP.** Drosophila melanogaster as a model to study the multiple phenotypes, related to genome stability of the fragile-X syndrome. Frontiers in genetics. **2019** Feb 13;10:10.

45. **Sutherland GR.** Heritable fragile sites on human chromosomes I. Factors affecting expression in lymphocyte culture. American journal of human genetics. **1979** Mar;31(2):125.

46. **Taha MS, Haghighi F, Stefanski A, Nakhaei-Rad S, Kazemein Jasemi NS, Al Kabbani MA, Görg B, Fujii M, Lang PA, Häussinger D, Piekorz RP.** Novel FMRP interaction networks linked to cellular stress. The FEBS journal. **2021** Feb;288(3):837-60.

47. **Tang S, Qin F, Wang X, Liang Z, Cai H, Mo L, Huang Y, Liang B, Wei X, Ao Q, Xu Y.** H2O2 induces PP2A demethylation to downregulate mTORC1 signaling in HEK293 cells. Cell Biology International. **2018** Sep;42(9):1182-91.

48. **Vasic V, Jones MS, Haslinger D, Knaus LS, Schmeisser MJ, Novarino G, Chiocchetti AG.** Translating the Role of mTOR-and RAS-Associated Signalopathies in Autism Spectrum Disorder: Models, Mechanisms and Treatment. Genes. **2021** Nov;12(11):1746.

49. **Vattem KM, Wek RC.** Reinitiation involving upstream ORFs regulates ATF4 mRNA translation in mammalian cells. Proceedings of the National Academy of Sciences. **2004** Aug 3;101(31):11269-74.

50. **Verkerk AJ, Pieretti M, Sutcliffe JS, Fu YH, Kuhl DP, Pizzuti A, Reiner O, Richards S, Victoria MF, Zhang F, Eussen BE.** Identification of a gene (FMR-1) containing a CGG repeat coincident with a breakpoint cluster region exhibiting length variation in fragile X syndrome. Cell. **1991** May 31;65(5):905- 14.

51. **Virág L.** Poly (ADP-ribosyl) ation in asthma and other lung diseases. Pharmacological research. **2005** Jul 1;52(1):83-92.

52. **Wallace AM, Hardigan AA, Gaffney A, Mirochnitchenko O, Thankachen J, Poon K, Arellanos L, Salim S, Thompson V, D'Armiento JM, Foronjy R.** Redox Regulation Of Protein Phosphatase 2A (PP2A) Phosphorylation Prevents Smoke-Induced Lung Injury. InD97. EMERGING OXIDATIVE STRESS-RELATED MECHANISMS IN INJURY AND REPAIR **2011** May (pp. A6142-A6142). American Thoracic Society.

53. **Wheeler AC, Bailey Jr DB, Berry-Kravis E, Greenberg J, Losh M, Mailick M, Milà M, Olichney JM, Rodriguez-Revenga L, Sherman S, Smith L.** Associated features in females with an FMR1 premutation. Journal of neurodevelopmental disorders. **2014** Dec;6(1):1-4.

54. **White B, Schmidt M, Murphy C, Livingstone W, O'toole D, Lawler M, O'Neill L, Kelleher D, Schwarz HP, Smith OP.** Activated protein C inhibits lipopolysaccharide-induced nuclear translocation of nuclear factor κB (NF-κB) and tumour necrosis factor α (TNF-α) production in the THP-1 monocytic cell line. British journal of haematology. **2000** Jul;110(1):130-4.

55. **Xu J, Ji L, Liang Y, Wan Z, Zheng W, Song X, Gorshkov K, Sun Q, Lin H, Zheng X, Chen J.** CircRNA-SORE mediates sorafenib resistance in hepatocellular carcinoma by stabilizing YBX1. Signal transduction and targeted therapy. **2020** Dec 26;5(1):1-4.

56. **Yao M, Wang X, Tang Y, Zhang W, Cui B, Liu Q, Xing L.** Dicer mediating the expression of miR-143 and miR-155 regulates hexokinase II associated cellular response to hypoxia. American Journal of Physiology-Lung Cellular and Molecular Physiology. **2014** Dec 1;307(11):L829-37.

57. **Zalfa F, Bagni C.** Molecular insights into mental retardation: multiple functions for the Fragile X mental retardation protein?. Current issues in molecular biology. **2004**;6(2):73-88.

58. **Zhou Z, Cao M, Guo Y, Zhao L, Wang J, Jia X, Li J, Wang C, Gabriel G, Xue Q, Yi Y.** Fragile X mental retardation protein stimulates ribonucleoprotein assembly of influenza A virus. Nature communications. **2014** Feb 10;5(1):

Chapter 2

Material and Methods

2.1 Animal handling

All animal work reported here has been approved by the Internal Animal UsersCommittee (IAUC) and the Institutional Animal Ethics Committee (IAEC) at inStem. Any procedure that could conceivably cause distress to the animals employed pre-procedural anesthesia with isofluorane gas (Baxter Healthcare Corp.), delivered by an anesthetic vaporizing machine. All animals were monitored for signs of distress and euthanized if in distress. The analysis of human biopsies was approved by Institutional Ethics Committee of JSS Medical College.

2.2 Mouse strains

Fmr1 knockout mice (*Mus musculus*) strain was maintained on a C57B6/J background at the Brain Development and Disease Mechanisms (BDDM), inStem.

2.3 Genotyping

Genotyping of the animals was done using established protocols (Bakker CE et al., 1994). Tissue from mouse tail was digested at 56°C temperature overnight with the help of lysis buffer and protease K. DNA was extracted from the lysed sample with the help of QIAprep Spin Miniprep kit (Qiagen,USA, 27104). This extracted DNA, 3 primers (Sequence and other details in Table 2.1) and Kapa green mix were mixed and the PCR products were run in a 12% agarose gel. A 431 BP band was detected for KO, 130 BP band was detected for wild type and both bands were detected in case of heterogeneous females (Fig 2.1).

Table 2.1 Sequences, melting temperature and molecular weight of FMR1 genotyping primers

Serial number	Sequence	Details
1	5’-CTTCTGGCACCTCCAGCTT	Tm=64.5 °C; MW = 5691
2	5’-TGTGATAGAATATGCAGCATGTGA	Tm=64.1 °C, MW = 7456
3	5’-CACGAGACTAGTGAGACGTG	Tm=58.6 °C, MW = 6191

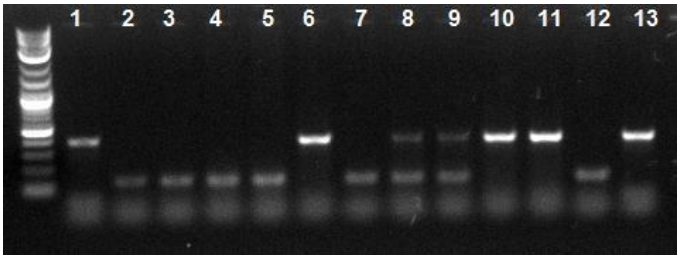

Figure 2.1. Picture of an agarose gel with PCR products from KO, WT and Het animals. Single band at 130 BP position on the lane number 2, 3, 4, 5, 7 and 12 are detecting WT, single band at around 430 BP position on the lane number 1, 6, 10, 11 and 13 are detecting KO. Two bands one at 130, another at 430 BP position on the lane number 8 and 9 are detecting heterogeneous animals (het female).

2.4 Human samples

Human (*Homo sapiens*) lung tissue was obtained from five subjects at autopsy by a forensic pathologist from JSS Medical College, Mysore. The cause of death was not attributed to lung trauma. Deidentified samples were fixed in 4% paraformaldehyde at 4 °C overnight, embedded in paraffin, and processed for immunohistochemical analysis.

2.5 Lung tissue harvesting and processing

For harvesting lung tissue first the animal was anesthetized with the help of isoflurane gas (Baxter Healthcare Corp.) and killed by cervical dislocation. The chest cavity was opened up by cutting the rib cage. Lungs were inflated with fixative (4% (vol/vol) Paraformaldehyde (Alfa Aesar, 30525-89-4) in PBS) solution through a small incision in the trachea. Fully inflated lungs were tied with a thread on the trachea below the incision and cut out carefully. The harvested tissue was cleaned by removing other tissues (like, food pipe, muscles and blood clots) and placed in 4% paraformaldehyde solution for 8 hours at 4°C. After fixation tissue was placed in 0.85% (wt/vol) NaCl solution for 30 minutes and then 1:1 mixture of 0.85% NaCl and ethanol for another 30 minutes. For gradual dehydration tissue was then placed in to 70%, 90% and absolute ethanol for 1 hour in each. After absolute ethanol step, tissue was placed in to Xylene for 30 minutes inside a chemical hood. After 30 minutes

fresh Xylene was added and kept for another 30 minutes. As the tissue became transparent, it was then placed into 1:1 Xylene and paraffin mix and placed inside a vacuum oven at 60°C for 2 hours. After 2 hours tissue was placed intomelted paraffin for 1 hour inside an oven at 60°C temperature. Tissue was then placed into a molder and paraffin block was prepared using melted paraffin. Blocks were kept at room temperature overnight for cooling and kept in a cool,dry place for further use. Paraffin blocks were cut using a microtome machine for generating 5um thick paraffin sections of tissue. Tissue sections were takenon charged slides for staining.

2.6 Cell culture

Human lung (BEAS-2B) non-ciliated airway epithelial origin cell line and human alveolar basal epithelial adenocarcinomic (A549) cell line were obtained from Johns Hopkins University (kind gift from Prof. S. Biswal) (Singh A et al., 2009; Singh A et al., 2013). The murine Club cell line (C22) was purchased from ECACC, UK (cat no.07021401, #07D022). All cell lines were tested for mycoplasma contamination and found to be negative. BEAS-2B were grown in DMEM: F12K (Gibco, USA, 21127030) (1:1) media and A549 cells were grownin DMEM media, supplemented with 10% FBS (Gibco, USA, 10082147) and Penicillin-Streptomycin (Gibco, USA, 1540122) at 37°C, 5% CO_2. Culture conditions for the C22 cell line were different from other two cell lines. C22 cells were maintained in a proliferative state at 33°C temperature and 10% CO_2 (Karnati S et al, 2016). The C22 cells were grown in proliferation media containing DMEM, 4% FBS, Penicillin-Streptomycin, other supplements like, Endothelin-1 (Sigma, USA, E7764), Insulin (Sigma, USA, I1882), Transferrin (Sigma, USA, T3309), Endothelial Cell Growth Supplement (ECGS) (Sigma, USA, E0760), EpidermalGrowth Factor (Sigma, USA, E9644), Hydrocortisone (Sigma, USA, H0888), T3(Sigma, USA, T2877) and IFN-γ (Sigma, USA, I3265). Before experiments cellswere transferred to 37°C temperature and in absence of IFN-γ in the culture media. Under this differentiation condition cells were incubated for 24h, so that they stop proliferation and differentiate into more mature type of club cells. Experiments were conducted within 3rd to 7th passages for BEAS-2B, A549 and within 3rd to 12th passages for C22.

2.7 Models for xenobiotic stress

For Naphthalene (Nap) injury in mice, wild type or Fmr1 knockout mice aged (≥8 weeks of age) were injected intraperitoneally with Corn Oil (vehicle, Sigma, USA, C8267) or with Nap dissolved in corn oil (300 mg kg-1, (Sigma, USA, 147141) using established protocols (Guha A et al., 2014; Guha A et al., 2012). Animals were sacrificed 12 h, 24 h, 48 h after injection for analysis.

To establish an assay for Nap injury in C22 cells, we first determined that these cells expressed the cytochrome Cyp2f2 that converts Nap to stress-inducing derivatives (Buckpitt A et al, 2002). Having established this, we tested a range of concentrations of Nap (50µg ml^{-1} to 500µg ml^{-1}, in DMSO/DMEM). Nap was found to be stable in solution at concentrations up to 100µg mL^{-1} and unstable at higher concentrations leading to cell death within 3h post exposure. Nap exposure at 50-75µg ml^{-1} (DMSO/DMEM, DMSO final concentration 0.7%) for short (1 h) and long duration (24 h) led to a progressive increase in expression of stress markers and mild cytotoxicity after a 24 h period. The vehicle alone (0.7% DMSO) did not impose any significant cytotoxicity to the Sc or Fmr1 Si treated C22 cells under experimental condition. To probe the effects of FMRP/ATF4 deficiency on susceptibility to Nap, cells were exposed to Nap at 75µg ml^{-1} (DMSO/DMEM, DMSO final concentration 0.7%) for a period 1h. Cells were then washed in PBS and chased for varying periods of time in complete medium.

It has been reported previously that 9,10-Phenanthrenequinone (PQ) causes a sharp decrease in the viability of BEAS-2B cells when administered to cells for 24 h at concentrations greater than 1µM (Koike E et al., 2014). We reconfirmed these findings and determined the LD50 dose to be ~1.5µm (Sigma, USA, 275034), dissolved in DMSO/DMEM, DMSO final concentration 0.00002%). To probe the effects of FMRP/ATF4 deficiency on susceptibility to PQ, cells were exposed to PQ at 1.5µm (DMSO/DMEM, DMSO final concentration 0.00002%) for a period 1h. Cells were then washed with PBS and fresh complete media and chased for varying period's time in complete medium.

2.8 siRNA based knockdown of FMR1/ATF4 expression

Several studies have demonstrated that multiple siRNA administered together or sequentially work more efficiently for silencing gene expression than a single siRNA (Wang Z et al., 2016; Fähling M et al., 2009; Zhang P et al., 20015; Hatch EM et al., 2010). For our studies we used 2 or 3 distinct siRNAs for each targeted gene. siRNAs were administered to cells sequentially, 12 h apart, to silence the gene expression. siRNA transfections were done with Lipofectamine 2000 (Thermofisher Scientific, USA, 11668027). All xenobiotic stress assays in C22 cells were performed 36 h after treatment with the last siRNA. C22 cells were transferred from proliferation to differentiation-inducing media 12 h after the last siRNA treatment and utilized for xenobiotic stress assays 24 h thereafter. All xenobiotic stress assays in BEAS-2B cells were performed 12 h after treatment with the last siRNA. All siRNAs were obtained from Ambion: murine *Fmr1* (Ambion, USA, 4390771), murine *Atf4* (Ambion, USA, 16708), murine *Cyp2f2* (Ambion, USA, 4390771), human *FMR1* (Ambion, USA, 4392420) and human *ATF4* (Ambion, USA, 16708), and Scrambled (Negative control, Ambion, USA, 4390843). The assay IDs for each of siRNAs are as follows: Mouse *Fmr1* siRNA (Assay ID: 5315, 5317, s66177), Human *FMR1* siRNA (Assay ID: 5315, 5316, 5317), Mouse *Atf4* siRNA (Assay ID: 160775, 160776, 160777), Mouse *Cyp2f2* siRNA (Assay ID: s64735, s64734), Human *ATF4* siRNA (Assay ID: 122168, 122287, 122372).

2.9 Cell Cytotoxicity assay

C22 and BEAS-2B cells were inoculated into a 96-well plate and treated with Nap or PQ for 1h, as described above, and harvested for analysis 24 h later. Cell viability was assayed using WST-1 reagent (Sigma, USA, 5015944001)). Cells were incubated with WST-1 for 4h and absorbance readings were taken at 450nm and 650nm. Optical density (OD) at 650nm was taken as a baseline control, and deducted from the OD value at 450nm to get the actual OD value of each well. As per manufacturer's protocol cytotoxicity was calculated using the following formula; Cytotoxicity percentage=100 X [(OD (450nm-650nm) of

untreated cells-OD (450nm-650nm) of treated cells)/ OD (450nm-650nm) of untreated cells].

2.10 Histology, Immunofluorescence and Imaging

Lungs were inflated with 4% (wt/vol) Paraformaldehyde (Alfa Aesar, USA, 30525-89-4) in PBS and fixed for 8 hours at 4°C. Fixed lungs were subsequently embedded in paraffin, sectioned (5 µm) and processed for immunohistochemical analysis post heat-mediated antigen retrieval at pH 6.0 (Vector Labs, USA, H-3300) except sections stained with anti-SOD1 antisera that were subject to antigen retrieval at pH 9.0 (Vector Labs, USA, H-3301). For cellular immunostaining, cells were seeded on coated coverslips (0.1% gelatin, Sigma, USA, G9391, as per manufacturer's protocol). Post-treatment, cells were fixed with 4% PFA for 30 minutes and blocked with 2%FBS, 0.2% BSA and 0.1% Triton X 100 in 1X PBS for an hour and stained. Primary antibodies were diluted using the same blocking solution. Immunohistochemical analysisutilized the following antisera: rabbit anti-FMRP (Abcam, UK, 17722, 1:500) (Giampetruzzi A et al, 2013; Yang YM et al, 2017), rabbit anti-FMRP (Sigma, USA, F4055 1:200), goat anti-Scgb1a1 (Santa Cruz, USA, Sc365992, 1:500) (Wu YF et al, 2020), mouse anti-acetylated tubulin (Sigma, USA, T7451, 1:1000), mouse anti-4HNE (Abcam, UK, ab48506, 1:500) (Hall SE et al, 2017), rabbit anti- γ-H2AX (Novus biological, USA, NB100-384, 1:1000) (Hwang JR et al, 2020), mouse anti-Cyp2f2 (Santa Cruz,USA, SC374540, 1:100) (Malvin NP et al, 2019), mouse anti-ATF4 (Sigma, USA, WH0000468M1,1:200)(Selvarajah B et al, 2019), goat-Anti-Tia1 (Santa Cruz, USA, SC1751, 1:200) (Vanderweyde T et al, 2012), rabbit anti-ATF3 (Sigma, USA, HPA001562, 1:200) (Cheng X et al, 2017), rabbit anti-SOD1 (Abcam, UK, ab16831, 1:200), mouse-Anti-human G3BP clone 23 (BD Biosciences, USA, 611126 1:200), purified mouse anti-Ataxin2 clone 22 (BD Biosciences, USA, 611378, 1:200) and Alexa 488/568/647-conjugated donkey anti-mouse/rabbit/goat secondary antibodies (Invitrogen, USA, A 21447, A 21202, A 21206, A10037, A10042, A31571, 1:300). Stained sections were mounted in ProLong Diamond (Invitrogen, USA, P36962). All samples were imaged on a FV3000 4-laser and FV3000 5-laser

confocal microscope or on a Zeiss LSM-780 (Carl Zeiss AG, Germany) laser-scanning confocal microscope. For Haematoxylin-Eosin staining sections were stained with Haematoxylin for 10 sec and Eosin for 30sec, dried and mounted in DPX (Cardiff RD et al, 2014) and imaged on a Nikon Eclipse Ti2 microscope (Nikon, Japan).

2.11 Quantitative fluorescence microscopy

Frequencies of Club cells/mm airway, and total cellular fluorescence in Club cells, in lung sections, were determined from single tiled optical sections acquired on a confocal microscope using ImageJ software. For Club cell frequency analysis, cells attached to the basement membrane were counted per section per animal. Total cellular fluorescence intensity was calculated by subtracting a “background” value per section from the integrated density per cell (outlined using the software) (for FMRP, 4HNE, γ-H2AX and ATF4) (Smolders LA et al, 2012; Chakraborty J and Das S, 2014). The “background” value was determined by sampling integrated density of regions on the section devoid of cells. Total cellular fluorescence of C22 and BEAS-2B cells was estimated from single optical sections on a confocal microscope using ImageJ software. In all experiments involving C22 and BEAS-2B cells, ≥25 cells were analyzed per time point, per experiment, n=3 experiments. The images of Scgb1a1 and Cyp2f2 expression in C22 cells, and of stress granule markers in BEAS-2B and C22 cells, are maximum intensity projection images of z-stacks acquired on a confocal microscope.

2.12 Western blot analysis

Protein was extracted from cell lysates using RIPA buffer (Thermofisher Scientific, USA, 89900) containing Sigmafast EDTA free protease inhibitor cocktail (Sigma, USA, s8830) and Phosstop (Merk, USA, 4906845001). Total protein was run on a 12% SDS PAGE, transferred onto a nitrocellulose membrane (Amersham, UK, 10600002), and the membrane was stained with reversible MemCode (Thermofisher Scientific, USA, 24580) for total protein estimation (imaged on ImageQuant600 (Amersham, UK) and quantified using ImageJ). The membrane was subsequently de-stained, blocked with 5% BSA

(Sigma, USA, A9418) for 1 h and probed using the following primary antisera: rabbit anti-Phospho-eIF2α (Ser51) (Cell Signalling Technology, USA, 9721S, 1:1000) (Banerjee S et al, 2022), mouse anti-eIF2α (Cell Signalling Technology, USA, 2103S, 1:1000) (Halliday M et al, 2017), rabbit anti-Phospho-PKR (Sigma, USA, SAB4504517,1:3000), mouse anti- PKR (Santa Cruz, USA, Sc-6282, 1:1000) (De Lucca FL et al, 2002), rabbit anti-GCN2 (Cell Signalling Technology, USA, 3302s), mouse anti-Phospho-GCN2 (Cell Signalling Technology, USA, 3301S), rabbit anti-PERK (Cell Signalling Technology, USA, 3192s, 1:1000), rabbit anti-Phospho-PERK (Cell Signalling Technology, USA, 3179s), mouse anti-HRI (Santa Cruz, USA, sc-365239). Primary antisera was detected using the following secondary antisera: HRP-conjugated anti-rabbit (abcam, UK, 6721, 1:3000) and HRP-conjugated anti-mouse secondary (Invitrogen, USA, # 62-6520 1:5000) antibodies and ECL (BioRad, USA, 1620177) and analyzed (images on ImageQuant600 (Amersham, UK) and quantified using ImageJ). The levels of eIF2α, phospho-eIF2α, PKR and Phospho-PKR were normalized to the total protein content of the respective lanes. For analysis of SOD1 expression from murine brain and lung tissue lysate, tissues were collected after dissection washed with PBS and protein was extracted with RIPA buffer and protease inhibitor cocktail. Total protein was run on a 12% SDS PAGE, transferred onto a nitrocellulose membrane. We have used 5% non-fat dry milk (Santa Cruz, USA, Sc-2325) solution in PBS forblocking and probed the blots with anti-SOD1 (Abcam, UK, ab16831) and anti- β-tubulin (CST, USA, 15115S) antisera. Levels of SOD1 were normalized to corresponding β-tubulin levels.

2.13 Quantitative PCR (qPCR) analysis

RNA from cell lysates was extracted using Trizol (Invitrogen, USA, 15596018, as per manufacturer's protocol) and qPCR was performed using the primers listed in the following table. The qPCR assays were constituted with the Maxima SYBR green/ROX qPCR Mastermix (2X) (Thermo Scientific, USA, K0221) andanalyzed on a BioRad CFX3 real-time PCR system (BioRad, USA).

Table 2.2 Primer Sequences for qPCR analysis

Gene	**Sequence**
ATF3 Human Forward primer	GTACCCAGGCTTTAGCATTA
ATF3 Human Reverse primer	TTAATAGACAGTAGCCAGCG
Beta actin Human Forward primer	AAAACTGGAACGGTGAAGGT
Beta actin Human Reverse primer	ACAACGCATCTCATATTTGGAA
ATF3 Mouse Forward primer	GAGATGTCAGTCACCAAGTC
ATF3 Mouse Reverse primer	TCCAGTTTCTCTGACTCTTTC
Beta actin Mouse Forward primer	CTTCCAGCAGATGTGGATCAG
Beta actin Mouse Reverse primer	AAAACGCAGCTCAGTAACAGT

2.14 Statistical Analysis

Statistical significance of datasets was assessed using unpaired two-tailed t-tests post Shapiro-Wilk tests for normality. Data were also analyzed using a two-way ANOVA to compare changes in two groups with respect to time, genotype and interaction parameters. ANOVA data and normality test results for each figure are presented (Table 3.1-4.2) in a tabular format.

References

1. **Bakker CE, Verheij C, Willemsen R, van der Helm R, Oerlemans F, Vermey M, Bygrave A, Hoogeveen A, Oostra BA, Reyniers E, De Boule K.** Fmr1 knockout mice: a model to study fragile X mental retardation. Cell. **1994** Jul 15;78(1):23-33.

2. **Banerjee S, Smith C, Geballe AP, Rothenburg S, Kitzman JO, Brennan G.** Gene amplification acts as a molecular foothold to facilitate cross-species adaptation and evasion of multiple antiviral pathways. Virus Evolution. **2022**;8(2):veac105.

3. **Buckpitt A, Boland B, Isbell M, Morin D, Shultz M, Baldwin R, Chan K, Karlsson A, Lin C, Taff A, West J.** Naphthalene-induced respiratory tract toxicity: metabolic mechanisms of toxicity. Drug metabolism reviews. **2002** Jan 1;34(4):791-820.

4. **Cardiff RD, Miller CH, Munn RJ.** Manual hematoxylin and eosin staining of mouse tissue sections. Cold Spring Harbor Protocols. **2014** Jun 1;2014(6):pdb-rot073411.

5. **Chakraborty J, Das S.** Characterization and cadmium-resistant gene expression of biofilm-forming marine bacterium Pseudomonas aeruginosa JP-11. Environmental Science and Pollution Research. **2014** Dec; 21:14188-201.

6. **Cheng X, Liu J, Shan H, Sun L, Huang C, Yan Q, Jiang R, Ding L, Jiang Y, Zhou J, Yan G.** Activating transcription factor 3 promotes embryo attachment via up-regulation of leukemia inhibitory factor in vitro. Reproductive Biology and Endocrinology. **2017** Dec;15:1-1.

7. **De Lucca FL, Serrano SV, Souza LR, Watanabe MA.** Activation of RNA-dependent protein kinase and nuclear factor-kB by regulatory RNA from lipopolysaccharide-stimulated macrophages: implications for cytokine production. European journal of pharmacology. **2002** Aug 16;450(1):85-9.

8. **Fähling M, Mrowka R, Steege A, Kirschner KM, Benko E, Förstera B, Persson PB, Thiele BJ, Meier JC, Scholz H.** Translational regulation of the human achaete-scute homologue-1 by fragile X mental retardation protein. Journal of Biological Chemistry. **2009** Feb 13;284(7):4255-66.

9. **Giampetruzzi A, Carson JH, Barbarese E.** FMRP and myelin protein expression in oligodendrocytes. Molecular and Cellular Neuroscience. **2013** Sep 1;56:333-41.

10. **Guha A, Vasconcelos M, Cai Y, Yoneda M, Hinds A, Qian J, Li G, Dickel L, Johnson JE, Kimura S, Guo J.** Neuroepithelial body microenvironment is a niche for a distinct subset of Clara-like precursors in the developing airways. Proceedings of the National Academy of Sciences. **2012** Jul 31;109(31):12592-7.

11. **Guha A, Vasconcelos M, Zhao R, Gower AC, Rajagopal J, Cardoso WV.**

Analysis of Notch signaling-dependent gene expression in developing airways reveals diversity of Clara cells. PLoS One. **2014** Feb 21;9(2):e88848.

12. **Hall SE, Aitken RJ, Nixon B, Smith ND, Gibb Z.** Electrophilic aldehyde products of lipid peroxidation selectively adduct to heat shock protein 90 and arylsulfatase A in stallion spermatozoa. Biology of Reproduction. **2017** Jan 1;96(1):107-21.

13. **Halliday M, Radford H, Zents KA, Molloy C, Moreno JA, Verity NC, Smith E, Ortori CA, Barrett DA, Bushell M, Mallucci GR.** Repurposed drugs targeting eIF2α-P-mediated translational repression prevent neurodegeneration in mice. Brain. **2017** Jun 1;140(6):1768-83.

14. **Hartig SM.** Basic image analysis and manipulation in ImageJ. Current protocols in molecular biology. **2013** Apr;102(1):14-5.

15. **Hatch EM, Kulukian A, Holland AJ, Cleveland DW, Stearns T.** Cep152 interacts with Plk4 and is required for centriole duplication. Journal of Cell Biology. **2010** Nov 15;191(4):721-9.

16. **Hwang JR, Kim WY, Cho YJ, Ryu JY, Choi JJ, Jeong SY, Kim MS, Kim JH, Paik ES, Lee YY, Han HD.** Chloroquine reverses chemoresistance via upregulation of p21WAF1/CIP1 and autophagy inhibition in ovarian cancer. Cell death & disease. **2020** Dec 4;11(12):1034.

17. **Karnati S, Palaniswamy S, Alam MR, Oruqaj G, Stamme C, Baumgart-Vogt E.** C22-bronchial and T7-alveolar epithelial cell lines of the immortomouse are excellent murine cell culture model systems to study pulmonary peroxisome biology and metabolism. Histochemistry and cell biology. **2016** Mar; 145:287-304.

18. **Koike E, Yanagisawa R, Takano H.** Toxicological effects of polycyclic aromatic hydrocarbons and their derivatives on respiratory cells. Atmospheric environment. **2014** Nov 1;97:529-36.

19. **Malvin NP, Kern JT, Liu TC, Brody SL, Stappenbeck TS.** Autophagy proteins are required for club cell structure and function in airways. American Journal of Physiology-Lung Cellular and Molecular Physiology. **2019** Aug 1;317(2):L259-70.

20. **Selvarajah B, Azuelos I, Platé M, Guillotin D, Forty EJ, Contento G, Woodcock HV, Redding M, Taylor A, Brunori G, Durrenberger PF.** mTORC1 amplifies the ATF4-dependent de novo serine-glycine pathway to supply glycine during TGF-β1–induced collagen biosynthesis. Science signaling. **2019** May 21;12(582):eaav3048.
21. **Singh A, Ling G, Suhasini AN, Zhang P, Yamamoto M, Navas-Acien A, Cosgrove G, Tuder RM, Kensler TW, Watson WH, Biswal S.** Nrf2-dependent sulfiredoxin-1 expression protects against cigarette smoke-induced oxidative stress in lungs. Free Radical Biology and Medicine. **2009** Feb 1;46(3):376-86.

22. **Smolders LA, Meij BP, Riemers FM, Licht R, Wubbolts R, Heuvel D, Grinwis GC, Vernooij HC, Hazewinkel HA, Penning LC, Tryfonidou MA.** Canonical Wnt signaling in the notochordal cell is upregulated in early intervertebral disk degeneration. Journal of Orthopaedic Research. **2012** Jun;30(6):950-7.

23. **Vanderweyde T, Yu H, Varnum M, Liu-Yesucevitz L, Citro A, Ikezu T, Duff K, Wolozin B.** Contrasting pathology of the stress granule proteins TIA-1 and G3BP in tauopathies. Journal of Neuroscience. **2012** Jun 13;32(24):8270-83.

24. **Wang Z, Sun W, Cao J, Cui H, Ma Z.** Repeated Aurora-A siRNA Transfection Results in Effective Apoptosis of A549 Cells Compared to Single Transfection. Clinical laboratory. **2016** Jan 1;62(4):697-703.

25. **Wu YF, Li ZY, Dong LL, Li WJ, Wu YP, Wang J, Chen HP, Liu HW, Li M, Jin CL, Huang HQ.** Inactivation of MTOR promotes autophagy-mediated epithelial injury in particulate matter-induced airway inflammation. Autophagy. **2020** Mar 3;16(3):435-50.

26. **Yang YM, Arsenault J, Bah A, Krzeminski M, Fekete A, Chao OY, Pacey LK, Wang A, Forman-Kay J, Hampson DR, Wang LY.** Identification of a molecular locus for normalizing dysregulated GABA release from interneurons in the Fragile X brain. Molecular psychiatry. **2020** Sep;25(9):2017-35.

27. **Zhang P, Abdelmohsen K, Liu Y, Tominaga-Yamanaka K, Yoon JH, Ioannis G, Martindale JL, Zhang Y, Becker KG, Yang IH, Gorospe M.** Novel RNA-and FMRP-binding protein TRF2-S regulates axonal mRNA transport and presynaptic plasticity. Nature communications. **2015** Nov 20;6(1):1-5.

Chapter 3

FMRP protects lung from xenobiotic stress via activation of Integrated stress Response

3.1 FMRP could be important for stress response in the lung

The goal of this study was to probe the role of FMRP in regulation of stress response in the pulmonary epithelial cells. Continuous exposure of lung epithelium to environmental toxicants, particulate matters and other biological agents leads to increased oxidative, genotoxic and endoplasmic reticulum stress. Such stresses, when unmitigated, lead to cellular damage, inflammation and in the long term to decreased lung capacity and functionality.

The capacity of the lung to manage xenobiotic stress is dependent on stress response proteins that are induced upon insult. In this regard, the Integrated Stress Response (ISR) pathway is an evolutionarily conserved pathway that is integral to how the lung copes with environmental challenges (Pakos-Zebrucka K et al., 2016; van 't Wout EF et al., 2014; Konsavage WM et al., 2012). The ISR is triggered by the activation of one or more of the four stress-responsive kinases GCN2, PKR, PERK and HRI. The activation of these kinases, in turn, sets in motion two separate but interdependent processes that enable cells to mount a restorative response (Wong HR & Wispe JR, 1997). First, these kinases phosphorylate the Eukaryotic Initiation Factor 2α (eIF2α) and shut off ongoing programs of protein synthesis. The inhibition of translation leads to the sequestration of translationally active mRNAs into stress-induced condensates or stress granules (SGs). Second, activation of the kinases also induces specialized modes of protein translation leading to the expression of stress response proteins. More specifically, these specialized translation regimes upregulate expression of Activating Transcription Factor 4 (ATF4) (Pakos-Zebrucka K et al., 2016; van 't Wout EF et al., 2014) and, in turn, ATF4 targets such as *ATF3*. ATF4 also synergizes with other transcription factors activated in response to stress like Nrf2, to induce the expression of stress response genes (He CH et al., 2001; Sarcinelli C et al., 2020).

The Fragile X Mental Retardation Protein (FMRP) is a multifunctional protein that is expressed in the brain and other organs, in humans and other animals alike. Deficiencies in FMRP lead to Fragile X Mental Retardation Syndrome (FXS), a disease characterized by mild-to-moderate intellectual disability (Zhou

Z et al., 2014). FMRP function has been most intensively studied in the neuronal context wherein the protein has been shown to regulate synaptic plasticity by multiple mechanisms (Santoro MR et al., 2012). Aside from this well-established role, several studies indicate that FMRP also has a role in facilitating stress responses. At a cellular level, FMRP has been shown to play an essential role in SG biogenesis in response to arsenite and heat shock (Didiot MC et al., 2009; Linder B et al., 2008). A recent study on fibroblasts derived from *Fmr1* KO mice showed that FMRP is required for a specialized DNA Damage Response (DDR) in response to agents like Aphidicolin, 5-Hydroxyurea (5-HU) and UV (Alpatov R et al., 2014). The central finding of this study is that FMRP has a chromatin-dependent role in resolving stalled replication forks and single strand breaks in DNA (Alpatov R et al., 2014) but not in response to other types of genotoxic stress.

The lung is routinely exposed to a variety of environmental toxicants that cause many different types of stress. Our interest in candidate proteins that regulate the pulmonary stress response led us to explore the role of FMRP in the lung. We immunostained murine and human lungs for FMRP to find that the protein is expressed in the airway epithelium and more broadly. To probe the role of FMRP in stress responses in the airways, we subjected *Fmr1* KO mice to Naphthalene injury, a well-established model for oxidative and genotoxic stress. We found that the airways of *Fmr1* KO mice exhibited higher expression of markers of oxidative and genotoxic stress, and greater cell death, than wild type. These findings led us to investigate the role of FMRP in airway stress responses, and in the Integrated Stress Response pathway, in mice and in the human lung.

3.2 Results

3.2.1 FMRP is expressed in the airways and more broadly in the murine lung and protects airway Club cells from Naphthalene induced stress

To characterize the role of FMRP in the pulmonary stress response, we examined the expression of the protein in adult lungs from wild-type (WT) and *Fmr1* KO animals. Lung sections from WT mice were stained with anti-FMRP antisera and examined under a confocal microscope (5 µm, n=8). FMRP expression was detected throughout the lung (Fig. 3.1A). We detected widespread protein expression in airway epithelium, both in secretory Club cells (CCs, marked by expression of Scgb1a1, Fig. 3.1A, C) and in ciliated cells (marked by expression of Acetylated Tubulin, AcTub, Fig. 3.1A, C). Outside of the airways, we noted intermittent expression in the alveolar parenchyma (Fig. 3.1A). Lung sections of *Fmr1* KO mice stained with the same anti-FMRP antisera did not show any specific staining (airways shown in Fig. 3.1B, D, n=3). Together, these experiments showed that FMRP is expressed in the murine lung, in the airways and more broadly. Next we examined H&E stained lung sections from WT and *Fmr1* KO mice to compare morphologies of the lungs. We found that lungs from WT and *Fmr1* KO were comparable (Fig. 3.2 A-B).

To investigate the role of FMRP in the pulmonary stress response, we focused our attention on FMRP-expressing airway CCs. Airway CCs are highly sensitive to the polycyclic hydrocarbon Naphthalene (Nap) (Stripp BR et al., 1995; Van Winkle LS et al., 1995). Nap administration leads to the loss of the vast majority of CCs from the airway epithelium within 24-48 h and is a well-established model for lung injury (Guha A et al., 2014; Guha A et al., 2017). The susceptibility of airway CCs to Nap is due to the expression, in CCs, of the cytochrome P450 enzyme Cyp2f2 (Buckpitt A et al., 2002). Cyp2f2 converts Nap to Naphthalene oxide that causes DNA damage. Naphthalene oxide is also converted to

Naphthoquinones that cause oxidative stress (Buckpitt A et al., 2002). Thus, to probe the role of FMRP in the pulmonary stress response in mice we decided to utilize the Nap injury model. Interestingly, the Cyp2f2 isoform that converts Nap to cytotoxic derivatives is not expressed in humans and consequently Nap does not affect humans in the same way.

We exposed WT and *Fmr1* KO animals to Nap and harvested lungs for analysis at different timepoints post injury (regimen shown schematically in Fig. 3.1E). To assess the extent of injury, we quantified frequencies of CCs across timepoints and examined expression of markers of oxidative and genotoxic stress. We found that the frequencies of CCs in WT were significantly higher than in *Fmr1* KO at 12h, 24 h and 48 h respectively (Fig. 3.1F, n=3 mice per genotype per timepoint). In other words, cell loss was greater and faster in *Fmr1* KOs. Next, we stained sections from mouse lung prior to and post Nap injury with two antisera: anti-4- Hydroxynonenal (4HNE, a product of lipid peroxidation and a marker of oxidative stress) and anti-γ-H2AX (a phosphorylated histone variant that is a marker of double stranded DNA breaks and genotoxic stress). We did not detect expression of either marker in the lungs from uninjured WT and *Fmr1* KO mice (Fig. 3.1G i, ii, 1H i, ii). In contrast, the expression of both markers was dramatically increased in CCs in Nap-injured lungs (Fig.1G, H). Pertinently, we noted that the levels of 4HNE and γ-H2AX expression in CCs were lower in WT than in *Fmr1* KOs at all time points examined (Fig. 3.1G iii-vi, 1H iii-vi, also see quantitation in Fig. 3.2 C-D, n=3 mice per genotype per time point). Based on these data we concluded that CCs in *Fmr1* KO animals are more susceptible to Nap- induced stress.

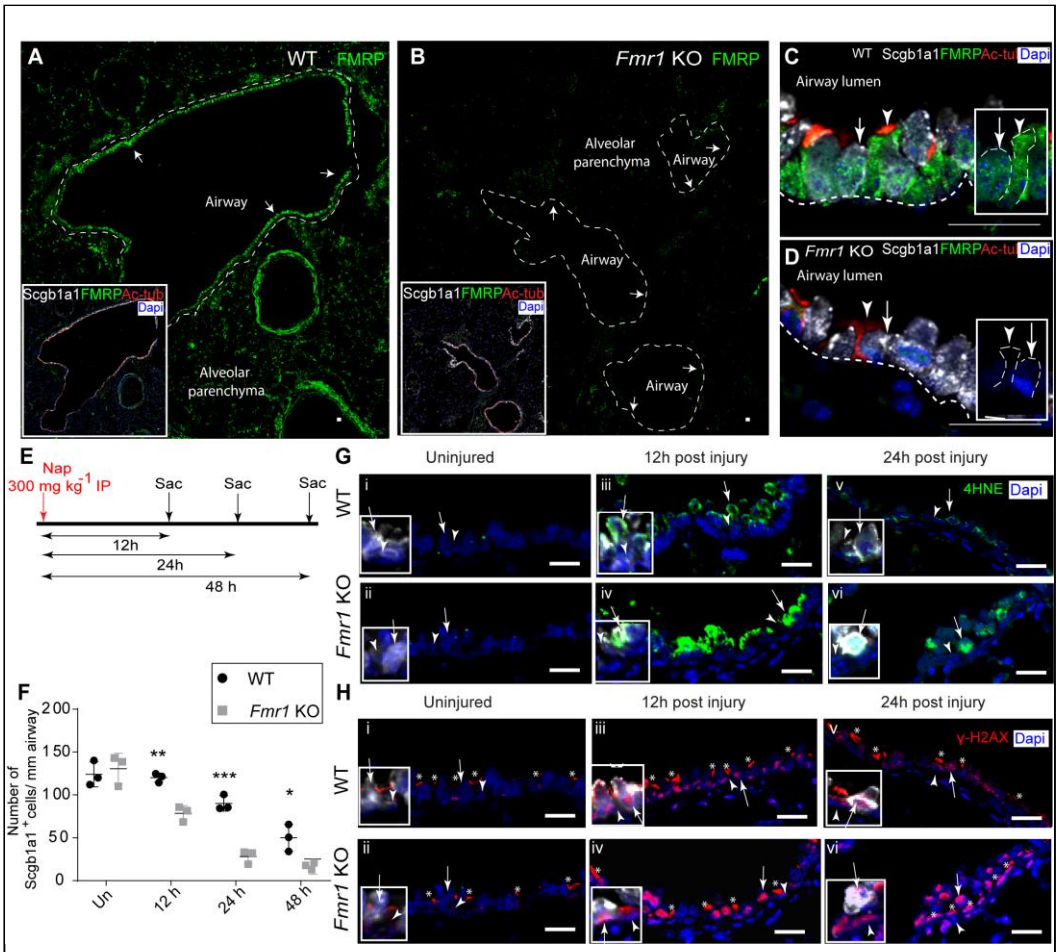

Figure 3.1: FMRP is expressed in the airways and more broadly and protects airway Club cells from Naphthalene induced stress. (A-D) FMRP expression in the murine lung. **(A)** Tiled image showing FMRP immunostaining (green, white arrow) in the airway epithelium (demarcated by white dotted lines) and in the parenchyma of the murine lung. The airways are identified by expression of the Club cell (CC) marker Scgb1a1 (white, inset) and of the ciliated cell marker Acetylated-Tubulin (red, inset). **(B)** Tiled image showing FMRP immunostaining in *Fmr1* knockout (*Fmr1* KO) mice. Note absence of FMRP (green) in both airways (demarcated by white dotted lines, inset) and parenchyma. **(C-D)** High resolution image of FMRP immunostaining (green) in airway epithelial cells. Here CCs are shown in white (white arrowhead in panel alongside) and ciliated cells are in red (red arrowhead in panel alongside) in wild type **(C)** and *Fmr1* KO **(D)**. **(E-H)** Susceptibility of CCs to Naphthalene (Nap) injury in control and *Fmr1* KO. **(E)** Schematic showing regimen for Nap injury. **(F)** Frequencies of Scgb1a1^{+} cells in wild type (black circle) and *Fmr1* KO (grey square) from uninjured (Un) and Nap-injured mice at different timepoints post injury. Data represents all three data points in the scattered plots with mean ± s.e.m. **(G-H)** Expression of markers of oxidative (4HNE) and genotoxic (γ-H2AX) stress in airways from wild-type and *Fmr1* KO mice prior to and post Nap injury. Note white arrowheads showing ciliated cells and white arrows showing CCs on the airways and in insets (counterstained with Scgb1a1 antisera, white). **(G i-G vi)** 4HNE immunostaining (green) in the airways of wild-type

(upper panel) and *Fmr1* KO (lower panel) mice prior to and post Nap injury. **(H i- H vi)** γ-H2AX immunostaining (red) in the airways of control (upper panel) and *Fmr1* KO (lower panel) prior to and post Nap injury. Asterisks showing cilia of ciliated cells marked with γ-H2AX **(H i- H vi).** Also see Fig. 3.2. Statistical significance was assessed by an unpaired two-tailed t-test (see methods, p< .05*, p< .01**, p< .001***). The changes in the two groups over time, across genotype and interaction parameters were also assessed by two-way ANOVA and found to be statistically significant. For Shapiro-Wilk normality test and two-way ANOVA see Table 3.1. Scale Bar=20 μm.

Table 3.1: Two-way ANOVA to show time-wise and genotype-wise changes in the graphical data used in Fig 3.1

Figure number	Variables	Sum of Squares	F statistic	P value	Normality (Shapiro-Wilk normality test)
Figure 3.1F	Interaction Time Genotype	3746 32659 6825	F (3, 12) = 8.862 F (3, 12) = 77.27 F (1, 4) = 64.9	P=0.0023 P<0.0001 P=0.0013	Passed

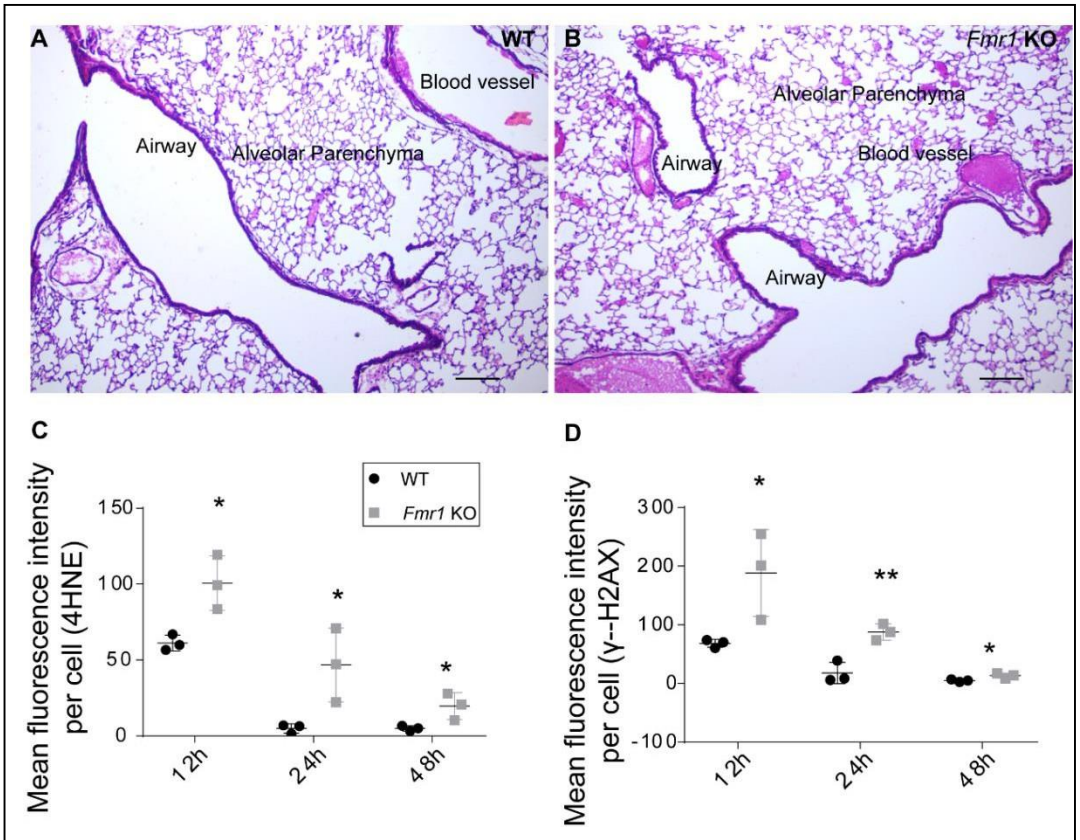

Figure 3.2: FMR KO animals express markers of oxidative and genotoxic stress in the airways in response to Nap. (A-B) Lung morphology in control and *Fmr1* KO animals. H&E stained lung sections from control **(A)** and *Fmr1* KO **(B)** (n=2 animals

each). Scale Bar=200um. (C-D) Quantitation of levels of expression of 4HNE and γ-H2AX in CCs in wild-type and Fmr1 KO lungs post Nap. (C) Quantitation of total 4HNE immunofluorescence per CC at different timepoints (≥ 50 cells were analysed per time point/per animal, n=3 animals). Data represents mean ± SEM. (D) Quantitation of total γ-H2AX immunofluorescence per CC at different timepoints (≥ 50 cells were analysed per time point/per animal, n=3 animals). Unpaired two-tailed t-test (p< .05*, p< .01**, p< .001***). For normality test and two-way ANOVA see Table 3.2.

Table 3.2: Two-way ANOVA to show time-wise and genotype-wise changes in the graphical data used in Fig 3.2

Figure number	Variables	Sum of Squares	F statistic	P value	Normality (Shapiro-Wilk normality test)
Figure 3.2C	Interaction Time Genotype	 6786923 158536285 46216894	 F (2, 8) = 1.428 F (2, 8) = 33.37 F (1, 4) = 115.1	 P=0.2948 P=0.0001 P=0.0004	Passed
Figure 3.2D	Interaction Time Genotype	 93896384 437685349 196523094	 F (2, 8) = 3.971 F (2, 8) = 18.51 F (1, 4) = 29	 P=0.0634 P=0.0010 P=0.0057	Passed

3.2.2 The Club cell-like C22 cell line deficient in FMRP is also more susceptible to Nap induced stress

To further probe the role of FMRP in stress responses in CCs, we turned to the murine Club cell-like cell line, C22. C22 cells were derived from H-2Kb-tsA58 mice expressing a temperature sensitive isoform of the SV40 Large T antigen under the H-2Kb promoter (Demello DE et al., 2002). To characterize these cells, we stained C22 cells with markers of CCs and other airway and alveolar lineages. Consistent with previous reports,these cells expressed the CC marker Scgb1a1 and did not express markers of other lineages (Fig. 3.4A, data not shown). We then performed a series of experiments to determine whether C22 could be utilized as a model for Nap injury, and to probe the role of FMRP therein.

First, C22 cells were stained with antisera against Cyp2f2 and FMRP. We found that C22 cells expressed modest levels of Cyp2f2 (Fig. 3.4B,

n=6 experiments) and expressed FMRP (Fig. 3.4C, n=9 experiments). Next we optimized methods for the knockdown of gene expression in C22 cells using siRNAs and methods for Nap challenge. We established that treatment with 2 different *Cyp2f2* siRNAs and 3 different FMRP siRNAs was sufficient to reduce Cyp2f2/FMRP expression by 80% or greater (see methods, compare Cyp2f2/FMRP expression in scrambled siRNA-treated cells, Sc, and *Cyp2f2/Fmr1* siRNA-treated cells, Si, in Supplementary Fig. 3.3 A-C, n=3 experiments, and Fig. 3.4D respectively, n=9 experiments). Careful titration of Nap dosage and time of exposure (see methods) showed that a 1 h pulse of Nap was sufficient to induce expression of oxidative and genotoxic stress markers in C22 cells and marginally increase cell death 24 h post exposure (see methods). We subsequently incubated control (scrambled siRNA-treated cells, Sc) and Cyp2f2-depleted (*Cyp2f2* siRNA-treated cells, Si) cells with Nap for 1 h and harvested cells at different timepoints for analysis (regimen is shown schematically in Fig. 3.3 D, see methods). Levels of 4HNE and γ-H2AX increased in Sc-cells within 6 h and returned to baseline by 24 h (Fig. 3.3 E-H, n=3 experiments each). In contrast, levels of expression in Si-cells remained at baseline levels at all timepoints (Fig. 3.3 E-H, n=3 experiments each). These data showed that C22 cells are susceptible to Nap-induced stress in a Cyp2f2-dependent manner like CCs *in vivo*.

To explore the possibility that FMRP regulates susceptibility to Nap in C22 cells, we incubated control (scrambled siRNA-treated cells, Sc) and FMRP-depleted (*Fmr1* siRNA-treated cells, Si) cells with Nap for 1 h and the harvested cells at different timepoints for analysis (shown schematically in Fig. 3.4E). To assess levels of oxidative and genotoxic stress, we again stained cells with anti-4HNE and anti-γ-H2AX respectively (Fig. 3.4 F, H). In order to assess the cytotoxicity of Nap, we subject the cells to a WST-1 assay 24 h post exposure. We found that levels of 4HNE and γ-H2AX (Fig. 3.4 F-I) were elevated in *Fmr1*-depleted cells at all timepoints (n=3 experiments each) and that *Fmr1*-depleted cells exhibited greater cell death in response to Nap (Fig. 3.4J).

These data correlated well with the increased susceptibility of CCs to Nap in *Fmr1* KO animals and demonstrated that FMRP has a cell intrinsic role in protecting cells from Nap.

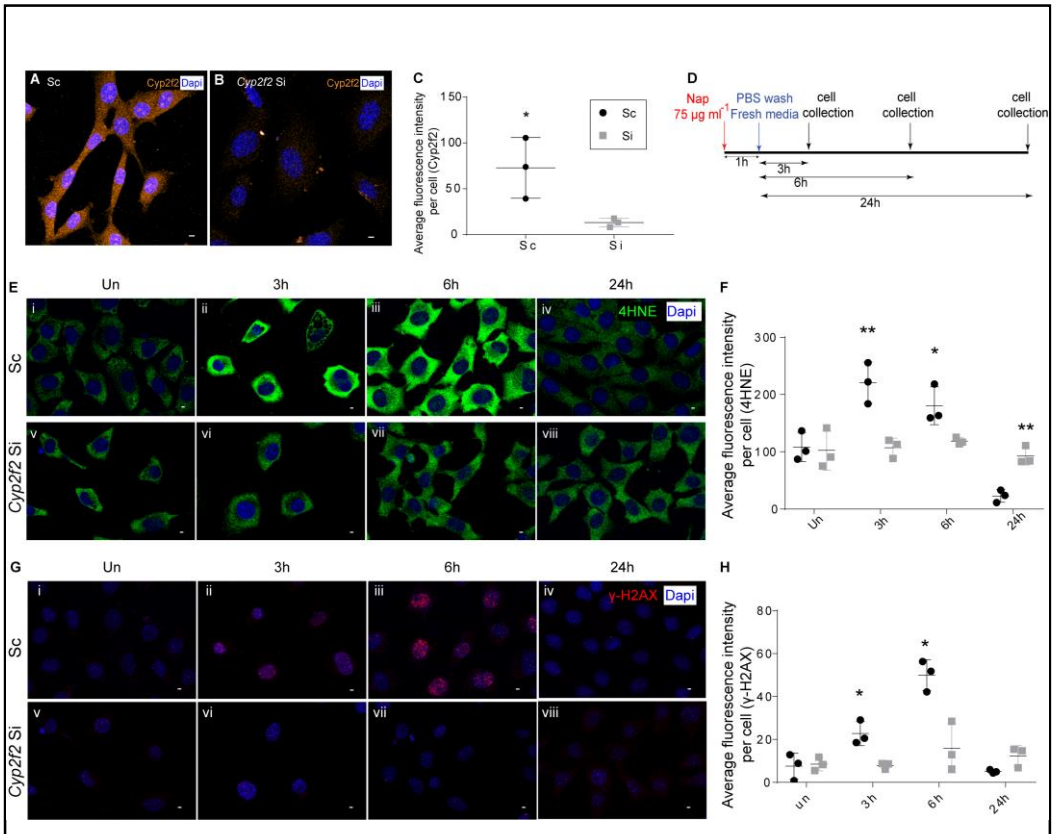

Figure 3.3: Validation of Cyp2f2 dependent Nap injury in C22 cells. (A-C) Cyp2f2 immunostaining and quantitation. **(A-B)** Cyp2f2 (orange) immunostaining in scrambled siRNA-treated (Sc) **(A)** and Cyp2f2 siRNA-treated (Si) **(B)** C22 cells. **(C)** Quantitation of Cyp2f2 immunofluorescence per cell in Sc and Si treated cells. (**D-G)** Cyp2f2 siRNA-treated (Si) C22 cells fail to respond to Nap induced stress. **(D i- D viii)** 4HNE immunostaining (green) in Sc and Si cells prior to and post Nap. **(E)** Quantitation of 4HNE immunofluorescence per cell in Sc and Si cells prior to and post Nap. Note the level of 4HNE in Si treated cells remains unchanged prior to and post Nap. **(F i- F viii)** γ-H2AX immunostaining (red) in Sc and Si cells prior to and post Nap. **(G)** Quantitation of γ-H2AX immunofluorescence per cell in Sc and Si cells post Nap. Black circle (Sc), Grey square (Si). (≥ 25 cells were analysed per timepoint/per experiment, n=3 experiments). Data represents mean ± SEM Unpaired two-tailed t-test (p< .05*, p<

Table 3.3: Two-way ANOVA to show time-wise and genotype-wise changes in the graphical data used in Fig 3.3

Figure number	Variables	Sum of Squares	F statistic	P value	Normality (Shapiro-Wilk normality test)
Figure 3.3E	Interaction Time Genotype	277282829 413013067 46317078	F (3, 12) = 16.47 F (3, 12) = 24.53 F (1, 4) = 5.944	P=0.0001 P<0.0001 P=0.0714	Passed
Figure 3.3G	Interaction Time Genotype	15397110 24262281 6287973	F (3, 12) = 14.84 F (3, 12) = 23.39 F (1, 4) = 15.82	P=0.0002 P<0.0001 P=0.0164	Passed

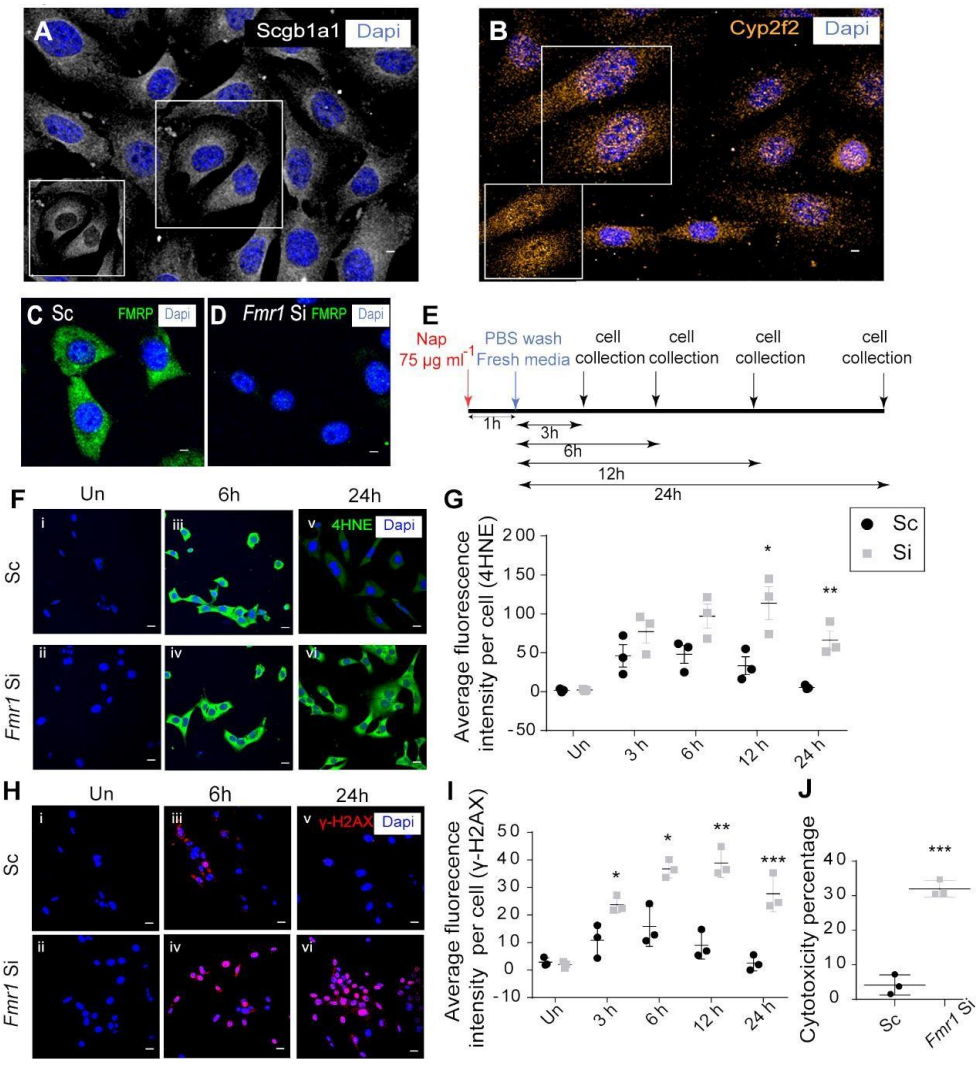

Figure 3.4: FMRP deficient Club cell-like C22 cells are susceptible to Nap-induced stress. (A-D) Phenotypic characterization of C22 cells. **(A)** Scgb1a1 immunostaining (white) in C22 cells. **(B)** Cyp2f2 (orange) immunostaining in C22 cells. Also see Fig. 3.3. **(C-D)** FMRP immunostaining in C22 cells **(C)** and in C22 cells treated

with *Fmr1* siRNA **(D)**. **(E-J)** Susceptibility of C22 cells to Nap (control is scrambled siRNA-treated, (Sc) and *Fmr1* siRNA-treated (Si)). **(E)** Schematic showing regimen for Nap injury. **(F-I)** Expression of markers of oxidative (4HNE) and genotoxic (γ-H2AX) stress in Sc and Si cells prior to and post Nap. **(F i- F vi)** 4HNE immunostaining (green) in Sc and Si cells prior to and post Nap. **(G)** Quantitation of 4HNE immunofluorescence per cell in Sc and Si cells prior to and post Nap. **(H i- H vi)** γ-H2AX immunostaining (red) in Sc and Si cells prior to and post Nap. **(I)** Quantitation of γ-H2AX immunofluorescence per cell in Sc and Si cells post Nap. **(J)** Cytotoxicity of Nap in Sc and Si cells 24 h post Nap (n=3 experiments). For immunofluorescence analysis ≥ 25 cells were analysed per timepoint/per experiment, n=3 experiments. Graphical data represents mean ± s.e.m. Black circle (Sc), Grey square (Si). Unpaired two-tailed t-test (p< .05*, p< .01**, p< .001***). For normality test and two-way ANOVA see Table 3.4. Scale Bar=5 μm.

Table 3.4: Two-way ANOVA to show time-wise and genotype-wise changes in the graphical data used in Fig 3.4

Figure number	Variables	Sum of Squares	F statistic	P value	Normality (Shapiro-Wilk normality test)
Figure 3.4G	Interaction Time Genotype	5525054195 22221659115 14690673188	F (4, 16) = 5.999 F (4, 16) = 24.13 F (1, 4) = 10.73	P=0.0038 P<0.0001 P=0.0306	Passed
Figure 3.4I	Interaction Time Genotype	872823942 2103967406 2326731004	F (4, 16) = 8.556 F (4, 16) = 20.62 F (1, 4) = 408.7	P=0.0007 P<0.0001 P<0.0001	Passed

3.2.3 FMRP is required for the induction of the Integrated Stress Response pathway that protects from Naphthalene induced stress

The increased susceptibility of FMRP-deficient CCs and C22 cells to Nap led us to investigate the role of FMRP in the Nap induced stress response. As previously mentioned, the ISR is induced when one of four stress-responsive kinases (GCN2, PERK, HRI, PKR) phosphorylated eIF2α at Serine 51. Phosphorylation of eIF2α arrests conventional translation, stimulates genesis of SIGs and enables specialized translation of stress response proteins like ATF4 (Pakos-Zebrucka K et al., 2016; van't Wout EF et al., 2014). To probe the status of the ISR in C22 cells post Nap, we examined the phosphorylation state of eIF2α.

We exposed C22 cells to Nap for 1 h, harvested cells at various time points and quantified the levels of expression of both eIF2α and phosphorylated eIF2α (p-eIF2α). Western blot-based ratiometric quantitation of total and p-eIF2α in Sc cells showed that p-eIF2α levels increased 3 and 6 h post injury and decreased to baseline levels thereafter (Fig. 3.5A, Fig. 3.6 A-B, n=5 experiments). We probed p-eIF2α and total eIF2α proteins on two different blots prepared simultaneously from the same sample (Fig 3.6 A, B and Fig 3.10 A, B). Similarly PKR and p-PKR blots were also prepared (Fig 3.6 D, E and Fig 3.10 D, E). Due to technical difficulties, we could not do this from the same blot. We inferred that the ISR is induced in C22 in response to Nap. We then exposed Si cells to Nap for 1 h and found that, contrary to controls, the levels of p-eIF2α did not increase post Nap (Fig. 3.5A, Fig. 3.6 A-B, n=5 experiments). The analysis of p-eIF2α suggested the FMRP-depletion might inhibit the ISR.

Next, we examined the expression of ATF4 and its target, *ATF3*, in control and FMRP-deficient cells. Sc and Si cells were stained with an anti-ATF4 antibody prior to and post Nap. In Sc, the expression of ATF4 was undetectable in untreated cells, increased dramatically 3, 6, 12 h post Nap treatment and then approached baseline levels at 24 h (Fig. 3.5 B-C, n=5 experiments). In Si cells, levels of ATF4 were negligible in untreated cells and showed no appreciable increase post Nap (Fig. 3.5 B-C, n=5 experiments). Next, we assayed *ATF3* levels by quantitative real-time PCR (qPCR). For this, RNA was isolated from Sc and Si cells at different timepoints and subjected to qPCR analysis. In Sc, levels of *ATF3* mRNA increased at 3, 6 h post Nap and returned to baseline thereafter (Fig. 3.6 C, n=3 experiments). In Si, the levels *ATF3* did not rise appreciably above baseline post Nap (Fig. 3.6 C). These findings were also validated with anti-ATF3 immunostaining (data not shown). Based on these data we concluded that both ATF4 and ATF3 expression are perturbed in FMRP-deficient cells post Nap. Taken together, the findings showed that the ISR is perturbed in FMRP-deficient cells post Nap.

Next, we decided to investigate whether the upstream kinases that phosphorylate eIF2α and induce the ISR become activated (phosphorylated) in FMRP-deficient cells. We probed the expression of GCN2, PERK, HRI, PKR and their phosphorylated isoforms in Nap-treated C22 cells using commercially available antibodies (see methods). Among all pairs of antisera tested, antisera for PKR and p-PKR provided reproducible results. Western blot-based ratiometric quantitation of p-PKR and total PKR in Sc and Si cells showed that the p-PKR levels increase in both Sc and Si 3 h post Nap (Fig. 3.6 D-F, n=3 experiments). Importantly, we noted that levels of p-PKR returned to baseline in Sc at 6 h and later timepoints, but remained significantly higher in Si at later time points (Fig. 3.6 D-F). This suggested that at least one of the stress responsive kinases (PKR) is activated in FMRP-deficient cells post Nap.

Perturbations to the ISR provided a plausible explanation for why FMRP-deficient C22 cells are more susceptible to Nap. To test this, we decided to probe how perturbing the ISR, by knocking down levels of *Atf4*, would impact susceptibility to Nap. Control (Scrambled siRNA) and *Atf4* siRNA treated C22 cells were exposed to Nap as described earlier and cells were harvested at different time points for analysis. ATF4 immunostaining of control and *Atf4* siRNA-treated cells showed that siRNA treatment eliminated ATF4 expression in cells post Nap exposure (Fig. 3.5 D). We also found that ATF4-depleted cells exhibited increased expression of 4HNE (Fig. 3.5E, representative images shown in Fig. 3.6 G) and γ-H2AX (Fig. 3.5F, representation images shown in Fig. 3.6 H) at all time points examined (n=3 experiments each, quantitation of cell

fluorescence based on n≥25 cells per experiment) and increased cell death 24 h post injury (Fig. 3.5G). We concluded that the increased levels of oxidative and genotoxic stress and increased cytotoxicity observed in FMRP-deficient cells could be due to a failure to induce the ISR and upregulate ATF4.

In light of the findings in C22 cells, we examined whether perturbations to the ISR are also observed in FMRP-deficient CCs in Nap-treated mice. We counterstained sections from control and *Fmr1* KO lungs post Nap with antisera to both ATF4 and ATF3. Although ATF4 immunostaining was inconclusive, we noted that the levels of ATF3 were negligible in CCs in the control lung and upregulated post Nap (Fig. 3.6 I-J, sections from n=3 mice). Pertinently, the levels of ATF3 in CCs in *Fmr1* KO did not increase post Nap. These results are consistent with a role for FMRP in the induction of ISR in CCs post Nap.

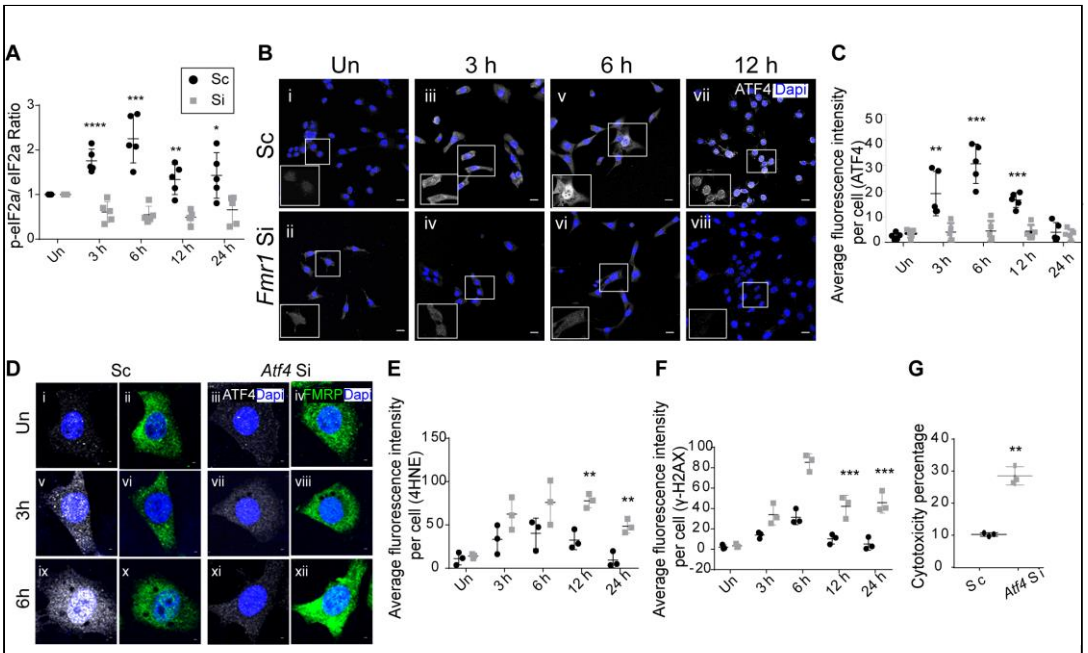

Figure 3.5: FMRP deficient C22 cells fail to upregulate the Integrated Stress Response and induce ATF4, essential for protection from Nap-induced stress. FMRP deficient C22 cells fail to upregulate the Integrated Stress Response and to induce ATF4, essential for protection from Nap-induced stress. (A) Western blot-based quantitation of phospho-eIF2α /eIF2α ratios in Sc and Si cells prior to and post Nap treatment (n=5 experiments). See Fig. S3 for representative blots used for quantitation. **(B i - B viii)** ATF4 immunostaining (white) in Sc (upper panel) and Si cells (lower panel) prior to and post Nap. Note nuclear accumulation of ATF4 in Sc cells by 6 h post Nap (inset). **(C)** Quantitation of ATF4 immunofluorescence per cell in Sc and Si cells prior to and post Nap (n=5 experiments). **(D-G)** Susceptibility of C22 cells to Nap in control (Scrambled siRNA-treated, Sc) and *Atf4* siRNA-treated (Si) cells. **(D i - D xii)** Analysis of ATF4 levels (white) in Sc and Si cells prior to and post Nap treatment. Immunostaining for ATF4 (white) and FMRP (green) in Sc (left panel) and Si (right panel) cells. **(E)** Quantitation of 4HNE immunofluorescence per cell in Sc and Si cells prior to and post Nap. See Fig. S3 for representative images. (F) Quantitation of γ-H2AX immunofluorescence per cell in Sc and Si. See Fig. S3 for representative

experiments). For immunofluorescence analysis ≥ 25 cells were analysed per time point/per experiment. Graphical data represents mean ± s.e.m. Black circle (Sc), Grey square (Si). Unpaired two-tailed t-test (p< .05*, p< .01**, p< .001***). For normality test and two-way ANOVA see Table 3.5. Scale Bar=5 μm.

Table 3.5: Two-way ANOVA to show time-wise and genotype-wise changes in the graphical data used in Fig 3.5

Figure number	Variables	Sum of Squares	F statistic	P value	Normality (Shapiro-Wilk normality test)
Figure 3.5A	Interaction Time Genotype	3.844 1.437 10	F (4, 32) = 12.66 F (4, 32) = 4.733 F (1, 8) = 57.8	P<0.0001 P=0.0041 P<0.0001	Passed
Figure 3.5C	Interaction Time Genotype	1227296089 1496657239 1452261497	F (4, 32) = 21.54 F (4, 32) = 26.27 F (1, 8) = 33.42	P<0.0001 P<0.0001 P=0.0004	Passed
Figure 3.5E	Interaction Time Genotype	1629028646 8957959343 6959867445	F (4, 16) = 4.11 F (4, 16) = 22.6 F (1, 4) = 11.66	P=0.0177 P<0.0001 P=0.0269	Passed
Figure 3.5F	Interaction Time Genotype	2412881952 9546744357 6562205063	F (4, 16) = 9.973 F (4, 16) = 39.46 F (1, 4) = 271.4	P=0.0003 P<0.0001 P<0.0001	Passed

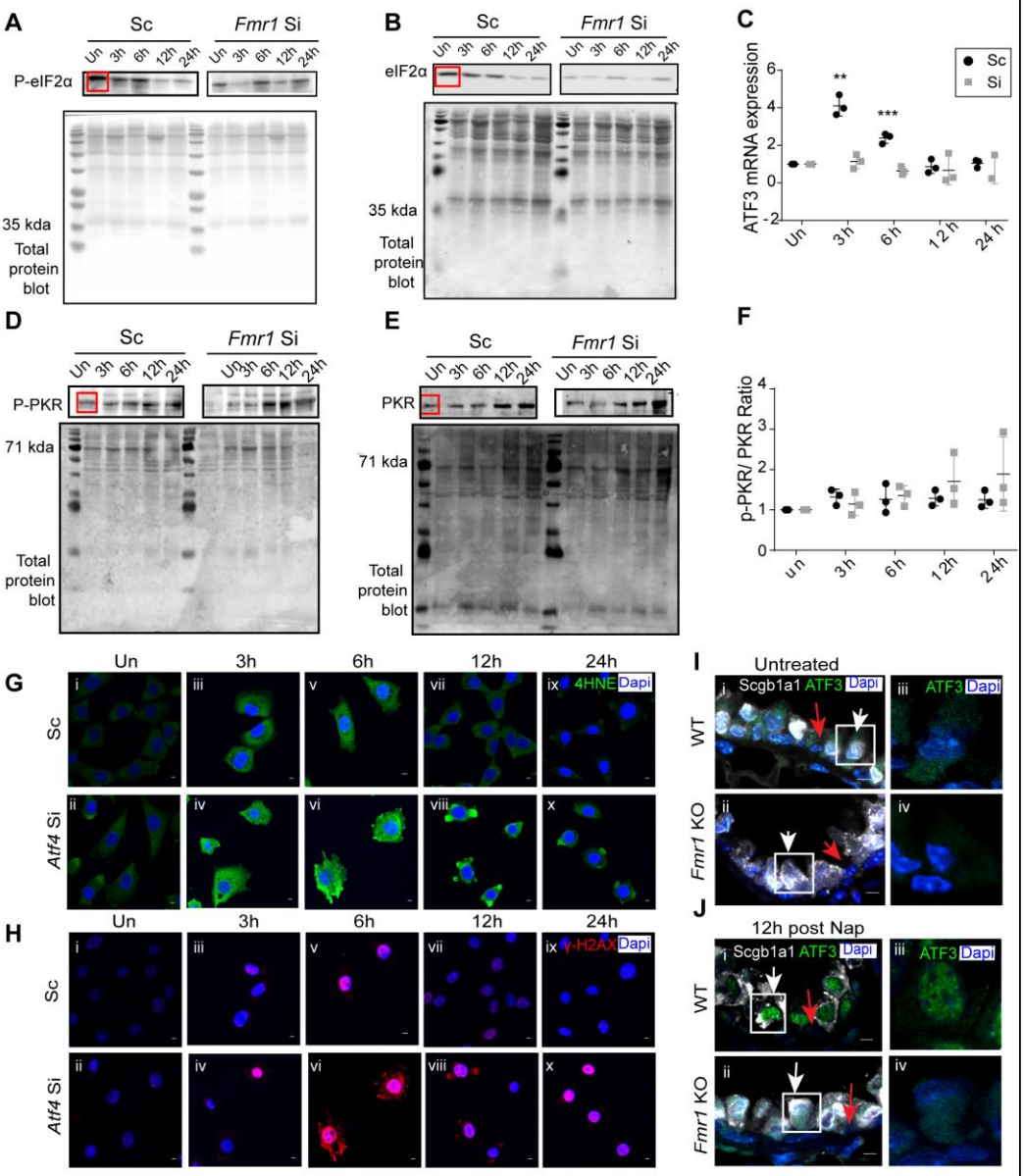

Figure 3.6: Regulation and requirement of the Integrated Stress Response post Nap. (A-B) Blots used for ratiometric quantitation of phospho-eIF2α **(A)** and eIF2α **(B)** in Sc and Si cells prior to and post Nap. Upper panels show blots probed with either anti-phosphorylated eIF2α **(A)** or with anti-eIF2α **(B)** antibodies. Red boxes indicate the area sampled for quantitation of band intensity. Lower panels show respective MemCode stained membranes used for quantitation of total protein/well. **(C)** Quantitative RT-PCR-based analysis of ATF4 target gene *ATF3* in Sc and Si cells prior to and post Nap (n=3 experiments). **(D-E)** Blots used for ratiometric quantitation of phospho-PKR **(D)** and PKR **(E)** in Sc and Si cells prior to and post Nap. Upper panels show blots probed with anti-phospho-PKR **(D)** or anti-PKR **(E)** antibodies. Red box indicates the area sampled for quantitation of band intensity. Lower panels show respective MemCode stained membranes used for quantitation of total protein/well. **(F)** Western blot-based quantitation of phospho-PKR/ PKR ratios in Sc and Si cells prior to and post Nap treatment (n=3 experiments). **(G i - G x)** Immunostaining for 4HNE

(green) in control (Sc) and ATF4-deficient (*Atf4* Si) cells prior to and post Nap. **(H i-H x)** Immunostaining for γ-H2AX (red) Sc and Si cells prior to and post Nap. **(I-J)** Expression of ATF3 in the airways in wild type and *Fmr1* KO mice prior to and post Naphthalene exposure. **(I i – I iv)** ATF3 (green) and Scgb1a1 (white) immunostaining in uninjured wild type **(i, iii)** and *Fmr1* KO **(ii, iv)** mice. **(J i – J iv)** ATF3 (green) and Scgb1a1 (white) immunostaining in wild type **(i, iii)** and *Fmr1* KO **(ii, iv)** mice 12 h post Nap. Note increased nuclear ATF3 expression in CCs in wild type but not *Fmr1* KO (white arrow showing Scgb1a1^{+} cell, red arrow showing ciliated cell). Unpaired two-tailed t-test ($p< .05$*, $p< .01$**, $p< .001$***). For normality tests and two-way ANOVA see Table 3.6. Scale Bar=5μm

Table 3.6: Two-way ANOVA to show time-wise and genotype-wise changes in the graphical data used in Fig 3.6

Figure number	Variables	Sum of Squares	F statistic	P value	Normality (Shapiro-Wilk normality test)
Figure 3.6C	Interaction Time Genotype	9.668 14.04 8.417	F (4, 16) = 17.56 F (4, 16) = 25.49 F (1, 4) = 22.54	P<0.0001 P<0.0001 P=0.0090	Passed
Figure 3.6F	Interaction Time Genotype	1.925 3.227 3.401	F (4, 16) = 1.813 F (4, 16) = 3.039 F (1, 4) = 72.97	P=0.1758 P=0.0484 P=0.0010	Passed

3.2.4 FMRP is also required for protecting C22 cells from 9, 10-PQ induced stress via induction of the Integrated Stress Response

Though Naphthalene is a well-established injury model for mouse lung, more specifically club cells, this model has limitations. Nap is not toxic for the human lung, as it cannot be metabolized in human bronchial cells. So, we tested another chemical 9, 10-Phenanthrenequinone (PQ), which is more generally toxic to different cell types including human bronchial cells (Matsunaga T et al, 2009; Yang M et al, 2018). PQ is an air pollutant that is present at high levels in diesel exhaust particles and is known to trigger oxidative and genotoxic stress (Lavrich KS et al., 2018). As part of our characterization of PQ, we first exposed control (scrambled

siRNA-treated cells) and FMRP-depleted (Fmr1 siRNA-treated cells) C22 cells to a pulse of PQ for 1 h (see Chapter 2) and harvested cells at different timepoints for analysis (shown schematically in Fig. 3.7A). Consistent with our findings in the Nap model, we found that FMRP-depleted C22 cells exhibited increased expression of 4HNE (Fig. 3.7B) and γ-H2AX (Fig. 3.7C) and increased cell death 24 h post exposure (Fig. 3.7D). We then examined ATF4 expression to find that although ATF4 levels increased in Sc cells at 3 h, 6 h post PQ, no expression wasdetected in Si cells (Fig. 3.7E). These experiments showed that PQ treatment does lead to oxidative and genotoxic stress and that FMRP-deficient C22 cells are more susceptible.

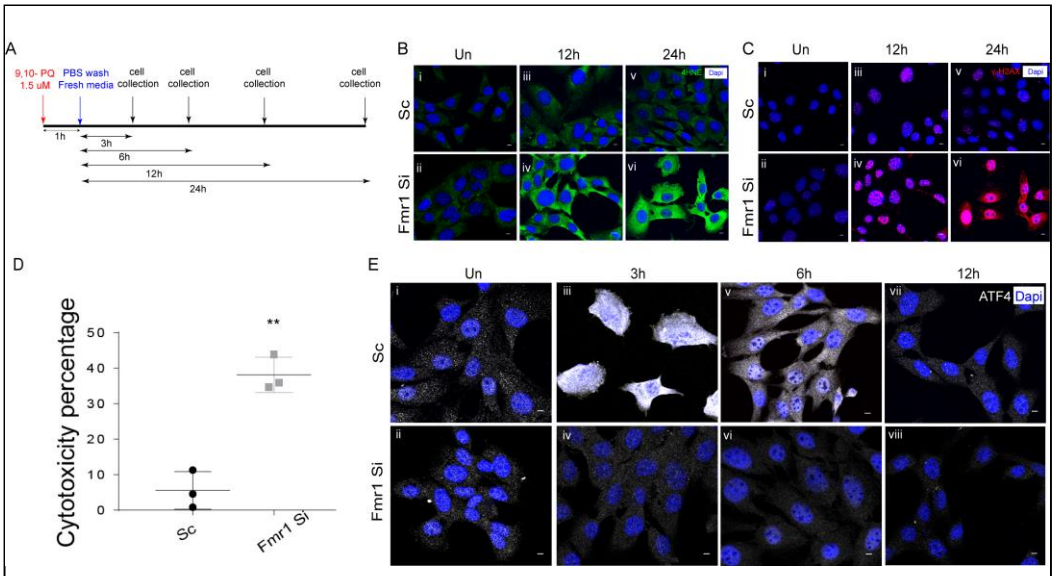

Figure 3.7: FMRP deficient C22 cells fail to upregulate the Integrated Stress Response and induce ATF4 upon 9, 10-Phenanthrenequinone challenge. (A) Schematic showing regimen for PQ injury. **(B i – B vi)** 4HNE immunostaining (green) in Control (Scrambled si-RNA treated, Sc) and Fmr1 si-RNA treated (Si) cells prior to and post PQ (n=3 experiments) **(C i – C vi)** γ-H2AX immunostaining (red) in Sc and Si cells prior to and post PQ (n= 3 experiments). **(D)** Cytotoxicity of PQ in Sc (black circles) and Si (grey squares) cells 24 h post PQ (n=3 experiments). **(E)** ATF4 immunostaining (white) in Sc Si cells prior to and post PQ treatment (n= 3 experiments). Unpaired two-tailed t-test (p< .05*, p< .01**, p< .001***). Scale Bar=5um

3.2.5 FMRP is expressed in the airways of the human lung and protects human bronchial BEAS-2B cells from 9, 10-Phenanthrenequinone induced stress

The findings in the murine lung led us to ask whether FMRP has a conserved role in the human lung. To investigate this possibility, we first examined the distribution of FMRP in the human lung. Paraffin sections stained with FMRP antisera showed that FMRP is expressed throughout the airways and more broadly (Fig. 3.8 A i, ii, iv, n=2 sections each from n=5 independent lung biopsies). Triple labeling experiments with markers for ciliated cells and CCs showed that FMRP is expressed in both ciliated and non-ciliated cells, including CCs. Based on the distribution of FMRP we surmised that the protein could play a role in the airways in the human lung as well.

The BEAS-2B cell line is derived from normal human airways. These cells do not express markers of ciliated cells and, akin to CCs, have characteristics of non-ciliated cells. We stained BEAS-2B cells with FMRP antisera to find that these cells expressed FMRP (Fig. 3.8B, n=6 experiments). We then proceeded to develop an assay to probe the role of FMRP in stress responses in these cells.

Since the susceptibility of airway CCs to Nap is not recapitulated in the human lung or in BEAS-2B cells (data not shown), we utilized a different injury model to probe the role of FMRP in stress responses in human cells. 9, 10-Phenanthrenequinone (PQ) is an air pollutant that is present at high levels in diesel exhaust particles and is known to trigger oxidative and genotoxic stress (Lavrich KS et al., 2018). As part of our characterization of PQ, we first exposed control (scrambled siRNA-treated cells) and FMRP-depleted (*Fmr1* siRNA-treated cells) C22 cells to a pulse of PQ for 1 h and harvested cells at different timepoints for analysis. Consistent with our findings in the Nap model, we found that FMRP-depleted C22 cells exhibited increased expression of 4HNE and γ-H2AX and increased cell death 24 h post exposure (Fig 3.7). We then

examined ATF4 expression to find that although ATF4 levels increased in Sc cells at 3 h, 6 h post PQ, no expression was detected in Si cells (data not shown). These experiments showed that PQ treatment does lead to oxidative and genotoxic stress, that FMRP-deficient C22 cells are more susceptible, and led us to examine the effects of PQ on BEAS-2B cells.

To test the role of FMRP in BEAS-2B cells we determined that the protocol for the knockdown led to a 90% reduction in the levels of FMRP post treatment (Fig. 3.8B-C, n=6 experiments). Next we exposed control (scrambled siRNA-treated cells) and FMRP-depleted (FMR1 siRNA-treated cells) BEAS-2B cells to a pulse of PQ for 1 h and harvested them at different timepoints for analysis (shown schematically in Fig. 3.8D). We found that FMRP-depleted cells exhibited increased expression of 4HNE (Fig. 3.8E-F) and γ-H2AX (Fig. 3.8G-H) at all timepoints examined (n=3 experiments each, quantitation of cell fluorescence based on n≥25 cells per experiment) and increased cell death 24 h post injury (Fig. 3.8I). These experiments showed that FMRP-deficient BEAS2B cells are moresusceptible to PQ.

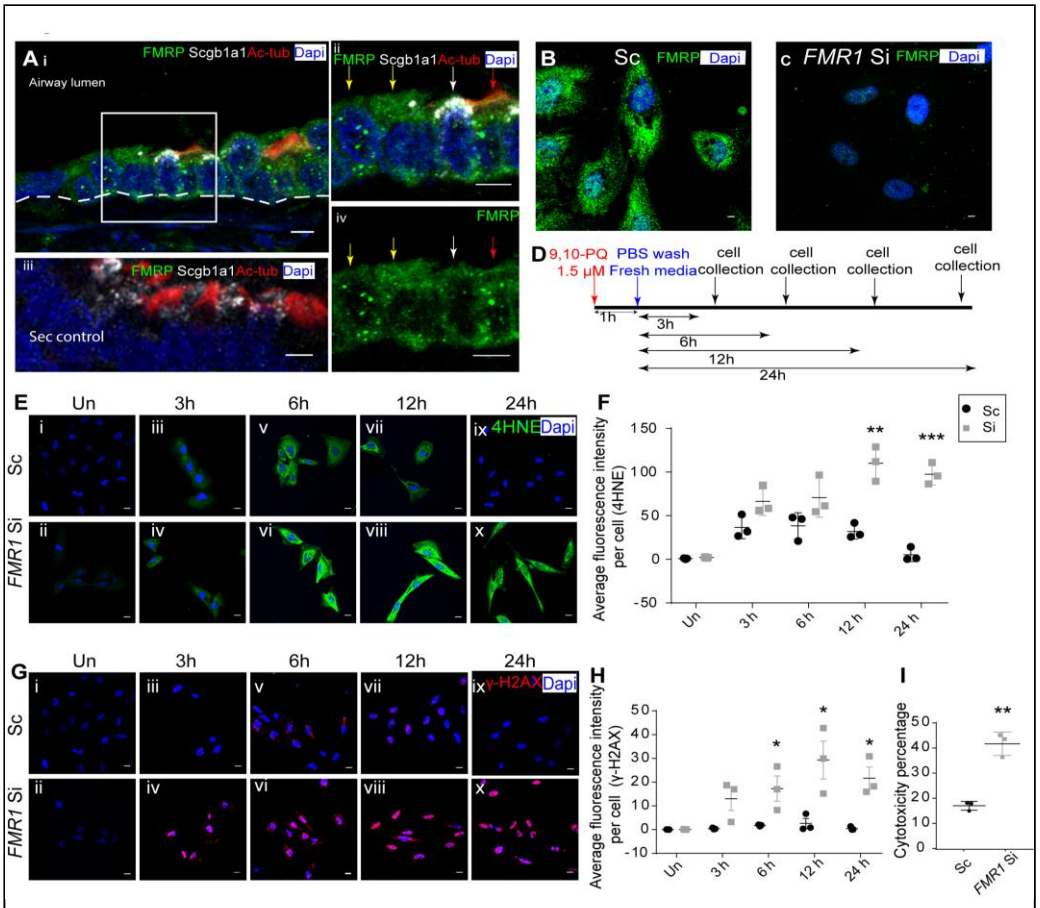

Figure 3.8: FMRP is expressed in the human airways and protects human bronchial BEAS-2B cells from 9, 10-Phenanthrenequinone-induced stress. (A-C) FMRP expression in the human lung and in BEAS-2B cells, a cell line derived from the human bronchial epithelium. **(A i - A iv)** FMRP immunostaining (green) in the distal airways of the human lung. **(A i, A ii, A iv)** Stained section showing FMRP expression in airway non-ciliated cells (Scgb1a1^{+} (white), white arrows; Scgb1a1-, yellow arrows) and ciliated cells (red, red arrow). Boxed area shown at higher magnification in top and bottom panels on the right **(A ii** and **A iv)**. Negative control (secondary alone) for FMRP immunostaining shown in **A iii**. **(B)** FMRP immunostaining of BEAS-2B cells (Control, scrambled siRNA-treated, Sc). **(C)** FMRP immunostaining of *FMR1* siRNA-treated BEAS-2B cells. **(D-I)** Susceptibility of BEAS-2B cells to PQ injury in control (Scrambled siRNA-treated, Sc) and *FMR1* siRNA-treated (Si) cells. **(D)** Schematic showing regimen for PQ injury. **(E-H)** Expression of markers of oxidative (4HNE) and genotoxic (γ-H2AX) stress in Sc and Si cells prior to and post PQ. **(E i - E x)** 4HNE immunostaining (green) in Sc and Si cells prior to and post PQ. **(F)** Quantitation of 4HNE immunofluorescence per cell in Sc and Si cells prior to and post PQ (n=3 experiments). **(G i - G x)** γ-H2AX immunostaining (red) in Sc and Si cells prior to and post PQ. **(H)** Quantitation of γ-H2AX immunofluorescence per cell in Sc and Si cells prior to and post PQ. **(I)** Cytotoxicity of PQ in Sc and Si cells 24 h post PQ exposure (n=3 experiments). For immunofluorescence analysis ≥ 25 cells were analysed per

timepoint/per experiment. Graphical data represents mean ± s.e.m. Black circle (Sc), Grey square (Si). Unpaired two-tailed t-test (p< .05*, p< .01**, p< .001***). For normality tests and two-way ANOVA see Table 3.8. Scale Bar=5 μm.

Table 3.8: Two-way ANOVA to show time-wise and genotype-wise changes in the graphical data used in Fig 3.8

Figure number	Variables	Sum of Squares	F statistic	P value	Normality (Shapiro-Wilk normality test)
Figure 3.8F	Interaction Time Genotype	8452531801 16492731939 16448237473	F (4, 16) = 12.1 F (4, 16) = 23.62 F (1, 4) = 72.34	P=0.0001 P<0.0001 P=0.0010	Passed
Figure 3.8H	Interaction Time Genotype	606376703 825663994 1730144538	F (4, 16) = 3.198 F (4, 16) = 4.354 F (1, 4) = 76.47	P=0.0414 P=0.0143 P=0.0009	Passed

3.2.6 FMRP is required for the induction of the Integrated Stress Response pathway that protects from 9, 10-Phenanthrenequinone induced stress in BEAS2B cells

Next, we determined whether FMRP is required for the induction of the ISR in BEAS-2B cells. As described previously, we probed the phosphorylation status of eIF2α (Fig. 3.9 A, Fig. 3.10 A–B, n=5), the levels of ATF4 induction (Fig. 3.9 B-C, n=5) and the levels of *ATF3* induction (Fig. 3.10 C, n=3), and the ratio of phosphorylation status of PKR (Fig. 3.10 D-F) at different times post PQ. These experiments showed that although p-PKR levels were increased in both Sc and Si post PQ, all of the downstream processes of the ISR were perturbed in Si. We concluded that FMRP is required for the ISR in BEAS-2B cells post PQ.

We then investigated whether the loss of ATF4 would recapitulate the loss of FMRP post PQ. Control (Scrambled siRNA) and *ATF4* siRNA treated BEAS-2B cells were exposed to PQ as previously described and cells were harvested at different timepoints for analysis. Consistent with expectations, *ATF4* siRNA-treated cells showed no anti-ATF4

immunostaining post PQ exposure (Fig. 3.9 D, n=3 experiments). We found that ATF4-depleted BEAS-2B cells exhibited increased expression of 4HNE (Fig. 3.9 E, representative images shown in Fig. 3.10 G) and γ-H2AX (Fig. 3.9 F, representative images shown in Fig. 3.10 H) and increased cell death 24 h post injury (see methods, Fig. 3.9G). These data indicated that the loss of ATF4 largely phenocopies the loss of FMRP in PQ-treated BEAS-2B cells.

The findings in BEAS-2B cells suggested that the role of FMRP in the actuation of the ISR pathway is conserved. To probe whether this finding is more broadly applicable to the lung, we performed the assays described above in another cell line of epithelial origin: A549 cells. We found that although A549 cells are of alveolar origin, they also express FMRP (Fig. 3.11A). Importantly, PQ exposure assays showed that A549 lacking FMRP exhibit higher levels of oxidative and genotoxic stress and fail to ATF4 expression (Fig. 3.11 B-I). Taken together, the studies in BEAS-2B and A549 strongly suggest that FMRP also regulates the induction of the ISR in the human respiratory epithelium.

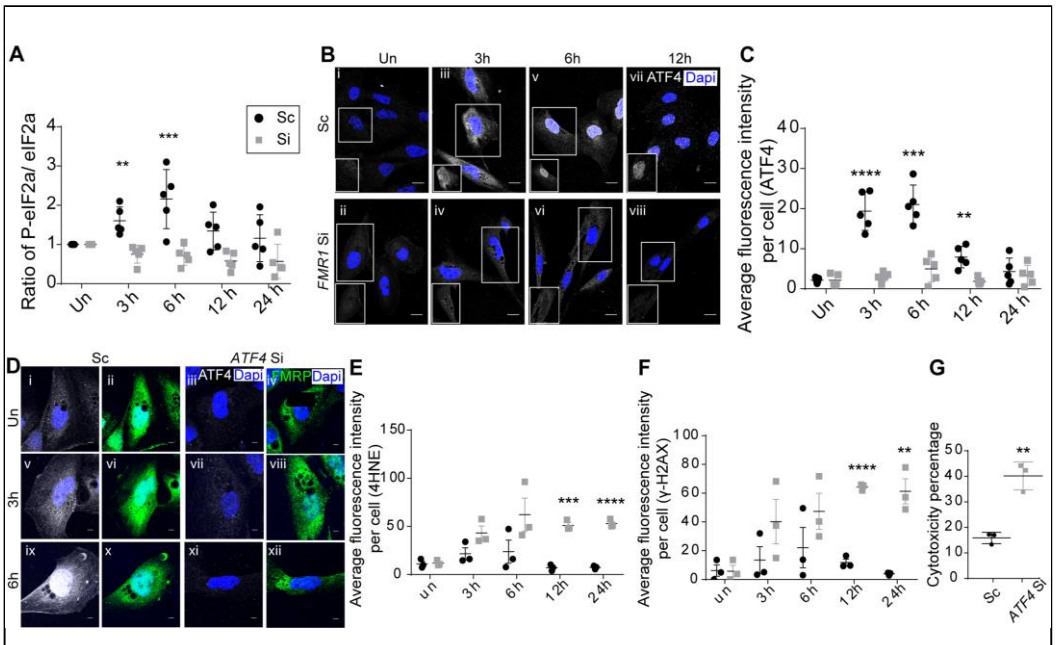

Figure 3.9: FMRP deficient BEAS-2B cells fail to upregulate the Integrated Stress Response and induce ATF4, essential for protection from 9, 10-Phenanthrenequinone induced stress. (A) Western blot-based quantitation of phospho-eIF2α /eIF2α ratios in Sc and Si cells prior to and post PQ treatment (n=5

experiments). See Fig. S4 (A-B) for representative blots used for quantitation. **(B-C)** Analysis of ATF4 prior to and post PQ. **(B i- B viii)** ATF4 immunostaining (white) in Sc (upper panel) and Si cells (lower panel) prior to and post PQ treatment. Note nuclear accumulation of ATF4 in Sc cells by 6 h post PQ treatment (inset). **(C)** Quantitation of ATF4 immunofluorescence per cell in Sc and Si cells prior to and post PQ (n=5 experiments). **(D-G)** Susceptibility of BEAS-2B cells to PQ in control (Scrambled siRNA-treated, Sc) and *ATF4* siRNA-treated (Si) cells. **(D i - D xii)** Analysis of ATF4 levels (white) and FMRP (green) in Sc (left panel) and Si (right panel) cells prior to and post PQ treatment. **(E)** Quantitation of 4HNE immunofluorescence per cell in Sc and Si. See Fig. S4 G for representative images. **(F)** Quantitation of γ-H2AX immunofluorescence per cell in Sc and Si. See Fig. S4 H for representative images. **(G)** Cytotoxicity of PQ in Sc and Si cells 24 h post PQ treatment (n=3 experiments). For immunofluorescence analysis ≥ 25 cells were analysed per timepoint/per experiment. Graphical data represents mean ± s.e.m. Black circle (Sc), Grey square (Si). Unpaired two-tailed t-test (p< .05*, p< .01**, p< .001***). For normality tests and two-way ANOVA see Table 3.9. Scale Bar=5 μm.

Table 3.9: Two-way ANOVA to show time-wise and genotype-wise changes in the graphical data used in Fig 3.9

Figure number	Variables	Sum of Squares	F statistic	P value	Normality (Shapiro-Wilk normality test)
Figure 5A	Interaction Time Genotype	2.693 2.027 6.657	F (4, 32) = 4.493 F (4, 32) = 3.381 F (1, 8) = 30.61	P=0.0054 P=0.0204 P=0.0006	Passed
Figure 5C	Interaction Time Genotype	671166420 865757156 833533615	F (4, 32) = 18.27 F (4, 32) = 23.57 F (1, 8) = 108.7	P<0.0001 P<0.0001 P<0.0001	Passed
Figure 5E	Interaction Time Genotype	2140882670 3078466752 6767050455	F (4, 16) = 3.972 F (4, 16) = 5.711 F (1, 4) = 22.36	P=0.0200 P=0.0047 P=0.0091	Passed
Figure 5F	Interaction Time Genotype	3271361264 3918054177 7807658529	F (4, 16) = 7.662 F (4, 16) = 9.177 F (1, 4) = 10.24	P=0.0012 P=0.0005 P=0.0329	Passed

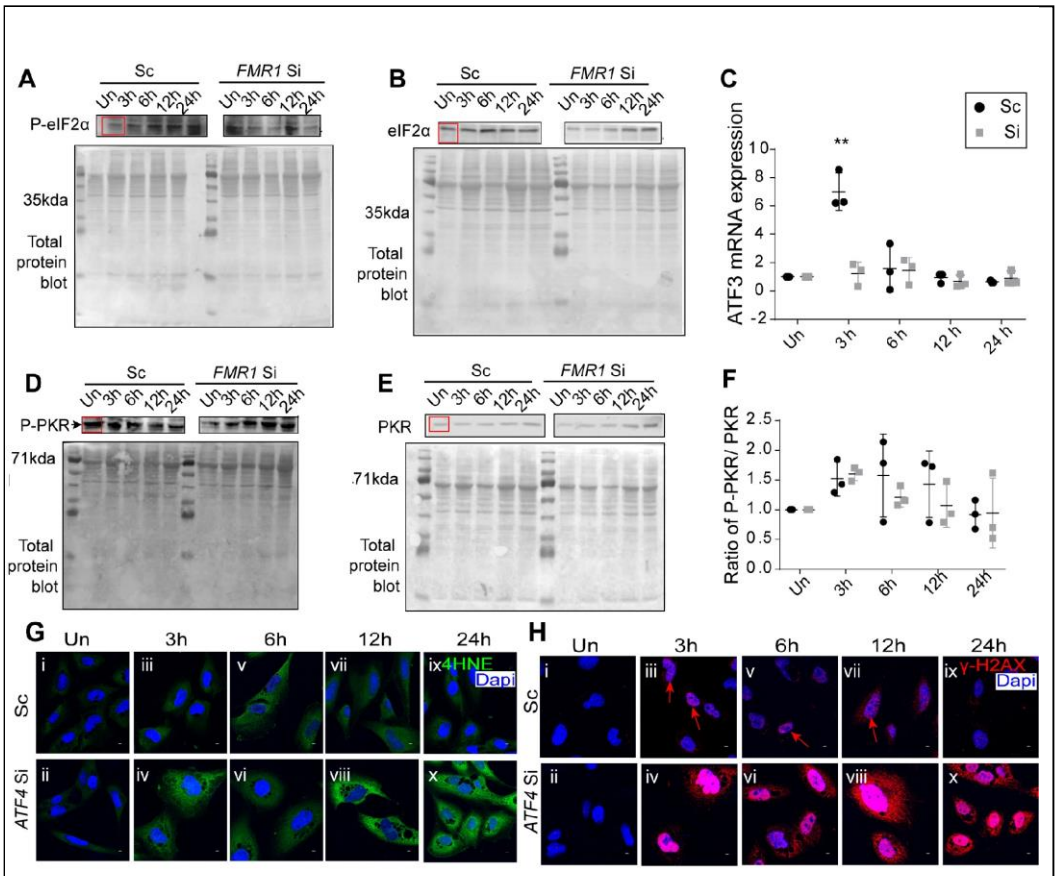

Figure 3.10: Regulation and requirement of the Integrated Stress Response post PQ in BEAS-2B cells. (A-B) Blots used for ratiometric quantitation of phospho-eIF2α **(A)** and eIF2α **(B)** in Sc and Si cells prior to and post PQ. Upper panels show blots probed with either anti-phospho-eIF2α **(A)** or anti-eIF2α **(B)** antibodies. Red boxes indicate the area sampled for quantitation of band intensity. Lower panels show respective MemCode stained membranes used for quantitation of total protein/well. **(C)** Quantitative RT-PCR-based analysis of expression of *ATF3* in Sc and Si cells prior to and post PQ (n=3 experiments). **(D-E)** Blots used for ratiometric quantitation of phospho-PKR **(D)** and PKR **(E)** in Sc and Si cells prior to and post PQ. Upper panels show blots probed with anti-phospho-PKR **(D)** or anti-PKR **(E)** antibodies. Red boxes indicate the area sampled for quantitation of band intensity. Lower panels show respective MemCode stained membranes used for quantitation of total protein/well**. (F)** Western blot-based quantitation of phospho-PKR/ PKR ratios in Sc and Si cells prior to and post PQ treatment (n=3 experiments). **(G i – G x)** Immunostaining for 4HNE (green) in control (Scrambled siRNA treated, Sc) and *ATF4*-siRNA treated (Si) cells prior to and post PQ. **(H i - H x)** Immunostaining for γ-H2AX (red) Sc and Si cells prior to and post PQ. Unpaired two-tailed t-test (p< .05*, p< .01**, p< .001***). For normality test and two-way ANOVA see Table 3.10. Scale Bar=5μm

Table 3.10: Two-way ANOVA to show time-wise and genotype-wise changes in the graphical data used in Fig 3.10

Figure number	Variables	Sum of Squares	F statistic	P value	Normality (Shapiro-Wilk normality test)
Figure 3.10C	Interaction Time Genotype	39.81 48.27 10.59	F (4, 16) = 14.69 F (4, 16) = 17.81 F (1, 4) = 18.4	P<0.0001 P<0.0001 P=0.0128	Passed
Figure 3.10F	Interaction Time Genotype	0.2878 1.675 0.1134	F (4, 16) = 0.9184 F (4, 16) = 5.346 F (1, 4) = 0.2715	P=0.4772 P=0.0063 P=0.6298	Passed

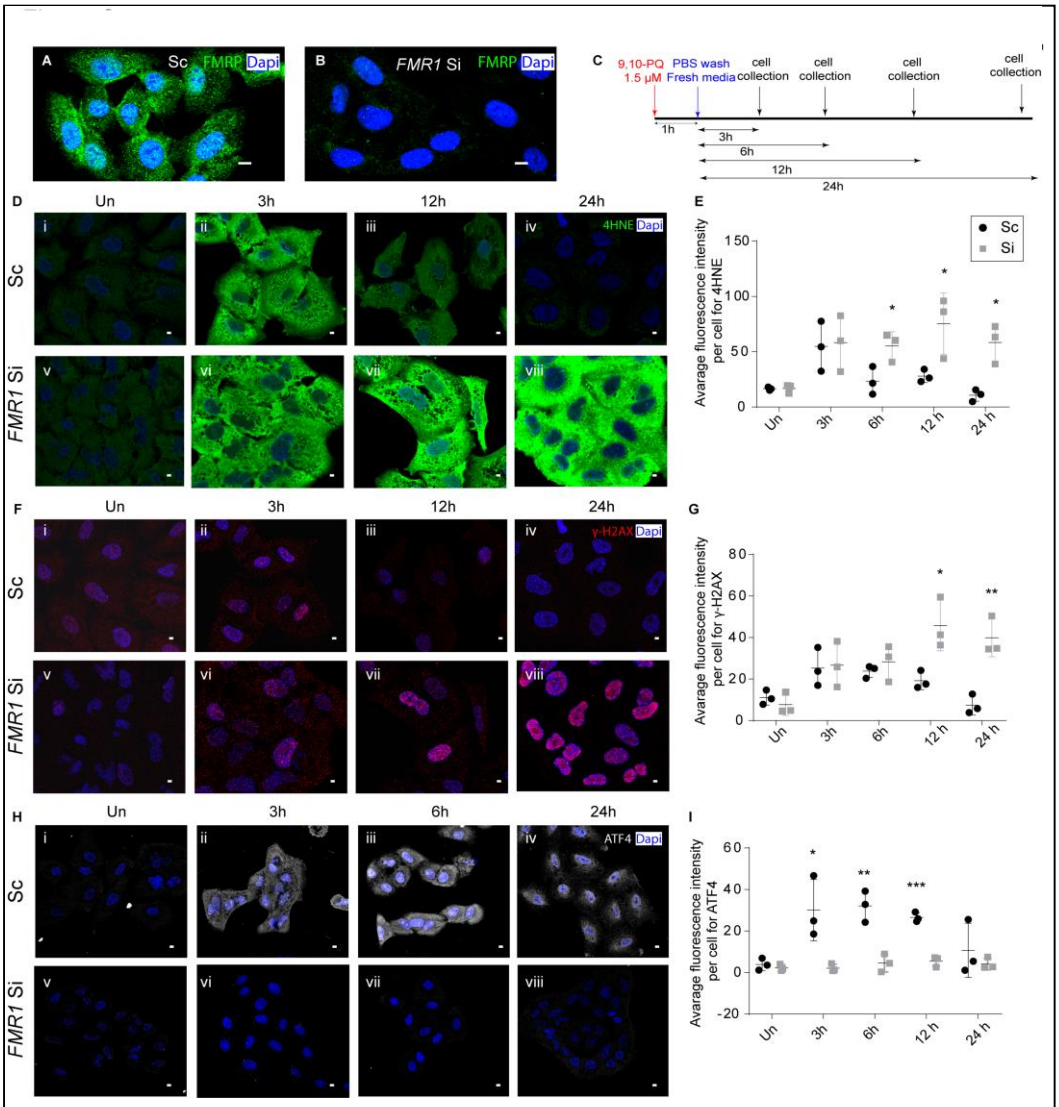

Figure 3.11: FMRP is expressed in human A549 cells and protects it from 9, 10-Phenanthrenequinone-induced stress. (A-B) FMRP expression in the A549 cells. **(A)** FMRP immunostaining of A549 cells. **(B)** FMRP immunostaining of *FMR1* siRNA-treated A549 cells. **(C)** Schematic showing regimen for PQ injury. **(D-I)** Susceptibility of FMRP-deficient A549 cells to PQ injury. **(D-G)** Expression of markers of oxidative (4HNE) and genotoxic (γ-H2AX) stress in (Control,Scrambled siRNA treated) Sc and (*FMR1* siRNA treated) Si cells prior to and post PQ. **(D i - D viii)** 4HNE immunostaining (green) in Sc and Si cells prior to and post PQ. **(E)** Quantitation of 4HNE immunofluorescence per cell in Sc and Si cells post PQ. **(F i- F viii)** γ-H2AX immunostaining (red) in Sc and Si cells prior to and post PQ. **(G)** Quantitation of γ-H2AX immunofluorescence per cell in Sc and Si cells post PQ. **(H i - H viii)** Immunostaining of ATF4 levels (white) in Sc and Si cells prior to and post PQ treatment. (I) Quantitation of ATF4 immunofluorescence per cell in Sc and Si cells prior to and post Nap. ≥ 25 cells were analysed per time point/per experiment, n=3 experiments. Black circle (Sc), Grey square (Si). Graphical data represents mean ±

SEM. Unpaired two-tailed t-test (p< .05*, p< .01**, p< .001***). For normality tests and two-way ANOVA see Table 3.11. Scale Bar=5 μm.

Table 3.11: Two-way ANOVA to show time-wise and genotype-wise changes in the graphical data used in Fig 3.11

Figure number	Variables	Sum of Squares	F statistic	P value	Normality (Shapiro-Wilk normality test)
Figure 3.11E	Interaction Time Genotype	3210672601 5874063911 5128674934	F (4, 16) = 6.877 F (4, 16) = 12.58 F (1, 4) = 6.088	P=0.0020 P<0.0001 P=0.0691	Passed
Figure 3.11G	Interaction Time Genotype	15464281 17602971 11380216	F (4, 16) = 5.435 F (4, 16) = 6.187 F (1, 4) = 63.39	P=0.0059 P=0.0033 P=0.0013	Passed
Figure 3.11I	Interaction Time Genotype	889643528 1043483050 2155934395	F (4, 16) = 3.84 F (4, 16) = 4.505 F (1, 4) = 125.8	P=0.0226 P=0.0125 P=0.0004	Passed

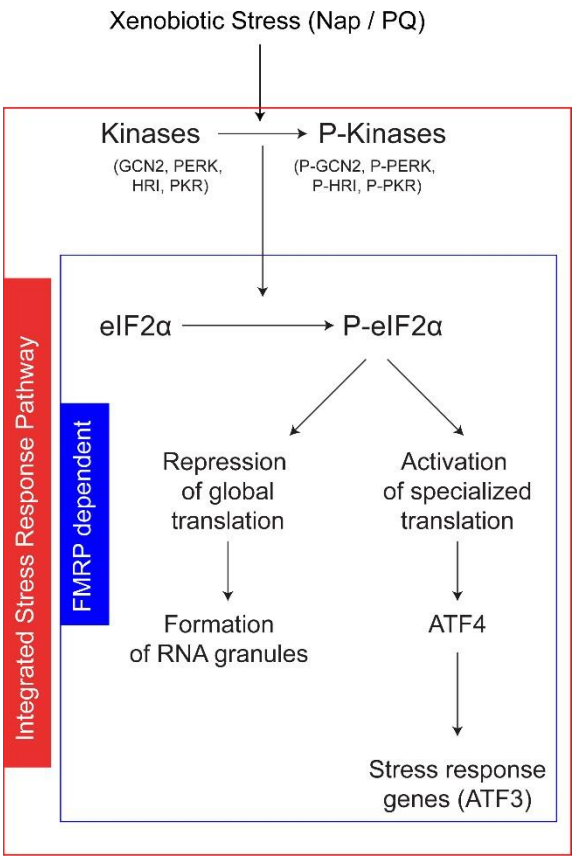

3.12: Model for the role of FMRP in the regulation of the Integrated Stress Response in the lung. Exposure to xenobiotics such as Naphthalene (Nap) and 9,10-Phenanthrenequinone (PQ) result in the activation of at least one of four stress-responsive kinases (GCN2, PERK, PKR, HRI) and to the induction of Integrated Stress Response Pathway (ISR, outlined in red). Our findings suggest that FMRP has an essential role downstream to phosphorylation of kinases (outlined in blue).

3.3 Conclusion

These data from mouse and murine lung derived C22 cells suggest that FMRP is expressed broadly in murine lung epithelium, predominantly in the airways, as well as in C22 cells. Fmr1 knockout mice do not show any marked difference in the lung histology or in the level of stress marker expression under uninjured conditions. But, upon injury, FMRP deficient club cells and club-like c22 cells become more susceptible to cellular stress and stress-mediated cell death. The data shows that FMRP regulates ISR in C22 cells, which is a key pathway of cellular stress response during xenobiotic stress induced by Nap treatment. The

data also shows that in absence of FMRP C22 cells fail to actuate ISR. We found that at multiple steps, like phosphorylation of eIF2α, activation of ATF4 and ATF3, ISR has not been actuated in FMRP deficient C22 cells. Though the underlined mechanism has not been elucidated in great detail.

FMRP has been detected in both human lung and human lung derived cell lines BEAS2B and A549. On this basis, human bronchial cell line BEAS2B and alveolar cell line A549 have been used to investigate the role of FMRP in human lungs. It has been found that in these human lung derived cell lines also, FMRP is required to protect the cells from chemical (9, 10 PQ) induced stress and activation of ISR. Altogether these data indicate FMRP may play a crucial role in protecting the lung from xenobiotic stress.

The study gives an indication that FMRP may act downstream to kinases, as it has been found that phosphorylation of PKR remains unaffected in absence of FMRP. In many cases it has been found that activation of one kinase is sufficient to activate eIF2α. Though in these particular cases of Nap or PQ injury, there is no evidence to say that other kinases are not involved. As the study could not comment on the activation status of other three kinases (GCN2, PERK and HRI) it cannot be strongly concluded that FMRP acts downstream to the stress responsive kinases. Although the molecular mechanism of eIF2α phosphorylation by FMRP, remains to be examined.

Contribution:

Conceptualization and experiment design: Dr. Arjun Guha, Deblina Sain Basu

Data collection and analysis: Deblina Sain Basu, Rital Bhavsar, Imtiyaz Gulami, Saraswati Chavda, Sai Manoz Lingamallu

Troubleshooting advises and critical review: Dr. Arjun Guha, Dr. Ravi Muddashetty, Dr. Rajesh Thimmulappa, Dr. Sumantra Chatterji, Dr. Aditi Bhattacharya

Sample collection (human lung tissue): Dr. Chandrakanth Veeranna

References

1. **Adjibade P, St-Sauveur VG, Bergeman J, Huot ME, Khandjian EW, Mazroui R.** DDX3 regulates endoplasmic reticulum stress-induced ATF4 expression. Scientific reports. **2017** Oct 23;7(1):1-2.

2. **Alpatov R, Lesch BJ, Nakamoto-Kinoshita M, Blanco A, Chen S, Stützer A, Armache KJ, Simon MD, Xu C, Ali M, Murn J.** A chromatin-dependent role of the fragile X mental retardation protein FMRP in the DNA damage response. Cell. **2014** May 8;157(4):869-81.

3. **Anderson P. KedershaN.(2006)**. RNA Granules. J. Cell Biol.;172:803-8.

4. **Anderson P, Kedersha N.** Stress granules: the Tao of RNA triage. Trends in biochemical sciences. **2008** Mar 1;33(3):141-50.

5. **Bechara EG, Didiot MC, Melko M, Davidovic L, Bensaid M, Martin P, Castets M, Pognonec P, Khandjian EW, Moine H, Bardoni B.** A novel function for fragile X mental retardation protein in translational activation. PLoS Biol. **2009** Jan 20;7(1):e1000016.

6. Buckpitt A, Boland B, Isbell M, Morin D, Shultz M, Baldwin R, Chan K, Karlsson A, Lin C, Taff A, West J. Naphthalene-induced respiratory tract toxicity: metabolic mechanisms of toxicity. Drug metabolism reviews. 2002 Jan 1;34(4):791-820.

7. **Demello DE, Mahmoud S, Ryerse J, Hoffmann JW.** Generation and characterization of a conditionally immortalized lung clara cell line from the H-2K b-tsA58 transgenic mouse. In Vitro Cellular & Developmental Biology-Animal. **2002** Mar 1;38(3):154-64.

8. **Didiot MC, Subramanian M, Flatter E, Mandel JL, Moine H.** Cells lacking the fragile X mental retardation protein (FMRP) have normal RISC activity but exhibit altered stress granule assembly. Molecular biology of the cell. **2009** Jan 1;20(1):428-37.

9. **El Bekay R, Romero-Zerbo Y, Decara J, Sanchez-Salido L, Del Arco-Herrera I, Rodríguez-de Fonseca F, De Diego-Otero Y.** Enhanced markers of oxidative stress, altered antioxidants and NADPH-oxidase activation in brains from Fragile X mental retardation 1-deficient mice, a pathological model for Fragile X syndrome. European Journal of Neuroscience. **2007** Dec;26(11):3169-80.

10. **He CH, Gong P, Hu B, Stewart D, Choi ME, Choi AM, Alam J.** Identification of activating transcription factor 4 (ATF4) as an Nrf2-interacting protein: implication for heme oxygenase-1 gene regulation. Journal of biological chemistry. **2001** Jun 15;276(24):20858-65.

11. **Konsavage WM, Zhang L, Wu Y, Shenberger JS.** Hyperoxia-induced activation of the integrated stress response in the newborn rat lung. American Journal of Physiology-Lung Cellular and Molecular Physiology. **2012** Jan 1;302(1):L27-35.

12. **Lavrich KS, Corteselli EM, Wages PA, Bromberg PA, Simmons SO, Gibbs-Flournoy EA, Samet JM**. Investigating mitochondrial dysfunction in human lung cells exposed to redox-active PM components. Toxicology and applied pharmacology. **2018** Mar 1;342:99-107.

13. **Li G, Scull C, Ozcan L, Tabas I.** NADPH oxidase links endoplasmic reticulum stress, oxidative stress, and PKR activation to induce apoptosis. Journal of Cell Biology. **2010** Dec 13;191(6):1113-25.

14. **Lima-Cabello E, Garcia-Guirado F, Calvo-Medina R, el Bekay R, Perez-Costillas L, Quintero-Navarro C, Sanchez-Salido L, de Diego-Otero Y.** An abnormal nitric oxide metabolism contributes to brain oxidative stress in the mouse model for the fragile X syndrome, a possible role in intellectual disability. Oxidative medicine and cellular longevity. **2016** Oct;2016.

15. **Linder B, Plöttner O, Kroiss M, Hartmann E, Laggerbauer B, Meister G, Keidel E, Fischer U.** Tdrd3 is a novel stress granule-associated protein interacting with the Fragile-X syndrome protein FMRP. Human molecular genetics. **2008** Oct 15;17(20):3236-46.

16. **Lozon TI, Eastman AJ, Matute-Bello G, Chen P, Hallstrand TS, Altemeier WA.** PKR-dependent CHOP induction limits hyperoxia-induced lung injury. American Journal of Physiology-Lung Cellular and Molecular Physiology. **2011** Mar 1.

17. **Li ZM, Xue CJ, Wang JH, Wang QM.** Comparative study of the characteristics of typical mineral deposits in Xinjiang, China, and its neighboring countries and regions. Geology in China. **2006**;33(1):160-8.

18. **Matsunaga T, Arakaki M, Kamiya T, Endo S, El-Kabbani O, Hara A.** Involvement of an aldo-keto reductase (AKR1C3) in redox cycling of 9, 10-phenanthrenequinone leading to apoptosis in human endothelial cells. Chemico-biological interactions. **2009** Sep 14;181(1):52-60.

19. **Reineke LC, Kedersha N, Langereis MA, van Kuppeveld FJ, Lloyd RE.** Stress granules regulate double-stranded RNA-dependent protein kinase activation through a complex containing G3BP1 and Caprin1. MBio. **2015** May 1;6(2).

20. **Romero-Zerbo Y, Decara J, El Bekay R, Sanchez-Salido L, Del Arco-Herrera I, De Fonseca FR, De Diego-Otero Y.** Protective effects of melatonin against oxidative stress in Fmr1 knockout mice: a therapeutic

research model for the fragile X syndrome. Journal of pineal research. **2009** Mar;46(2):224-34.

21. **Santoro MR, Bray SM, Warren ST**. Molecular mechanisms of fragile X syndrome: a twenty-year perspective. Annual Review of Pathology: Mechanisms of Disease. **2012** Feb 28;7:219-45.

22. **Sarcinelli C, Dragic H, Piecyk M, Barbet V, Duret C, Barthelaix A, Ferraro-Peyret C, Fauvre J, Renno T, Chaveroux C, Manié SN.** ATF4-Dependent NRF2 transcriptional regulation promotes antioxidant protection during endoplasmic reticulum stress. Cancers. **2020** Mar;12(3):569.

23. S**olomon S, Xu Y, Wang B, David M, Schubert P, Kennedy D, Schrader JW.** Distinct structural features of Caprin-1 mediate its interaction with G3BP-1 and its induction of phosphorylation of eIF2α, entry to cytoplasmic stress granules, and selective interaction with a subset of mRNAs. Molecular and Cellular Biology. **2007** Jan 8.

24. **Song G, Napoli E, Wong S, Hagerman R, Liu S, Tassone F, Giulivi C.** Altered redox mitochondrial biology in the neurodegenerative disorder fragile X-tremor/ataxia syndrome: use of antioxidants in precision medicine. Molecular Medicine. **2016** Jan;22(1):548-59.

25. **Stripp BR, Maxson KA, Mera RA, Singh G.** Plasticity of airway cell proliferation and gene expression after acute naphthalene injury. American Journal of Physiology-Lung Cellular and Molecular Physiology. **1995** Dec 1;269(6):L791-9.

26. **Taha MS, Haghighi F, Stefanski A, Nakhaei-Rad S, Kazemein Jasemi NS, Al Kabbani MA, Görg B, Fujii M, Lang PA, Häussinger D, Piekorz RP.** Novel FMRP interaction networks linked to cellular stress. The FEBS journal. **2021** Feb;288(3):837-60.

27. **van't Wout EF, Hiemstra PS, Marciniak SJ.** The integrated stress response in lung disease. American journal of respiratory cell and molecular biology. **2014** Jun;50(6):1005-9.

28. **Van Winkle LS. Buckpitt AR, Nishio SJ, Isaac JM, Plopper CG.** Cellular response in naphthalene-induced Clara cell injury and bronchiolar epithelial repair in mice. Am J Physiol Lung Cell Mol Physiol. **1995**;269:L800-18.

29. **Wong HR, Wispe JR.** The stress response and the lung. American Journal of Physiology-Lung Cellular and Molecular Physiology. **1997** Jul 1;273(1):L1-9.

30. **Zhou Z, Cao M, Guo Y, Zhao L, Wang J, Jia X, Li J, Wang C, Gabriel G, Xue Q, Yi Y.** Fragile X mental retardation protein stimulates ribonucleoprotein assembly of influenza A virus. Nature communications. **2014** Feb 10;5(1):1-2.

31. **Yang M, Ahmed H, Wu W, Jiang B, Jia Z.** Cytotoxicity of air pollutant 9, 10-Phenanthrenequinone: role of reactive oxygen species and redox signaling. BioMed research international. **2018** Jun 10;2018.

Chapter 4

Probing possible alternate mechanisms by which FMRP may regulate stress responses in the lung

4.1 Possible explanation for FMRP phenotype in the lung

As discussed in the Introduction (chapter- I) there are mainly three existing models to describe the role of FMRP in cellular stress response; FMRP dependent regulation of SOD1, perturbation of SG biogenesis in FMRP deficient cells, and FMRP dependent DNA damage response in replication stress. We tried to probe whether these roles for FMRP are also relevant to the lung in the context of the injury models that we have tested. The following sections will shed light on these possibilities to explain FMRP phenotype in the context of our injury models.

4.2 Regulation of Superoxide dismutase 1 expression by FMRP in the lung

4.2.1 Superoxide dismutase as a group of metalloprotein enzymes

Superoxide dismutase (SOD) is a group of enzymes that catalyze the conversion of superoxide radicals into oxygen (O_2) and hydrogen peroxides (H_2O_2) (Younus H, 2018; Zelko IL, 2002). There are three known forms of SOD present in humans and most other mammals. Among these, SOD1 is cytoplasmic, SOD2 is mitochondrial, and SOD3 is secreted form that is found in the extracellular matrix. SOD1 and SOD3 have Cu-Zn at their active site, whereas SOD2 has Mn^{+2} at its reactive center (Zelko IL et al, 2002; Okado-Matsumoto A, 2001). SODs play an important role in quenching reactive oxygen species (ROS) during oxidative stress and are extremely important for lung health. Mutation of SOD1 gene causes pulmonary restriction (a decrease in total volume of air due to decreased elasticity of the lung) at very early developmental stages, and also Amyotrophic lateral sclerosis (ALS), a neurodegenerative disease (Stoica L et al, 2017; Tankersley CG et al, 2007; Noor R et al, 2002). Impaired activity of SOD2 is related to asthma pathophysiology and SOD3 has been shown to protect the lung from oxidative stress mediated injury (Zelko IL et al, 2002; Constantino L et al, 2014; Siedlinski M et al, 2009).

4.2.2 FMRP dependent Superoxide dismutase1 expression in the mouse brain

Superoxide dismutase 1 (SOD1) is a cytoplasmic protein that exists as a homodimer of 32 kDa. The study of Bechara et al (Bechara et al, 2009) on murine brain, revealed that in absence of FMRP SOD1 translation was reduced in brain tissue, hence resulted in elevated level of oxidative stress. They also showed that FMRP physically interact with SOD1 mRNA and positively regulates translation of SOD1 in brain. SOD1 mRNA has a conserved 64 nucleotide fragment with three independent stem loop structures called SoSLIP domain, which interacts with the C-terminal domain of FMRP. This finding led us to investigate the interaction between SOD1 and FMRP in the lung. The idea was to find out whether decreased level of FMRP-dependent SOD1 expression can explain the susceptibility of FMRP deficient lung or lung derived cells to xenobiotic stress. This could also potentially reveal the role of FMRP in directly modulating the expression of stress related genes other than those involved in the ISR pathway.

4.3 Results

4.3.1 FMRP does not regulate SOD1 expression in the lung

To investigate whether FMRP has any role in SOD1 expression in the lung, we first tried to validate finding of Bechara et al in our mouse model. To do this we used Western blot technique and analysed brain lysates from WT and Fmr1 KO mice. We could recapitulate the the decreased level of SOD1 expression in Fmr1 KO mice as compared to the WT (n=3; Fig 4.1A i –ii).

Next, we analysed the whole lung lysates through western blot and probed for SOD1 levels. This data shows no significant difference (n=3) in the levels of SOD1 between WT and Fmr1 KO lung (Fig 4.1A

iii- iv). Taken together the results suggest that unlike in the brain, SOD1 translation is not affected in the lungs of Fmr1 KO mice.

To further confirm the finding, we examined the expression of SOD1 in adult lungs from wild-type (WT) and Fmr1 KO animals by immunostaining. Lung sections from WT mice were stained with anti-SOD1 antisera and examined under a confocal microscope (5μm, n=3 mice). We observed that SOD1 is predominantly expressed in airway club cells, but failed to detect any noticeable difference in the levels of SOD1 between WT (Figure 4.1B; SOD1 in green, acetylated tubulin in red, marking the cilia of ciliated cells and Scgb1a1 in white, marking the club cells) and KO (Fig 4.1C) lung tissues.

We also examined the expression of SOD1 in C22 (mouse clara cell line) and BEAS-2B (human bronchial non-ciliated cell line) cells with and without FMRP. Control (Scrambled siRNA treated) and Fmr1 si RNA treated C22 cells were stained with anti-SOD1 antisera and images were taken with a confocal microscope (Fig 4.1D, 4.1E). Total cell fluorescence was analyzed in 25 cells (number of experiments=3) using ImageJ software (Fig 4.1F). No obvious difference was detected in the level of SOD1 protein in the presence or absence (~80% reduction) of FMRP. We analyzed BEAS-2B cells in a similar way, but could not detect any significant difference in the level of SOD1 between control (Sc- treated, Figure 4.1G) and FMR1 si-RNA treated (Fig 4.1H) cells. Average fluorescence intensity per cell from control and FMRP-deficient cells were represented in a scatter plot (Fig 4.1I), which also reveals the same (number of experiments =3). Taken together these data suggest that though SOD1 expression is decreased in the brain tissue of Fmr1 KO mice compared to the WT littermate, there is no obvious difference in the level of SOD1 in the lung or bronchial cell lines in the presence or absence of FMRP. So, we may conclude that there is no role of FMRP in regulation of SOD1 expression in the lung at homeostatic

condition and that reduced levels of SOD1 is unlikely to be a major fact in determining susceptibility to Nap induced stress.

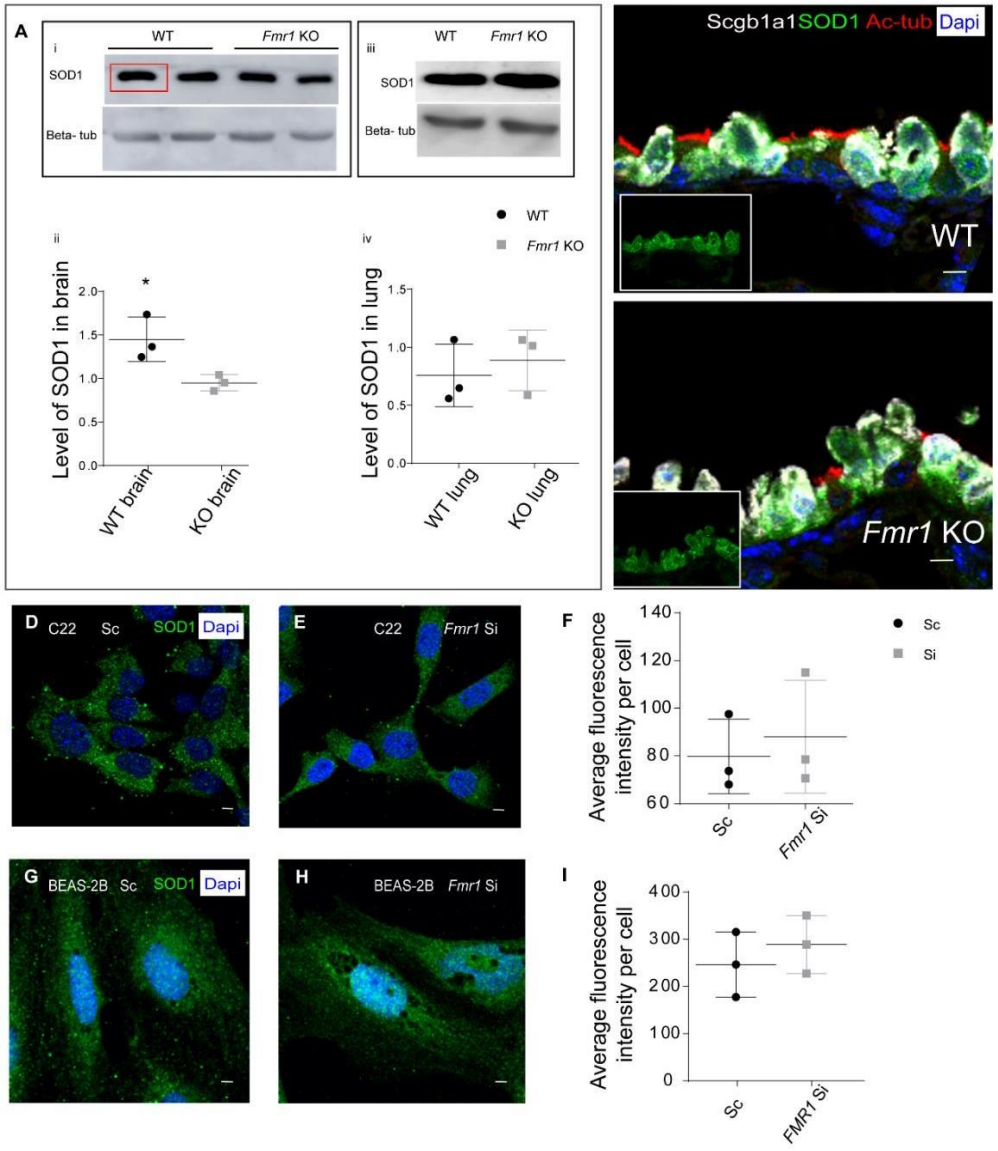

Figure 4.1: FMRP does not regulate SOD1 expression in lung and bronchial cell lines (A i- A iv) Western blot-based quantitation of SOD1 in WT and Fmr1 KO brain and lung (n=3 experiments). Blots used for quantitation of SOD1 from brain **(A i)** and lung **(A iii)** tissue lysate in WT and Fmr1 KO mice. Upper panels show blots probed with anti-SOD1 and lower panels show blots probed with anti-β-tubulin **(A i, Aiii)** antibodies. Red boxes indicate the area sampled for quantitation of band intensity. **(B-C)** SOD1 expression in the murine lung. SOD1 immunostaining (green) in airway epithelial cells. Shown here are CCs (white, Scgb1a1) and ciliated cells (red, acetylated-tubulin) in wild-type **(B)** and Fmr1 KO **(C)**. **(D-F)** SOD1 expression in the C22 cell line with or without FMRP. SOD1 immunostaining (green) in control

(Scrambled siRNA-treated, Sc) **(D)** and Fmr1 siRNA-treated (Si) cells **(E)**. **(F)** Quantitation of SOD1 immunofluorescence per cell in Sc (black bars) and Si (grey bars). **(G-I)** SOD1 expression in the BEAS-2B cell line with or without FMRP. SOD1 immunostaining (green) in control (Scrambled siRNA-treated, Sc) **(G)** and Fmr1 siRNA-treated (Si) cells **(H)**. **(I)** Quantitation of SOD1. Immunofluorescence per cell in Sc (black bars) and Si (grey bars). Graphical data represents mean ± s.e.m. Unpaired two-tailed t-test ($p < .05$*, $p < .01$**, $p < .001$***). Scale bar= 5µm.

4.3.2 FMRP may regulate SOD1 expression post injury in a context specific way

From our preliminary experiments it was quite clear to us that SOD1 translation is not under the regulation of FMRP, at least in the homeostatic lung. This led us to investigate if there was any inter-relation between FMRP and SOD1 expressions in the lung during stress, such as Naphthalene injury. In order to do this, we stained sections from mouse lung, both prior to and post Nap injury (12h and 24h) with anti-SOD1 antisera, and examined under confocal microscope. We observed a dramatic increase of SOD1 expression in WT lung from 12h to 24h post nap injury (Fig 4.2A ii- iii). We did not detect any change in the Fmr1 KO lung (Fig 4.2A v- vi) during 12h to 24 h post Nap. These data suggest FMRP may have a role inregulating translation of SOD1 post injury in the mouse lung.

Next, we examined SOD1 expression in C22 cells with and without FMRP, prior to and post Nap injury by immunostaining method. Control (Sc treated) and Fmr1 si RNA treated C22 cells were incubated with 75µg ml^{-1} Naphthalene for 1 h, then washed and fresh media was added. Cells were analyzed at 3h, 6h and 12h post injury (Fig 4.2B). The analysis showed up-regulation of SOD1 expression in control (Fig 4.2C i-iv, Sc) at 3h and 6h post injury, and theexpression came down to baseline at 12h post injury. However, levels of SOD1 did not show any increase in the Fmr1 deficient C22 cells post injury at any time point (Fig 4.2C v-vi, Si). The analysis of average fluorescence intensity showed significant difference

between control and Fmr1 knocked down cells at 3h and 6h (Fig 4.2D). We also examined C22 cells prior to and post 9,10-Phenanthrenequinone (PQ) injury in the presence and absence of FMRP (Fig 4.2E). This experiment revealed that SOD1 up-regulation is partially dependent on FMRP post PQ in C22 cells. There were some increases in the level of SOD1 at 3h and 6h even in FMRP deficient cells (Fig 4.2F v-vii), however, the increase was not up to the level of SOD1 increase in control (Fig 4.2F i- iii). Analysis of average fluorescence intensity showed significant difference in the level of SOD1 expression post PQ between control (Sc) and FMRP deficient C22 cells (Fig 4.2G), but also showed some increase in SOD1 level in Fmr1 si treated cells post PQ. These results suggest SOD1 up-regulation in C22 cells could be dependent on FMRP post Nap injury.

Then we analyzed BEAS-2B cells post PQ at 3h, 6h and 12h. Unexpectedly, we failed to detect any difference between control and FMR1 siRNA treated cell population (Fig 4.2H, 4.2I). Both control and FMRP deficient BEAS-2B cells were almost equally able to up-regulate SOD1 expression post PQ. These infers post injury SOD1 up-regulation is dependent on FMRP in mice but not in humans.

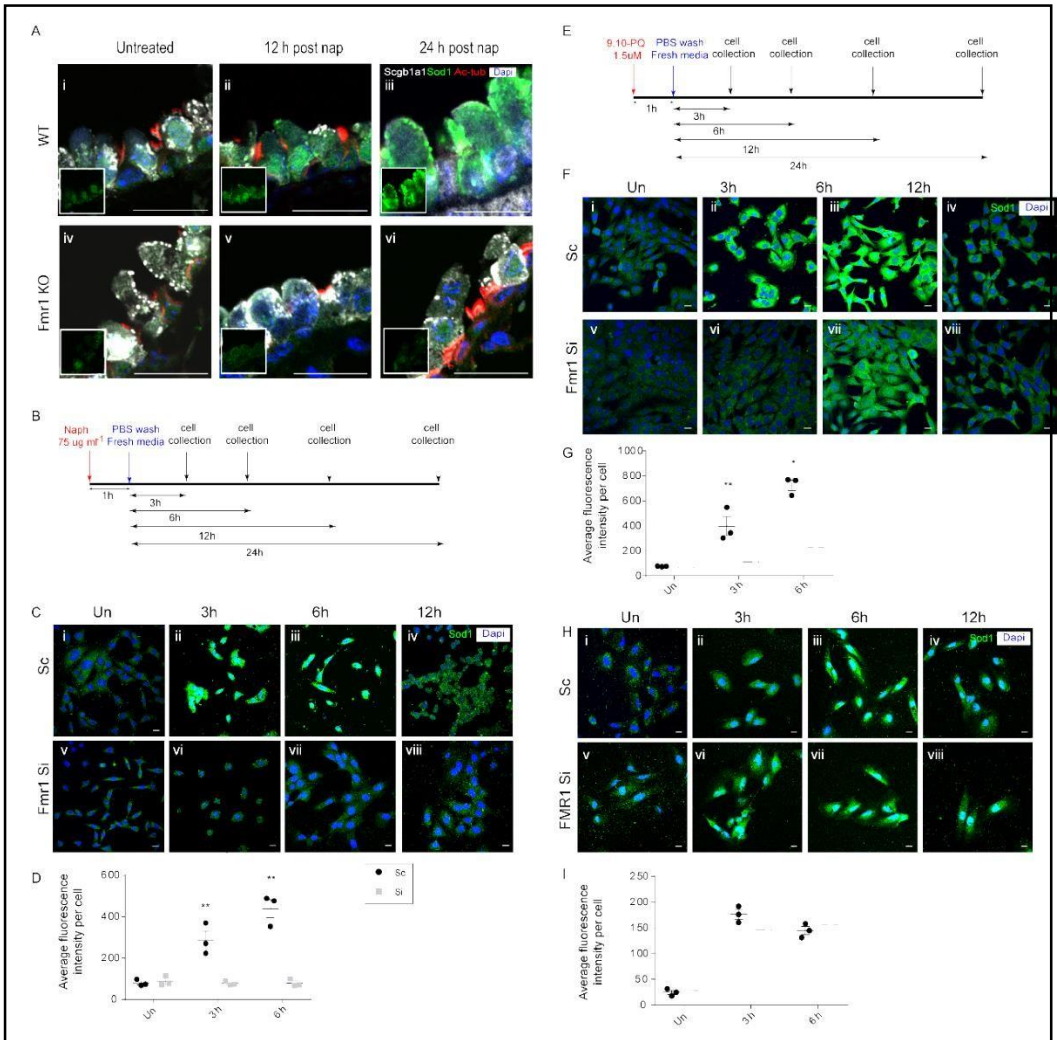

Figure 4.2: FMRP partially regulates Superoxide Dismutase 1 (SOD1) expression post xenobiotic stress in mouse but not in human. (A) SOD1 immunostaining (green, shown in insets) in control and *Fmr*1 KO lungs prior to and post Nap treatment. In control lungs (upper panel) SOD1 immunostaining is detected in the airways in Club cells (Scgb1a1, white) prior to Nap treatment and increased in intensity post Nap treatement. In *Fmr*1 KO lungs (lower panel) SOD1 immunostaining is detected in Clubcells prior to Nap but not increased at 12, 24 hr post Nap. **(B)** Schematic showing regimen for Nap treatment on C22 cells. **(C i – C viii)** Immunostaining for SOD1 in control (Sc) and FMRP-deficient (FMR1 Si) C22 cells at different points post Nap exposure. **(D)** Quantitation of levels of SOD1 immunostaining per cell in Sc (black bars) and Si (grey bars). For SOD1 total cell fluorescence ≥ 25 cells were analysed per timepoint, per experiment (n=3 different sets of experiment). (**E)** Schematic showing regimen for 9, 10-PQ treatment on C22 cells. **(F i- F viii)** Immunostaining for SOD1 in control (Sc) and FMRP-deficient (FMR Si) C22 cells at different points post PQ exposure. In contrast to Nap exposure, the levels of SOD1 show a slight increase in C22 cells post PQ (see figures 6 hr timepoint). **(G)** Quantitation of levels of SOD1

immunostaining per cell in Sc (black bars) and Si (grey bars). For SOD1 total cell fluorescence ≥ 25 cells were analysed per timepoint, per experiment (n=3 different sets of experiment). **(H i – H viii)** Immunostaining for SOD1 in control (Sc) and FMRP-deficient (FMR Si) BEAS-2B cells at different points post PQ exposure. Note that the levels of SOD1 immunostaining are comparable in Sc (upper panel) and Si (lower panels) at all timepoints post PQ. **(I)** Quantitation of levels of SOD1 immunostaining per cell in Sc (black bars) and Si (grey bars). For SOD1 total cell fluorescence ≥ 25 cells were analysed per timepoint, per experiment (n=3 different sets of experiment). Scale Unpaired two-tailed t-test (p< .05*, p< .01**, p< .001***). Graphical data represents mean ± s.e.m. Unpaired two-tailed t-test (p< .05*, p< .01**, p< .001***). For normality tests see Table 4.2. Scale bar= 5µm.

Table 4.2. Two-way ANOVA to show time-wise and genotype-wise changes in the graphical data used in Fig 4.2

Figure number	Variables	Sum of Squares	F statistic	P value	Normality (Shapiro-Wilk normality test)
Figure 4.2D	Interaction Time Genotype	1037389574 919440281 1574610165	F (2, 12) = 22.78 F (2, 12) = 20.19 F (1, 12) = 69.15	P<0.0001 P=0.0001 P<0.0001	passed
Figure 4.2G	Interaction Time Genotype	1780486850 4957728271 3189319886	F (2, 8) = 22.59 F (2, 8) = 62.89 F (1, 4) = 45.72	P=0.0005 P<0.0001 P=0.0025	passed
Figure 4.2I	Interaction Time Genotype	14111297 671415182 837589	F (2, 8) = 2.737 F (2, 8) = 130.2 F (1, 4) = 0.3589	P=0.1243 P<0.0001 P=0.5814	passed

4.4 Context specific dependency of post injury SOD1 expression on FMRP does not explain the FMRP phenotype under all experimental conditions, whereas the role of FMRP in the ISR can account for the phenotype more generally

According to the study, we can conclude that unlike the murine brain, under uninjured conditions, SOD1 translation is not dependent on FMRP in the murine lung. SOD1 gene could be partially under the regulation of FMRP in mouse lung and lung derived bronchial cells in an injury-dependent manner. Depending on the type of injury, FMRP dependent SOD1 up-regulation mayvary to different extent. It may also indicate that there could be other

mechanisms of SOD1 translation in the lung, which is not dependent on FMRP. The study also reveals that SOD1 up-regulation is not likely to be dependent on FMRP in human lungs. Taken together, this data does not adequately explain susceptibility of FMRP deficient C22 cells across injury models or in human BEAS2b to PQ injury. This suggests that perturbation of ISR is a more parsimonious reason for the susceptibility of FMRP deficient bronchial epithelial cells to xenobiotic stress, and not the regulation of SOD1 by FMRP.

4.5 FMRP dependent stress granule formation in lung derived cell lines

4.5.1 Stress granule

Stress granules (SGs) are membrane-less condensates of the translation initiation complex, ribosomes, mRNAs and RNA binding proteins (Youn JY et al, 2019). These are dynamic compartments formed due to stress induced translation arrest, and are used for storage of mRNAs. Depending on the post stress fate of the cell, these granules are either resolved. There are a number of proteins and mRNAs associated with SGs. Tia1 was found to promote SG biogenesis by its prion-like self- aggregation activity and RNA binding capacity (Gliks N et al, 2004). Apart from Tia1, Atx2, G3BP, TDP 43 are the other well-known markers of SGs (Tsang B et al, 2016; Bakthavachalu B et al, 2018; Nonhoff U et al, 2007). Biochemically isolated SGs have two distinct layers, the more dynamic outer shell, and an inner core structure (Protter DSW and Parker R, 2016). SGs are categorized into two main types: canonical andnon-canonical. Canonical SG biogenesis is dependent on phosphorylation of eIF2α (Reineke LC et al, 2012; Eiermann N et al, 2022), whereas non-canonical SG formation does notrequire eIF2α phosphorylation (Grousl, T. et al, 2009; Dang Y et al, 2006; Emara MM et al, 2012). On the other hand, certain type of stresses may lead to eIF2α phosphorylation without SG biogenesis (Zhai X et al, 2018; Montero H et al, 2008). Depending on the stressor, SG formationcan follow a canonical or non-canonical pathway.

4.5.2 Role of stress granules in the cell

SGs have multiple roles in maintaining cellular health. They are involved in localization, compartmentalization, degradation and translation of mRNAs. SG dynamics is crucial for functionality of the cell. Neurodegenerative diseases may cause increased SG formation or defective clearance of SGs (Protter DSW and Parker R, 2016). SG formation may induce stress response and cell survival pathways, or pro-death pathways during chronic stress (Reineke LC et al, 2018).

4.5.3 Stress granule biogenesis and role of FMRP in the process

FMRP interacts with several SG associated proteins like G3BP, ATXN2L, Caprin1, and PABP1. FMRP has been found to be a SG protein itself. Moreover, the study of Didiot and coworkers showed that FMRP deficient cells were unable to form SGs in response to heat shock and arsenite stress. Interestingly they report that along with Tia1, FMRP could also be an early SG assembly protein (Didiot MC et al, 2009).

As FMRP has been found to have a role in stress granule biogenesis, we wanted to investigate whether FMRP regulates the efficacy of stress response by regulating stress granule biogenesis in lung epithelial cellsduring xenobiotic stress induced by Nap or PQ.

4.6 Results

4.6.1 In response to Arsenite stress, Stress Granule biogenesis is affected in FMRP deficient bronchial epithelial cell lines

FMRP was found to be associated with SGs in many studies. Didiot MC et al report showed perturbation of Tia-1 granule formation in post arsenite and heat shock stress in the FMRP deficient mouse fibroblast cells. This report does not talk about the effect of the perturbation to SG biogenesis on cell health, and it is currently unclear whether a defect in

SG biogenesis alone can render cells more susceptibility to stressful stimuli (Adjibade P et al., 2017). We decided to explore the possibility of FMRP dependent SG biogenesis as a mechanism behind the susceptibility of FMRP deficient bronchial epithelial cells to Naphthalene and PQ induced stress.

In order to investigate this, we first exposed murine C22 cells with (Control, treated with Scrambled siRNA, Sc) and without FMRP (*Fmr1* siRNA treated, Si) to 250μM concentration of sodium arsenite (Linero FN, 2011; Reineke LC et al, 2018) dissolved in water for an hour (Fig 4.3A). After an hour of exposure, cells were washed and fixed. Cells were stained with anti-Tia1 and anti-FMRP antisera prior to and post arsenite treatment to detect Tia1 and FMRP condensates. Confocal analysis showed both control (Sc) and FMRP deficient (Si) C22, having a more or less diffuse pattern of Tia1 staining (Fig 4.3B i, Fig 4.3C i). Under the same conditions, FMRP anti-sera appeared to detect very small granules, predominantly in the cytoplasm of the control cells (Fig 4.3B ii) but not in the siRNA treated cells (Fig 4.3C ii). We observed what appeared to be large cytoplasmic granules post arsenite exposure for Tia1 (Red, white arrowhead, Fig 4.3B iv) and FMRP (Green, white arrows, Fig 4.3B v) in the Sc treated control cells, but not in the FMRP deficient cells (Fig 4.3C iv-vi). The large overlapping of Tia-1 and FMRP granules (white double arrowhead, Fig 4.3 B vi) and presence of small non-overlapping Tia1 granules (white arrowhead, Fig
4.3 B vi) and FMRP granules (white arrow, Fig 4.3 B vi) in post arsenite Sc treated C22 cells.

Next, we performed the arsenite experiment with human BEAS2b cells (Fig 4.3 D-E). The human BEAS2b cells with (Scrambled siRNA treated control, Sc) and without FMRP (FMR1 siRNA treated, Si) were exposed to 250μM concentration of sodium arsenite dissolved in water for an hour. As before, we observed, various sized overlapping (white double arrowhead, Fig 4.3 D vi) and non-overlapping Tia1 (red, white arrowhead, Fig 4.3 B vi) and FMRP (Green, white arrow, Fig 4.3 D vi)

granules in post arsenite Sc treated BEAS2b cells, but not in FMRP deficient BEAS2b cells (Fig 4.3E iv-vi).

These results validated the finding of Didiot MC et al in the bronchial epithelial cell lines C22 and BEAS2b.

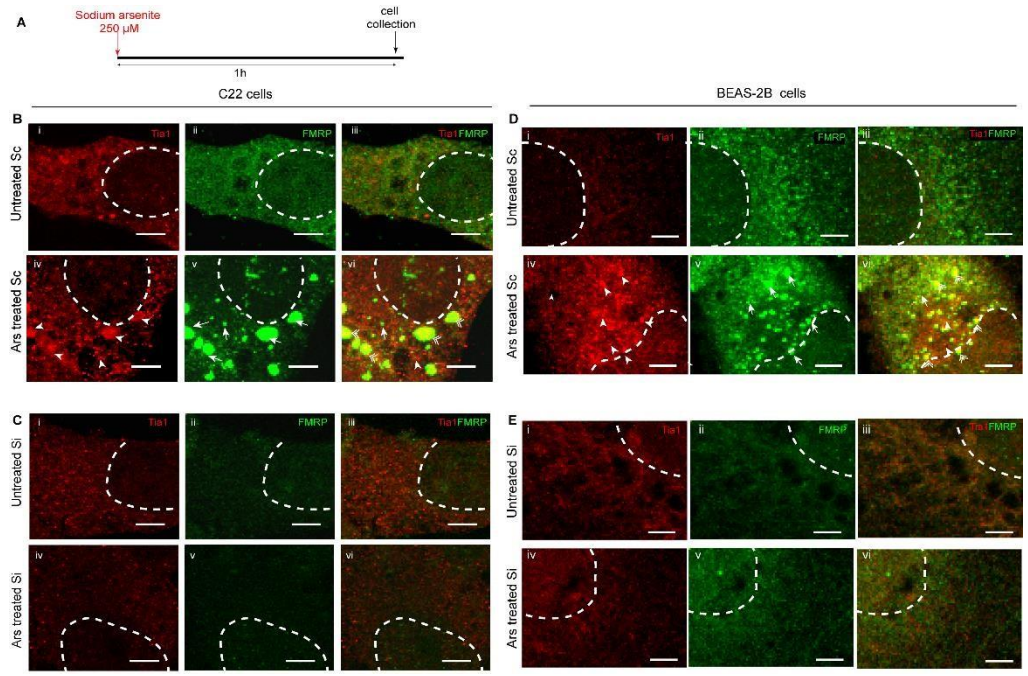

Figure 4.3: Stress granule biogenesis is affected in FMRP deficient cells post Arsenite exposure. (A) Schematic showing regimen of sodium arsenite injury. **(B-C)** Tia1 (red) and FMRP (green) immunostaining prior to and post arsenite in control and FMRP-depleted C22 cells (Scrambled siRNA treated, Sc and Fmr1 siRNA treated, Si). **(B i- B iii)** Tia1 and FMRP staining in uninjured Sc. **(B iv- B vi)** Tia1 and FMRP immunostaining in Sc post arsenite. Tia1 granules indicated with white arrowheads, FMRP granules indicated with white arrow, Tia1, FMRP co-expressing granules shown with double arrowheads. Note the presence of granules with overlapping and non-overlapping expressions of these markers. **(C i- C iii)** Tia1 and FMRP staining in uninjured Si. **(C iv- C vi)** Tia1 and FMRP immunostaining in Si post arsenite. Note absence of both Tia1 and FMRP granules in Si cells (n= 2 experiments). **(D-E)** Tia1 (red) and FMRP (green) immunostaining prior to and post arsenite in control and FMRP-depleted BEAS-2B cells (Scrambled siRNA treated, Sc and Fmr1 siRNA treated, Si). **(D i- D iii)** Tia1 and FMRP staining in uninjured Sc. **(D iv- D vi)** Tia1 and FMRP immunostaining in Sc post arsenite. Tia1 granules indicated with white arrowheads, FMRP granules indicated with white arrow, Tia1, FMRP co-expressing granules shown with double arrowheads. Note the presence of granules with

overlapping and non-overlapping expressions of these markers. **(E i- E iii)** Tia1 and FMRP staining in uninjured Si. **(E iv- E vi)** Tia1 and FMRP immunostaining in Si post arsenite. Note absence of both Tia1 and FMRP granules in Si cells. n= 3 experiments. Scale bar= 5μm.

4.6.2 In response to Nap and PQ stress, Tia1 expression is affected in FMRP deficient cells

In an effort to characterize the role of FMRP in the stress response, we probed SG biogenesis in control and FMRP-depleted C22 cells post Nap. To determine whether the SG biogenesis was inhibited in FMRP-deficient C22 cells 1 h post Nap, we stained Sc and Si cells with antisera against TIA1/FMRP (anti-TIA1 immunostaining shown in red, white arrowhead, and anti-FMRP immunostaining shown in green, white arrow, Fig. 4.4 A; n=3 experiments). Confocal analysis showed that unlike arsenite, Nap does not induce formation of large Tia1-FMRP punctae during the time course of the experiment. Rather, we observed very small, mostly non-overlapping granular appearances of Tia1 and FMRP in Sc cells (Fig 4.4A i-v), but not in Si cells (Fig 4.4A vi-x). This observation primarily led us to consider that SG biogenesis has been perturbed in FMRP-depleted cells. Then images were analyzed carefully by using the particle count tool of Fiji software to determine the sizes and intensity of condensates. It was found that the maximum number of condensates was very small (< 0.5 μ) and not changing significantly prior to and post treatment. We also observed that a very small percentage of total intensity of light is coming from the condensates. So, we concluded that Tia1 or FMRP granules that we observed here, may not be considered as any kind of condensates, specifically stress granules. Though the total intensity of the Tia1 staining increased at 3h post nap compared to untreated condition and this pattern was not observed in FMRP deficient C22 or BEAS2B cells.

As described previously, we probed the formation of SG (Fig. 4.4B) in BEAS2b cells. These cells also showed very small, partially overlapping Tia1 and FMRP granules.

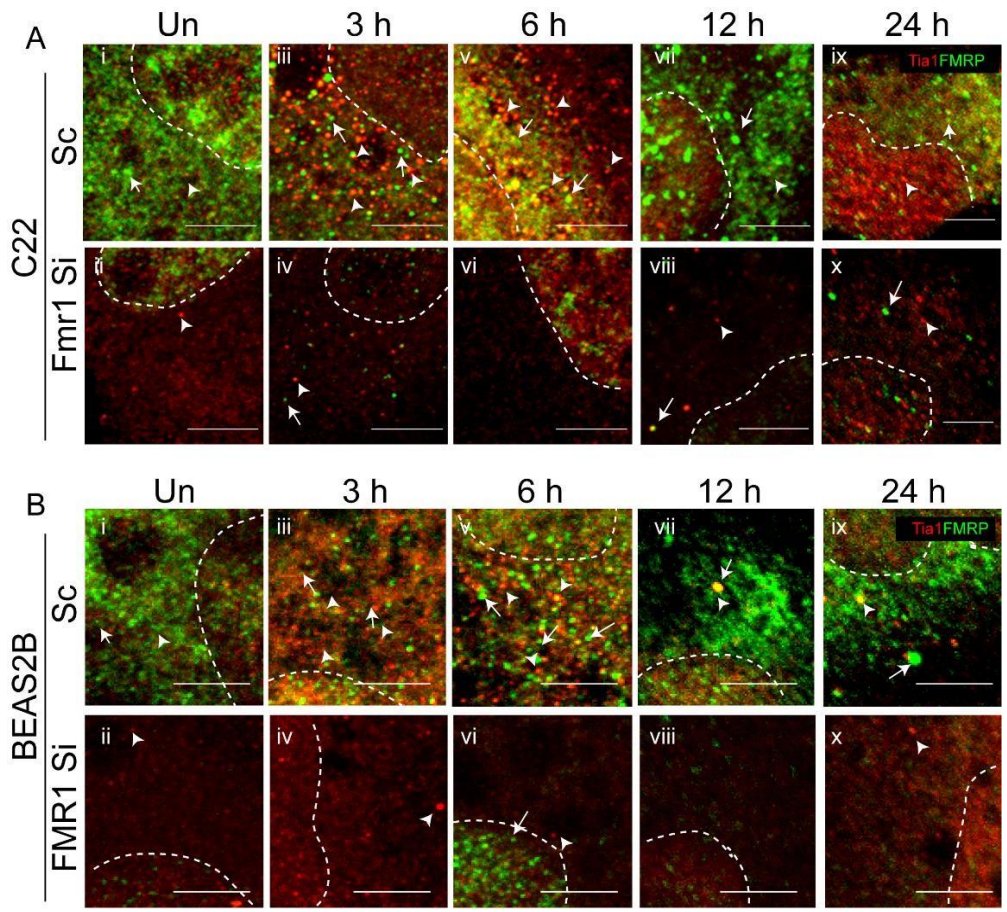

Fig 4.4: Loss of Tia1 expression in C22 and BEAS2B cells in absence of FMRP post injury. (A i - A x) Expression of Tia-1(red, white arrowheads) in control (Scrambled siRNA-treated, Sc) and Fmr1 siRNA-treated (Si) cells prior to and post Nap. Note that FMRP expression in the same cells (green, white arrows) does not completely overlap with Tia-1. **(B i-B x)** Expression of the stress granule marker Tia-1(red, white arrowheads) in control (Scrambled siRNA-treated, Sc) and FMR1 siRNA-treated (Si) cells prior to and post PQ. Note that FMRP expression in the same cells (green, white arrow) does not completely overlap with Tia-1.

4.7 Stress granule biogenesis does not sufficiently explain the susceptibility of FMRP deficient cells to Xenobiotic stress

There was no prior data that suggests nap and PQ can induce SG biogenesis in these cells. Moreover, the results did not allow us to unambiguously conclude that the granular appearances could be considered as some sort of RNA granules. Though interestingly, we observed loss of Tia1 intensity in the FMRP deficient cells post injury as compared to the control (Sc). This may suggest that post injury expression of Tia1 could be FMRP dependent. However, we

concluded that the perturbation of SG biogenesis is not enough to explain the FMRP phenotype in the pulmonary epithelial cells.

4.8 FMRP dependent γ-H2AX docking as a marker of DNA damage response during the course of injury in the lung and lung derived cells

A report by Alpatov et al, 2016 introduced the role of FMRP during replication stress. Among many of their observations, two seemed crucial to us, as we observed increased stress in FMRP depleted cells in response to Nap or PQ. First, according to the study FMRP is required to induce DNA damage response by docking of γ-H2AX to the DNA damage site on the chromosome during replication stress. As a result, they observed loss of γ-H2AX foci formation in FMRP depleted cells, when subjected to aphidicolin, hydroxyurea or UV radiation. Second, the study also reports γ-H2AX foci induced by gamma irradiation do not require FMRP for their formation. This suggests that there are certain types of genotoxic stress, where γ-H2AX foci formation is not dependent on FMRP. In fact, γ-H2AX foci may increase in absence of FMRP as a result of increased DNA damage and impaired DNA damage repair (Liu W et al, 2012).

4.8.1 FMRP dependent DNA damage response during replication stress does not explain the susceptibility of FMRP deficient cells to Xenobiotic stress in the lung or lung derived cell lines

When we analyzed our observations in the light of the Alpatov study, we found the following. First, our study shows increased γ-H2AX foci formation and longer persistence of the stress marker in the FMRP depleted cells and tissues (see chapter III). This tells us, xenobiotic stress induced by nap and PQ could be a type of stress where γ-H2AX foci formation is not dependent on FMRP. Second, lung epithelium is largely quiescent (Peng et al, 2015; Verckist L et al, 2018). A very small percentage of cells in the lung airway and alveolar compartments remain mitotically active (positive for cell cycle marker Ki67) under homeostatic conditions and the cells start proliferating after 36-48h

post Nap treatment. So, replication stress is unlikely to explain the susceptibility of *Fmr1* KO mice lung to nap injury. Experiments on C22 and BEAS2B cells were performed within 24h, which is almost half the doubling time of C22 and BEAS2B cells. Moreover, C22 cell experiments were performed under differentiated conditions, where cells were not in the replication cycle. In case of BEAS2B and A549 cells, we cannot argue that the large percentage of cells were not in cycle during the regimen of injury, as the doubling time of BEAS2B cells may vary from passage to passage, and the approximate doubling time of A549 cells is 22h. Though the experimental results suggest that γ-H2AX foci formation was increased in FMRP deficient BEAS2B and A549 cells. If γ-H2AX foci formation was dependent on FMRP as described by Alpatov et al, in case of replication stress, we could have observed no γ-H2AX foci formation in absence of FMRP. Thus, we conclude that FMRP dependent DNA damage response in replication stress is not applicable in case of Nap or PQ induced stress in lung or lung derived cell lines.

4.9 Conclusion

Considering the discussion and results in the above sections, we must conclude that the existing models of FMRP in regulating cellular stress do not justify the phenotype we observe in the murine lung and lung derived cell lines in response to nap and PQ. The perturbation of ISR seems to be a more plausible reason behind the susceptibility of these pulmonary epithelial cells to xenobiotic stress. Along with that, we do appreciate that FMRP is a multifunctional protein which may regulate different pathways during the stress response, depending on the type and the system of injury.

Contribution:

Conceptualization and experiment design: Dr. Arjun Guha, Deblina Sain Basu

Data collection and analysis: Deblina Sain Basu

Troubleshooting advises and critical review: Dr. Arjun Guha, Dr. Ravi Muddashetty, Dr. Rajesh Thimulappa, Dr. Sumantra Chatterji, Dr. Aditi Bhattacharya

References

1. **Adjibade P, Grenier St-Sauveur V, Bergeman J, Huot ME, Khandjian EW, Mazroui R**. DDX3 regulates endoplasmic reticulum stress-induced ATF4 expression. Scientific reports. **2017** Oct 23;7(1):1-2.

2. **Alpatov R, Lesch BJ, Nakamoto-Kinoshita M, Blanco A, Chen S, Stützer A, Armache KJ, Simon MD, Xu C, Ali M, Murn J.** A chromatin-dependent role of the fragile X mental retardation protein FMRP in the DNA damage response. Cell. **2014** May 8;157(4):869-81.

3. **Bakthavachalu B, Huelsmeier J, Sudhakaran IP, Hillebrand J, Singh A, Petrauskas A, Thiagarajan D, Sankaranarayanan M, Mizoue L, Anderson EN, Pandey UB.** RNP-granule assembly via ataxin-2 disordered domains is required for long-term memory and neurodegeneration. Neuron. **2018** May 16;98(4):754-66.

4. **Bechara EG, Didiot MC, Melko M, Davidovic L, Bensaid M, Martin P, Castets M, Pognonec P, Khandjian EW, Moine H, Bardoni B.** A novel function for fragile X mental retardation protein in translational activation. PLoS Biol. **2009** Jan 20;7(1):e1000016.

5. **Constantino L, Gonçalves RC, Giombelli VR, Tomasi CD, Vuolo F, Kist LW, de Oliveira GM, de Bittencourt Pasquali MA, Bogo MR, Mauad T, Horn A.** Regulation of lung oxidative damage by endogenous superoxide dismutase in sepsis. Intensive care medicine experimental. **2014** Dec;2(1):1-1.

6. **Dang Y, Kedersha N, Low WK, Romo D, Gorospe M, Kaufman R, Anderson P, Liu JO.** Eukaryotic initiation factor 2α-independent pathway of stress granule induction by the natural product pateamine A. Journal of Biological Chemistry. **2006** Oct 27;281(43):32870-8.

7. **Didiot MC, Subramanian M, Flatter E, Mandel JL, Moine H.** Cells lacking the fragile X mental retardation protein (FMRP) have normal RISC activity but exhibit altered stress granule assembly. Molecular biology of the cell. **2009** Jan 1;20(1):428-37.

8. **Eiermann N, Stoecklin G, Jovanovic B.** Mitochondrial inhibition by sodium azide induces assembly of eIF2α phosphorylation-independent stress granules in mammalian cells. International Journal of Molecular Sciences. **2022** May 17;23(10):5600.

9. **Emara MM, Fujimura K, Sciaranghella D, Ivanova V, Ivanov P, Anderson P.** Hydrogen peroxide induces stress granule formation

independent of eIF2α phosphorylation. Biochemical and biophysical research communications. **2012** Jul 13;423(4):763-9.

10. **Gilks N, Kedersha N, Ayodele M, Shen L, Stoecklin G, Dember LM, Anderson P.** Stress granule assembly is mediated by prion-like aggregation of TIA-1. Molecular biology of the cell. **2004** Dec;15(12):5383-98.

11. **Grousl, T., Ivanov, P., Frydlová, I., Vasicová, P., Janda, F., Vojtová, J., Malínská, K., Malcová, I., Nováková, L., Janosková, D. and Valásek, L., 2009.** Robust heat shock induces eIF2α-phosphorylation-independent assembly of stress granules containing eIF3 and 40S ribosomal subunits in budding yeast, Saccharomyces cerevisiae. Journal of cell science, 122(12), pp.2078-2088.

12. **Linero FN, Thomas MG, Boccaccio GL, Scolaro LA.** Junin virus infection impairs stress-granule formation in Vero cells treated with arsenite via inhibition of eIF2α phosphorylation. Journal of general virology. **2011** Dec;92(12):2889-99.

13. **Liu W, Jiang F, Bi X, Zhang YQ.** Drosophila FMRP participates in the DNA damage response by regulating G2/M cell cycle checkpoint and apoptosis. Human molecular genetics. **2012** Nov 1;21(21):4655-68.

14. **Montero H, Rojas M, Arias CF, López S.** Rotavirus infection induces the phosphorylation of eIF2α but prevents the formation of stress granules. Journal of virology. **2008** Feb 1;82(3):1496-504.

15. **Nonhoff U, Ralser M, Welzel F, Piccini I, Balzereit D, Yaspo ML, Lehrach H, Krobitsch S.** Ataxin-2 interacts with the DEAD/H-box RNA helicase DDX6 and interferes with P-bodies and stress granules. Molecular biology of the cell. **2007** Apr;18(4):1385-96.

16. **Noor R, Mittal S, Iqbal J.** Superoxide dismutase--applications and relevance to human diseases. Medical science monitor: international medical journal of experimental and clinical research. **2002** Sep 1;8(9):RA210-5.

17. **Peng T, Frank DB, Kadzik RS, Morley MP, Rathi KS, Wang T, Zhou S, Cheng L, Lu MM, Morrisey EE**. Hedgehog actively maintains adult lung quiescence and regulates repair and regeneration. Nature. **2015** Oct;526(7574):578-82.

18. **Protter DS, Parker R.** Principles and properties of stress granules. Trends in cell biology. **2016** Sep 1;26(9):668-79.

19. **Reineke LC, Cheema SA, Dubrulle J, Neilson JR.** Chronic starvation induces noncanonical pro-death stress granules. Journal of cell science. **2018** Oct 1;131(19):jcs220244.

20. **Reineke LC, Dougherty JD, Pierre P, Lloyd RE.** Large G3BP-induced granules trigger eIF2α phosphorylation. Molecular biology of the cell. **2012** Sep 15;23(18):3499-510.

21. **Siedlinski M, van Diemen CC, Postma DS, Vonk JM, Boezen HM.** Superoxide dismutases, lung function and bronchial responsiveness in a general population. European Respiratory Journal. **2009** May 1;33(5):986-92.

22. **Stoica L, Keeler AM, Xiong L, Kalfopoulos M, Desrochers K, Brown Jr RH, Sena-Esteves M, Flotte TR, ElMallah MK.** Restrictive lung disease in the Cu/Zn superoxide-dismutase 1 G93A amyotrophic lateral sclerosis mouse model. American journal of respiratory cell and molecular biology. **2017** Mar;56(3):405-8.

23. **Tankersley CG, Haenggeli C, Rothstein JD.** Respiratory impairment in a mouse model of amyotrophic lateral sclerosis. Journal of applied physiology. **2007** Mar;102(3):926-32.

24. **Tsang B, Arsenault J, Vernon RM, Lin H, Sonenberg N, Wang LY, Bah A, Forman-Kay JD.** Phosphoregulated FMRP phase separation models activity-dependent translation through bidirectional control of mRNA granule formation. Proceedings of the National Academy of Sciences. **2019** Mar 5;116(10):4218-27.

25. **Verckist L, Pintelon I, Timmermans JP, Brouns I, Adriaensen D.** Selective activation and proliferation of a quiescent stem cell population in the neuroepithelial body microenvironment. Respiratory Research. **2018**Dec;19:1-7.

26. **Youn JY, Dyakov BJ, Zhang J, Knight JD, Vernon RM, Forman-Kay JD, Gingras AC.** Properties of stress granule and P-body proteomes. Molecular cell. **2019** Oct 17;76(2):286-94.

27. **Younus H.** Therapeutic potentials of superoxide dismutase. International journal of health sciences. **2018** May;12(3):88.

28. **Zelko IN, Mariani TJ, Folz RJ.** Superoxide dismutase multigene family: a comparison of the CuZn-SOD (SOD1), Mn-SOD (SOD2), and EC-SOD (SOD3) gene structures, evolution, and expression. Free Radical Biology and Medicine. **2002** Aug 1;33(3):337-49.

29. **Zhai X, Wu S, Lin L, Wang T, Zhong X, Chen Y, Xu W, Tong L, Wang Y, Zhao W, Zhong Z.** Stress granule formation is one of the early antiviral mechanisms for host cells against coxsackievirus B infection. Virologica Sinica. **2018** Aug;33:314-22.

Chapter 5

Discussion and Future Prospects

FMRP is well researched in the context of the brain or neuron due to its connection with FXS. It was also reported previously that FMRP regulates oxidative stress in the brain. Though FMRP was initially discovered as a neuronal protein, recent studies have shown that expression of FMR1 mRNA and protein is not tissue specific, rather they are present throughout the body. Recent studies have started exploring the role of FMRP in organs apart from the brain. Our study has taken a step ahead to connect the protein with lung health. Taken together, these studies will give a bigger picture of the functionality of FMRP for a better improvement of clinical strategies.

5.1 FMRP is a multifunctional protein

FMR1 gene is highly conserved across species. It contains 17 exons and can be alternatively spliced. The gene spans about 40 kilobases (kb) of DNA and the gene product is an mRNA of 3.9 kb. Human FMRP protein is a 71 KDa protein. FMRP has different domains that can interact with RNA, DNA, proteins and ribosomes.

5.1.1 FMRP may be involved in multiple stress related pathways,like ISR

FMRP interacting proteins are found to be associated with multiple stress related pathways. Among these, proteins like YBX1, APC are found to be associated with TNFα pathway (Pasciuto E et al, 2014; Blackwell E et al, 2011; Mateu-Regue, A. et al 2019; Xu J et al 2020; White B et al, 2020). Proteins PARP1, RPS6K and PP2A have important roles in mTOR and ERK pathways (Pasciuto E et al, 2014; Luo X et al, 2012; Tang S et al, 2018; Vasic V et al, 2021). Proteins DICER1, YBX1, PARP1, PRMP5 and others are found to be important for Nrf2 pathway (Nabih HK et al, 2020; Cheever A et al, 2009; Diao C et al, 2019; Gong C et al, 2021; Pietrzak J et al, 2018). FMRP interacting partners caprin1,G3BP1, TIA1, Trdr3, EIF4E, DDX3X, PKR were found to be associated with Integrated Stress Response pathway (ISR) (Reineke LC et al, 2015;Linder B et al, 2008; Shih JW et al, 2012). Our

study demonstrates that FMRP itself is necessary for the actuation of ISR in lung epithelial cells in response to xenobiotic stress.

FMRP interacting partners establish strong connections with multiple stress related pathways, like mTOR, PI3K/AKT, Nrf2, ERK and ISR. On the other hand, FMRP may directly regulate another subset of mRNAs like SOD1. Our study showed that unlike in the brain, FMRP does not regulate SOD1 at homeostatic level in the lung, but it may regulate post injury SOD1 expression in a context specific way.

5.1.2 Post transcriptional modification sites (PMTs) provide morecomplexity to the functionality of FMRP

Along with prominent RNA and protein binding domains, FMRP contains post-translational modification sites (PMTs), which modulate FMRP activity by phosphorylation, sumoylation or methylation. Phosphorylation site S499 (Fig 1.3) at the C-terminal end is very important in the context of translational repression by FMRP. Based on the studies in the neuronal system, Phosphorylation of this serine residue does not affect the overall amount of mRNA associated with the protein, but causes ribosome stalling and inhibits translation. PP2A dependent dephosphorylation of FMRP resumes the global translation machinery. Phosphorylation site S500 of human FMRP is important for translational regulation and synaptic plasticity (Prieto M et al, 2020).

Sumoylation is the association of Small Ubiquitine-like Modifier proteins to specific lysine residues of target proteins. Sumoylation seems to be a key regulator for neuronal activity. Two residues at the N-terminal end of FMRP, L88 and L130 are the sites for sumoylation. Expression of a SUMO-deficient FMRP in neurons impairs neuronal maturation (Khayachi et al, 2018).

FMRP has been reported to be methylated by an unknown protein-arginine methyltransferase present in the brain lysate. These arginine methylation sites are located at the RGG box (R533, R538, R543 and

R545) (Fig 1.3). Methylation of these sites on FMRP regulates their binding to mRNAs.

We have not observed any obvious change in the level of FMRP in BEAS2B and C22 cells or in the mouse lung tissue during the course of injury. This may indicate towards post transcriptional modification of FMRP, which kicks in the process of ISR initiation. Testing this hypothesis was out of the scope of this study. Our future studies may shed light on the post-translational modification of FMRP, which facilitates activation of ISR in the context of lung injury.

5.2 FMRP interaction with Caprin1 and G3BP1, may reveal a possiblemechanism for FMRP dependent activation of ISR

A major finding of our study is that FMRP is required for the actuation of the ISR pathway. More specifically, we find that the stress responsive kinase PKR is activated in FMRP-deficient cells but that the phosphorylation of the PKR substrate, eIF2α, is perturbed. The mechanism by which FMRP regulates this step is currently unknown. The analysis of FMRP-binding proteins in neuronal and other tissues has identified numerous interacting partners. Interestingly, among these interacting partners, Caprin1 and G3BP have independently been implicated in the induction of the ISR pathway in response to stress (Taha MS et al., 2020; Wu Y et al., 2016). Pertinently, both Caprin1 and G3BP1 have been shown to be important for eIF2α phosphorylation (Reineke LC et al., 2015). Also, the crystal structure of Caprin1 has revealed that Caprin1 can physically interact with FMRP and G3BP1 together (Yuhong Wu et al, 2016). Thus, it is plausible that FMRP acts in concert with Caprin1 and G3BP1 to facilitate eIF2α phosphorylation. Although eIF2α phosphorylation is an early event in the ISR pathway and perturbations at this stage are likely to affect all downstream processes, our data do not allow us to rule out the possibility that FMRP has independent roles in downstream processes. Our future experiments will probe these possibilities.

5.3 Clinical prospects of the study

5.3.1 Mutation and phenotypes associated with FXS

With further advancement of studies on FXS, it became evident that the CGG repeat sequence has a spectrum of expansion (copy number) in the population. According to the size of expansion there are four groups: normal alleles (5-44 repeats), grey zone alleles (45-54 repeats), premutation alleles (55-200 repeats) and fully mutated alleles (more than 200 repeats) (Debrey SM et al, 2016; Wheeler AC et al, 2014; Devys D et al, 1993). The population groups having different numbers of CGG repeats in the FMR1 gene, also possess variation in the level of FMR1 mRNA and protein expression. Fully mutated groups however, lack FMR1 mRNA or protein, the premutation group has a higher level of FMR1 mRNA but due inefficient translation there is less FMRP expression (Schneider A et al, 2020). Grey zone group has also been found to have higher levels of FMR1 mRNA as compared to the normal group (Loesch DZ et al, 2007). Of these four genotypic groups, only the premutation and fully mutated groups are associated with clinical conditions.

Fully mutated group with transcriptionally silenced FMR1 gene and complete loss of FMR protein (FMRP) production is associated with autism spectrum disorder (ASD). Almost 98% of Fragile X patients belong to this group. People who fall in this group possess mild to moderate intellectual disability, speech disorder, and some characteristic physical features like, elongated facial structure, prominent jaw and forehead, large pinnae, macroorchidism (in case of male), flat foot, unusually flexible digits etc. Occurrence of full mutation in population is about 1 in 4000 to 5000 males and about 1 in 8000 in females (Zalfa F et al, 2004; Protic D et al, 2019).

As compared to the frequency of full mutation groups, premutation is more common in the population. Based on US population studies, prevalence ofpremutation has been reported to be about 1 in 200 females

and about 1 in 300-400 males. Premutation could be more frequent in certain populations. For a long time, it was thought that individuals who fall under the permutation groups are only carriers, having a high chance of propagating breakage of X-chromosome to the next generation, but with no health issues. However, rigorous research has established a firm correlation with a subset of FMR1 premutation group and two clinical conditions, Fragile X-associated Tremor/ Ataxia Syndrome (FXTAS) and Fragile X-associated Primary Ovarian Insufficiency (FXPOI). Along with reproductive issues, some other medical problems have been found to be possibly or strongly related to premutation, such as thyroid disorder, hypertension, migraines, neuropathy, estrogen deficiency, general intelligence, memory and language related disorders (Wheeler AC et al, 2014).

'Grey zone' allele carriers are considered to be clinically fit. However, a recent case-study based report has shown that 'Grey zone' allele carriers had early onset of Parkinson's disease, dementia, atypical Parkinsonism and tremor at an average age of 53 (Devys D et al, 1993). Important to note here, that a computational study on the data of FMR1-informed biobank has found that male and female individuals carrying FMR1 premutation (55-200 CGG repeats) have significantly higher rates of respiratory diseases or symptoms along with digestive and endocrine problems (Movaghar et al, 2019).

Under these circumstances, there could be two possibilities to consider the role of FMRP in lung health. First, according to our study FMRP is required for actuation of ISR in the lung, thus important for lung health. Second, FMRP or FMRP interacting proteins could be directly or indirectly involved in lung diseases or other stress response pathway in the lung. For example, a study based on mutation screening has found that FMRP interacting protein CYFIP2 is significantly associated with the development of atopic asthma in humans (Noguchi E et al, 2005). Interestingly, some of the FMRP interacting proteins, like PP2A, PARP1, DICER, Myosin 5a, PRMP5 have been found to be associated with smoke induced lung injury, asthma and

oxidative stress in lung (Wallace AM et al, 2011; Virág L, 2005; Yao M et al, 2014; Hernandez K et al, 2017; Diao C et al, 2019).

Taken together, the data suggest that FMRP and its interacting partners play an important role in maintaining lung health. More studies on molecular interactions and clinical data will reveal the mechanism of this process.

5.3.2 People with FXS who are living in areas of higher pollutant load could be more susceptible to lung damage/disease

This study demonstrates a role for FMRP in the lung, and points to a potential vulnerability in individuals with an FMR1 deficiency. Clinically, the bulk of the case studies on FXS patients are derived from geographic regions where the load of pulmonary environmental stressors is low. Our study suggests that individuals with FXS living in areas of higher pollutant load may be more susceptible to lung damage/disease and FMRP status in the lung may be a strong correlate of resilience to pulmonary insults.

References

1. **Bardoni B, Schenck A, Mandel JL.** The Fragile X mental retardation protein. Brain research bulletin. **2001** Nov 1;56(3-4):375-82.

2. **Blackwell E, Ceman S.** A new regulatory function of the region proximal to the RGG box in the fragile X mental retardation protein. Journal of cell science. **2011** Sep 15;124(18):3060-5.

3. **Casingal CR, Kikkawa T, Inada H, Sasaki Y, Osumi N.** Identification of FMRP target mRNAs in the developmental brain: FMRP might coordinate Ras/MAPK, Wnt/β-catenin, and mTOR signaling during corticogenesis. Molecular brain. **2020** Dec;13(1):1-3.

4. **Chen E, Joseph S.** Fragile X mental retardation protein: a paradigm for translational control by RNA-binding proteins. Biochimie. **2015** Jul 1;114:147-54.

5. **Darnell JC, Mostovetsky O, Darnell RB.** FMRP RNA targets: identification and validation. Genes, Brain and Behavior. **2005** Aug;4(6):341-9.

6. **Davis JK, Broadie K.** Multifarious functions of the fragile X mental retardation protein. Trends in Genetics. **2017** Oct 1;33(10):703-14

7. **Hu Y, Chen Z, Fu Y, He Q, Jiang L, Zheng J, Gao Y, Mei P, Chen Z, Ren X.** The amino-terminal structure of human fragile X mental retardation protein obtained using precipitant-immobilized imprinted polymers. Nature communications. **2015** Mar 23;6(1):1-1.

8. **Myrick LK, Hashimoto H, Cheng X, Warren ST.** Human FMRP contains an integral tandem Agenet (Tudor) and KH motif in the amino terminal domain. Human molecular genetics. **2015** Mar 15;24(6):1733-40.

9. **Pasciuto E, Bagni C.** SnapShot: FMRP interacting proteins. Cell. **2014** Sep 25;159(1):218-.

10. **Piazzon N, Rage F, Schlotter F, Moine H, Branlant C, Massenet S.** In vitro and in cellulo evidences for association of the survival of motor neuron complex with the fragile X mental retardation protein. Journal of Biological Chemistry. **2008** Feb 29;283(9):5598-610.

11. **Pietrzak J, Spickett CM, Płoszaj T, Virág L, Robaszkiewicz A.** PARP1 promoter links cell cycle progression with adaptation to oxidative environment. Redox biology. **2018** Sep 1;18:1-5.

12. **Ramos A, Hollingworth D, Adinolfi S, Castets M, Kelly G, Frenkiel TA, Bardoni B, Pastore A.** The structure of the N-terminal domain of the fragile X mental retardation protein: a platform for protein-protein interaction. Structure. **2006** Jan 1;14(1):21-31.

13. **Richter JD, Zhao X.** The molecular biology of FMRP: new insights into fragile X syndrome. Nature Reviews Neuroscience. **2021** Feb 19:1-4.

14. **Santoro MR, Bray SM, Warren ST.** Molecular mechanisms of fragile X syndrome: a twenty-year perspective. Annual Review of Pathology: Mechanisms of Disease. **2012** Feb 28;7:219-45.

15. **Taha MS, Haghighi F, Stefanski A, Nakhaei- Rad S, Kazemein Jasemi NS, Al Kabbani MA, Görg B, Fujii M, Lang PA, Häussinger D, Piekorz RP.** Novel FMRP interaction networks linked to cellular stress. The FEBS journal. **2021** Feb;288(3):837-60.

16. **Vasic V, Jones MS, Haslinger D, Knaus LS, Schmeisser MJ, Novarino G, Chiocchetti AG.** Translating the Role of mTOR-and RAS-Associated Signalopathies in Autism Spectrum Disorder: Models, Mechanisms and Treatment. Genes. **2021** Nov;12(11):1746.

17. **Vasic V, Jones MS, Haslinger D, Knaus LS, Schmeisser MJ, Novarino G, Chiocchetti AG**. Translating the Role of mTOR-and RAS-Associated Signalopathies in Autism Spectrum Disorder: Models, Mechanisms and Treatment. Genes. **2021** Nov;12(11):1746.

18. **Vasilyev N, Polonskaia A, Darnell JC, Darnell RB, Patel DJ, Serganov A.** Crystal structure reveals specific recognition of a G-quadruplex RNA by a β-turn in the RGG motif of FMRP. Proceedings of the National Academy of Sciences. **2015** Sep 29;112(39):E5391-400.

19. **Wallace AM, Hardigan AA, Gaffney A, Mirochnitchenko O, Thankachen J, Poon K, Arellanos L, Salim S, Thompson V, D'Armiento JM, Foronjy R.** Redox Regulation Of Protein Phosphatase 2A (PP2A) Phosphorylation Prevents Smoke-Induced Lung Injury. InD97. EMERGING OXIDATIVE STRESS-RELATED MECHANISMS IN INJURY AND REPAIR **2011** May (pp. A6142-A6142). American Thoracic Society.

20. **Zhou Z, Cao M, Guo Y, Zhao L, Wang J, Jia X, Li J, Wang C, Gabriel G, Xue Q, Yi Y.** Fragile X mental retardation protein stimulates ribonucleoprotein assembly of influenza A virus. Nature communications. **2014** Feb 10;5(1):1-2.

© 2022. Published by The Company of Biologists Ltd | Journal of Cell Science (2022) 135, jcs258652. doi:10.1242/jcs.258652

RESEARCH ARTICLE

FMRP protects the lung from xenobiotic stress by facilitating the integrated stress response

Deblina Sain Basu[1,2], Rital Bhavsar[1], Imtiyaz Gulami[1,2], Saraswati Chavda[1], Sai Manoz Lingamallu[1,3], Ravi Muddashetty[1], Chandrakanth Veeranna[4], Sumantra Chattarji[1,5,6], Rajesh Thimmulappa[7], Aditi Bhattacharya[1,5] and Arjun Guha[1,*]

ABSTRACT

Stress response pathways protect the lung from the damaging effects of environmental toxicants. Here we investigate the role of the fragile X mental retardation protein (FMRP), a multifunctional protein implicated in stress responses, in the lung. We report that FMRP is expressed in murine and human lungs, in the airways and more broadly. Analysis of airway stress responses in mice and in a murine cell line *ex vivo*, using the well-established naphthalene injury model, reveals that FMRP-deficient cells exhibit increased expression of markers of oxidative and genotoxic stress and increased cell death. Further inquiry shows that FMRP-deficient cells fail to actuate the integrated stress response pathway (ISR) and upregulate the transcription factor ATF4. Knockdown of ATF4 expression phenocopies the loss of FMRP. We extend our analysis of the role of FMRP to human bronchial BEAS-2B cells, using a 9,10-phenanthrenequinone air pollutant model, to find that FMRP-deficient BEAS-2B cells also fail to actuate the ISR and exhibit greater susceptibility. Taken together, our data suggest that FMRP has a conserved role in protecting the airways by facilitating the ISR.

This article has an associated First Person interview with the first author of the paper.

KEY WORDS: Stress response, Lung, Integrated stress response, *FMR1*, FMRP

INTRODUCTION

The epithelial lining of the respiratory tract is continually challenged by a diverse array of environmental toxicants, including gases, particulates and biological agents. Exposure to these agents leads to increased oxidative, genotoxic and endoplasmic reticulum stress. Such stresses lead to cellular damage, inflammation and, in the long term, to lung damage and decreased lung functionality. The goal of this study was to probe the mechanisms by which lungs cope with environmental insults.

The capacity of the lung to manage xenobiotic stress is dependent on stress response proteins that are induced upon insult. In this regard, the integrated stress response (ISR) pathway is an evolutionarily conserved pathway that is integral to how the lung copes with environmental challenges (Pakos-Zebrucka et al., 2016; van 't Wout et al., 2014; Konsavage et al., 2012). The ISR is triggered by the activation of one or more of the four stress-responsive kinases GCN2 (also known as EIF2AK4), PKR (EIF2AK2), PERK (EIF2AK3) and HRI (EIF2AK1). The activation of these kinases, in turn, sets in motion two separate but interdependent processes that enable cells to mount a restorative response (Wong and Wispe, 1997). First, these kinases phosphorylate eukaryotic initiation factor 2α (eIF2α, also known as EIF2S1) and shut off ongoing programs of protein synthesis. The inhibition of translation leads to the sequestration of translationally active mRNAs into stress-induced condensates of various types. Second, activation of the kinases also induces specialized modes of protein translation, leading to the expression of stress response proteins. More specifically, these specialized translation regimes upregulate expression of activating transcription factor 4 (ATF4) (Pakos-Zebrucka et al., 2016; van 't Wout et al., 2014) and, in turn, ATF4 targets such as *ATF3*. ATF4 also synergizes with other transcription factors activated in response to stress, such as Nrf2 (NFE2L2), to induce the expression of stress response genes (He et al., 2001; Sarcinelli et al., 2020).

The fragile X mental retardation protein (FMRP, encoded by *FMR1*) is a multifunctional protein that is expressed in the brain and other organs, in humans and other animals alike. Deficiencies in FMRP lead to fragile X mental retardation syndrome (FXS), a disease characterized by mild-to-moderate intellectual disability (Zhou et al., 2014). FMRP function has been most intensively studied in the neuronal context, wherein the protein has been shown to regulate synaptic plasticity by multiple mechanisms (Santoro et al., 2012). Aside from this well-established role, several studies indicate that FMRP also has a role in facilitating stress responses. At a cellular level, FMRP has been shown to play an essential role in genesis of stress granules in response to arsenite and heat shock (Didiot et al., 2009; Linder et al., 2008). A recent study on fibroblasts derived from *Fmr1* knockout (KO) mice showed that FMRP is required for a specialized DNA damage response (DDR) in response to agents such as aphidicolin, 5-hydroxyurea (5-HU) and UV (Alpatov et al., 2014). The central finding of this study is that FMRP has a chromatin-dependent role in resolving stalled replication forks and single-strand breaks in DNA (Alpatov et al., 2014), but not in response to other types of genotoxic stress.

The lung is routinely exposed to a variety of environmental toxicants that cause many different types of stress. Our interest in mechanisms that regulate the pulmonary stress response led us to explore the role of FMRP in the lung. We immunostained murine and human lungs for FMRP to find that the protein is expressed in the airway epithelium and more broadly. To probe the role of FMRP in stress responses in the airways, we subjected *Fmr1* KO mice to

[1]Institute for Stem Cell Science and Regenerative Medicine (inStem), GKVK Campus, Bangalore 560065, India. [2]Trans Disciplinary University, Yelahanka, Bangalore 560064, India. [3]Manipal Academy of Higher Education, Madhav Nagar, Manipal 576104, India. [4]Department of Forensic Medicine, JSS Medical College, Mysore 570015, India. [5]Brain Development and Disease Mechanisms (BDDM), inStem, GKVK Campus, Bangalore 560065, India. [6]National Centre for Biological Sciences, GKVK Campus, Bangalore 560065, India. [7]JSS Medical College, JSS Academy of Higher Education & Research, Mysore 570015, India.

*Author for correspondence (arjung@instem.res.in)

R.B., 0000-0003-4646-2326; A.G., 0000-0002-3753-1484

Handling Editor: Kathleen Green
Received 17 March 2021; Accepted 8 March 2022

Journal of Cell Science (2022) 135, jcs258652. doi:10.1242/jcs.258652

naphthalene (Nap) injury, a well-established model for oxidative and genotoxic stress. We found that the airways of *Fmr1* KO mice exhibited higher expression of markers of oxidative and genotoxic stress, and greater cell death, than wild type. These findings led us to investigate the role of FMRP in airway stress responses, and in the ISR pathway, in mice and in the human lung.

RESULTS

FMRP is expressed in the airways and more broadly in the murine lung and protects airway club cells from Nap-induced stress

To characterize the role of FMRP in the pulmonary stress response, we examined the expression of the protein in adult lungs from wild-type (WT) and *Fmr1* KO animals. Lung sections from WT mice were stained with anti-FMRP antisera and examined under a confocal microscope (5 µm, *n*=8). FMRP expression was detected throughout the lung (Fig. 1A). We detected widespread protein expression in airway epithelium, both in secretory club cells (CCs, marked by expression of Scgb1a1, Fig. 1A,C) and in ciliated cells (marked by expression of acetylated tubulin, Ac-tub, Fig. 1A,C). Outside the airways, we noted intermittent expression in the alveolar parenchyma (Fig. 1A). Lung sections of *Fmr1* KO mice stained with the same anti-FMRP antisera did not show any specific staining (airways shown in Fig. 1B,D, *n*=3). Taken together, these experiments showed that FMRP is expressed in the murine lung, in the airways and more broadly. Next we examined hematoxylin and eosin (H&E)-stained lung sections from WT and *Fmr1* KO mice to compare morphologies of the lungs. We found that lungs from WT and *Fmr1* KO were comparable (Fig. S1A,B).

To investigate the role of FMRP in the pulmonary stress response, we focused our attention on FMRP-expressing airway CCs. Airway CCs are highly sensitive to the polycyclic hydrocarbon Nap (Stripp et al., 1995; Van Winkle et al., 1995). Nap administration leads to the loss of the vast majority of CCs from the airway epithelium within 24–48 h and is a well-established model for lung injury (Guha et al., 2014, 2017). The susceptibility of airway CCs to Nap is a result of the expression, in CCs, of the cytochrome P450 enzyme Cyp2f2 (Buckpitt et al., 2002). Cyp2f2 converts Nap to naphthalene oxide, which causes DNA damage. Naphthalene oxide is also converted to naphthoquinones, which cause oxidative stress (Buckpitt et al., 2002). Thus, to probe the role of FMRP in the pulmonary stress response in mice, we decided to utilize the Nap injury model. Interestingly, the Cyp2f2 isoform that converts Nap to cytotoxic derivatives is not expressed in humans and consequently Nap does not affect humans in the same way.

We exposed WT and *Fmr1* KO animals to Nap and harvested lungs for analysis at different timepoints post injury (regimen shown schematically in Fig. 1E). To assess the extent of injury, we quantified frequencies of CCs across timepoints and examined expression of markers of oxidative and genotoxic stress. We found that the frequencies of CCs in WT were significantly higher than in *Fmr1* KO at 12 h, 24 h and 48 h, respectively (Fig. 1F, *n*=3 mice per genotype per timepoint). In other words, cell loss was greater and faster in *Fmr1* KOs. Next, we stained sections from mouse lung prior to and post Nap injury with two antisera: anti-4-hydroxynonenal (4HNE, a product of lipid peroxidation and a marker of oxidative stress) and anti-γ-H2AX (a phosphorylated histone variant that is a marker of double-stranded DNA breaks and genotoxic stress). We did not detect expression of either marker in the lungs from uninjured WT and *Fmr1* KO mice (Fig. 1Gi,ii,Hi,ii). In contrast, the expression of both markers was dramatically increased in CCs in Nap-injured lungs (Fig. 1G,H). Pertinently, we noted that the levels of 4HNE and γ-H2AX expression in CCs were lower in WT than in *Fmr1* KOs at all timepoints examined (Fig. 1Giii–vi,Hiii–vi; see also the quantification in Fig. S1C,D, *n*=3 mice per genotype per timepoint). Based on these data, we concluded that CCs in *Fmr1* KO animals are more susceptible to Nap-induced stress.

The club-cell-like C22 cell line deficient in FMRP is also more susceptible to Nap-induced stress

To further probe the role of FMRP in stress responses in CCs, we turned to the murine club-cell-like cell line C22. C22 cells were derived from H-2Kb-tsA58 mice expressing a temperature-sensitive isoform of the SV40 large T antigen under the H-2Kb promoter (Demello et al., 2002). To characterize these cells, we stained C22 cells with markers of CCs and other airway and alveolar lineages. Consistent with previous reports, these cells expressed the CC marker Scgb1a1 (Fig. 2A) and did not express markers of other lineages (data not shown). We then performed a series of experiments to determine whether C22 could be utilized as a model for Nap injury, and to probe the role of FMRP therein.

First, C22 cells were stained with antisera against Cyp2f2 and FMRP. We found that C22 cells expressed modest levels of Cyp2f2 (Fig. 2B, *n*=6 experiments) and expressed FMRP (Fig. 2C, *n*=9 experiments). Next, we optimized methods for the knockdown of gene expression in C22 cells using siRNAs and methods for Nap challenge. We established that treatment with two different *Cyp2f2* siRNAs and three different FMRP siRNAs was sufficient to reduce Cyp2f2 and FMRP expression, respectively, by 80% or greater (see the Materials and Methods; compare Cyp2f2 or FMRP expression in scrambled siRNA-treated cells, Sc, and *Cyp2f2* or *Fmr1* siRNA-treated cells, Si, in Fig. S2A–C, *n*=3 experiments, and Fig. 2D, respectively, *n*=9 experiments). Careful titration of Nap dosage and time of exposure (see the Materials and Methods) showed that a 1 h pulse of Nap was sufficient to induce expression of oxidative and genotoxic stress markers in C22 cells and marginally increase cell death 24 h post exposure (see the Materials and Methods). We subsequently incubated control (scrambled siRNA-treated cells, Sc) and Cyp2f2-depleted (*Cyp2f2* siRNA-treated cells, Si) cells with Nap for 1 h and harvested cells at different timepoints for analysis (regimen shown schematically in Fig. S2D; see the Materials and Methods). Levels of 4HNE and γ-H2AX increased in Sc cells within 6 h and returned to baseline by 24 h (Fig. S2E–H, *n*=3 experiments each). In contrast, levels of expression in Si-cells remained at baseline levels at all timepoints (Fig. S2E–H, *n*=3 experiments each). These data showed that C22 cells are susceptible to Nap-induced stress in a Cyp2f2-dependent manner like CCs *in vivo*.

To explore the possibility that FMRP regulates susceptibility to Nap in C22 cells, we incubated control (scrambled siRNA-treated cells, Sc) and FMRP-depleted (*Fmr1* siRNA-treated cells, Si) cells with Nap for 1 h and then harvested cells at different timepoints for analysis (shown schematically in Fig. 2E). To assess levels of oxidative and genotoxic stress, we again stained cells with anti-4HNE and anti-γ-H2AX, respectively (Fig. 2F,H). In order to assess the cytotoxicity of Nap, we subject the cells to a WST-1 assay 24 h post exposure. We found that levels of 4HNE and γ-H2AX (Fig. 2F–I) were elevated in *Fmr1*-depleted cells at all timepoints (*n*=3 experiments each) and that *Fmr1*-depleted cells exhibited greater cell death in response to Nap (Fig. 2J). These data correlated well with the increased susceptibility of CCs to Nap in *Fmr1* KO animals and demonstrated that FMRP has a cell-intrinsic role in protecting cells from Nap.

Journal of Cell Science (2022) 135, jcs258652. doi:10.1242/jcs.258652

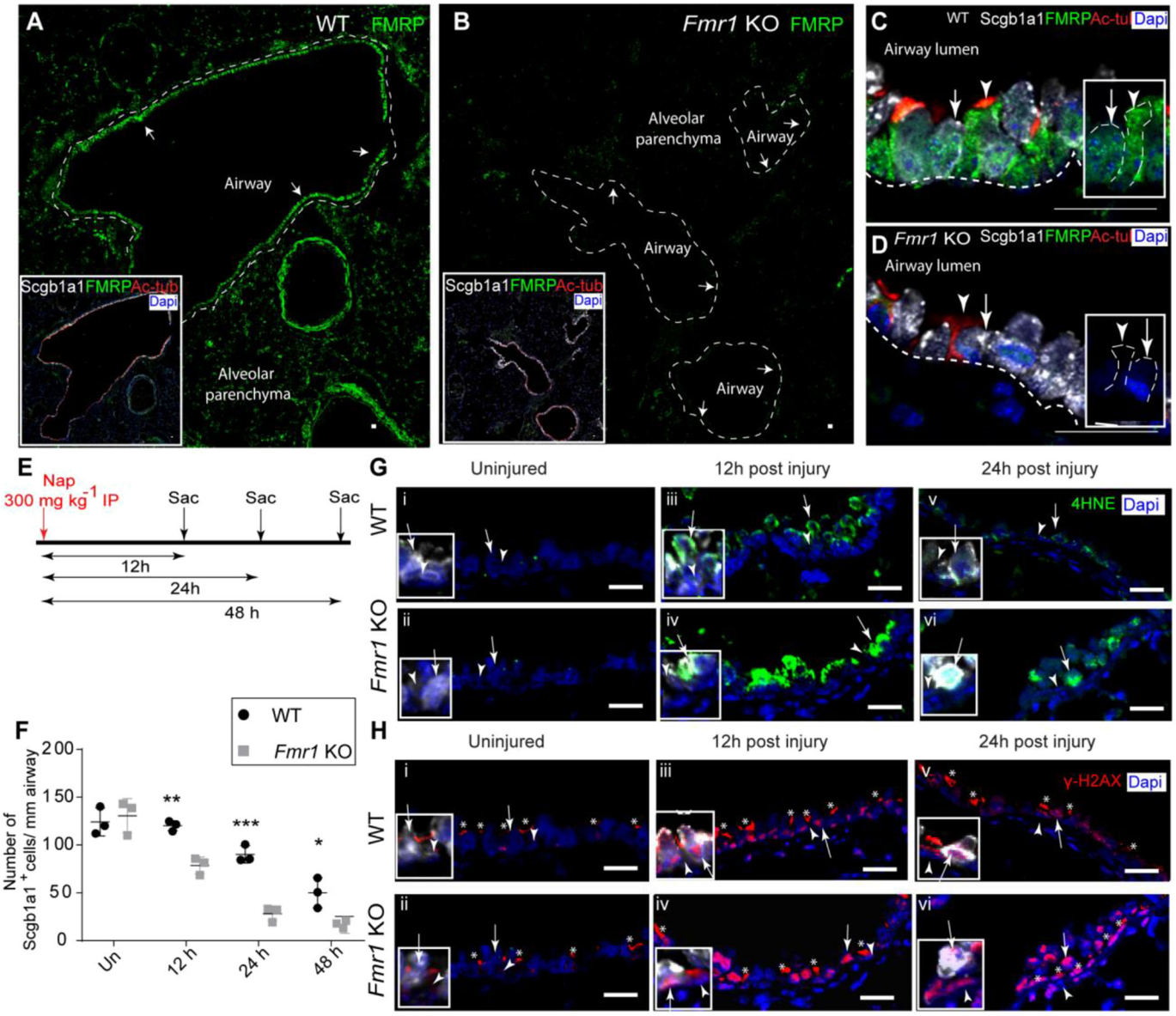

Fig. 1. FMRP is expressed in the airways and more broadly, and protects airway club cells from Nap-induced stress. (A–D) FMRP expression in the murine lung. (A) Tiled image showing FMRP immunostaining (green, white arrows) in the airway epithelium (demarcated by white dashed lines) and in the parenchyma of the murine lung. The airways are identified by expression of the club cell (CC) marker Scgb1a1 (white, inset) and of the ciliated cell marker acetylated tubulin (Ac-tub, red, inset). (B) Tiled image showing FMRP immunostaining in *Fmr1* knockout (*Fmr1* KO) mice. Note the absence of FMRP (green) in both airways (demarcated by white dashed lines, inset) and parenchyma. (C,D) High-resolution image of FMRP immunostaining (green) in airway epithelial cells. Here, CCs are shown in white (white arrow in inset) and ciliated cells are in red (white arrowhead in inset) in wild type (C) and *Fmr1* KO (D). (E–H) Susceptibility of CCs to Nap injury in control and *Fmr1* KO. (E) Schematic showing regimen for Nap injury. (F) Frequencies of Scgb1a1^{+} cells in wild type (black circles) and *Fmr1* KO (gray squares) from uninjured (Un) and Nap-injured mice at different timepoints post injury. Each data point in the scatter plot represents multiple sections from a single animal (n=3 mice) with mean±s.e.m. (G,H) Expression of markers of oxidative (4HNE) and genotoxic (γ-H2AX) stress in airways from wild-type and *Fmr1* KO mice prior to and post Nap injury. Note white arrowheads showing ciliated cells and white arrows showing CCs on the airways and in insets (counterstained with Scgb1a1 antisera, white). (G i–vi) 4HNE immunostaining (green) in the airways of wild-type (i,iii,v) and *Fmr1* KO (ii,iv,vi) mice prior to and post Nap injury. (H i–vi) γ-H2AX immunostaining (red) in the airways of control (i,iii,v) and *Fmr1* KO (ii,iv,vi) mice prior to and post Nap injury. Asterisks show cilia of ciliated cells marked with γ-H2AX (H i–vi). See also Fig. S1. Statistical significance was assessed by an unpaired two-tailed *t*-test: **P*<0.05; ***P*<0.01; ****P*<0.001. The changes in the two groups over time, across genotype and interaction parameters were also assessed by two-way ANOVA and found to be statistically significant. For Shapiro–Wilk normality test and two-way ANOVA, see Table S1. Scale bars: 20 µm.

FMRP is required for induction of the ISR pathway, which protects from Nap-induced stress

A role for FMRP in mediating stress responses has been reported previously. One of these studies has pointed towards a role for the protein in stress granule biogenesis in response to arsenite or heat shock (Didiot et al., 2009). This study suggests that FMRP may have a role in the induction of the ISR, a pathway necessary for stress granule biogenesis, or a more specific role in the induction of stress granule biogenesis, or both. As the ISR has been shown to be important for stress responses in the lung, we decided to examine the possibility that FMRP may be required for the induction of the ISR in C22 cells post Nap. We note that FMRP-deficient cells also fail to recruit γ-H2AX to stalled replication forks and single-strand breaks in response to aphidicolin, 5HU and UV

Journal of Cell Science (2022) 135, jcs258652. doi:10.1242/jcs.258652

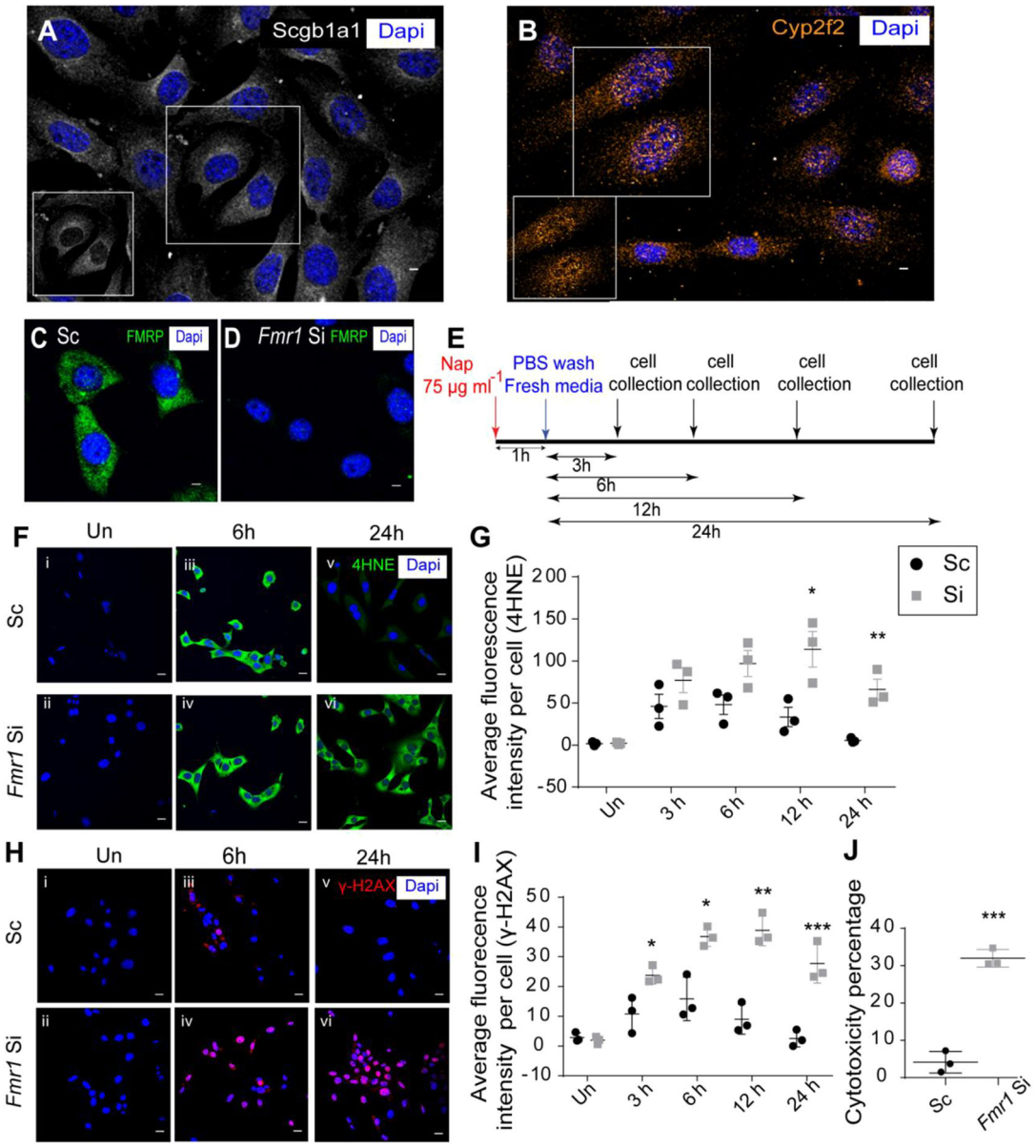

Fig. 2. FMRP-deficient club-cell-like C22 cells are susceptible to Nap-induced stress. (A–D) Phenotypic characterization of C22 cells. (A) Scgb1a1 immunostaining (white) in C22 cells. Inset shows Scgb1a1 staining alone in C22 cells from the same field. (B) Cyp2f2 (orange) immunostaining in C22 cells. Inset shows Cyp2f2 staining alone in C22 cells from the same field. See also Fig. S2. (C,D) FMRP immunostaining (green) in C22 cells treated with scrambled siRNA (C) and in C22 cells treated with *Fmr1* siRNA (D). (E–J) Susceptibility of C22 cells to Nap [control is scrambled siRNA-treated (Sc), and *Fmr1* siRNA-treated (Si)]. (E) Schematic showing regimen for Nap injury. (F–I) Expression of markers of oxidative (4HNE) and genotoxic (γ-H2AX) stress in Sc and Si cells prior to and post Nap. (Fi–vi) 4HNE immunostaining (green) in Sc and Si cells prior to and post Nap. (G) Quantification of 4HNE immunofluorescence per cell in Sc and Si cells prior to and post Nap. Un, uninjured. (Hi–vi) γ-H2AX immunostaining (red) in Sc and Si cells prior to and post Nap. (I) Quantification of γ-H2AX immunofluorescence per cell in Sc and Si cells post Nap. (J) Cytotoxicity of Nap in Sc and Si cells 24 h post Nap (*n*=3 experiments). For immunofluorescence analysis, ≥25 cells were analyzed per timepoint per experiment, *n*=3 experiments. Graphical data represent mean±s.e.m. Black circles, Sc; gray squares, Si. **P*<0.05; ***P*<0.01; ****P*<0.001 (unpaired two-tailed *t*-test). For normality test and two-way ANOVA, see Table S2. Scale bars: 5 µm.

(Alpatov et al., 2014). Although it is plausible that FMRP serves a similar role in Nap-treated cells, we noted that the nuclear accumulation of γ-H2AX in FMRP-deficient CCs and C22 cells post Nap was greater than in the respective controls. This suggested to us that the DDR was at least partially active in FMR-deficient cells and, more importantly, that extent of DNA damage (as reported by nuclear γ-H2AX accumulation) was greater in FMR-deficient cells than in controls (see the Discussion). Taken together, the findings led us to investigate the role of FMRP in the ISR pathway.

As previously mentioned, the ISR is induced when one of four stress-responsive kinases (GCN2, PERK, HRI, PKR) phosphorylate eIF2α at serine-51. Phosphorylation of eIF2α arrests conventional translation, promotes sequestration of mRNAs being actively translated and enables specialized translation of mRNAs encoding stress response proteins such as ATF4 (Pakos-Zebrucka et al., 2016; van 't Wout et al., 2014). To probe the status of the ISR in C22 cells post Nap, we examined the phosphorylation state of eIF2α. We exposed C22 cells to Nap for 1 h, harvested cells at various timepoints and quantified the levels of expression of both eIF2α and

Journal of Cell Science (2022) 135, jcs258652. doi:10.1242/jcs.258652

phosphorylated eIF2α (p-eIF2α). Western-blot-based ratiometric quantification of total and p-eIF2α in Sc cells showed that p-eIF2α levels increased 3 and 6 h post injury and decreased to baseline levels thereafter (Fig. 3A; Fig. S3A,B, *n*=5 experiments). We inferred that the ISR is induced in C22 cells in response to Nap. We then exposed Si cells to Nap for 1 h and found that, contrary to controls, the levels of p-eIF2α did not increase post Nap (Fig. 3A; Fig. S3A,B, *n*=5 experiments). The analysis of p-eIF2α suggested that FMRP depletion might inhibit the ISR.

Next, we examined the expression of ATF4 and its target, *ATF3*, in control and FMRP-deficient cells. Sc and Si cells were stained with an anti-ATF4 antibody prior to and post Nap treatment. In Sc, the expression of ATF4 was undetectable in untreated cells, increased dramatically at 3, 6 and 12 h post Nap treatment and then approached baseline levels at 24 h (Fig. 3B,C, *n*=5 experiments). In Si cells, levels of ATF4 were negligible in untreated cells and showed no appreciable increase post Nap treatment (Fig. 3B,C, *n*=5 experiments). Next, we assayed *ATF3* levels by quantitative real-time PCR (qPCR). For this, RNA was isolated from Sc and Si cells at different timepoints and subjected to qPCR analysis. In Sc, levels of *ATF3* mRNA increased at 3 and 6 h post Nap and returned to baseline thereafter (Fig. S3C, *n*=3 experiments). In Si, the *ATF3* levels did not rise appreciably above baseline post Nap (Fig. S3C). These findings were also validated with anti-ATF3 immunostaining (data not shown). Based on these data, we concluded that both ATF4 and ATF3 expression are perturbed in FMRP-deficient cells post Nap. Taken together, the findings showed that the ISR is perturbed in FMRP-deficient cells post Nap.

We also probed whether the upstream kinases that phosphorylate eIF2α and induce the ISR become activated (phosphorylated) in FMRP-deficient cells. We probed the expression of GCN2, PERK, HRI, PKR and their phosphorylated isoforms in Nap-treated C22 cells using commercially available antibodies (see the Materials and Methods). Among all pairs of antisera tested, antisera for PKR and p-PKR provided reproducible results. Western-blot-based ratiometric quantification of p-PKR and total PKR in Sc and Si cells showed that the p-PKR levels increase in both Sc and Si 3 h post Nap (Fig. S3D–F, *n*=3 experiments). Importantly, we noted that levels of p-PKR returned to baseline in Sc at 6 h and later timepoints, but remained significantly higher in Si at later timepoints (Fig. S3D–F). This suggested that at least one of the stress-responsive kinases (PKR) is activated in FMRP-deficient cells post Nap.

Perturbations to the ISR provided a plausible explanation for why FMRP-deficient C22 cells are more susceptible to Nap. To test this, we decided to probe how perturbing the ISR, by knocking down levels of *Atf4*, would impact susceptibility to Nap. Control (scrambled siRNA) and *Atf4* siRNA-treated C22 cells were exposed to Nap as described earlier and cells were harvested at different timepoints for

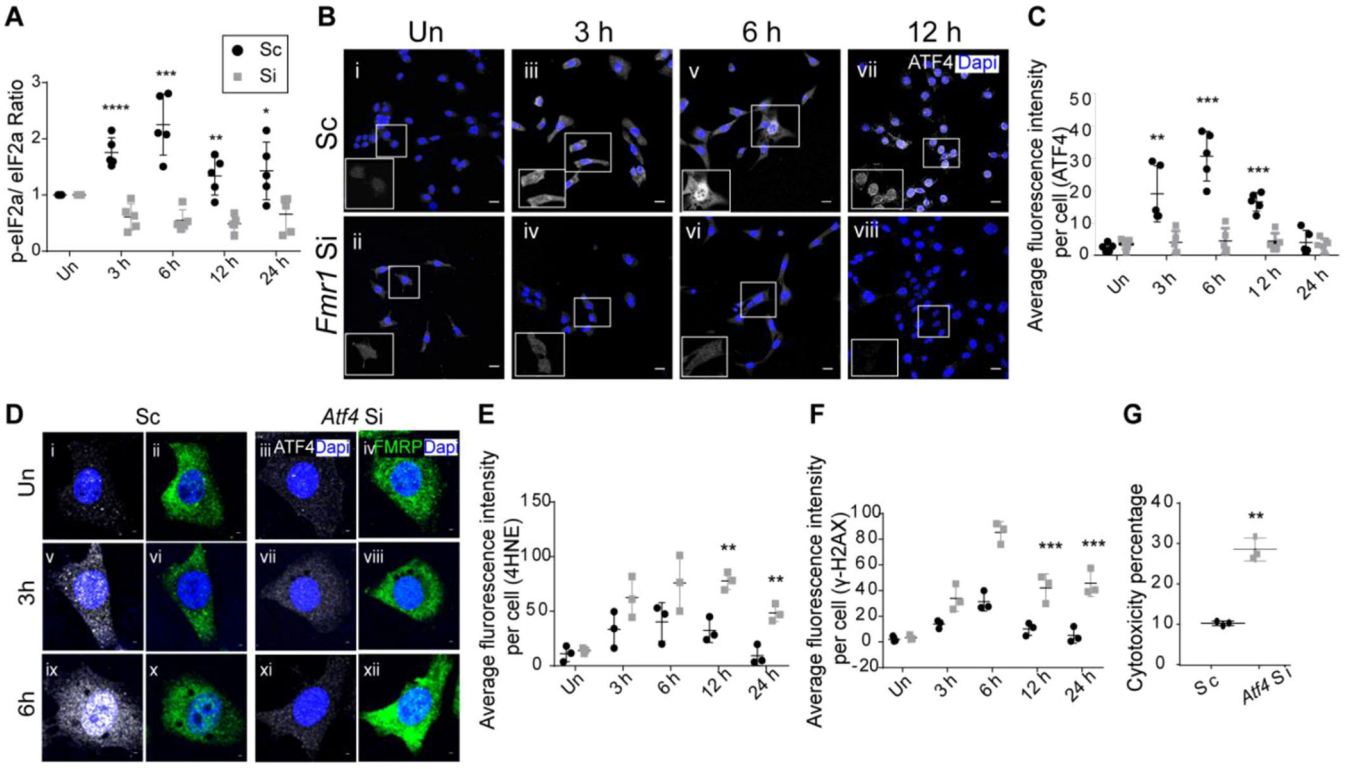

Fig. 3. FMRP-deficient C22 cells fail to upregulate the integrated stress response and to induce ATF4, essential for protection from Nap-induced stress. (A) Western blot-based quantification of phospho-eIF2α:eIF2α ratios in Sc and Si cells prior to and post Nap treatment (*n*=5 experiments). See Fig. S3 for representative blots used for quantification. Un, uninjured. (Bi–viii) ATF4 immunostaining (white) in Sc (i,iii,v,vii) and Si (ii,iv,vi,viii) cells prior to and post Nap. Note nuclear accumulation of ATF4 in Sc cells by 6 h post Nap (inset). (C) Quantification of ATF4 immunofluorescence per cell in Sc and Si cells prior to and post Nap (*n*=5 experiments). (D–G) Susceptibility of C22 cells to Nap in control (scrambled siRNA-treated, Sc) and *Atf4* siRNA-treated (Si) cells. (Di–xii) Analysis of ATF4 levels (white) and FMRP levels (green) in Sc and Si cells prior to and post Nap treatment. Immunostaining for ATF4 (white) and FMRP (green) in Sc (i,ii,v,vi,ix,x) and Si (iii,iv,vii,viii,xi,xii) cells. (E) Quantification of 4HNE immunofluorescence per cell in Sc and Si cells prior to and post Nap. See Fig. S3 for representative images. (F) Quantification of γ-H2AX immunofluorescence per cell in Sc and Si. See Fig. S3 for representative images. (G) Cytotoxicity of Nap in Sc and Si cells 24 h post Nap exposure (*n*=3 experiments). For immunofluorescence analysis, ≥25 cells were analyzed per timepoint per experiment. Graphical data represent mean±s.e.m. Black circles, Sc; gray squares, Si. **P*<0.05; ***P*<0.01; ****P*<0.001; *****P*<0.0001 (unpaired two-tailed *t*-test). For normality test and two-way ANOVA, see Table S3. Scale bars: 5 µm.

Journal of Cell Science (2022) 135, jcs258652. doi:10.1242/jcs.258652

analysis. ATF4 immunostaining of control and *Atf4* siRNA-treated cells showed that siRNA treatment eliminated ATF4 expression in cells post Nap exposure (Fig. 3D). We also found that ATF4-depleted cells exhibited increased expression of 4HNE (Fig. 3E; representative images shown in Fig. S3G) and γ-H2AX (Fig. 3F; representative images shown in Fig. S3H) at all timepoints examined (n=3 experiments each, quantification of cell fluorescence based on $n\geq25$ cells per experiment) and increased cell death 24 h post injury (Fig. 3G). We concluded that the increased levels of oxidative and genotoxic stress and increased cytotoxicity observed in FMRP-deficient cells could be the result of a failure to induce the ISR and upregulate ATF4.

In light of the findings in C22 cells, we examined whether perturbations to the ISR are also observed in FMRP-deficient CCs in Nap-treated mice. We counterstained sections from control and *Fmr1* KO lungs post Nap with antisera to both ATF4 and ATF3. Although ATF4 immunostaining was inconclusive, we noted that the levels of ATF3 were negligible in CCs in the control lung and upregulated post Nap (Fig. S3I,J, sections from n=3 mice). Pertinently, the levels of ATF3 in CCs in *Fmr1* KO did not increase post Nap. These results are consistent with a role for FMRP in the induction of ISR in CCs post Nap.

FMRP is expressed in the airways of the human lung and protects human bronchial BEAS-2B cells from 9,10-phenanthrenequinone-induced stress

The findings in the murine lung led us to ask whether FMRP has a conserved role in the human lung. To investigate this possibility, we first examined the distribution of FMRP in the human lung. Paraffin sections stained with FMRP antisera showed that FMRP is expressed throughout the airways and more broadly (Fig. 4Ai,ii,iv, n=2 sections each from n=5 independent lung biopsies). Triple labeling experiments with markers for ciliated cells and CCs showed that FMRP is expressed in both ciliated and non-ciliated cells, including CCs. Based on the distribution of FMRP, we surmised that the protein could also play a role in the airways in the human lung.

The BEAS-2B cell line is derived from normal human airways. These cells do not express markers of ciliated cells and, akin to CCs, have characteristics of non-ciliated cells. We stained BEAS-2B cells with FMRP antisera to find that these cells expressed FMRP (Fig. 4B, n=6 experiments). We then proceeded to develop an assay to probe the role of FMRP in stress responses in these cells.

Since the susceptibility of airway CCs to Nap is not recapitulated in the human lung or in BEAS-2B cells (data not shown), we utilized a different injury model to probe the role of FMRP in stress responses in human cells. 9,10-Phenanthrenequinone (PQ) is an air pollutant that is present at high levels in diesel exhaust particles and is known to trigger oxidative and genotoxic stress (Lavrich et al., 2018). As part of our characterization of PQ, we first exposed control (scrambled siRNA-treated cells) and FMRP-depleted (*Fmr1* siRNA-treated cells) C22 cells to a pulse of PQ for 1 h and harvested cells at different timepoints for analysis (data not shown). Consistent with our findings in the Nap model, we found that FMRP-depleted C22 cells exhibited increased expression of 4HNE and γ-H2AX and increased cell death 24 h post exposure (data not shown). We then examined ATF4 expression to find that although ATF4 levels increased in Sc cells at 3 h and 6 h post PQ, no expression was detected in Si cells (data not shown). These experiments showed that PQ treatment does lead to oxidative and genotoxic stress, and that FMRP-deficient C22 cells are more susceptible, and led us to examine the effects of PQ on BEAS-2B cells.

To test the role of FMRP in BEAS-2B cells, we determined that the protocol for the knockdown led to a 90% reduction in the levels of FMRP post treatment (Fig. 4B,C, n=6 experiments). Next, we exposed control (scrambled siRNA-treated cells) and FMRP-depleted (*FMR1* siRNA-treated cells) BEAS-2B cells to a pulse of PQ for 1 h and harvested them at different timepoints for analysis (shown schematically in Fig. 4D). We found that FMRP-depleted cells exhibited increased expression of 4HNE (Fig. 4E,F) and γ-H2AX (Fig. 4G,H) at all timepoints examined (n=3 experiments each, quantification of cell fluorescence based on $n\geq25$ cells per experiment) and increased cell death 24 h post injury (Fig. 4I). These experiments showed that FMRP-deficient BEAS2B cells are more susceptible to PQ.

FMRP is required for the induction of the ISR pathway, which protects from PQ-induced stress

Next, we determined whether FMRP is required for the induction of the ISR in BEAS-2B cells. As described previously, we probed the phosphorylation status of eIF2α (Fig. 5A; Fig. S4A,B, n=5), the levels of ATF4 induction (Fig. 5B,C, n=5) and the levels of *ATF3* induction (Fig. S4C, n=3), and the ratio of phosphorylation status of PKR (Fig. S4D–F) at different times post PQ. These experiments showed that although p-PKR levels were increased in both Sc and Si post PQ, all of the downstream processes of the ISR were perturbed in Si.

We then investigated whether the loss of ATF4 would recapitulate the loss of FMRP post PQ. Control (scrambled siRNA) and *ATF4* siRNA-treated BEAS-2B cells were exposed to PQ as described previously, and cells were harvested at different timepoints for analysis. Consistent with expectations, *ATF4* siRNA-treated cells showed no anti-ATF4 immunostaining post PQ exposure (Fig. 5D, n=3 experiments). We found that ATF4-depleted BEAS-2B cells exhibited increased expression of 4HNE (Fig. 5E; representative images shown in Fig. S4G) and γ-H2AX (Fig. 5F; representative images shown in Fig. S4H) and increased cell death 24 h post injury (see the Materials and Methods, Fig. 5G). These data indicated that the loss of ATF4 largely phenocopies the loss of FMRP in PQ-treated BEAS-2B cells.

The findings in BEAS-2B cells suggested that the role of FMRP in the actuation of the ISR pathway is conserved. To probe whether this finding is more broadly applicable to the lung, we performed the assays described above in another cell line of epithelial origin: A549 cells. We found that although A549 cells are of alveolar origin, they also express FMRP (Fig. S5A). Importantly, PQ exposure assays showed that A549 cells lacking FMRP exhibit higher levels of oxidative and genotoxic stress and fail to actuate ATF4 expression (Fig. S5B–I). Taken together, the studies in BEAS-2B and A549 strongly suggest that FMRP also regulates the induction of the ISR in the human respiratory epithelium.

DISCUSSION

The aim of this study was to probe the role of FMRP in stress responses in the lung. We report that FMRP plays an essential role in protecting the airways in mice, and potentially in humans, from the deleterious effects of xenobiotic stress. Our studies provide strong evidence that FMRP protects the lung by facilitating the induction of the ISR (see model, Fig. 6). In the paragraphs that follow we will discuss the plausible mechanism(s) by which FMRP may regulate the ISR, the possibility that FMRP regulates stress response pathways in addition to the ISR, and the clinical implications of the findings reported here.

Journal of Cell Science (2022) 135, jcs258652. doi:10.1242/jcs.258652

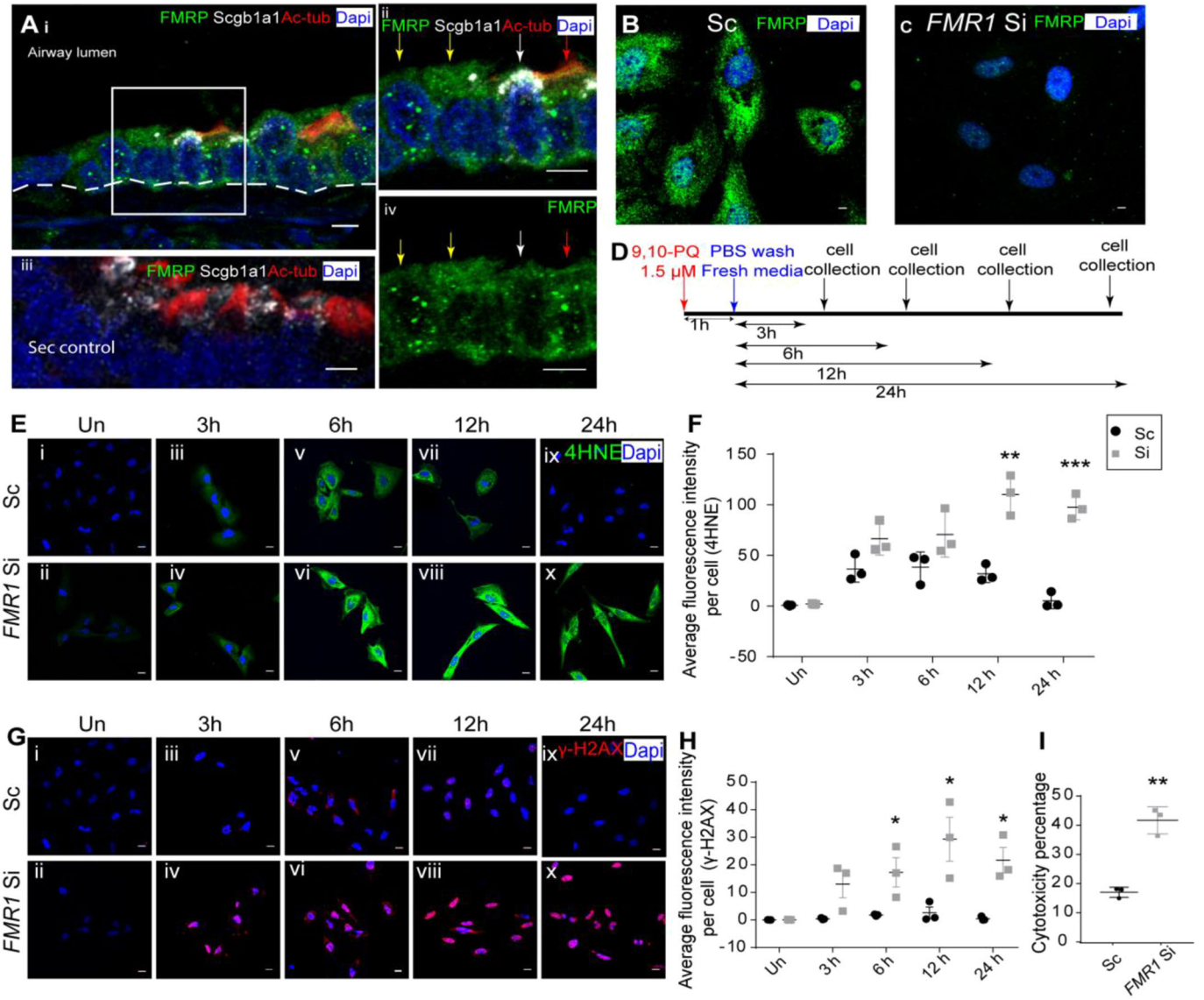

Fig. 4. FMRP is expressed in the human airways and protects human bronchial BEAS-2B cells from PQ-induced stress. (A–C) FMRP expression in the human lung and in BEAS-2B cells, a cell line derived from the human bronchial epithelium. (Ai–iv) FMRP immunostaining (green) in the distal airways of the human lung. (Ai,ii,iv) Stained section showing FMRP expression in airway non-ciliated cells [Scgb1a1$^+$ (white), white arrows; Scgb1a1$^-$, yellow arrows] and ciliated cells (red, red arrow). The white dashed line indicates airway epithelium. The boxed area in i is shown at higher magnification in ii and iv. Negative control [secondary antibody (Sec) alone] for FMRP immunostaining is shown in iii. (B) FMRP immunostaining (green) of BEAS-2B cells (control, scrambled siRNA-treated, Sc). (C) FMRP immunostaining (green) of *FMR1* siRNA-treated BEAS-2B cells. (D–I) Susceptibility of BEAS-2B cells to PQ injury in control (scrambled siRNA-treated, Sc) and *FMR1* siRNA-treated (Si) cells. (D) Schematic showing regimen for PQ injury. (E–H) Expression of markers of oxidative (4HNE) and genotoxic (γ-H2AX) stress in Sc and Si cells prior to and post PQ. Un, uninjured. (Ei–x) 4HNE immunostaining (green) in Sc and Si cells prior to and post PQ. (F) Quantification of 4HNE immunofluorescence per cell in Sc and Si cells prior to and post PQ (*n*=3 experiments). (Gi–x) γ-H2AX immunostaining (red) in Sc and Si cells prior to and post PQ. (H) Quantification of γ-H2AX immunofluorescence per cell in Sc and Si cells prior to and post PQ. (I) Cytotoxicity of PQ in Sc and Si cells 24 h post PQ exposure (*n*=3 experiments). For immunofluorescence analysis, ≥25 cells were analyzed per timepoint per experiment. Graphical data represent mean±s.e.m. Black circles, Sc; gray squares, Si. **P*<0.05; ***P*<0.01; ****P*<0.001 (unpaired two-tailed *t*-test). For normality tests and two-way ANOVA, see Table S4. Scale bars: 5 µm.

A major finding of our study is that FMRP is required for the actuation of the ISR pathway. The mechanism by which FMRP regulates this step is currently unknown. We find that the stress-responsive kinase PKR is activated in FMRP-deficient cells but that the phosphorylation of the PKR substrate, eIF2α, is perturbed. This suggests that the role of FMRP may be downstream to the activation of stress-responsive kinases. The analysis of FMRP-binding proteins in neuronal and other tissues has identified numerous interacting partners. Among these interacting partners are the proteins Caprin1 and G3BP1, which have independently been implicated in the induction of the ISR pathway in response to stress (Taha et al., 2020; Wu et al., 2016). Pertinently, both Caprin1 and G3BP1 have been shown to be important for eIF2α phosphorylation (Reineke et al., 2015; Solomon et al., 2007). Thus, it is plausible that FMRP acts in concert with Caprin1 and G3BP1 to facilitate eIF2α phosphorylation. Although eIF2α phosphorylation is an early event in the ISR pathway and perturbations at this stage are likely to affect all downstream processes, our data do not allow us to rule out the possibility that FMRP has independent roles either upstream

Journal of Cell Science (2022) 135, jcs258652. doi:10.1242/jcs.258652

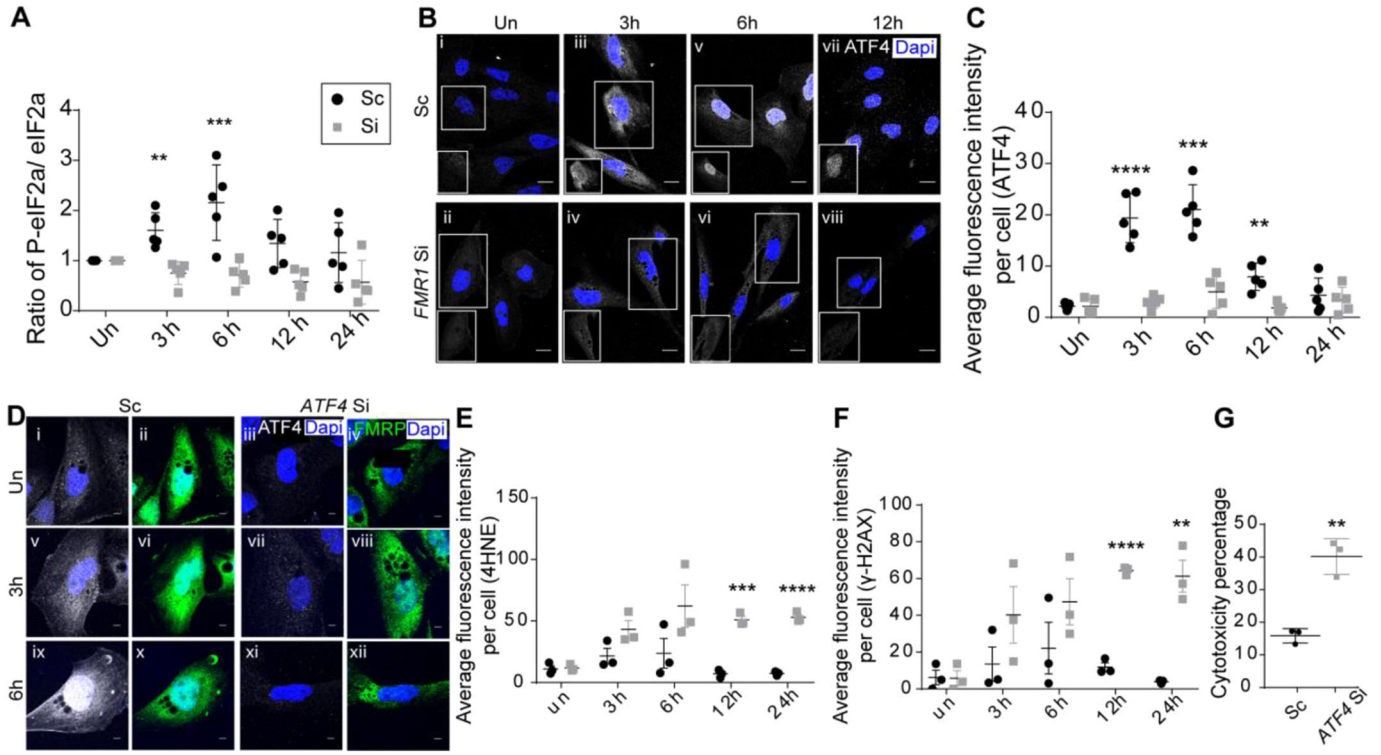

Fig. 5. FMRP-deficient BEAS-2B cells fail to upregulate the integrated stress response and to induce ATF4, essential for protection from PQ-induced stress. (A) Western blot-based quantification of phospho-eIF2α:eIF2α ratios in Sc and Si cells prior to and post PQ treatment (n=5 experiments). Un, uninjured. See Fig. S4A,B for representative blots used for quantification. (B,C) Analysis of ATF4 prior to and post PQ. (Bi–viii) ATF4 immunostaining (white) in Sc (i,iii,v,vii) and Si (ii,iv,vi,viii) cells prior to and post PQ treatment. Note nuclear accumulation of ATF4 in Sc cells by 6 h post PQ treatment (inset). (C) Quantification of ATF4 immunofluorescence per cell in Sc and Si cells prior to and post PQ (n=5 experiments). (D–G) Susceptibility of BEAS-2B cells to PQ in control (scrambled siRNA-treated, Sc) and *ATF4* siRNA-treated (Si) cells. (Di–xii) Analysis of ATF4 levels (white) and FMRP levels (green) in Sc (i,ii,v,vi,ix,x) and Si (iii,iv,vii,viii,xi,xii) cells prior to and post PQ treatment. (E) Quantification of 4HNE immunofluorescence per cell in Sc and Si. See Fig. S4G for representative images. (F) Quantification of γ-H2AX immunofluorescence per cell in Sc and Si. See Fig. S4H for representative images. (G) Cytotoxicity of PQ in Sc and Si cells 24 h post PQ treatment (n=3 experiments). For immunofluorescence analysis, ≥25 cells were analyzed per timepoint per experiment. Graphical data represent mean±s.e.m. Black circles, Sc; gray squares, Si. **P<0.01; ***P<0.001; ****P<0.0001 (unpaired two-tailed t-test). For normality test and two-way ANOVA, see Table S5. Scale bars: 5 µm.

or downstream. Our future experiments will probe these possibilities.

Studies that have examined the role of FMRP vis-à-vis stress responses suggest that FMRP could protect cells from stress in myriad ways. For example, it has been demonstrated that FMRP plays a chromatin-dependent role in inducing the DDR. This could be relevant in the context of the lung. Along the same lines, there is also evidence that FMRP regulates the expression of superoxide dismutase 1 (SOD1) in the brain (Bechara et al., 2009). Levels of SOD1 are reduced in the brains of *Fmr1* KO animals. As SOD1 has an important role in protecting cells from stress, FMRP could alter the susceptibility of tissues to stressful stimuli by altering the baseline levels of SOD1. To investigate this possibility, we probed levels of SOD1 in the brain and lung using both western blot and immunohistochemical approaches (Fig. S6). Although we did observe that SOD1 levels in the brain were lower in *Fmr1* KO than wild type, the levels of SOD1 in the lung were comparable (Fig. S6A,B). Moreover, we also analyzed SOD1 levels in the bronchial cell lines (C22 and BEAS-2B) with or without FMRP to find that SOD1 levels were comparable (Fig. S6D–I). Taken together, these data show FMRP is unlikely to regulate SOD1 expression in the lung. Nevertheless, the role of FMRP in the DDR (Alpatov et al., 2014), and in the regulation of SOD1 expression in the brain, show that FMRP can contribute towards protecting tissues from stress by ISR-independent mechanisms as well.

Although FMRP is expressed in many tissues in humans and mice alike (https://www.genecards.org/cgi-bin/carddisp.pl?gene=FMR1), historically, FMRP has almost exclusively been studied in a neural context because of its connection with intellectual disability. An important finding of this study is that it demonstrates a role for FMRP in the lung. Although the data implicating a role for FMRP in the human lung is based on findings in cell lines and requires validation in more physiologic assays, the data clearly point towards a potential vulnerability in individuals with an *FMR1* deficiency. Clinically, the bulk of the case studies on FXS patients are derived from geographic regions where the load of pulmonary environmental stressors is low. Our study suggests that individuals with FXS living in areas of higher pollutant load may be more susceptible to lung damage and disease, and FMRP status in the lung may be a strong correlate of resilience to pulmonary insults.

MATERIALS AND METHODS

All animal work reported here has been approved by the Internal Animal Users Committee (IAUC) and the Institutional Animal Ethics Committee (IAEC) at inStem. Any procedure that could conceivably cause distress to the animals employed pre-procedural anesthesia with isoflurane gas (Baxter Healthcare Corp.), delivered by an anesthetic vaporizing machine. All animals were monitored for signs of distress and killed if in distress. The analysis of human biopsies was approved by the Institutional Ethics Committee of JSS Medical College.

Journal of Cell Science (2022) 135, jcs258652. doi:10.1242/jcs.258652

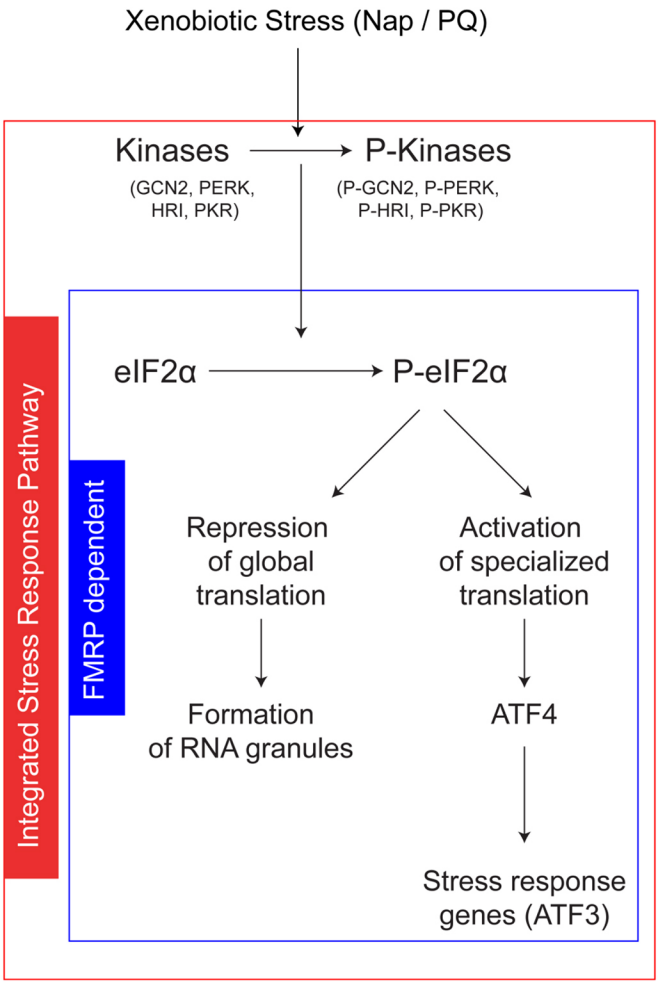

Fig. 6. Model for the role of FMRP in the regulation of the integrated stress response in the lung. Exposure to xenobiotics such as Nap and PQ result in the activation of at least one of four stress-responsive kinases (GCN2, PERK, PKR, HRI) and in the induction of the ISR pathway (outlined in red). Our findings suggest that FMRP has an essential role downstream of phosphorylation of kinases (outlined in blue).

Mouse strains

An *Fmr1* knockout (Fmr1 tm1 Cgr) mouse (*Mus musculus*) strain was maintained on a C57BL/6J background at Brain Development and Disease Mechanisms (BDDM), inStem. Genotyping of the animals was performed using established protocols (Bakker et al., 1994).

Human samples

Human (*Homo sapiens*) lung tissue was obtained from five subjects at autopsy by a forensic pathologist from JSS Medical College, Mysore. The cause of death was not attributed to lung trauma. De-identified samples were fixed in 4% paraformaldehyde (PFA) at 4°C overnight, embedded in paraffin, and processed for immunohistochemical analysis. All human tissues were obtained following due protocols and all clinical investigations have been conducted according to the principles expressed in the Declaration of Helsinki.

Cell lines and culture conditions

Human lung (BEAS-2B) non-ciliated airway epithelial origin cell line and human alveolar basal epithelial adenocarcinomic (A549) cell line were obtained from Johns Hopkins University (kind gifts from Prof. Shyam Biswal, Department of Environmental Health and Engineering, Johns Hopkins Bloomberg School of Public Health, USA; Singh et al., 2009, 2013). The murine club cell line (C22) was purchased from ECACC, UK (cat. no. 07021401, #07D022). All cell lines were tested for mycoplasma contamination and found to be negative. BEAS-2B were grown in DMEM: F12K (Gibco, USA, 21127030) (1:1) medium and A549 cells were grown in DMEM, supplemented with 10% FBS (Gibco, USA, 10082147) and penicillin-streptomycin (Gibco, USA, 1540122) at 37°C and 5% CO_2. The C22 cell line was maintained in a proliferative state as per the supplier's instructions, and experiments were performed 24 h post differentiation. Experiments were conducted within the 3rd to 7th passages for BEAS-2B and A549, and within the 3rd to 12th passages for C22.

Models for xenobiotic stress

For Nap injury in mice, wild-type or *Fmr1* KO mice aged ≥8 weeks of age (2 males and 1 female per timepoint per genotype) were injected intraperitoneally with corn oil (vehicle, Sigma, USA, C8267) or with Nap dissolved in corn oil (300 mg kg^{-1}, Sigma, USA, 147141) using established protocols (Guha et al., 2014, 2012). Animals were killed 12 h, 24 h or 48 h after injection for analysis.

To establish an assay for Nap injury in C22 cells, we first determined that these cells expressed Cyp2f2, which converts Nap to stress-inducing derivatives. Having established this, we tested a range of concentrations of Nap (50 µg ml^{-1} to 500 µg ml^{-1}, in DMSO in DMEM). Nap was found to be stable in solution at concentrations up to 100 µg ml^{-1} and unstable at higher concentrations, leading to cell death within 3 h post exposure. Nap exposure at 50–75 µg ml^{-1} (DMSO in DMEM, DMSO final concentration 0.7%) for short (1 h) and long (24 h) duration led to a progressive increase in expression of stress markers and mild cytotoxicity after a 24 h period. To probe the effects of FMRP or ATF4 deficiency on susceptibility to Nap, cells were exposed to Nap at 75 µg ml^{-1} (DMSO in DMEM, DMSO final concentration 0.7%) for a period of 1 h. Cells were then washed in PBS and chased for varying periods of time in complete medium.

It has been reported previously that PQ causes a sharp decrease in the viability of BEAS-2B cells when administered to cells for 24 h at concentrations greater than 1 µM (Koike et al., 2014). We reconfirmed these findings and determined the LD_{50} to be ∼1.5 µM (Sigma, USA, 275034; dissolved in DMSO in DMEM, DMSO final concentration 0.00002%). To probe the effects of FMRP or ATF4 deficiency on susceptibility to PQ, cells were exposed to PQ at 1.5 µM (DMSO in DMEM, DMSO final concentration 0.00002%) for a period of 1 h. Cells were then washed with PBS, and fresh complete medium was added and chased for varying periods of time in complete medium. A549 cells were also treated with a 1.5 µM dose of PQ for 1 h. Cells were washed with PBS and kept in fresh complete medium and collected at different timepoints for analysis.

siRNA-based knockdown of FMRP, Cyp2f2 and ATF4 expression

Several studies have demonstrated that multiple siRNAs administered together or sequentially work more efficiently for silencing gene expression than a single siRNA (Wang et al., 2016; Fähling et al., 2009; Zhang et al., 2015; Hatch et al., 2010). For our studies we used three or two distinct siRNAs for each targeted gene. siRNAs were administered to cells sequentially, 12 h apart, to silence the gene expression. siRNA transfections were performed with Lipofectamine 2000 (Thermo Fisher Scientific, USA, 11668027). All xenobiotic stress assays in C22 cells were performed 36 h after treatment with the last siRNA. C22 cells were transferred from proliferative to differentiation-inducing medium 12 h after the last siRNA treatment and utilized for xenobiotic stress assays 24 h thereafter. All xenobiotic stress assays in BEAS-2B cells were performed 12 h after treatment with the last siRNA. All siRNAs were obtained from Ambion, USA: murine *Fmr1* (4390771), murine *Atf4* (16708), murine *Cyp2f2* (4390771), human *FMR1* (4392420) and human *ATF4* (16708), and scrambled (negative control, 4390843). The assay IDs for each of the siRNAs are as follows: mouse *Fmr1* siRNA (Assay ID: 5315, 5317, s66177), Human *FMR1* siRNA (Assay ID: 5315, 5316, 5317), mouse *Atf4* siRNA (Assay ID: 160775, 160776, 160777), Mouse *Cyp2f2* siRNA (Assay ID: s64735, s64734), and human *ATF4* siRNA (Assay ID: 122168, 122287, 122372).

Cell cytotoxicity assay

C22 and BEAS-2B cells were inoculated into a 96-well plate and treated with Nap or PQ for 1 h, as described above, and harvested for analysis 24 h later. Cell viability was assayed using WST-1 reagent (Sigma, USA, 5015944001). Briefly, cells were incubated with WST-1 for 4 h and absorbance readings were taken and analyzed as per the manufacturer's protocols. Cytotoxicity percentage=100 [(OD (450 nm–650 nm) of untreated cells – OD (450 nm–650 nm) of treated cells)/OD (450 nm–650 nm) of untreated cells].

Histology, immunofluorescence and imaging

Lungs were inflated with 4% (w/v) PFA (Alfa Aesar, USA, 30525-89-4) in PBS and fixed for 8 h at 4°C. Fixed lungs were subsequently embedded in paraffin, sectioned (5 µm) and processed for immunohistochemical analysis post heat-mediated antigen retrieval at pH 6.0 (Vector Labs, USA, H-3300) except for sections stained with anti-SOD1 antisera, which were subject to antigen retrieval at pH 9.0 (Vector Labs, USA, H-3301). For cellular immunostaining, cells were seeded on coated coverslips (0.1% gelatin, Sigma, USA, G9391), as per the manufacturer's protocol. Post treatment, cells were fixed with 4% PFA for 30 min and blocked with 2% FBS, 0.2% BSA and 0.1% Triton X-100 in 1× PBS for 1 h and stained. Primary antibodies were diluted using the same blocking solution. Immunohistochemical analysis utilized the following antisera: rabbit anti-FMRP (Abcam, UK, 17722, 1:500), rabbit anti-FMRP (Sigma, USA, F4055 1:200), goat anti-Scgb1a1 (Santa Cruz, USA, Sc365992, 1:500), mouse anti-acetylated tubulin (Sigma, USA, T7451, 1:1000), mouse anti-4HNE (Abcam, UK, ab48506, 1:500), rabbit anti-γ-H2AX (Novus Biologicals, USA, NB100-384, 1:1000), mouse anti-Cyp2f2 (Santa Cruz, USA, SC374540, 1:100), mouse anti-ATF4 (Sigma, USA, WH0000468M1, 1:200), rabbit anti-ATF3 (Sigma, USA, HPA001562, 1:200), rabbit anti-SOD1 (Abcam, UK, ab16831, 1:200) and Alexa Fluor 488, 568 or 647-conjugated donkey anti-mouse, -rabbit or -goat IgG secondary antibodies (Invitrogen, USA, A21447, A21202, A21206, A10037, A10042, A31571, 1:300). Stained sections were mounted in ProLong Diamond (Invitrogen, USA, P36962). All samples were imaged on a FV3000 4-laser and FV3000 5-laser confocal microscope or on a Zeiss LSM-780 laser-scanning confocal microscope (Carl Zeiss AG, Germany). For H&E staining, sections were stained with hematoxylin for 10 s and eosin for 30 s, dried and mounted in DPX and imaged on a Nikon Eclipse Ti2 microscope (Nikon, Japan).

Quantitative fluorescence microscopy

Frequencies of club cells/mm of airway, and total cellular fluorescence in club cells, in lung sections, were determined from single tiled optical sections acquired on a confocal microscope using ImageJ software. For club cell frequency analysis, cells attached to the basement membrane were counted per section per animal. Total cellular fluorescence intensity was calculated by subtracting a 'background' value per section from the integrated density per cell (outlined using the software) (for FMRP, 4HNE, γ-H2AX and ATF4). The 'background' value was determined by sampling integrated density of regions on the section devoid of cells. Total cellular fluorescence of C22 and BEAS-2B cells was estimated from single optical sections on a confocal microscope using ImageJ software. In all experiments involving C22, BEAS-2B and A549 cells, ≥25 cells were analyzed per timepoint, per experiment. The images of Scgb1a1 and Cyp2f2 expression in C22 cells are maximum intensity projection images of z-stacks acquired on a confocal microscope.

Western blot analysis

Protein was extracted from cell lysates using RIPA buffer (Thermo Fisher Scientific, USA, 89900) containing Sigmafast EDTA-free protease inhibitor cocktail (Sigma, USA, s8830) and PhosSTOP (Merck, USA, 4906845001). Total protein was run on a 12% SDS PAGE gel, transferred onto a nitrocellulose membrane (Amersham, UK, 10600002), and the membrane was stained with reversible MemCode (Thermo Fisher Scientific, USA, 24580) for total protein estimation [imaged on ImageQuant600 (Amersham, UK) and quantified using ImageJ]. The membrane was subsequently destained, blocked with 5% BSA (Sigma, USA, A9418) for 1 h and probed using the following primary antisera: rabbit anti-Phospho-eIF2α (Ser51) (Cell Signaling Technology, USA, 9721S, 1:1000), mouse anti-eIF2α (Cell Signaling Technology, USA, 2103S, 1:1000), rabbit anti-phospho-PKR (Sigma, USA, SAB4504517, 1:3000), mouse anti-PKR (Santa Cruz, USA, Sc-6282, 1:1000), rabbit anti-GCN2 (Cell Signaling Technology, USA, 3302s), mouse anti-phospho-GCN2 (Cell Signaling Technology, USA, 3301S), rabbit anti-PERK (Cell Signaling Technology, USA, 3192s, 1:1000), rabbit anti-phospho-PERK (Cell Signaling Technology, USA, 3179s), mouse anti-HRI (Santa Cruz, USA, sc-365239). Primary antisera was detected using the following secondary antisera: HRP-conjugated anti-rabbit (Abcam, UK, 6721, 1:3000) and HRP-conjugated anti-mouse secondary (Invitrogen, USA, # 62-6520 1:5000) antibodies and ECL (BioRad, USA, 1620177) and analyzed (imaged on ImageQuant600 and quantified using ImageJ). The levels of eIF2α, phospho-eIF2α, PKR and Phospho-PKR were normalized to the total protein content of the respective lanes. For analysis of SOD1 expression from murine brain and lung tissue lysate, tissues were collected after dissection, washed with PBS and protein was extracted with RIPA buffer and protease inhibitor cocktail. Total protein was run on a 12% SDS PAGE gel and transferred onto a nitrocellulose membrane. We used 5% non-fat dry milk (Santa Cruz, USA, Sc-2325) solution in PBS for blocking and probed the blots with anti-SOD1 (Abcam, UK, ab16831) and anti-β-tubulin (CST, USA, 15115S) antisera. Levels of SOD1 were normalized to corresponding β-tubulin levels.

Quantitative PCR analysis

RNA from cell lysates was extracted using TRIzol (Invitrogen, USA, 15596018, as per the manufacturer's protocol) and qPCR was performed using the primers listed in Table S11. The qPCR assays were constituted with the Maxima SYBR Green/ROX qPCR Master Mix (2×) (Thermo Scientific, USA, K0221) and analyzed on a BioRad CFX3 real-time PCR system (BioRad, USA).

Statistical analysis

Statistical significance of datasets was assessed using unpaired two-tailed *t*-tests post Shapiro–Wilk tests for normality. Data were also analyzed using a two-way ANOVA with a Sidak post-hoc test to compare changes in two groups with respect to time, genotype and interaction parameters. ANOVA data and normality test results for each figure are presented in a tabular format (Tables S1–S10).

Acknowledgements

We thank Joseph Jomon, National Centre for Cell Science (NCCS), Pune for sharing antibodies; Aditya Deshpande, inStem, for assistance in animal experiments; Sarfaraz Nawaz and Sudhriti Ghosh Dastidar, inStem, for their assistance with biochemical analyses; Harlin Kaur, Binita Dam, Arnab Karmakar and Mamta Yadav for technical assistance; and the Central Imaging and Flow Cytometry Facility (CIFF) and Animal Care and Resource Center (ACRC) Facility at Bangalore Life Science Cluster (BLiSC) for their constant support.

Competing interests

The authors declare no competing or financial interests.

Author contributions

Conceptualization: D.S.B., R.B., S. Chavda, R.M., S. Chattarji, R.T., A.B., A.G.; Methodology: D.S.B., R.M., C.V., S. Chattarji, A.G.; Validation: D.S.B., R.B., I.G., S.M.L., R.T., A.B.; Formal analysis: D.S.B., R.M., S. Chattarji, R.T., A.B., A.G.; Investigation: D.S.B., R.B., I.G., S. Chavda, S.M.L., C.V.; Writing - original draft: D.S.B., A.G.; Writing - review & editing: S. Chavda; Visualization: D.S.B., A.G.; Supervision: A.G.; Project administration: D.S.B., A.G.; Funding acquisition: A.G.

Funding

This work was funded by Institute for Stem Cell Science and Regenerative Medicine core funds and the Ramalingaswami Reentry Fellowship (A.G., R.B.), and fellowships from the Department of Biotechnology (S.M.L.), Indian Council of Medical Research (I.G.) and University Grants Commission – Council of Scientific and Industrial Research (D.S.B.).

Peer review history

The peer review history is available online at https://journals.biologists.com/jcs/article-lookup/doi/10.1242/jcs.258652.

References

Alpatov, R., Lesch, B. J., Nakamoto-Kinoshita, M., Blanco, A., Chen, S., Stützer, A., Armache, K. J., Simon, M. D., Xu, C., Ali, M. et al. (2014). A chromatin-dependent role of the fragile X mental retardation protein FMRP in the DNA damage response. *Cell.* **157**, 869-881. doi:10.1016/j.cell.2014.03.040

Bakker, C. E., Verheij, C., Willemsen, R., van der Helm, R., Oerlemans, F., Vermey, M., Bygrave, A., Hoogeveen, A., Oostra, B. A., Reyniers, E. et al. (1994). Fmr1 knockout mice: a model to study fragile X mental retardation. *Cell.* **78**, 23-33. doi:10.1016/0092-8674(94)90569-X

Bechara, E. G., Didiot, M. C., Melko, M., Davidovic, L., Bensaid, M., Martin, P., Castets, M., Pognonec, P., Khandjian, E. W., Moine, H. et al. (2009). A novel function for fragile X mental retardation protein in translational activation. *PLoS. Biol.* **7**, e16. doi:10.1371/journal.pbio.1000016

Buckpitt, A., Boland, B., Isbell, M., Morin, D., Shultz, M., Baldwin, R., Chan, K., Karlsson, A., Lin, C., Taff, A. et al. (2002). Naphthalene-induced respiratory tract toxicity: metabolic mechanisms of toxicity. *Drug. Metab. Rev.* **34**, 791-820. doi:10.1081/DMR-120015694

Demello, D. E., Mahmoud, S., Ryerse, J. and Hoffmann, J. W. (2002). Generation and characterization of a conditionally immortalized lung clara cell line from the H-2Kb-tsA58 transgenic mouse. *In. Vitro. Cell. Dev. Biol. Anim.* **38**, 154-164. doi:10.1290/1071-2690(2002)038<0154:GACOAC>2.0.CO;2

Didiot, M.-C., Subramanian, M., Flatter, E., Mandel, J.-L. and Moine, H. (2009). Cells lacking the fragile X mental retardation protein (FMRP) have normal RISC activity but exhibit altered stress granule assembly. *Mol. Bio. Cell* **20**, 428-437. doi:10.1091/mbc.e08-07-0737

Fähling, M., Mrowka, R., Steege, A., Kirschner, K. M., Benko, E., Förstera, B., Persson, P. B., Thiele, B. J., Meier, J. C. and Scholz, H. (2009). Translational regulation of the human achaete-scute homologue-1 by fragile X mental retardation protein. *J. Bio. Chem.* **284**, 4255-4266. doi:10.1074/jbc.M807354200

Guha, A., Vasconcelos, M., Cai, Y., Yoneda, M., Hinds, A., Qian, J., Li, G., Dickel, L., Johnson, J. E., Kimura, S. et al. (2012). Neuroepithelial body microenvironment is a niche for a distinct subset of Clara-like precursors in the developing airways. *Proc. Natl. Acad. Sci. USA* **109**, 12592-12597. doi:10.1073/pnas.1204710109

Guha, A., Vasconcelos, M., Zhao, R., Gower, A. C., Rajagopal, J. and Cardoso, W. V. (2014). Analysis of Notch signaling-dependent gene expression in developing airways reveals diversity of Clara cells. *PLoS. ONE* **9**, e88848. doi:10.1371/journal.pone.0088848

Guha, A., Deshpande, A., Jain, A., Sebastiani, P. and Cardoso, W. V. (2017). Uroplakin 3a+ cells are a distinctive population of epithelial progenitors that contribute to airway maintenance and post-injury repair. *Cell Rep.* **19**, 246-254. doi:10.1016/j.celrep.2017.03.051

Hatch, E. M., Kulukian, A., Holland, A. J., Cleveland, D. W. and Stearns, T. J. (2010). Cep152 interacts with Plk4 and is required for centriole duplication. *Cell Biol.* **191**, 721-729. doi:10.1083/jcb.201006049

He, C. H., Gong, P., Hu, B., Stewart, D., Choi, M. E., Choi, A. M. K. and Alam, J. (2001). Identification of activating transcription factor 4 (ATF4) as an Nrf2-interacting protein. Implication for heme oxygenase-1 gene regulation. *J. Biol. Chem.* **276**, 20858-20865. doi:10.1074/jbc.M101198200

Koike, E., Yanagisawa, R. and Takano, H. (2014). Toxicological effects of polycyclic aromatic hydrocarbons and their derivatives on respiratory cells. *Atmos. Environ.* **97**, 529-536. doi:10.1016/j.atmosenv.2014.04.003

Konsavage, W. M., Zhang, L., Wu, Y. and Shenberger, J. S. (2012). Hyperoxia-induced activation of the integrated stress response in the newborn rat lung. *Am. J. Physiol. Lung. Cell. Mol. Physiol.* **302**, L27-L35. doi:10.1152/ajplung.00174.2011

Lavrich, K. S., Corteselli, E. M., Wages, P. A., Bromberg, P. A., Simmons, S. O., Gibbs-Flournoy, E. A. and Samet, J. M. (2018). Investigating mitochondrial dysfunction in human lung cells exposed to redox-active PM components. *Toxicol. Appl. Pharmacol.* **342**, 99-107. doi:10.1016/j.taap.2018.01.024

Linder, B., Plöttner, O., Kroiss, M., Hartmann, E., Laggerbauer, B., Meister, G., Keidel, E. and Fischer, U. (2008). Tdrd3 is a novel stress granule-associated protein interacting with the Fragile-X syndrome protein FMRP. *Hum. Mol. Genet.* **17**, 3236-3246. doi:10.1093/hmg/ddn219

Pakos-Zebrucka, K., Koryga, I., Mnich, K., Ljujic, M., Samali, A. and Gorman, A. M. (2016). The integrated stress response. *EMBO Rep.* **17**, 1374-1395. doi:10.15252/embr.201642195

Reineke, L. C., Kedersha, N., Langereis, M. A., van Kuppeveld, F. J. M. and Lloyd, R. E. (2015). Stress granules regulate double-stranded RNA-dependent protein kinase activation through a complex containing G3BP1 and Caprin1. *M. Bio.* **6**, e02486-14. doi:10.1128/mBio.02486-14

Santoro, M. R., Bray, S. M. and Warren, S. T. (2012). Molecular mechanisms of fragile X syndrome: a twenty-year perspective. *Annu. Rev. Pathol.* **7**, 219-245. doi:10.1146/annurev-pathol-011811-132457

Sarcinelli, C., Dragic, H., Piecyk, M., Barbet, V., Duret, C., Barthelaix, A., Ferraro-Peyret, C., Fauvre, J., Renno, T., Chaveroux, C. et al. (2020). ATF4-Dependent NRF2 transcriptional regulation promotes antioxidant protection during endoplasmic reticulum stress. *Cancers* **12**, 569. doi:10.3390/cancers12030569

Singh, A., Ling, G., Suhasini, A. N., Zhang, P., Yamamoto, M., Navas-Acien, A., Cosgrove, G., Tuder, R. M., Kensler, T. W., Watson, W. H. et al. (2009). Nrf2-dependent sulfiredoxin-1 expression protects against cigarette smoke-induced oxidative stress in lungs. *Free. Radic. Biol. Med.* **46**, 376-386. doi:10.1016/j.freeradbiomed.2008.10.026

Singh, A., Happel, C., Manna, S. K., Acquaah-Mensah, G., Carrerero, J., Kumar, S., Nasipuri, P., Krausz, K. W., Wakabayashi, N., Dewi, R. et al. (2013). Transcription factor NRF2 regulates miR-1 and miR-206 to drive tumorigenesis. *J. clin. Investing.* **123**, 2921-2934. doi:10.1172/JCI66353

Solomon, S., Xu, Y., Wang, B., David, M. D., Schubert, P., Kennedy, D. and Schrader, J. W. (2007). Distinct structural features of Caprin-1 mediate its interaction with G3BP-1 and its induction of phosphorylation of eIF2α, entry to cytoplasmic stress granules, and selective interaction with a subset of mRNAs. *J. Mol. Cell. Bio.* **27**, 2324-2342. doi:10.1128/MCB.02300-06

Stripp, B. R., Maxson, K., Mera, R. and Singh, G. (1995). Plasticity of airway cell proliferation and gene expression after acute naphthalene injury. *Am. J. Physiol.* **269**, L791-L799. doi:10.1152/ajplung.1995.269.6.L791

Taha, M. S., Haghighi, F., Stefanski, A., Nakhaei-Rad, S., Kazemein Jasemi, N. S., Al Kabbani, M. A., Görg, B., Fujii, M., Lang, P. A., Häussinger, D. et al. (2020). Novel FMRP interaction networks linked to cellular stress. *FEBS J.* **288**, 837-860. doi:10.1111/FEBS.15443

van 't Wout, E. F. A., Hiemstra, P. S. and Marciniak, S. J. (2014). The integrated stress response in lung disease. *Am. J. Respir. Cell. Mol. Bio.l* **50**, 1005-1009. doi:10.1165/rcmb.2014-0019TR

Van Winkle, L. S., Buckpitt, A. R., Nishio, S. J., Isaac, J. M. and Plopper, C. G. (1995). Cellular response in naphthalene-induced Clara cell injury and bronchiolar epithelial repair in mice. *Am. J. Physiol.* **269**, L800-L818. doi:10.1152/ajplung.1995.269.6.L800

Wang, Z., Sun, W., Cao, J., Cui, H. and Ma, Z. (2016). Repeated Aurora-A siRNA transfection results in effective apoptosis of A549 cells compared to single transfection. *Clin. Lab.* **62**, 697-703. doi:10.7754/clin.lab.2015.150836

Wong, H. R. and Wispe, J. R. (1997). The stress response and the lung. *Am. J. Physiol.* **273**, L1-L9. doi:10.1152/ajplung.1997.273.1.L1

Wu, Y., Zhu, J., Huang, X. and Du, Z. (2016). Crystal structure of a dimerization domain of human Caprin-1: insights into the assembly of an evolutionarily conserved ribonucleoprotein complex consisting of Caprin-1, FMRP and G3BP1. *Acta Crystallogr. Sec. D J. Struct. Bio.* **72**, 718-727. doi:10.1107/S2059798316004903

Zhang, P., Abdelmohsen, K., Liu, Y., Tominaga-Yamanaka, K., Yoon, J.-H., Ioannis, G., Martindale, J. L., Zhang, Y., Becker, K. G., Yang, I. H. et al. (2015). Novel RNA- and FMRP-binding protein TRF2-S regulates axonal mRNA transport and presynaptic plasticity. *Nat. Commun.* **6**, 8888. doi:10.1038/ncomms9888

Zhou, Z., Cao, M., Guo, Y., Zhao, L., Wang, J., Jia, X., Li, J., Wang, C., Gabriel, G., Xue, Q. et al. (2014). Fragile X mental retardation protein stimulates ribonucleoprotein assembly of influenza A virus. *Nat. Commun.* **5**, 3259. doi:10.1038/ncomms4259

RESEARCH ADVANCE

Duox-generated reactive oxygen species activate ATR/Chk1 to induce G2 arrest in *Drosophila* tracheoblasts

Amrutha Kizhedathu[1], Piyush Chhajed[1], Lahari Yeramala[2], Deblina Sain Basu[1,3], Tina Mukherjee[1], Kutti R Vinothkumar[2], Arjun Guha[1]*

[1]Regulation of Cell Fate, Institute for Stem Cell Science and Regenerative Medicine (inStem), Bangalore, India; [2]National Centre for Biological Sciences, Tata Institute of Fundamental Research, Bangalore, India; [3]Trans Disciplinary University, Bangalore, India

Abstract Progenitors of the thoracic tracheal system of adult *Drosophila* (tracheoblasts) arrest in G2 during larval life and rekindle a mitotic program subsequently. G2 arrest is dependent on ataxia telangiectasia mutated and rad3-related kinase (ATR)-dependent phosphorylation of checkpoint kinase 1 (Chk1) that is actuated in the absence of detectable DNA damage. We are interested in the mechanisms that activate ATR/Chk1 (Kizhedathu et al., 2018; Kizhedathu et al., 2020). Here we report that levels of reactive oxygen species (ROS) are high in arrested tracheoblasts and decrease upon mitotic re-entry. High ROS is dependent on expression of Duox, an H_2O_2 generating dual oxidase. ROS quenching by overexpression of superoxide dismutase 1, or by knockdown of Duox, abolishes Chk1 phosphorylation and results in precocious proliferation. Tracheae deficient in Duox, or deficient in both Duox and regulators of DNA damage-dependent ATR/Chk1 activation (ATRIP/TOPBP1/claspin), can induce phosphorylation of Chk1 in response to micromolar concentrations of H_2O_2 in minutes. The findings presented reveal that H_2O_2 activates ATR/Chk1 in tracheoblasts by a non-canonical, potentially direct, mechanism.

***For correspondence:** arjung@instem.res.in

Competing interest: The authors declare that no competing interests exist.

Funding: See page 15

Received: 24 March 2021
Preprinted: 25 March 2021
Accepted: 07 October 2021
Published: 08 October 2021

Reviewing Editor: Amin S Ghabrial, Columbia University, United States

Introduction

Ataxia telangiectasia mutated and rad3-related kinase (ATR, *Mei-41*) and its substrate, checkpoint kinase 1 (Chk1, *Grapes*), are essential for DNA damage repair and for normal development (***Artus and Cohen-Tannoudji, 2008***; ***Blythe and Wieschaus, 2015***; ***Cimprich and Cortez, 2008***). The mechanism by which ATR phosphorylates and activates Chk1 in response to DNA damage and the mechanism by which activated Chk1 induces cell cycle arrest have been well characterized (***Choi et al., 2010***; ***Cimprich and Cortez, 2008***; ***Delacroix et al., 2007***; ***Lee et al., 2012***; ***Xu and Leffak, 2010***). In contrast, the mechanisms for the activation of ATR/Chk1 during development, and the roles of these proteins therein, are less well understood. We reported recently that the ATR/Chk1 axis is co-opted during *Drosophila* development for inducing G2 arrest in progenitor cells (***Kizhedathu et al., 2018***; ***Kizhedathu et al., 2020***). The current study was designed to shed light on the mechanism by which the pathway is activated in this context and to probe if it is distinct from the mechanism for DNA damage-induced activation.

The progenitors of the adult tracheal (respiratory) system in *Drosophila* remain mitotically quiescent through larval life and rekindle cell divisions at the onset of pupariation. Progenitors of the tracheal branches of the second thoracic metamere (Tr2, hereafter referred to as tracheoblasts) are arrested in the G2 phase of the cell cycle for ~56 hr and divide thereafter (***Djabrayan et al., 2014***). Importantly, we have shown previously that G2 arrest in tracheoblasts is dependent on ATR-dependent

phosphorylation of Chk1. Two aspects of this process are striking and merit mention here. First, arrested tracheoblasts phosphorylate Chk1 (phosphorylated Chk1 [pChk1]) in the absence of detectable DNA damage. Second, Chk1 is upregulated by a Wnt signaling-dependent mechanism in arrested tracheoblasts and high levels of Chk1 expression are necessary to induce arrest (***Kizhedathu et al., 2018***; ***Kizhedathu et al., 2020***). In the absence of detectable DNA damage, the mechanism for the activation of ATR/Chk1 pathway in tracheoblasts has been unclear from the studies so far.

Although ATR and the related kinases ataxia telangiectasia mutated (ATM) and DNA-PK are the principal sensors of DNA damage and effectors of the DNA damage response (***Durocher and Jackson, 2001***), there is evidence that these kinases can also be activated by non-canonical mechanisms that are not dependent on DNA damage (***Guo et al., 2010***; ***Kumar et al., 2014***). Reactive oxygen species (ROS) are a group of oxygen-derived small molecules that interact avidly with macromolecules like proteins, lipids, and nucleic acids, and alter their function (***Corcoran and Cotter, 2013***). Pertinently, there is evidence that ROS can directly activate ATM by stabilizing ATM homodimers through the formation of intermolecular disulfide bridges (***Guo et al., 2010***). ROS-activated ATM can phosphorylate and activate substrates like checkpoint kinase 2 (Chk2). Whether ROS can activate ATR in the same manner is not known. There is evidence that ROS can activate ATR and lead to Chk1 phosphorylation via the induction of DNA damage (***Srinivas et al., 2019***; ***Willis et al., 2013***). A recent study has shown that mechanical stress on the nuclear envelope, arising during DNA replication (S phase) or in response to osmotic stress or mechanical stimulation, can lead to ATR activation (***Kumar et al., 2014***). This implies that ATR can also be activated by a non-canonical mechanism.

ROS are now generally recognized as important regulators of developmental processes (***Zhang et al., 2016***). The regulation of ROS levels in cells during development is orchestrated by altering rates of aerobic respiration in cells or by altering the levels of expression of ROS-producing enzymes like NADPH oxidases (NOXs). Interestingly, the *Drosophila* genome encodes two NADPH oxidases – NOX and dual oxidase (Duox) (***Kim and Lee, 2014***) – and one of these, Duox, is expressed at high levels in the larval tracheal system (***Robinson et al., 2013***). Duox catalyzes the oxidation of NADPH, leading to the generation of H_2O_2 (***Bedard and Krause, 2007***; ***Geiszt et al., 2003***).

Our interest in the mechanism for activation of ATR/Chk1 led us to probe the role of ROS in this context. We found that ROS levels are high when the cells are arrested in G2 and low after the cells rekindle cell division. We quenched ROS in tracheoblasts via overexpression of the superoxide dismutase 1 (SOD1) to find that the cells started dividing precociously in a manner similar to Chk1 mutants. These findings led us to probe the role of Duox in the regulation of ROS and the mechanism by which ROS regulate the ATR/Chk1 axis.

Results

High ROS is required for G2 arrest in larval tracheoblasts

The cells that comprise the tracheal branches of the second thoracic metamere (Tr2) of the larvae are differentiated adult progenitors that contribute to the development of pupal and adult tracheal structures (***Djabrayan et al., 2014***; ***Guha et al., 2008***; ***Guha and Kornberg, 2005***). The cells that make up the dorsal trunk (DT) in Tr2, hereafter referred to as tracheoblasts, are the focus of our studies. Tracheoblasts remain arrested in the G2 phase of the cell cycle during larval life and initiate mitosis thereafter. Analysis of the cell cycle phasing of tracheoblasts using the fluorescent ubiquitination-based cell cycle indicator (FUCCI) system (***Zielke et al., 2014***) has shown that the cells are in the G1 phase at the time the embryo hatches into a larva and that the cells transition from G1 to S to G2 in the first larval instar (L1). Tracheoblasts remain in G2 from the second larval instar (L2) till mid third larval instar (L3) (32–40 hr L3, ~56 hr) and divide rapidly thereafter (***Kizhedathu et al., 2018***; ***Kizhedathu et al., 2020***, ***Figure 1A***).

To probe the role of ROS in the regulation of G2 arrest in tracheoblasts, we assessed the levels of cytoplasmic ROS in tracheoblasts at L2, 0-8 hr L3, 16-24 hr L3 and 32–40 hr L3 using two well-established, redox-sensitive dyes: 2′,7′-dichlorodihydrofluorescein diacetate (H_2DCFDA) and dihydroethidium (DHE). Both H_2DCFDA and DHE are cell-permeable molecules that alter light emission upon oxidation (***Yang et al., 2014***). Analysis of H_2DCFDA and DHE staining in tracheoblasts at various stages revealed that levels of both reporters are readily detectable at L2 (***Figure 1B and F***, ***Figure 1—figure supplement 1A and B***, n ≥ 6 tracheae per condition per experiment, n = 3), 0–8 hr L3 (***Figure 1C***

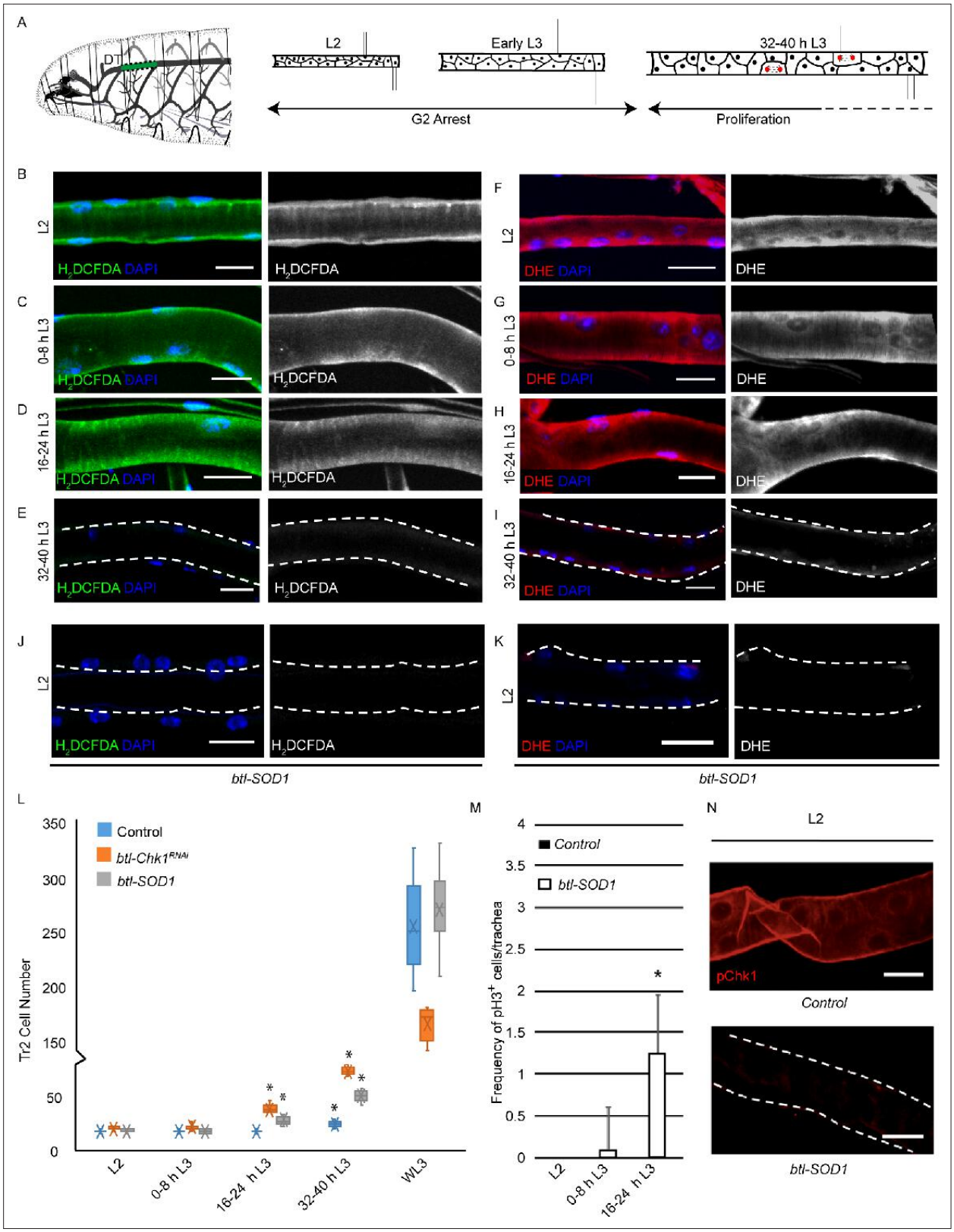

Figure 1. High levels of reactive oxygen species (ROS) are required for checkpoint kinase 1 (Chk1) activation and G2 arrest in tracheoblasts. (**A**) A diagram of the third instar larva showing the dorsal trunk (DT) of the second thoracic metamere (Tr2, colored in green and marked by dashed line). The diagram also shows the timecourse of G2 arrest and cell division in Tr2. The cells in Tr2 DT remain geographically isolated from tracheal cells in other branches during larval life. (**B–E**) Levels of the ROS reporter 2',7'-dichlorodihydrofluorescein diacetate (H_2DCFDA) in Tr2 DT during larval stages.

Figure 1 continued on next page

Figure 1 continued

Shown in the figures are H_2DCFDA staining in L2 (**B**), 0–8 hr L3 (**C**), 16–24 hr L3 (**D**), and 32–40 hr L3 (**E**) in wild type (*btl-Gal4*) animals. (**F–I**) Levels of the ROS reporter dihydroethidium (DHE) in Tr2 DT during larval stages. Shown in the figures are DHE staining in L2 (**F**), 0–8 hr L3 (**G**), 16–24 hr L3 (**H**), and 32–40 hr L3 (**I**) in wild type (*btl-Gal4*) animals. (**J, K**) Effect of *btl*-Gal4-dependent overexpression of superoxide dismutase 1 (SOD1) on levels of ROS reporters in Tr2 DT. (**J**) H_2DCFDA staining in *btl-SOD1* (*btl-GAL4/UAS-SOD1*)-expressing larvae (n ≥ 6 tracheae per condition per timepoint). (**K**) DHE staining in *btl-SOD1* larvae (n ≥ 6 tracheae per condition per timepoint). (**L**) Effect of SOD1 overexpression on cell numbers in Tr2 DT at different larval stages. Graph shows numbers of Tr2 tracheoblasts in wild type (*btl-Gal4), btl-SOD1 (btl-GAL4/UAS-SOD1*), and *btl-Chk1^{RNAi} (btl-GAL4/UAS-Chk1^{RNAi})* larvae at L2, 0–8 hr L3, 16–24 hr L3, 32–40 hr L3, and wandering L3 (WL3) (n ≥ 7 tracheae per condition per timepoint). (**M**) Effect of SOD1 overexpression on mitotic indices in Tr2 DT (see text). Graph shows mitotic indices in Tr2 DT in wild type and *btl-SOD1 (btl-GAL4/UAS-SOD1)*-expressing larvae at L2, 0–8 hr L3 and 16–24 hr L3 (mean values ± standard deviation, n ≥ 7 tracheae per condition per timepoint). (**N**) Effect of SOD1 overexpression on Chk1 phosphorylation in Tr2 tracheoblasts. Shown in the figure is phosphorylated Chk1 (pChk1, phospho-Chk1Ser^{345}) immunostaining (red) in Tr2 DT in wild type (*btl-GAL4*) and *btl-SOD1 (btl-GAL4/UAS-SOD1)* larvae at L2. Scale bars = 10 µm. Dashed lines outline the cuticular lumen of the tracheal tube here and elsewhere and are shifted outward to include the epithelial lining when they overlap with the signal. Student's t-test: *p<0.00001.

The online version of this article includes the following figure supplement(s) for figure 1:

Source data 1. Cell Frequencies in SOD1 overexpressing animals.

Source data 2. Mitotic indices in SOD1 overexpressing animals.

Figure supplement 1. Quantification of reactive oxygen species (ROS) levels in Tr2 tracheoblasts.

Figure supplement 2. Quantification of phosphorylated checkpoint kinase 1 (pChk1) levels in Tr2 tracheoblasts.

and G, ***Figure 1—figure supplement 1A and B***, n ≥ 6 tracheae per condition per experiment, n = 3), 16–24 hr L3 (***Figure 1D and H***, ***Figure 1—figure supplement 1A, B***, n ≥ 6 tracheae per condition per experiment, n = 3), and nearly undetectable at 32–40 hr L3 in wild type (*btl-Gal4*) animals (***Figure 1E, I***, ***Figure 1—figure supplement 1A and B***, n ≥ 6 tracheae per condition per experiment, n = 3). Taken together, the analysis of ROS reporters (***Figure 1***) showed that cytoplasmic ROS is high in arrested cells and low in mitotically active cells.

Next, we asked whether changes in ROS levels had any bearing on the cell cycle program. To answer this question, we adopted a genetic approach for quenching ROS in tracheoblasts. SOD1 is a cytoplasmic enzyme that scavenges ROS (***Blackney et al., 2014***). We overexpressed SOD1 in trachea (*btl-GAL4/UAS-SOD1*, hereafter *btl-SOD1*) and examined the effects of SOD1 overexpression on ROS levels by H_2DCFDA and DHE staining. Levels of H_2DCFDA and DHE were found to be significantly lower in *btl-SOD1*-expressing animals compared to controls (***Figure 1J and K***, ***Figure 1—figure supplement 1C and D***, compare with ***Figure 1B and F***, n ≥ 6 tracheae per condition per experiment, n = 3). This showed that SOD1 overexpression is an effective way to quench ROS in tracheae. We then determined whether SOD1 overexpression altered the cell cycle program of tracheoblasts. We counted the number of cells in Tr2 DT at L2, 0–8 hr L3, 16–24 hr L3, 32–40 hr L3, and wandering L3 (WL3) and quantified the frequencies of phospho-histone $H3^+$ ($pH3^+$) mitotic figures in Tr2 DT at L2, 0–8 hr L3, and 16–24 hr L3. Analysis of the cell numbers and frequency of $pH3^+$ figures in Tr2 showed that SOD1 overexpression resulted in precocious cell division from 0 to 8 hr L3 (***Figure 1L and M***, n ≥ 7 tracheae per timepoint, ***Figure 1—source data 1***; ***Figure 1—source data 2***). We noted that the precocious cell divisions in *btl-SOD1* tracheae are similar to that observed in Chk1 mutants (*btl-GAL4/UAS-Chk1^{RNAi}* (*btl*-Chk1^{RNAi}), ***Figure 1L***, ***Figure 1—source data 1***). Based on these data, we concluded that quenching of ROS phenocopies the loss of Chk1 in these cells. We also noted a difference in cell proliferation kinetics in *btl-Chk1^{RNAi}* and *btl-SOD1*-expressing animals. Tracheoblasts in *btl-Chk1^{RNAi}* rekindle mitoses earlier than wild type but divide more slowly thereafter. In contrast, tracheoblasts in *btl-SOD1* rekindle mitoses earlier than wild type but do not appear to divide more slowly than wild type cells (see Discussion).

The findings above led us to investigate the levels of phosphorylated (activated) Chk1 in tracheoblasts in wild type and *btl-SOD1* animals. As reported previously, pChk1 levels are high in L2 and early L3 and diminished at 32–40 hr L3. pChk1 immunostaining in *btl-SOD1*-expressing tracheae in L2 and early L3 showed that pChk1 levels were reduced in comparison to wild type at these respective stages (***Figure 1N***, ***Figure 1—figure supplement 2A***, n ≥ 6 tracheae per condition per experiment, n = 3). We inferred that high ROS levels are necessary for G2 arrest and that high ROS contributes in some manner to high levels of pChk1.

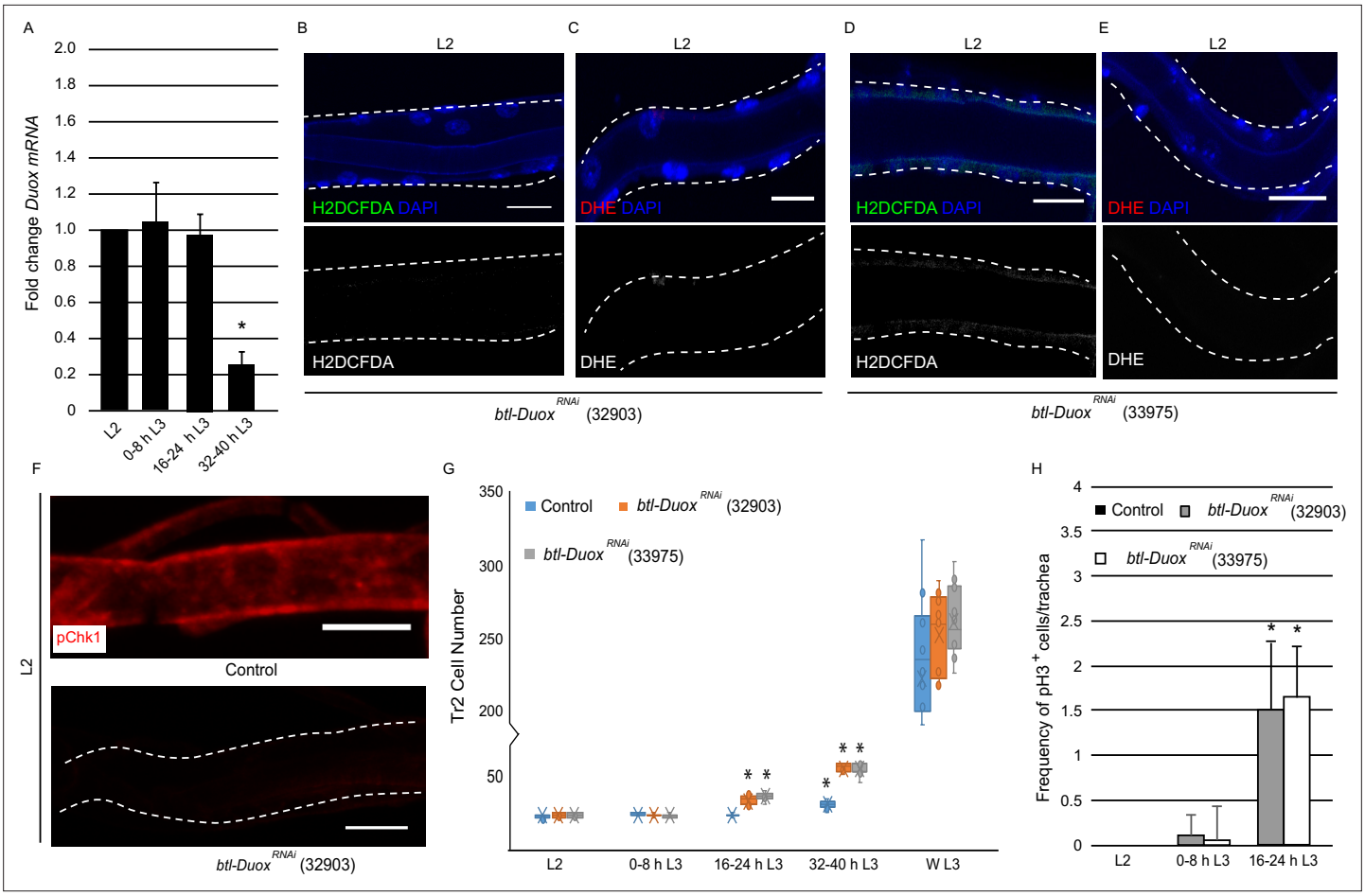

Figure 2. High reactive oxygen species (ROS) in tracheoblasts is dependent on *Duox* expression. (**A**) Quantitative PCR analysis of *Duox* mRNA levels in micro-dissected Tr2 dorsal trunk (DT) fragments at different stages. Graph shows fold change in *Duox* mRNA in Tr2 DT fragments from wild type (*btl-GAL4*) larvae at L2, 0–8 hr L3, 16–24 hr L3, and 32–40 hr L3. Fold change has been represented with respect to L2 (n = 3 experiments, n ≥ 15 Tr2 DT fragments/stage/experiment, mean ± standard deviation, p<0.0001). (**B–E**) Effect of the knockdown of *Duox* expression on the levels of ROS reporters in Tr2 DT in L2. Shown here are the results of the expression of two different Duox RNAi lines (32903 and 33975). (**B, D**) 2',7'-Dichlorodihydrofluoresce in diacetate (H_2DCFDA) staining and (**C, E**) dihydroethidium (DHE) staining in Tr2 DT in *btl-Duox^{RNAi}*. (**[B, C]** *btl-GAL4/+; UAS-Duox^{RNAi} (32903)/+* and **[D, E]** *btl-GAL4/+; UAS-Duox^{RNAi} (33975)/+*) larvae (n ≥ 6 tracheae per condition per timepoint). (**F**) Effect of reduction of *Duox* expression on levels of phosphorylated checkpoint kinase 1 (pChk1) in Tr2 DT in L2. pChk1 immunostaining (red) in Tr2 DT in wild type (*btl-Gal4*) and *btl-Duox^{RNAi} (btl-GAL4/+; UAS- Duox^{RNAi} (32903)/+*) larvae. (**G**) Effect of the knockdown of *Duox* expression on cell numbers in Tr2 DT at different larval stages. Graph shows cell numbers of Tr2 tracheoblasts in wild type (*btl-Gal4*) and *btl-Duox^{RNAi} (btl-GAL4/+; UAS-Duox^{RNAi} (32903)/+* and *btl-GAL4/+; UAS-Duox^{RNAi} (33975)/+*) larvae at L2, 0–8 hr L3, 16–24 hr L3, 32–40 hr L3, and WL3 (n ≥ 7 tracheae per condition per timepoint). (**H**) Effect of the knockdown of *Duox* expression on mitotic indices in Tr2 DT. Graph shows mitotic indices in Tr2 DT in wild type (*btl-Gal4*) and *btl-Duox^{RNAi} (btl-GAL4/+; UAS-Duox^{RNAi} (32903)/+* and *btl-GAL4/+; UAS-Duox^{RNAi} (33975)/+*) larvae at L2, 0–8 hr L3 and 16–24 hr L3 (mean values ± standard deviation, n ≥ 7 tracheae per condition per timepoint). Scale bars = 10 µm. Student's t-test: *p<0.0001

The online version of this article includes the following figure supplement(s) for figure 2:

Source data 1. Cell frequencies in Duox ^{RNAi} expressing animals.

Source data 2. Mitotic indices in Duox ^{RNAi} expressing animals.

High ROS in G2-arrested tracheoblasts is dependent on *Duox*

The identification of ROS as regulator of G2 arrest in tracheoblasts raises two questions. First, how are ROS levels regulated in the tracheoblasts? Second, how does high ROS translate into high levels of pChk1? As mentioned previously, the H_2O_2-generating enzyme Duox is expressed at high levels in larval tracheae (***Robinson et al., 2013***). To probe the role of Duox in the generation of ROS in tracheoblasts, we first examined Duox expression in tracheoblasts at different larval stages using quantitative RT-PCR (qPCR). We isolated mRNA from micro-dissected fragments of Tr2 DT at different timepoints

and utilized these samples to query Duox expression. Our analysis showed that Duox mRNA levels are higher at L2, 0–8 hr L3, and 16–24 hr L3 than at 32–40 hr L3 (***Figure 2A,*** n ≥ 15 tracheal fragments per timepoint per experiment, n = 3 experiments). We concluded that the timecourse of Duox mRNA expression correlates with the timecourse of ROS accumulation in the tracheae.

To probe whether Duox is the driver of ROS accumulation, we knocked down the levels of Duox in the tracheal system by RNA interference and examined its impact on the levels of ROS reporters. The reduction in the levels of Duox using two different RNAi lines (BDSC-32903, BDSC-33975, *btl-GAL4/+; UAS-Duox^{RNAi}/+ (btl-Duox^{RNAi})*) followed by H_2DCFDA and DHE staining showed that the reduction of Duox leads to a dramatic decrease in levels of both the reporters (***Figure 2B–E***, ***Figure 1—figure supplement 1E and F***, compare with ***Figure 1B and E***, n ≥ 6 tracheae per condition per experiment, n = 3). Based on these data, we inferred that the high levels of ROS in arrested tracheoblasts are dependent on Duox expression.

Next, we examined how the knockdown of Duox impacted Chk1 phosphorylation and the program of cell division. Consistent with the previous findings with SOD1 overexpression, we observed that the knockdown of Duox resulted in the loss of pChk1 (***Figure 2F***, ***Figure 1—figure supplement 2B***, n ≥ 6 tracheae per condition per experiment, n = 3). We counted the number of cells of tracheoblasts at L2, 0–8 hr L3, 16–24 hr L3, 32–40 hr L3, and WL3 and quantified the frequencies of pH3$^+$ nuclei in Tr2 DT at L2, 0–8 hr L3, and 16–24 hr L3. We found that *btl-Duox^{RNAi}*-expressing animals rekindle cell divisions sooner than their wild type counterparts. Interestingly, *btl-Duox^{RNAi}*-expressing animals also showed

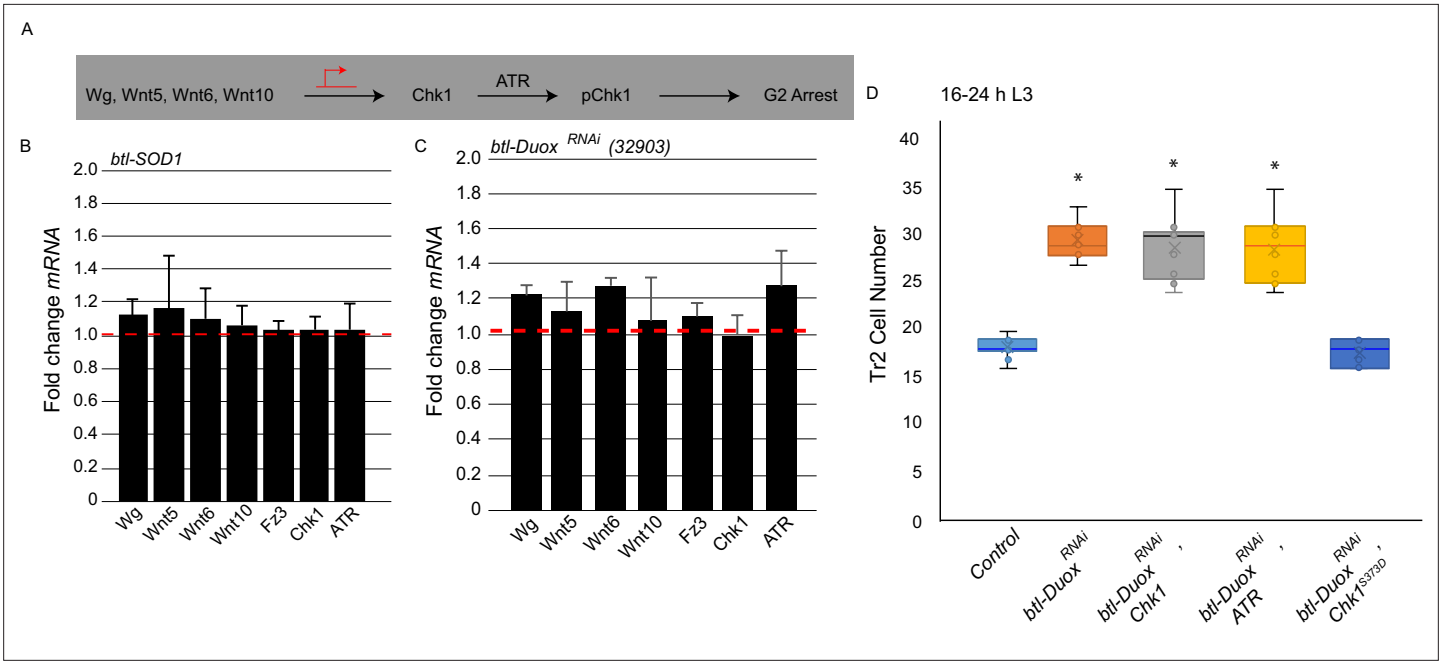

Figure 3. Reactive oxygen species (ROS) dependence identifies a novel pathway for the regulation of ataxia telangiectasia mutated-related kinase/checkpoint kinase 1 (ATR/Chk1) in tracheoblasts. (**A**) Model for G2 arrest mechanism in Tr2 tracheoblasts based on previous studies. Earlier work has shown that four Wnt ligands (*Wg, Wnt5, Wnt6, Wnt10*) act synergistically to upregulate Chk1 mRNA levels in arrested tracheoblasts. High levels of Chk1 expression are necessary for G2 arrest and Chk1 overexpression can rescue defects in Wnt signaling (***Kizhedathu et al., 2020***). (**B, C**) Effect of superoxide dismutase 1 (SOD1) overexpression and Dual oxidase (Duox) knockdown on expression of Wnts and Wnt-target genes. Quantitative PCR analysis of levels of *Wg, Wnt5, Wnt6, Wnt10, Fz3, Chk1,* and *ATR* mRNA in micro-dissected Tr2 DT fragments at L2. Graph shows fold change in *Wg, Wnt5, Wnt6, Wnt10, Fz3, Chk1,* and *ATR* mRNA levels in Tr2 dorsal trunk (DT) fragments expressing (**B**) *btl-SOD1 (btl-GAL4/UAS-SOD1)* and (**C**) *btl-Duox^{RNAi} (btl-GAL4/+; UAS-Duox^{RNAi} (32903)/+)*. Fold change has been represented with respect to wild type (*btl-Gal4*, shown by dashed red line, n = 3 experiments, n ≥ 15 Tr2 DT fragments/stage/experiment, mean ± standard deviation). (**D**) Effect of overexpression of a phosphomimic variant of Chk1 in *btl-Duox^{RNAi}* larvae at 16–24 hr L3. Graph shows numbers of Tr2 tracheoblasts in wild type (*btl-Gal4*), *btl-Duox^{RNAi} (btl-GAL4/+; UAS-Duox^{RNAi} (32903)/+)*, *btl-Duox^{RNAi}, Chk1 (btl-GAL4/+; UAS-Duox^{RNAi} (32903)/ UAS-Chk1)*, *btl-Duox^{RNAi}, ATR (btl-GAL4/+; UAS-Duox^{RNAi} (32903)/ UAS-ATR)* and *btl-Duox^{RNAi}, Chk1^{S373D} (btl-GAL4/+; UAS-Duox^{RNAi} (32903)/ UAS-Chk1^{S373D})* larvae at 16–24 hr L3 (n ≥ 7 tracheae per condition per timepoint). Student's t-test: *p<0.00001.

The online version of this article includes the following figure supplement(s) for figure 3:

Source data 1. Cell frequencies in Chk1S373D expressing animals.

no obvious slowdown in cell division rate after mitotic re-entry (***Figure 2G and H***, n ≥ 7 tracheae per timepoint, ***Figure 2—source data 1***, ***Figure 2—source data 2***).

ROS dependence reveals a novel mode of ATR/Chk1 regulation

Having identified the source for high ROS in arrested tracheoblasts, we turned our attention to addressing how ROS is coordinating G2 arrest. Our previous studies have shown that Wnt-dependent transcriptional upregulation of Chk1 is essential for G2 arrest. Wnt signaling in the trachea is mediated by four Wnt ligands – Wg, Wnt5, Wnt6, and Wnt10 – that are expressed by the tracheoblasts (***Figure 3A***). All ligands are expressed at high levels in arrested cells and downregulated post-mitotic entry. We have also shown that the four Wnts act synergistically to upregulate Chk1 expression but are redundant for expression of other Wnt targets like Fz3.

Our first step toward characterizing the role of ROS in G2 arrest was to analyze how ROS levels impacted Wnt signaling and the expression of Wnt target genes, particularly Chk1. We micro-dissected Tr2 fragments from *btl-SOD1* and *btl-Duox*^{RNAi} animals at L2, extracted mRNA, and analyzed expression of Wnts and Wnt target genes by qPCR. We found that the expression of all Wnt ligands, Fz3 and Chk1, was comparable in wild type, *btl-SOD1* and *btl-Duox*^{RNAi}-expressing animals (***Figure 3B and C***, red dashed line marks wild type levels, n ≥ 15 tracheal fragments per timepoint per experiment, n = 3 experiments). This showed that perturbations in ROS levels in the trachea do not impact Wnt signaling nor expression of Wnt targets like Chk1. We also assayed the levels of ATR in *btl-SOD1* and *btl-Duox*^{RNAi}-expressing animals by qPCR and found no change in ATR transcript levels compared to control (***Figure 3B and C***, red dashed line marks wild type levels). Together, the qPCR data suggested that ROS did not regulate the abundance of either Chk1 or ATR transcripts.

We have shown previously that precocious mitotic re-entry observed in Wnt signaling-deficient tracheoblasts (*btl-TCF*^{RNAi}) can be rescued by overexpression of Chk1 (***Kizhedathu et al., 2020***). Thus, to functionally test whether ROS levels impact Chk1 expression, we overexpressed Chk1 in *btl-Duox*^{RNAi}-expressing animals and examined cell proliferation. We counted numbers of tracheoblasts in *btl-GAL4/+; UAS-Duox*^{RNAi}*/UAS-Chk1* (*btl-Duox*^{RNAi}*, Chk1*) animals at 16–24 hr L3 to find that the numbers were considerably higher than wild type and comparable to the numbers in *btl-Duox*^{RNAi} animals (***Figure 3D***, n ≥ 7 tracheae, ***Figure 3—source data 1***). Along these lines, we also overexpressed ATR in *btl-Duox*^{RNAi} animals and counted the number of Tr2 tracheoblasts at 16–24 hr L3. We found that the numbers were higher than wild type and comparable to the numbers in *btl-Duox*^{RNAi} animals (***Figure 3D***, n ≥ 7 tracheae, ***Figure 3—source data 1***). Taken together, the analyses suggested that ROS does not regulate ATR/Chk1 gene expression.

In light of the findings that ROS depletion does not perturb Chk1 expression but does perturb Chk1 phosphorylation and function, we hypothesized that ROS may regulate Chk1 phosphorylation in some manner. The ATR-dependent phosphorylation of Chk1 at serine 373 is thought to be necessary for its activation (***Liu et al., 2000***; ***Patil et al., 2013***; ***Bayer et al., 2018***). Our immunohistochemical analyses are consistent with these findings. To probe the possibility that ROS facilitates Chk1 phosphorylation, we tested whether a phosphomimic variant of Chk1, in which the serine at the position 373 has been replaced by aspartic acid (Chk1^{S373D}), could rescue the Duox phenotype. We overexpressed Chk1^{S373D} in *btl-Duox*^{RNAi} animals and counted cell numbers in Tr2 at 16–24 hr L3. We found that Tr2 cell numbers in these animals were now comparable to wild type (and lower than in *btl-Duox*^{RNAi} animals, ***Figure 3D***, n ≥ 7 tracheae, ***Figure 3—source data 1***). The rescue of the Duox mutant phenotype by the phosphomimic variant of Chk1 suggested that ROS is required for ATR-dependent phosphorylation and activation of Chk1.

ROS-dependent activation of ATR/Chk1 does not require ATRIP/TOPBP1/claspin

The coincidence of high ROS levels and activated Chk1 in cells would typically implicate ROS-dependent genotoxic stress as the driver of Chk1 activation. However, our analysis of DNA damage in tracheoblasts, using the well-characterized marker for double-strand DNA breaks (γ-H2AX), found no detectable DNA damage in arrested cells (***Kizhedathu et al., 2018***). In light of the findings with respect to ROS, we decided to probe more rigorously the incidence of genotoxic stress in tracheoblasts and the role of the DNA damage response in Chk1 activation.

We re-evaluated the levels of DNA damage in tracheoblasts using two assays. First, we examined the accumulation of 8-oxo-2'-deoxyguanosine (8-oxo-dG), a marker for nucleotide oxidation. Second, we scored the frequencies of nuclear foci of RPA70, a protein that binds single-strand DNA breaks. To validate nuclear 8-oxodG as a marker of oxidative damage in tracheoblasts, tracheae from L2 larvae were dissected and treated ex vivo with different concentrations of H_2O_2 (100 µM, 500 µM, and 1 mM) for 30 min and stained with an antibody against 8-oxodG. Robust staining was detected in trachea at 1 mM H_2O_2(***Figure 4A***, n ≥ 6 tracheae per condition per experiment, n = 2), but no signal was detected at lower concentrations or in untreated tracheae. This showed that although 8-oxodG accumulation is responsive to oxidative stress, there is no 8-oxodG accumulation in G2-arrested tracheoblasts under normal conditions. An aspect of the 8-oxodG staining in tracheal cells merits mention here. The accumulation of 8-oxodG in Tr2 tracheoblasts was cytoplasmic unlike the tracheal cells in other metameres, where 8-oxodG was observed in both cytoplasm and nucleus (***Figure 4B***, n ≥ 6 tracheae per condition per experiment, n = 2). One reason for this difference could be that Tr2 DT are arrested in G2 and not engaged in DNA synthesis while cells in other metameres are actively endocycling and replicating DNA.

Next we probed the incidence of single-stranded DNA breaks in tracheoblasts with the help of a strain that ubiquitously expresses RPA70-GFP (***Blythe and Wieschaus, 2015***). RPA 70 has been shown to be uniformly distributed in the nucleus under normal conditions and to form focal nuclear aggregates at sites of single-strand DNA breaks (***Blythe and Wieschaus, 2015***). To validate RPA*70-GFP* as a marker for genotoxic stress in the tracheal system, L2 animals were exposed to either 0 (control) or 50 Gy of γ-irradiation and immunostained for GFP. Foci of GFP could be observed in the nuclei of tracheoblasts exposed to 50 Gy γ-irradiation (***Figure 4C***, n ≥ 6 tracheae per condition per experiment, n = 3) but no foci were detected in untreated tracheae at the same stage. In a parallel set of experiments, we also examined levels of γ-H2AX in L2 animals under these conditions. We observed foci of nuclear γ-H2AX staining in tracheoblasts exposed to 50 Gy of γ-irradiation (***Figure 4D***, n ≥ 6 tracheae per condition per experiment, n = 3) but not in untreated tracheae at the same stage. Taken together, our analysis of 8-oxodG, RPA70-GFP, and γ-H2AX further confirmed that there is no detectable DNA damage in arrested tracheoblasts.

To probe the relationship between DNA damage and Chk1 activation in tracheoblasts, we also utilized a genetic approach. The mechanism for ATR/Chk1 activation in response to DNA damage has been characterized in some detail. These studies show that the activation of ATR/Chk1 requires three major proteins: ATR interacting protein (ATRIP, *mus-304*), topoisomerase II binding protein 1 (TOPBP1, *mus-101*), and claspin. Breaks in DNA that are bound by single-strand DNA-binding proteins like RPA-1/RPA-70 recruit ATR via its partner ATRIP and, in turn, TOPBP1. This complex activates ATR, and consequently, in a claspin-dependent manner, Chk1 (***Choi et al., 2010***; ***Cimprich and Cortez, 2008***; ***Delacroix et al., 2007***; ***Lee et al., 2012***; ***Xu and Leffak, 2010***).

To determine if ATRIP, TOPBP1, and claspin are required in tracheal cells for DNA damage-dependent phosphorylation of Chk1, we examined pChk1 levels post γ-irradiation in tracheoblasts in which we simultaneously knocked down Duox and the aforementioned gene products. We exposed animals expressing *btl-Duox^{RNAi}*, *ATRIP^{RNAi} (btl-GAL4/ UAS-ATRIP^{RNAi}; UAS-Duox^{RNAi}/+)*, *btl-Duox^{RNAi}*, *TopBP1^{RNAi} (btl-GAL4/+; UAS-Duox^{RNAi}/UAS-TOPBP1^{RNAi})*, and *btl-Duox^{RNAi}*, *btl-Duox^{RNAi}*, *Claspin^{RNAi} (btl-GAL4/+; UAS-Duox^{RNAi}/UAS-Claspin^{RNAi})* to 50 Gy of γ-radiation and performed immunostaining for pChk1 1 hr after irradiation (***Figure 4—figure supplement 1A***). Although pChk1 could be detected post irradiation in animals expressing *btl-Duox^{RNAi}* (***Figure 5—figure supplement 1C***, n ≥ 6 tracheae per condition per experiment, n = 3), we did not detect pChk1 in *btl-Duox^{RNAi}*, *ATRIP^{RNAi}*, *btl-Duox^{RNAi}*, *TOPBP1^{RNAi}*, and *btl-Duox^{RNAi}*, *Claspin^{RNAi}*-expressing animals at the same stages (***Figure 4—figure supplement 1B–E***, n ≥ 6 tracheae per condition per experiment, n = 2). This shows that DNA damage-dependent phosphorylation of Chk1 in Tr2 DT cells requires ATRIP, TOPBP1, and claspin.

To determine if any of the components of DNA damage-dependent ATR activation are necessary for the phosphorylation of Chk1 in the trachea, we knocked down ATR, ATRIP, TOPBP1, and claspin and probed the levels of pChk1 in L2 (***Figure 4E–H***, n ≥ 6 tracheae per condition per experiment, n = 2). pChk1 staining of the tracheae from these animals revealed that the loss of ATR led to the loss of pChk1 (***Figure 4E***). In contrast, the knockdown of ATRIP, TOPBP1, or claspin did not lead to a loss of pChk1 in L2 (***Figure 4F–H***). We also counted the number of cells in Tr2 DT at L2 and 16–24 hr L3 in each of these genetic backgrounds. While the knockdown of ATR led to an increase in cell number

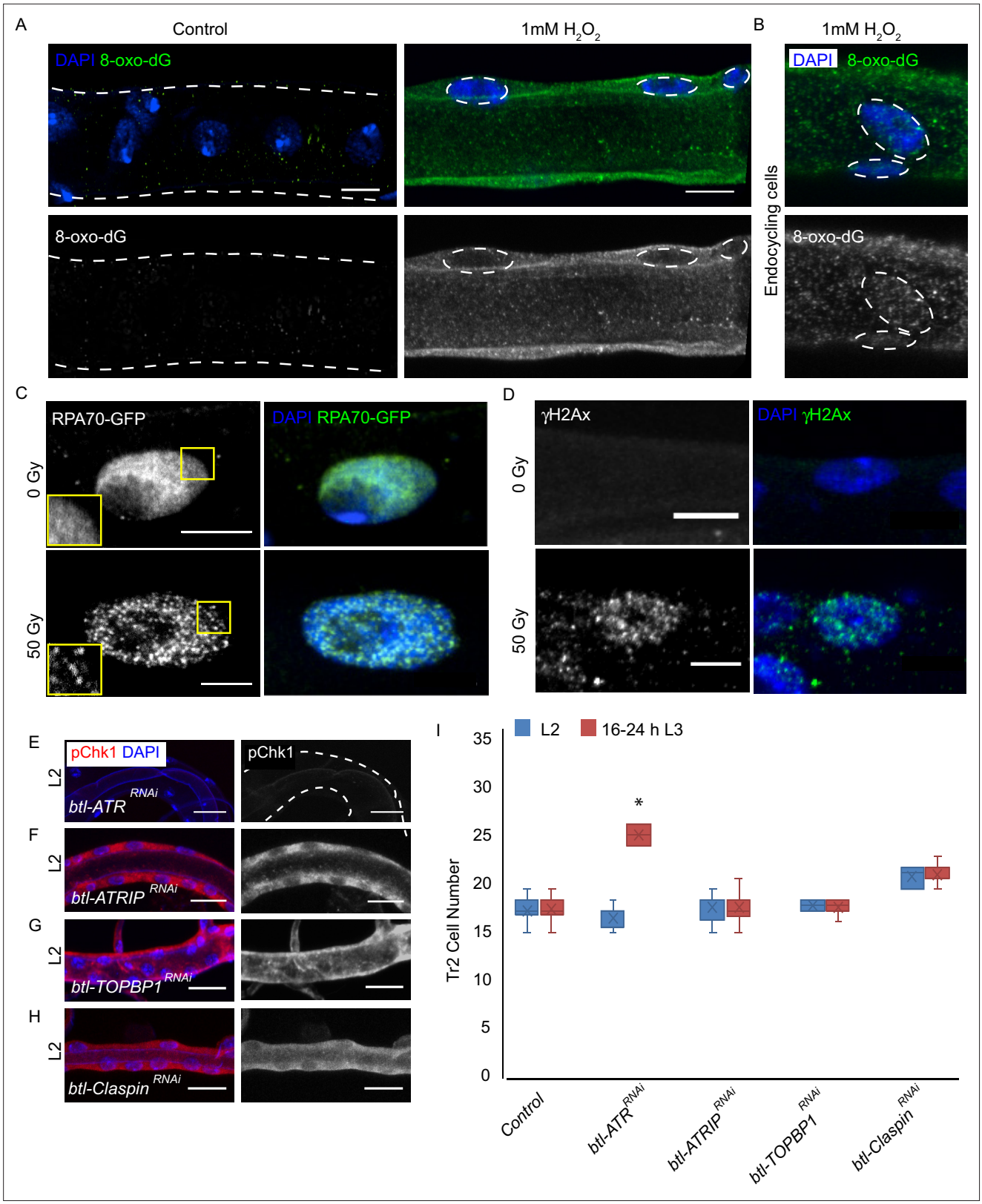

Figure 4. ATRIP, TOPBP1, and claspin are not required for reactive oxygen species (ROS)-mediated checkpoint kinase 1 (Chk1) activation in tracheoblasts. (**A–D**) Detailed analysis of DNA damage in Tr2 dorsal trunk (DT). Shown here are findings from three different reporters of genotoxic stress. (**A**) 8-Oxo-2'-deoxyguanosine (8-Oxo-dG) immunostaining in wild type (*btl-GAL4*) Tr2 DT in untreated tracheae (left panel) and tracheae exposed to 1 mM H_2O_2 for 30 min ex vivo (right panel) at L2. (**B**) 8-Oxo-dG immunostaining in wild type (*btl-GAL4*) endocycling cells of the tracheae exposed

Figure 4 continued on next page

Figure 4 continued

to 1 mM H_2O_2 for 30 min ex vivo at L2. (**C**) GFP immunostaining in non-irradiated and γ -irradiated larvae expressing RPA70-GFP. Shown in the figure are GFP immunostaining in non-irradiated larvae (top panel) and larvae exposed to 50 Gy of γ -radiation (bottom panel) at L2. (**D**) γ -H2AX^{Ser139} immunostaining in Tr2 DT in wild type (*btl-GAL4*) non-irradiated larvae (top panel) and larvae irradiated with 50 Gy of γ -radiation (bottom panel) at L2. (**E–H**) Analysis of the contribution of components of the DNA damage-dependent activation of ATR/Chk1 to Chk1 activation in Tr2 DT. Effects of the knockdown of *ATR, ATRIP, TOPBP1,* and *Claspin* on phosphorylated checkpoint kinase 1 (pChk1) levels in Tr2 DT at L2. pChk1 immunostaining (red) in Tr2 DT in (**E**) *btl-ATR^{RNAi}* (*btl-GAL4/UAS-ATR^{RNAi}*), (**F**) *btl-ATRIP^{RNAi}* (*btl-GAL4/UAS-ATRIP^{RNAi}*), (**G**) *btl-TOPBP1^{RNAi}* (*btl-GAL4/+; UAS-TOPBP1^{RNAi}/+*), and (**H**) *btl-Claspin^{RNAi}* (*btl-GAL4/+; UAS-Claspin^{RNAi}/+*) larvae at L2. (**I**) Effects of knockdown of *ATR, ATRIP, TOPBP1,* and *Claspin* on cell numbers in Tr2 DT. Graph shows numbers of Tr2 tracheoblasts in wild type (*btl-Gal4*), *btl-ATR^{RNAi}* (*btl-GAL4/UAS-ATR^{RNAi}*), *btl-ATRIP^{RNAi}* (*btl-GAL4/UAS-ATRIP^{RNAi}*), *btl-TOPBP1^{RNAi}* (*btl-GAL4/+; UAS-TOPBP1^{RNAi}/+*), and *btl-Claspin^{RNAi}* (*btl-GAL4/+; UAS-Claspin^{RNAi}/+*) at L2 and 16–24 hr L3 (mean values ± standard deviation, n ≥ 7 tracheae per condition per timepoint). Scale bars = 5 μm (**A–D**), 10 μm (**E–H**). Student's t-test: *p<0.00001.

The online version of this article includes the following figure supplement(s) for figure 4:

Source data 1. Cell frequencies in ATR ^{RNAi}, ATRIP ^{RNAi}, TOPBP1 ^{RNAi} and Claspin ^{RNAi} expressing animals.

Figure supplement 1. ATRIP, TOPBP1, and claspin are required for DNA damage-dependent activation ofATR/Chk1.

Figure supplement 2. Loss of ATRIP, TOPBP1, and claspin does not affect cell numbers at WL3.

at 16–24 hr L3, knockdown of ATRIP, TOPBP1, and claspin did not (***Figure 4I***, n ≥ seven tracheae per timepoint, ***Figure 4—source data 1***). These data indicate that ATR-dependent activation of Chk1 in G2-arrested tracheoblasts cells does not require ATRIP, TOPBP1, or claspin.

Collectively, these experiments lend support to the idea that the ROS-dependent Chk1 activation in tracheoblasts does not involve the DNA damage response pathway.

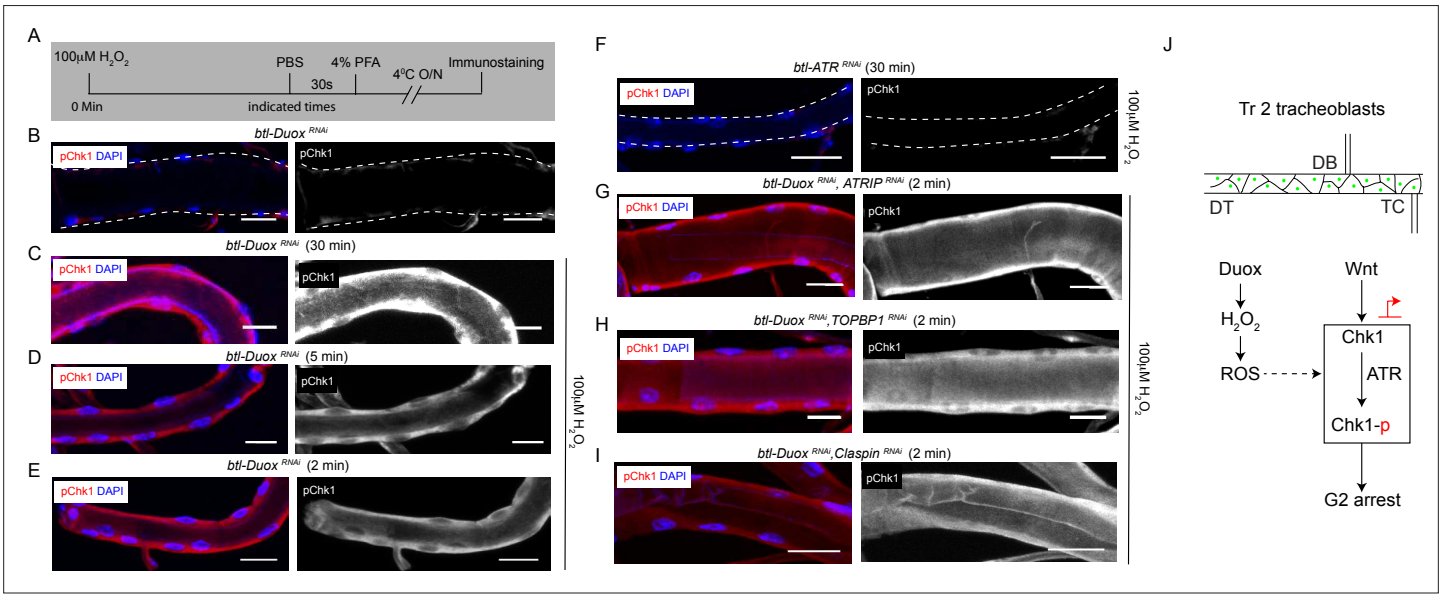

Figure 5. Incubation with H_2O_2 can restore phosphorylated checkpoint kinase 1 (pChk1) levels in Dual oxidase (Duox)-deficient tracheoblasts. (**A–E**) Kinetics of Chk1 phosphorylation upon exposure to H_2O_2 ex vivo. (**A**) Regimen for H_2O_2 treatment and analysis of pChk1 in Tr2 dorsal trunk (DT) in L2. pChk1 immunostaining (red) in Tr2 DT in (**B**) untreated *btl-Duox^{RNAi} (btl-GAL4/+; UAS-Duox^{RNAi} (32903)/+*)-expressing tracheae and treated with 100 μM H_2O_2 for (**C**) 30 min, (**D**) 5 min, and (**E**) 2 min. (**F**) Effect of knockdown of ATR on Chk1 activation in Tr2 DT upon exposure to H_2O_2 ex vivo. pChk1 immunostaining (red) in Tr2 DT in *btl-ATR^{RNAi} (btl-GAL4/UAS-ATR^{RNAi})* tracheae treated with 100 μM H_2O_2 for 30 min. (**G–I**) Effect of knockdown of *Duox* and *ATRIP* or *TOPBP1* or *Claspin* on pChk1 levels in Tr2 DT in tracheae exposed to 100 μM H_2O_2 at L2. pChk1 immunostaining (red) in Tr2 DT in (**G**) *btl-Duox^{RNAi}, ATRIP^{RNAi} (btl-GAL4/ UAS-ATRIP^{RNAi}; UAS-Duox^{RNAi} (32903)/+)*, (**H**) btl-*Duox^{RNAi}, TOPBP1^{RNAi} (btl-GAL4/+; UAS-Duox^{RNAi}(32903)/UAS-TOPBP1^{RNAi})* and (**I**) *btl-Duox^{RNAi}, Claspin^{RNAi} (btl-GAL4/+; UAS-Duox^{RNAi}(32903)/UAS-Claspin^{RNAi})* tracheae treated with 100 μM H_2O_2 for 2 min at L2. (**J**) Model for the regulation of ATR/Chk1 activation in Tr2 DT. We propose that H_2O_2 can induce ATR-dependent phosphorylation and activation of Chk1 in the absence of detectable DNA damage, leading to G2 arrest in Tr2 tracheoblasts. Scale bars = 10 μm.

The online version of this article includes the following figure supplement(s) for figure 5:

Figure supplement 1. Exposure to γ -radiation can restore phosphorylated checkpoint kinase 1 (pChk1) levels in dual oxidase (Duox)-deficient tracheoblasts.

H_2O_2 can rescue pChk1 levels in Duox-deficient tracheoblasts

The next obvious question was to ask if Chk1 phosphorylation can be induced in Duox mutants by the addition of H_2O_2. To investigate this possibility, we examined levels of pChk1 in *btl-Duox*^{RNAi} tracheae after exposure to different concentrations of H_2O_2 for different periods of time. Tracheae from L2 animals were exposed to PBS or H_2O_2 (PBS) ex vivo and immunostained for pChk1 (***Figure 5A***). We detected no pChk1 staining in tracheae exposed to buffer alone and robust pChk1 staining in tracheae incubated with H_2O_2 (***Figure 5B–E***, ***Figure 1—figure supplement 2C***, n ≥ 6 tracheae per condition per experiment, n = 3). Interestingly, we noted that exposure to H_2O_2 for periods as short as 2 min was sufficient to restore levels of pChk1 in *btl-Duox*^{RNAi} tracheae (***Figure 5E***). We also probed pChk1 levels in *btl-ATR*^{RNAi} (*btl-GAL4/UAS-ATR*^{RNAi}) tracheae post H_2O_2 treatment and found that there was no pChk1 accumulation (***Figure 5G***, ***Figure 1—figure supplement 2C***, n ≥ 6 tracheae per condition per experiment, n = 3). Together, these data show that H_2O_2 treatment is sufficient to induce Chk1 phosphorylation in an ATR-dependent manner and that H_2O_2 can induce pChk1 in minutes.

In an independent set of experiments, we examined the kinetics of DNA damage-dependent activation of Chk1 in tracheoblasts. As described earlier, we exposed L2 larvae to 50 Gy of γ-radiation and performed pChk1 immunostaining at different timepoints post irradiation (***Figure 5—figure supplement 1A***). We could detect pChk1 1 hr post irradiation (***Figure 5—figure supplement 1C***, n ≥ 6 tracheae per condition per experiment, n = 2) but not earlier (***Figure 5—figure supplement 1D*** and E, n ≥ 6 tracheae per condition per experiment, n = 2). Here again, pChk1 induction in response to γ-radiation was dependent on ATR as pChk1 was not detected in tracheoblasts expressing *btl-ATR*^{RNAi} (***Figure 5—figure supplement 1F***, n ≥ 6 tracheae per condition per experiment, n = 2). These experiments suggest that the kinetics of Chk1 phosphorylation in response to H_2O_2 could be significantly faster than in response to γ-radiation.

Next, we tested whether H_2O_2 could restore levels of pChk1 in the absence of ATRIP, TOPBP1, and claspin in *btl-Duox*^{RNAi}-expressing animals. To test this possibility, we exposed animals expressing *btl-Duox*^{RNAi}, *ATRIP*^{RNAi}, *btl-Duox*^{RNAi}, *TOPBP1*^{RNAi}, and *btl-Duox*^{RNAi}, *Claspin*^{RNAi}-expressing tracheae to 100 μM H_2O_2 and performed Chk1 immunostaining 2 min after exposure. pChk1 immunostaining showed that the knockdown of ATRIP, TOPBP1, and claspin did not prevent the activation of Chk1 (***Figure 5G–I***, ***Figure 1—figure supplement 2C***, n ≥ 6 tracheae per condition per experiment, n = 2). This strongly suggests that the H_2O_2-dependent phosphorylation of Chk1 is independent of ATRIP, TOPBP1, and claspin.

Discussion

ATR and Chk1 are essential for normal development in *Drosophila* and other animals. In this regard, both kinases are thought to serve as guardians of genomic integrity and loss of either is associated with increased genomic instability and catastrophic cell death. Our studies in the tracheal system reveal a different facet of ATR/Chk1 function . We have shown previously that the pathway is required to arrest tracheal progenitor cells in G2 and that the activation of ATR/Chk1 occurs in the absence of any detectable DNA damage. The findings presented here demonstrate that Duox-generated H_2O_2 is required for the activation of ATR/Chk1 axis in this context (see model in ***Figure 5J***). We discuss below the possible mechanisms by which ROS can activate ATR/Chk1, how ROS levels are regulated during tracheal development, and the clinical implication of the findings.

The precedence for ROS-based activation of PIKK-family kinases like ATR, ATM, and DNA-PK was set by studies on ATM. The formation of an intermolecular disulfide bond between cysteine residues located at the C-terminus of ATM was found to be essential for ATM homodimerization and activation (***Guo et al., 2010***). The structure of *Drosophila* ATR is not known, but the structure of human ATR in complex with ATRIP has been determined by cryoEM and the human ATR-ATRIP complex has been shown to dimerize (***Rao et al., 2017***). Using SWISS-MODEL and the kinase domain of human ATR as template, we modeled the *Drosophila* ATR monomer (the sequence range modeled was 855–2517, which has 33.6% sequence identity to human ATR). A model for the *Drosophila* ATR dimer was subsequently generated using the human ATR-ATRIP complex as the template (***Waterhouse et al., 2018***; ***Guex et al., 2009***). This model shows that there are no exposed cysteines that are close enough to form intermolecular disulfide bridges. Thus, there is a possibility that H_2O_2 regulates ATR in a different way than what has been proposed for ATM. The possibility that H_2O_2 can directly activate ATR by

other mechanisms seems likely. ROS can alter kinase activity either by modifying cysteine residues at or near the active site or more broadly, leading to conformational changes (***Corcoran and Cotter, 2013***). As indicated in the Introduction, ATR can be activated in response to mechanical stress by a mechanism that is likely to be dependent on ATRIP. Although our studies show that activation of ATR/Chk1 by ROS does not require ATRIP, future experiments will investigate all possibilities for non-canonical activation. ATR aside, ROS may also regulate Chk1 activation by modifying Chk1 in some manner or via recruitment of other factors (see model in ***Figure 5J***).

A comparison of the effects of ATR/Chk1 knockdown and SOD1 overexpression/Duox knockdown suggests that there may be other (ROS-independent) mechanisms for the non-canonical activation of ATR/Chk1. We have shown that loss of either ATR or Chk1 leads to slow rate of cell division post mitotic reentry (***Kizhedathu et al., 2018***). Since there is no evidence for any DNA damage post-mitotic re-entry and the knockdown of ATRIP, TOPBP1, and claspin does not recapitulate the ATR/Chk1 mutant phenotype (***Figure 4—figure supplement 2***, n ≥ 7 tracheae per timepoint), the mechanism for the activation of ATR/Chk1 post-mitotic re-entry is unclear. Interestingly, neither the overexpression of SOD1 nor the knockdown of Duox recapitulates the mitotic defect observed in ATR/Chk1 mutants (***Figures 1J and 2F***). This suggests that there are other non-canonical-mechanisms of ATR/Chk1 activation that are relevant to the roles of these kinases during development.

How are ROS levels regulated during development? Analysis of Duox mRNA levels in tracheoblasts shows that expression is high in L2 and early L3 and drops significantly at 32–40 hr L3. This parallels the expression of Chk1. We have previously shown that the levels of Chk1 mRNA are regulated transcriptionally by the Wnt signaling pathway. We determined whether Wnt signaling also regulates Duox expression and ROS levels. This analysis showed that ROS levels are unaffected in Wnt pathway mutants (data not shown). We infer that Wnt signaling pathway does not regulate Duox nor ROS levels. Juvenile hormone (JH) has been shown to act as a negative regulator of cell proliferation in tracheae (***Djabrayan et al., 2016***). Pertinently, the levels of JH are high in L2 and early L3 and drop mid L3 (***Dubrovsky, 2005***). Thus, the timecourse of JH levels parallels the timecourses of both Duox and Chk1 expression. Future experiments will test the possibility that JH signaling in trachea regulates Duox expression and potentially Wnt signaling/Chk1 expression as well.

The possibility that ROS can activate ATR/Chk1 without inducing DNA damage may be clinically relevant. It has been reported that ovarian cancer cells that express high levels of Duox1 and high levels of activated Chk1 are relatively Cisplatin-resistant (***Meng et al., 2018***). The authors suggest that high levels of Chk1 activation are critical for chemoresistance and that the high levels of Chk1 activation are likely the result of ROS-generated DNA damage. The findings presented here suggest that high ROS may independently activate Chk1 and contribute toward chemoresistance. Along the same lines, cancer cells that have high levels of ROS (***Gu et al., 2018***; ***Singh et al., 2020***) and an active DNA damage repair pathway have been shown to be relatively radioresistant (***Alsubhi et al., 2016***; ***Wang et al., 2013***). Here again, the enhanced radioresistance has been attributed to ROS-dependent DNA damage priming of the DNA damage response. We suggest that the ROS-based activation of ATR/Chk1 activation evidenced here may also contribute toward the observed chemo-/radioresistance of cancer cells.

Materials and methods

Key resources table

Reagent type (species) or resource	Designation	Source or reference	Identifiers	Additional information
Genetic reagent (*Drosophila melanogaster*)	*btl-GAL4*	***Shiga et al., 1996***	FLYB: FBtp0001208	This line was a gift from Dr. Shigeo Hayashi
Genetic reagent (*D. melanogaster*)	*UAS-Chk1^{RNAi}*	VDRC	110076	
Genetic reagent (*D. melanogaster*)	*UAS-Chk1^{S373D}*	This study		Please see Materials and methods for a detailed description. (Can be obtained through NCBS Fly Facility: https://bangalorefly.ncbs.res.in/)

Continued on next page

Continued

Reagent type (species) or resource	Designation	Source or reference	Identifiers	Additional information
Genetic reagent (*D. melanogaster*)	*RPA-70GFP*	***Blythe and Wieschaus, 2015***		This line was a gift from Dr. Eric F Wieschaus
Genetic reagent (*D. melanogaster*)	*UAS-Duox^{RNAi}*	BDSC	RRID:BDSC_33975 and RRID:BDSC_32903	
Genetic reagent (*D. melanogaster*)	*UAS-ATR*	***Bayer et al., 2018***		This line was a gift from Dr. Anja C Nagel
Antibody	Phospho-Chk1 (Ser345) (rabbit monoclonal) antibody	CST	Cat #2348 (RRID:AB_331212)	(1:200)
Antibody	Anti-8-hydroxy-2′-deoxyguanosine antibody (mouse monoclonal) antibody	Abcam	Cat #ab48508 (RRID:AB_867461)	(1:200)
Commercial assay or kit	Tyramide signal amplification system	Thermo Fisher Scientific	Cat #B40912	

Fly strains and handling

The following strains were obtained from repositories: *UAS-Sod1* (RRID:BDSC_24754), UAS-*Duox^{RNAi}* (RRID:BDSC_32903, RRID:BDSC_33975), UAS-*ATRIP^{RNAi}* (RRID:BDSC_61355), *UAS-TOPBP1^{RNAi}* (RRID:BDSC_43244), UAS-*Claspin^{RNAi}* (RRID:BDSC_32974) (Bloomington *Drosophila* Stock Center), *UAS-Chk1^{RNAi}* (RRID:FlyBase_FBst0473748), and *UAS-ATR^{RNAi}* (RRID:FlyBase_FBst0475838; Vienna *Drosophila* Resource Center). *UAS-Chk1* was generated in the in-house fly facility. The following strains were received as gifts: *btl-GAL4*, *UAS-ATR*, and *RPA70-GFP*. Strains were raised on a diet of cornmeal-agar and maintained at 25°C . All experiments were performed on animals raised at 25°C unless otherwise indicated.

Cloning of pUAST-Chk1^{S373D} and generation of transgenic flies

Drosophila Chk1 cDNA clone was ordered from DGRC in pOT2 vector. Serine at 373 (TCG) position was mutated to aspartic acid (GAT) using the primers *Chk1_S373D_Forward* and *Chk1_S373D_Reverse*. The complete plasmid was amplified by polymerase chain reaction (PCR) using Phusion polymerase. The PCR product was then digested with Dpn1 enzyme and further transformed into XL10 cells. The plasmid was isolated from a few colonies and sent for sequencing. The positive clone with the mutation (TCG to GAT) was then subcloned into the vector pUAST. Mutant Chk1 (Chk1 S373D) was amplified using the primers *pUAST_Chk1_Ecor1_Forward* and *pUAST_Chk1_Kpn1_Reverse*. The PCR fragment and the empty vector were then double digested using enzymes EcoR1 and Kpn1 at 37°C for 1 hr. The vector was purified using gel extraction and the PCR fragment was purified using the PCR clean-up kit (Qiagen). The digested vector and insert were mixed in the ratio 1:3 and ligated using T4 DNA ligase (NEB) at 16°C overnight. The ligation mixture was transformed into XL10 cells. Plasmid isolation was performed on the positive clones and sent for sequencing for further confirmation. The clone with the correct mutation pUAST-Chk1^{S373D} was used to establish five independent transgenic fly lines by P-element mediated germline transformation by the in-house fly facility.

The following primer sets were used for generating and cloning Chk1^{S373D}:

Chk1_S373D_Forward	5′ CAGTTACTCCTTCGATCAACCAGCTTTGCTTGATG 3′
Chk1_S373D_Reverse	5′ ATCGAAGGAGTAACTGAGCCGAGCCTCCTG 3′
pUAST_Chk1_EcoR1_Forward	5′ AGAGAATTCATGGCTGCAACGCTG 3′
pUAST_Chk1_Kpn1_Reverse	5′ AGAGGTACCCTAAGGCACCGAATTTG 3′

Larval staging

Larval staging was performed as previously described (***Guha and Kornberg, 2005***) based on the morphology of the anterior spiracles. L2 larvae were collected and examined to identify animals that had undergone the L2-L3 molt in 8 hr intervals (0–8 hr L3). 0–8 hr L3 cohorts collected in this method were staged for subsequent timepoints.

Immunostaining and imaging

Animals were dissected in PBS and fixed for 30 min with 4% (w/v) paraformaldehyde (PFA) in PBS. The following antisera were used for immunohistochemical analysis: chicken anti-GFP (Aves, 1:500, RRID:AB_10000240), rabbit anti-phospho Chk1 (CST, 1:200, RRID:AB_331212), rabbit anti-pH3 (Millipore, 1:500, RRID:AB_310177), mouse anti-8-hydroxy-2′-deoxyguanosine (Abcam, 1:200, RRID:AB_867461), and Alexa 488/568-conjugated donkey anti-chicken/rabbit/mouse secondary antibodies (Invitrogen, 1:200). Tyramide signal amplification was performed as per the manufacturer's recommendations for pChk1 detection. The following reagents were used as part of this protocol: tyramide amplification buffer and tyramide reagent (Thermo Fisher), vectastain A and B (Vector Labs), and biotinylated donkey anti-rabbit IgG (Jackson ImmunoResearch, 1:200, RRID:AB_2340593). Tracheal preparations were flat-mounted in ProLong Diamond Antifade Mountant with DAPI (Molecular Probes) and imaged on Zeiss LSM-780 laser-scanning confocal microscopes. All images were taken by adjusting the parameters (gain and laser power) such that there is no saturation in the positive control images. All images from the same experiment were acquired at the same settings. Images were processed using ImageJ (RRID:SCR_003070). For quantification of cell number, fixed specimens were mounted in ProLong Diamond Antifade Mountant with DAPI and the number of nuclei was counted from images collected with an Olympus BX 53 microscope. The DT of the second thoracic metamere was identified morphologically based on the cuticular banding pattern at anterior and posterior junctions.

ROS detection

Larvae of indicated stages were dissected in PBS, flipped inside out to expose the trachea, and incubated in 100 µM H_2DCFDA (Thermo Fisher) for 30 min or 10 µM DHE (Thermo Fisher) for 5 min at room temperature. The larvae were then washed in PBS and fixed mildly in 4% PFA for 5 min. Tracheae were flat mounted in ProLong Diamond and imaged immediately.

Fluorescence intensity quantification

Fluorescence intensities were quantified by doing a maximum intensity projection followed by background subtraction. In each image, three square regions of interest (ROIs) were selected at random within the tracheal boundaries. The intensity density values obtained from these ROIs were averaged and then divided by 1000 to obtain arbitrary unit values (AU). Fluorescence intensities of all the samples for H_2DCFDA, DHE staining, and pChk1 immunostaining were calculated in the same manner. ImageJ software was used to perform all the above operations.

RNA isolation and quantitative PCR

RNA extraction and qPCR were performed as described in ***Kizhedathu et al., 2018***. Primer sequences for *Chk1*, *Fz3*, *Wg*, *Wnt5*, *Wnt6*, *Wnt10*, *ATR*, *Duox*, and *GAPDH* (internal control) are provided below. Relative mRNA levels were quantified using the formula RE = $2^{-\Delta\Delta Ct}$ method.

The following primer sets were used:

GAPDH forward	5' CGTTCATGCCACCACCGCTA 3'
GAPDH reverse	5' CACGTCCATCACGCCACAA 3'
Chk1 forward	5' AACAACAGTAAAACGCGCTGG 3'
Chk1 reverse	5' TGCATATCTTTCGGCAGCTC 3'
Wg forward	5' AAATCGTTGATCGAGGCTGC 3'
Wg reverse	5' GGTGCAGGACTCTATCGTTCC 3'

Continued on next page

Continued	
Wnt5 forward	5' AGGATAACGTGCAAGTGCCA 3'
Wnt5 Reverse	5′ ACTTCTCGCGCAGATAGTCG 3′
Wnt6 Forward	5′ AGTTTCAATTCCGCAACCGC 3′
Wnt6 Reverse	5′ TCGGGAATCGCGCATTAAGA 3′
Wnt10 Forward	5′ CACGAATGGCCCGAAAACTG 3′
Wnt10 Reverse	5′ CCCACGGTGCCCTGTATATC 3′
Fz3 Forward	5′ ATGAATGTCGTTCAAAGTGG 3′
Fz3 Reverse	5′ TATAGTAAATGGGGCTTGCG 3′
ATR Forward	5' CCAGATAGCAGCGAGTGCAT 3'
ATR Reverse	5' CGAGGTCCAGGGAACTTAGC 3'
Duox Forward	5′ ATCTACACGGTGGATAGGAA 3′
Duox Reverse	5′ CAGCAGGATGTAAGGTTTCT 3′

γ-Irradiation of larvae

Second instar larvae were exposed to 50 Gy of γ-radiation at the rate of 2.56 Gy/min using Blood Irradiator 2000 (Board of Radiation and Isotope Technology, DAE, Mumbai). After irradiation, the larvae were transferred into media vials, maintained at 25°C for 3 hr (detection of *RPA-70GFP* and γ−H2AX) or indicated timepoints (detection of pChk1), after which they were sacrificed.

Hydrogen peroxide treatment

Animals were dissected in PBS and flipped inside out to expose the tracheae. They were then incubated with specific concentrations of H_2O_2 in PBS at room temperature. For detection of 8-oxo-dG, the larvae were immediately washed in PBS and fixed with 4% PFA and immunostaining was performed as described above. For detection of pChk1, the specimens were washed in PBS immediately and ice-cold PFA was added. The samples were fixed overnight at 4°C . Immunostaining was then performed as indicated above.

Acknowledgements

We thank Shigeo Hayashi, Eric F Wieschaus, and Anja C Nagel for fly lines. We also thank the Central Imaging and Flow Cytometry Facility (CIFF) at inStem and Fly Facility at C-CAMP for their support. Ramalingaswami Fellowship (Department of Biotechnology, Government of India, AG) and institutional funds from inStem (AK, PC) are acknowledged.

Additional information

Funding

Funder	Grant reference number	Author
Department of Biotechnology, Ministry of Science and Technology, India	inStem Core Funds	Arjun Guha

The funders had no role in study design, data collection and interpretation, or the decision to submit the work for publication.

Author contributions

Amrutha Kizhedathu, Conceptualization, Investigation, Methodology, Visualization, Writing – original draft, Writing – review and editing; Piyush Chhajed, Investigation, Methodology, Visualization, Writing – original draft, Writing – review and editing; Lahari Yeramala, Investigation, Methodology, Resources; Deblina Sain Basu, Investigation, Methodology; Tina Mukherjee, Resources; Kutti R Vinothkumar, Conceptualization, Resources, Writing – original draft; Arjun Guha, Conceptualization, Funding acquisition, Methodology, Supervision, Visualization, Writing – original draft, Writing – review and editing

Author ORCIDs

Piyush Chhajed http://orcid.org/0000-0002-8705-6773
Tina Mukherjee http://orcid.org/0000-0003-3776-5536
Arjun Guha http://orcid.org/0000-0002-3753-1484

Decision letter and Author response

Decision letter https://doi.org/10.7554/eLife.68636.sa1
Author response https://doi.org/10.7554/eLife.68636.sa2

Additional files

Supplementary files

- Transparent reporting form

Data availability

All data generated or analysed during this study are included in the manuscript and supporting file; Source Data files have been provided for Figures 1,2,3,4.

References

Alsubhi N, Middleton F, Abdel-Fatah TMA, Stephens P, Doherty R, Arora A, Moseley PM, Chan SYT, Aleskandarany MA, Green AR, Rakha EA, Ellis IO, Martin SG, Curtin NJ, Madhusudan S. 2016. Chk1 phosphorylated at serine345 is a predictor of early local recurrence and radio-resistance in breast cancer. *Molecular Oncology* **10**: 213–223. DOI: https://doi.org/10.1016/j.molonc.2015.09.009, PMID: 26459098

Artus J, Cohen-Tannoudji M. 2008. Cell cycle regulation during early mouse embryogenesis. *Molecular and Cellular Endocrinology* **282**: 78–86. DOI: https://doi.org/10.1016/j.mce.2007.11.008, PMID: 18164540

Bayer FE, Zimmermann M, Preiss A, Nagel AC. 2018. Overexpression of the Drosophila ATR homologous checkpoint kinase Mei-41 induces a G2/M checkpoint in Drosophila imaginal tissue. *Hereditas* **155**: 27. DOI: https://doi.org/10.1186/s41065-018-0066-4

Bedard K, Krause K-H. 2007. The NOX family of ROS-generating NADPH oxidases: physiology and pathophysiology. *Physiological Reviews* **87**: 245–313. DOI: https://doi.org/10.1152/physrev.00044.2005, PMID: 17237347

Blackney MJ, Cox R, Shepherd D, Parker JD. 2014. Cloning and expression analysis of Drosophila extracellular Cu Zn superoxide dismutase. *Bioscience Reports* **34**: 851–863. DOI: https://doi.org/10.1042/BSR20140133

Blythe SA, Wieschaus EF. 2015. Zygotic genome activation triggers the DNA replication checkpoint at the midblastula transition. *Cell* **160**: 1169–1181. DOI: https://doi.org/10.1016/j.cell.2015.01.050, PMID: 25748651

Choi JH, Lindsey-Boltz LA, Kemp M, Mason AC, Wold MS, Sancar A. 2010. Reconstitution of RPA-covered single-stranded DNA-activated ATR-Chk1 signaling. *PNAS* **107**: 13660–13665. DOI: https://doi.org/10.1073/pnas.1007856107, PMID: 20616048

Cimprich KA, Cortez D. 2008. ATR: An essential regulator of genome integrity. *Nature Reviews Molecular Cell Biology* **9**: 616–627. DOI: https://doi.org/10.1038/nrm2450, PMID: 18594563

Corcoran A, Cotter TG. 2013. Redox regulation of protein kinases. *The FEBS Journal* **280**: 1944–1965. DOI: https://doi.org/10.1111/febs.12224, PMID: 23461806

Delacroix S, Wagner JM, Kobayashi M, Yamamoto K, Karnitz LM. 2007. The Rad9-Hus1-Rad1 (9-1-1) clamp activates checkpoint signaling via TopBP1. *Genes & Development* **21**: 1472–1477. DOI: https://doi.org/10.1101/gad.1547007, PMID: 17575048

Djabrayan J-V, Cruz J, de Miguel C, Franch-Marro X, Casanova J. 2014. Specification of differentiated adult progenitors via inhibition of endocycle entry in the Drosophila trachea. *Cell Reports* **9**: 859–865. DOI: https://doi.org/10.1016/j.celrep.2014.09.043, PMID: 25437542

Djabrayan J.-V, Casanova J, Perrimon N. 2016. Snoo and Dpp Act as Spatial and Temporal Regulators Respectively of Adult Progenitor Cells in the *Drosophila* Trachea. *PLOS Genetics* **12**: e1005909. DOI: https://doi.org/10.1371/journal.pgen.1005909

Dubrovsky EB. 2005. Hormonal cross talk in insect development. *Trends in Endocrinology and Metabolism* **16**: 6–11. DOI: https://doi.org/10.1016/j.tem.2004.11.003, PMID: 15620543

Durocher D, Jackson SP. 2001. DNA-PK, ATM and ATR as sensors of DNA damage: variations on a theme? *Current Opinion in Cell Biology* **13**: 225–231. DOI: https://doi.org/10.1016/s0955-0674(00)00201-5, PMID: 11248557

Geiszt M, Witta J, Baff J, Lekstrom K, Leto TL. 2003. Dual oxidases represent novel hydrogen peroxide sources supporting mucosal surface host defense. *The FASEB Journal* **17**: 1–14. DOI: https://doi.org/10.1096/fj.02-1104fje

Gu H, Huang T, Shen Y, Liu Y, Zhou F, Jin Y, Sattar H, Wei Y. 2018. Reactive oxygen species-mediated tumor microenvironment transformation: The mechanism of radioresistant gastric cancer. *Oxidative Medicine and Cellular Longevity* **2018**: 5801209. DOI: https://doi.org/10.1155/2018/5801209, PMID: 29770167

Guex N, Peitsch MC, Schwede T. 2009. Automated comparative protein structure modeling with SWISS-MODEL and Swiss-PdbViewer: a historical perspective. *Electrophoresis* **30**: 162-173. DOI: https://doi.org/10.1002/elps.200900140, PMID: 19517507

Guha A, Kornberg TB. 2005. Tracheal branch repopulation precedes induction of the Drosophila dorsal air sac primordium. *Developmental Biology* **287**: 192–200. DOI: https://doi.org/10.1016/j.ydbio.2005.09.005, PMID: 16198330

Guha A, Lin L, Kornberg TB. 2008. Organ renewal and cell divisions by differentiated cells in Drosophila. *PNAS* **105**: 10832–10836. DOI: https://doi.org/10.1073/pnas.0805111105, PMID: 18664581

Guo Z, Kozlov S, Lavin MF, Person MD, Paull TT. 2010. ATM activation by oxidative stress. *Science* **330**: 517–521. DOI: https://doi.org/10.1126/science.1192912, PMID: 20966255

Kim SH, Lee WJ. 2014. Role of DUOX in gut inflammation: Lessons from Drosophila model of gut-microbiota interactions. *Frontiers in Cellular and Infection Microbiology* **3**: 116. DOI: https://doi.org/10.3389/fcimb.2013.00116

Kizhedathu A, Bagul AV, Guha A. 2018. Negative regulation of G2-m by ATR (mei-41)/Chk1(Grapes) facilitates tracheoblast growth and tracheal hypertrophy in Drosophila. *eLife* **7**: e29988. DOI: https://doi.org/10.7554/eLife.29988, PMID: 29658881

Kizhedathu A, Kunnappallil RS, Bagul AV, Verma P, Guha A. 2020. Multiple wnts act synergistically to induce chk1/grapes expression and mediate g2 arrest in *Drosophila tracheoblasts*. *eLife* **9**: e57056. DOI: https://doi.org/10.7554/eLife.57056, PMID: 32876044

Kumar A, Mazzanti M, Mistrik M, Kosar M, Beznoussenko GV, Mironov AA, Garrè M, Parazzoli D, Shivashankar GV, Scita G, Bartek J, Foiani M. 2014. ATR mediates a checkpoint at the nuclear envelope in response to mechanical stress. *Cell* **158**: 633–646. DOI: https://doi.org/10.1016/j.cell.2014.05.046, PMID: 25083873

Lee EM, Trinh TTB, Shim HJ, Park SY, Nguyen TTT, Kim MJ, Song YH. 2012. Drosophila Claspin is required for the G2 arrest that is induced by DNA replication stress but not by DNA double-strand breaks. *DNA Repair* **11**: 741–752. DOI: https://doi.org/10.1016/j.dnarep.2012.06.007, PMID: 22796626

Liu Q, Guntuku S, Cui XS, Matsuoka S, Cortez D, Tamai K, Luo G, Carattini-Rivera S, DeMayo F, Bradley A, Donehower LA, Elledge SJ. 2000. Chk1 is an essential kinase that is regulated by Atr and required for the G2/M DNA damage checkpoint. *Genes & Development* **14**: 1448. DOI: https://doi.org/10.1101/gad.14.12.1448

Meng Y, Chen C-W, Yung MMH, Sun W, Sun J, Li Z, Li J, Li Z, Zhou W, Liu SS, Cheung ANY, Ngan HYS, Braisted JC, Kai Y, Peng W, Tzatsos A, Li Y, Dai Z, Zheng W, Chan DW, et al. 2018. DUOXA1-mediated ROS production promotes cisplatin resistance by activating ATR-Chk1 pathway in ovarian cancer. *Cancer Letters* **428**: 104–116. DOI: https://doi.org/10.1016/j.canlet.2018.04.029, PMID: 29704517

Patil M, Pabla N, Dong Z. 2013. Checkpoint kinase 1 in DNA damage response and cell cycle regulation. *Cellular and Molecular Life Sciences* **70**: 4009–4021. DOI: https://doi.org/10.1007/s00018-013-1307-3, PMID: 23508805

Rao Q, Liu M, Tian Y, Wu Z, Hao Y, Song L, Qin Z, Ding C, Wang HW, Wang J, Xu Y. 2017. Cryo-EM structure of human ATR-ATRIP complex. *Cell Research* **28**: 143–156. DOI: https://doi.org/10.1038/cr.2017.158

Robinson SW, Herzyk P, Dow JAT, Leader DP. 2013. FlyAtlas: database of gene expression in the tissues of Drosophila melanogaster. *Nucleic Acids Research* **41**: 744-750. DOI: https://doi.org/10.1093/nar/gks1141, PMID: 23203866

Shiga Y, Tanaka-Matakatsu M, Hayashi S. 1996. A nuclear GFP/beta-galactosidase fusion protein as a marker for morphogenesis in living Drosophila. *Development, Growth and Differentiation* **38**: 99–106. DOI: https://doi.org/10.1046/j.1440-169X.1996.00012.x

Singh B, Patwardhan RS, Jayakumar S, Sharma D, Sandur SK. 2020. Oxidative stress associated metabolic adaptations regulate radioresistance in human lung cancer cells. *Journal of Photochemistry and Photobiology B* **213**: 112080. DOI: https://doi.org/10.1016/j.jphotobiol.2020.112080

Srinivas US, Tan BWQ, Vellayappan BA, Jeyasekharan AD. 2019. ROS and the DNA damage response in cancer. *Redox Biology* **25**: 101084. DOI: https://doi.org/10.1016/j.redox.2018.101084

Wang WJ, Wu SP, Liu JB, Shi YS, Huang X, Zhang QB, Yao KT. 2013. MYC regulation of CHK1 and CHK2 promotes radioresistance in a stem cell-like population of nasopharyngeal carcinoma cells. *Cancer Research* **73**: 1219–1231. DOI: https://doi.org/10.1158/0008-5472.CAN-12-1408

Waterhouse A, Bertoni M, Bienert S, Studer G, Tauriello G, Gumienny R, Heer FT, de Beer TAP, Rempfer C, Bordoli L, Lepore R, Schwede T. 2018. SWISS-MODEL: homology modelling of protein structures and complexes. *Nucleic Acids Research* **46**: W296–W303. DOI: https://doi.org/10.1093/nar/gky427, PMID: 29788355

Willis J, Patel Y, Lentz BL, Yan S. 2013. APE2 is required for ATR-Chk1 checkpoint activation in response to oxidative stress. *PNAS* **110**: 10592–10597. DOI: https://doi.org/10.1073/pnas.1301445110

Xu YJ, Leffak M. 2010. ATRIP from TopBP1 to ATR--in vitro activation of a DNA damage checkpoint. *PNAS* **107**: 13561–13562. DOI: https://doi.org/10.1073/pnas.1008909107

Yang C, Jiang L, Zhang H, Shimoda LA, Deberardinis RJ, Semenza GL. 2014. Analysis of hypoxia-induced metabolic reprogramming. *Methods Enzymol* **542**: 425–455. DOI: https://doi.org/10.1016/B978-0-12-416618-9.00022-4

Zhang J, Wang X, Vikash V, Ye Q, Wu D, Liu Y, Dong W. 2016. ROS and ROS-Mediated Cellular Signaling. *Oxidative Medicine and Cellular Longevity* **2016**: 1–18. DOI: https://doi.org/10.1155/2016/4350965

Zielke N, Korzelius J, van Straaten M, Bender K, Schuhknecht GFP, Dutta D, Xiang J, Edgar BA. 2014. Fly-FUCCI: A Versatile Tool for Studying Cell Proliferation in Complex Tissues. *Cell Reports* **7**: 588–598. DOI: https://doi.org/10.1016/j.celrep.2014.03.020